GEOMORPHOMETRIC CHARACTERIZATION OF TOPOGRAPHIC MORPHOLOGICAL STRUCTURE FOR MAPPING AND UNDERSTANDING MOUNTAIN ENVIRONMENTS

A Dissertation

by

BRENNAN WILLIAM YOUNG

Submitted to the Graduate and Professional School of
Texas A&M University
in partial fulfillment of the requirements for the degree of

DOCTOR OF PHILOSOPHY

Chair of Committee,	Michael P. Bishop
Committee Members,	Andrew G. Klein
	Anthony M. Filippi
	Ryan C. Ewing
Head of Department,	David M. Cairns

December 2021

Major Subject: Geography

ABSTRACT

The spatial morphological structure of the topography is notoriously difficult to map and characterize in relation to geodynamic processes due to the complex coupling of tectonic, geologic, climate, and surface processes that generate relief, as well as issues of topographic information representation, scale dependency, and spatial and semantic uncertainty. Consequently, we do not know where or at what rate relief production occurs except at specific sample locations. Furthermore, we lack the techniques to objectively extract process-related information from a digital elevation model even though much of that information is present and can be interpreted subjectively. The primary objective of this research was therefore to improve our understanding of mountain geodynamics by conceptualizing, designing, and implementing a framework for representing and interrogating the spatial topographic morphological structure (TMS) and process-form relationships for mapping and characterizing process regimes in northern Pakistan.

The TMS framework was found to be effective for mapping process regimes. Specifically, 31 basins in the central Karakoram were identified as predominantly shaped by glacier erosion or by bedrock river incision based on mapped terrain units and spatial constraints imposed by basin structure. Process regimes of glacial downwasting and supraglacial lake development and intermoraine drainage and sediment flux were mapped on the surface of Baltoro Glacier based on simple process-form relationships represented in TMS networks. The TMS-erosion relationship was also investigated, though no clear relationship could be identified between basin-averaged land-surface and terrain-unit parameters and predicted erosion rate and measured beryllium-10 concentrations. A linear relationship was identified between beryllium-10 production rate and concentrations, and further research will better characterize this relationship and determine if it can be used to predict cosmogenic nuclide concentrations and erosion rates. Future research on topics of semantic modeling, uncertainty characterization, scale dependency, and topographic influence on erosion rate will improve our understanding of process-form relationships and scale-dependent mountain geodynamics through objective, structure-based interpretations of the land surface.

DEDICATION

To Lucy and the kids, and to my parents and grandparents.

I wouldn't have made it without you.

ACKNOWLEDGMENTS

I extend thanks to my advisor and committee chair, Michael Bishop for his invaluable insight, support, and patience, who had the courage to engage in this endeavor with me. I also wish to thank the rest of my committee, Andrew Klein, Anthony Filippi, and Ryan Ewing, and honorary committee member Lewis Owen, for their tremendous patience and support. I wish to thank leadership and staff of the Department of Geography at Texas A&M University, who have facilitated this process. I thank Sandia National Laboratories and the National Park Service for research opportunities that gave me the opportunity to explore these ideas from different perspectives. Thanks to Da Huo and Zhaohui Chi, who provided support and insight throughout various stages of this dissertation.

I also wish thank family, friends, and associates, who provided invaluable support and guidance.

CONTRIBUTORS AND FUNDING SOURCES

Contributors

This work was supported by a dissertation committee consisting of Professor Michael P. Bishop [advisor], Professor Andrew G. Klein, and Associate Professor Anthony M. Filippi of the Department of Geography, Professor Ryan C. Ewing of the Department of Geology and Geophysics, and honorary committee member Professor Lewis A. Owen of the Department of Marine, Earth and Atmospheric Sciences at North Carolina State University.

A version of Chapter 2 has been submitted for publication as a research article in the Journal of Physical Geography. Preliminary work investigating object-oriented analysis and network analysis described in Chapter 3 was done in collaboration with Da Huo, a recent graduate of the Department of Geography. The beryllium-10 sample data for Chapter 4 were provided by Professor Lewis Owen, who also provided the methodological details for the field sampling and laboratory work described in the same chapter.

All other work conducted for the dissertation was completed by the student independently.

Funding Sources

Graduate study was supported by generous teaching assistant opportunities through the Department of Geography at Texas A&M University and research assistant opportunities funded by Sandia National Laboratories and the National Park Service. This dissertation does not represent the research conducted for those funding agencies.

TABLE OF CONTENTS

Page

LIST OF FIGURES

FIGURE Page

LIST OF TABLES

TABLE Page

1. INTRODUCTION

The study of mountain geodynamics involves characterization of the interaction of climate, surface, and tectonic processes across space and time (Schumm and Lichty, 1965; Barsch and Caine, 1984; Bishop et al., 2003; Phillips, 2003; Larsen and Montgomery, 2012; Bishop et al., 2018, 2020). Investigating such complex processes, feedback mechanisms, and systems couplings is notoriously difficult, but required for a complete understanding of the environment and for practical applications in hazards mitigation and resource management (Pike, 2000; Bishop et al., 2012; Lastochkin et al., 2018). Of special importance is understanding complex interactions between systems that result in relief production, including the spatial and temporal scales over which processes operate, the magnitudes of processes that drive and influence coupled systems, and their relationship with the spatial organizational structure of the land surface (Tate and Wood, 2001; Phillips, 2003; Larsen and Montgomery, 2012; Phillips, 2016).

From a mountain geodynamics perspective, relief is the product of the interaction between tectonic, geologic, surface, and climate systems (e.g., Phillips, 2003; Aalto et al., 2006; Phillips, 2007; Bishop and Dobreva, 2017). Couplings between these systems have been characterized in terms of sediment cascades (e.g., Heckmann and Schwanghart, 2013), climate forcing (e.g., Sweeney et al., 2015), tectonics (e.g., Roy et al., 2016; Gray et al., 2018), base-level forcing due to climate and tectonics (e.g., Roering et al., 2007), and relief-erosion feedbacks (e.g., Moon et al., 2017). Controls on relief production (topography, microclimate, topographic stress, etc.) are constrained by the boundary conditions imposed by the scale-dependent, hierarchical topographic context within which these systems operate, such as boundary geometry (Perron et al., 2008; Ewing and Kocurek, 2010). Self-organization and complexity emerges out of the scale-variant behavior of the topography and coupled systems under such constraints (Woldenberg, 1969; Hallet, 1990; de Boer, 1992; Brändli, 1996; Phillips, 2003; McDonnell et al., 2007; Ewing and Kocurek, 2010; Phillips, 2016). Despite this understanding of topographic self-organization under specific tectonic, climatic and hydrological, and topographic constraints, we do not know where relief production occurs due to

erosion-uplift coupling, the magnitudes of surface processes across space except at specific sample locations, or the spatial extents of where specific processes dominate (Bishop et al., 2012; Bishop and Houser, 2016). We also do not know how to map polygenetic evolution, address scale-dependencies of process-form relationships, or how to numerically characterize the degree to which the topography represents past and present geomorphic systems and processes (Beven, 1996; Phillips, 2007; Bishop et al., 2012; Bishop and Houser, 2016).

From a geographic information science and technololgy (GIST) and mapping perspective, geodynamics are related to the geometry and spatial topology of the land surface and its components, such that the hierarchical organization of diverse shapes, patterns, and spatial anisotropy provide a framework for characterizing spatial variation and for relating process to topography, and process-form relationships to coupled systems (e.g., Larin-Fonseca and Garea-Llano, 2010; Ode et al., 2010; Bishop et al., 2018). Associating processes and coupled systems with terrain morphometry and features is challenging, however, because many geomorphological concepts, objects, and boundaries remain semantically ill-defined (Burrough and Frank, 1996; Fisher et al., 2005; Deng, 2007), making the relationships between morphometry parameters, terrain features, geomorphic processes, and forcing factors mathematically intractible. Representing geometric and process-related characteristics of the topography with geomorphometric parameters can provide insight into specific properties of flow, roughness, and environmental conditions such as exposure or openness (Böhner and Antonić, 2009; Olaya, 2009; Bishop et al., 2012), but such characterizations are generally scale-dependent (Shary et al., 2005) and often yield little information into the systems that drive the spatial distributions of those parameters. Elemental or elementary forms, such as slope facets (Dikau, 1989; MacMillan and Shary, 2009), curvature forms (Dikau, 1989; Shary et al., 2005; MacMillan and Shary, 2009), and geomorphons (Jasiewicz and Stepinski, 2013) are spatial partitions of useful, usually flow-related, terrain elements, that might theoretically be organized based on process dynamics and/or aggregated into higher-order-scale entities that characterize the scale-variant behavior of a system (Band, 1989; Goodchild et al., 2007; Bishop et al., 2018).

From a GIST/geomorphometry perpsective, information regarding the spatial organization of

shapes and patterns of topographic form, including geometry, boundaries, and topological relationships related to landforms and surface processes are perceptible in visual representations of the altitude field or the fields of geomorphometric parameters or elementary forms, and are often interpreted in context of their relationship to process and system dynamics by an expert (Smith et al., 2013). Attempts to quantitatively extract that information, however, to map such fundamental features as valley bottoms (Gallant and Dowling, 2003; Gilbert et al., 2016; Zhao et al., 2019) and eminences (Deng and Wilson, 2008; Sinha and Mark, 2010), or semantically model hillslopes or process regimes dominated by fluvial incision, deposition, glaciation, or mass wasting is fraught with challenge due to uncertainty, subjectivity, and empiricism (Bishop et al., 2012; Bishop and Dobreva, 2017; Bishop and Houser, 2016; Bishop et al., 2018). Empirical methods, though perhaps useful for individual study areas, are difficult to repeat across various geologic, climatological, tectonic, and/or topographic regimes and do not generally account for associated process-form relationships (Bishop et al., 2012; Bishop and Dobreva, 2017; Bishop and Houser, 2016). It is clear that geomorphometric parameterization and empirical and pattern recognition techniques to map and characterize forms, processes, and systems are limited, and semantic models are required to objectively map specific terrain entities and associate geomorphic forms with the various factors that drive heterogeneous relief production (Sinha and Mark, 2010; Bishop and Houser, 2016). Numerous conceptual and methodological issues exist for transforming the altitude field into terrain entities and process-related information, including issues of length-scale (Shary et al., 2005), anisotropy (e,g, Roy et al., 2016; Newman et al., 2018), heterogeneity (e.g., Moglen and Bras, 1995; Zhang et al., 2020), nonlinearity (Phillips, 2003, 2007), inherited topography (Ritter, 1988; Phillips, 2007), empiricism (Bishop et al., 2012), uncertainty (Beven, 1996; Fisher et al., 2005), indeterminate boundaries (Burrough and Frank, 1996), semantics (Dehn et al., 2001; Deng, 2007; Lingua and Noardo, 2015), ontologies (Smith and Mark, 2003), and interoperability (Boucher and Zimányi, 2010). Some progress has been made in the theory and application in these areas, but there as-yet exists no formalized framework for characterizing the spatial complexity and scale-dependency of surface processes and geodynamics of a region based upon the hierarchical

spatial organization of the topography (Bishop et al., 2012).

Lastochkin et al. (2018) recommends a "system-morphological approach" for geomorphological research and applications, with a workflow consisting of (1) data accumulation; (2) general geomorphologic mapping and land-surface partitioning; (3) evaluating the structure of systems through the perspective of characteristic points, links, elementary forms, and vector fields; and (4) evaluating dynamics based on geomorphologic and structural characterizations. Though Lastochkin et al. (2018) presented this framework as a manual workflow driven by expert knowledge, it serves as a useful basis for formulating a new framework for evaluating the topographic morphological structure (TMS) of a region in order to numerically characterize the spatial organization of the land surface and relating the TMS, as characterized in one or more topographic morphological structural frameworks, to processes and geomorphic complexity (McDonnell et al., 2007; Ode et al., 2010). The scope of research for generating such a framework is inherently multidisciplinary, drawing on knowledge accumulated within both Earth science and GIST.

1.1 Research Objectives

The primary objective of this research is to improve our understanding of process-form relationships that can be used to characterize mountain geodynamics in the central Karakoram Himalaya. Specific sub-objectives include:

1. Conceptualize, design, and implement a topographic morphological structural framework (TMS framework) that will permit the characterization of terrain entities that serve as the basis for establishing nodes for characterizing a topographic morphological network system with unique topological and properties that result from the influence of surface and geological processes. This component of the research aims to utilize terrain-entity properties, topological relationships between terrain entities, and scale-hierarchical-organizational signals to generate a composite signature that encapsulates information about erosion, uplift, deformation, and threshold slopes to permit characterization and mapping of coupled systems and the polygenetic character of the topography. More specifically, it is important to

evaluate this approach for mapping surface-process regimes. This sub-objective is driven by such questions as: What is the TMS and how do we represent it for characterizing geomorphological systems? How may the scale-dependent TMS be characterized within a GIS spatial analysis and modeling framework? What are the formal relationships between mountain TMS and surface processes and geodynamic subsystems, specifically fluvial incision, and glacial erosion? Answers to these questions come through exploration of spatial topological characteristics formalized within a TMS framework that can be incorporated into process-regime mapping, geomorphometric parameterization, object-oriented analysis, and network analysis to investigate the geometry and topology of the TMS as captured within a TMS framework.

2. Evaluate the TMS framework to gain insight into the presence or absence of spatial constraints that govern the operational scale dependencies of process regimes on a glacier surface. Specifically, process-form relationships should be able to differentiate and map the high-altitude glacial sediment transfer system versus variation in the ablation dynamics at different altitudes associated with the development of supraglacial lakes on debris-covered glaciers. In this way, process regimes can be mapped and polygenetic evolution can be evaluated. This objective is driven by questions regarding matter, form, and process dominence, and indeterminate boundaries that cause significant problems in geomorphological mapping (Bishop et al., 2012). Spatial variations in process dominance, such as ablation dynamics caused by water versus debris-load forcing versus suprafluvial and drainage transport, alter the topography of glacier surfaces. Collectively, the spatial locations of such process regimes and their degree of spatial overprinting may govern the sensitivity of the glacier system to respond to climate change and may even control glacier state and system resilience to change. This objective therefore involves development and evaluation of specific TMS frameworks for characterizing the process-regime system via object-oriented analysis and network analysis.

3. Evaluate the utilization of terrain entities and a TMS framework to characterize parameters that can be used in erosion simulations to predict basin-wide average erosion rates. These will be calibrated with erosion rate estimates from beryllium-10 cosmogenic isotope concentrations. Important questions that drive this sub-objective are: Can terrain features and the basin TMS be used to facilitate erosion simulations and the accurate prediction of basin erosion rates? What properties of the TMS correlate well with measured erosion rate estimates for specific basins? Can topographic information be used to modulate beryllium-10 production rates to predict beryllium-10 concentrations? To reduce the complexity of the problem, geomorphometric parameters and terrain object properties will be evaluated in association with hillslope and fluvial processes in an unglaciated environment. The Hazara region south of the Karakoram in Kashmir, northeastern Pakistan, is well-suited for this because it represents an unglaciated mountainous environment. Simple erosion laws will be implemented within a GIS framework to model topographic evolution, sediment flux, cosmogenic isotope production for comparison with measured beryllium-10 concentrations to evaluate erosion rates and erosion-rate modulation with topographic information.

These objectives permit the testing of a number of hypotheses:

- H_0 : The spatial and hierarchical organization of topographic forms/entities/objects is not related to formative processes or systems coupling. This null hypothesis can be demonstrated false by implementing a TMS framework and extracting process-related information from TMS signals, morphometric parameters, terrain entities, and network properties that unique characterize and permit mapping of deformation zones, tectonic zones, and surface-process regimes. We expect to be able to uniquely characterize geomorphological units as described in objectives 1, 2, and 3. This should be possible, as the topography inherently records information about the nature of mountain geodynamics in the Himalaya up to perhaps back to 65-70 ka (Bishop and Shroder, 2000; Bishop et al., 2001; Seong et al., 2007, 2009a).

- H_1 : The spatial organization of terrain entities and patterns in geomorphometric parame-

ter fields can be used to characterize specific surface process regimes. Terrain entities are related through specific topological relationships that arise through the self-organization of the topography in response to such processes as uplift, crustal shear, mass wasting, fluvial incision, glacial erosion, ice ablation, and matter and energy transport under the influence of gravity. This hypothesis is difficult to test as process-form relationships must be characterized to represent a process regime. Different process regimes can exhibit different process-form relationships and scale dependencies. This hypothesis can be shown to be true within the context of this research by implementing unique TMS frameworks that are useful for characterizing and mapping the spatial extents, morphometric properties, system properties, and scale dependencies of a particular process regime. Under the assumption of unique process-regime structure, we also hypothesize that we can determine the degree of spatial overprinting of multiple process regimes operating over a geographic area. Object-oriented analysis and network analysis permits the integration and synthesis of information to permit such capabilities, and preliminary findings in Bishop et al. (2018) demonstrate that the process of glacierization can be differentiated from processes operating on adjacent hillslopes.

- H_2 : A topographic structural framework facilitates the prediction of basin erosion rates. This hypothesis involves the development of a TMS framework that encapsulates terrain features associated with hillslope and fluvial processes, and permits the identification of relationships between morphometric parameters that causally govern erosion and transport, and that ultimately govern the basin erosion rate. Terrain entities exhibit unique slope morphometries that accelerate or decelerate transport and that ultimately determine the direction of transport. Meso-scale relief properties control topographic stress and fracturing that control local erosion rates. Collectively, the integration of this information should explain the variation in basin rates, as individual basins are structurally different, and topographic forcing modulates erosion and deposition. Therefore, we can expect that we can use morphometric properties and terrain structure to explain the variation in basin erosion rates estimated using beryllium-10 cosmogenic nuclides and modulate cosmogenic production rate predictions

with topographic information.

Testing these hypotheses requires the establishment of a TMS framework which will facilitate the characterization of process regimes, coupled systems, erosion rates, and provide some insight into mountain the polygenetic evolution of the topography.

1.2 Research Significance

The morphological properties of the topography are widely utilized in mapping efforts, and also serve as the basis for establishing basic process-form relationships, but the process-form linkage concept lacks formalization that permits system characterization and interoperability between disciplines or even between studies (Bishop et al., 2012; Smith et al., 2013; Bishop and Houser, 2016). The proposed research will formalize the TMS concept within a spatial organizational and mathematical framework that utilizes morphological parameters, topographic features/objects and topological and hierarchical spatial organizational structure to characterize numerous components of geomorphological systems and teh coupling of systems that govern mountain geodynamics. This will be accomplished through the use of an innovative methodological approach that formalizes spatial and system concepts, makes use of hierarchy and graph theory, and encapsulates information from object-oriented and network analysis. This approach should enable the formalization of the concepts of operational scale dependencies and degree of polygenetic topographic evolution, which have yet to be adequately addressed (Bishop et al., 2012, 2018, 2020). Doing so will enable quantitative investigation of process-form relationships and the identification of coupled system zones, which is a hallmark of mountain geodynamics. The approach will also improve disciplinary interoperability, reduce subjectivity, increase replicability, address various multi-faceted uncertainty issues, and accelerate efforts to characterize and map geomorphological phenomena, systems, and their interactions (Church, 2010; Kasprak et al., 2017; Lastochkin et al., 2018). This will be the first TMS framework to provide new insights into mountain geodynamics based solely on a digital elevation model and the organization of terrain entities represented in it, bridging the fields of geomorphology and GIST.

Information of the spatial variability of surface uplift rates and denudation processes is difficult to acquire. This is particularly true in areas that are remote, have high relief, and/or have high geomorphic complexity, such as the Himalaya. Efforts to formalize a topographic morphological structural framework will enable more robust remote analysis of challenging regions and provide insights into: (1) the amount of information that is encoded into the terrain about geologic and climatic conditions; (2) spatially heterogeneous uplift-erosion dynamics; (3) factors that control fluvial and glacial erosion; and (4) the coupling between topographic morphological structure, lithology, geologic structure, and landscape evolution. Outcomes of this research are therefore extendable and multipurpose, and can facilitate studies from many other disciplines. Furthermore, a formalized TMS framework has practical implications, as multi-scale information can be used to inform decision-making regarding water management, various forms of geohazards mitigation, resource exploration, and other applications where the TMS may be important (Pike, 2000; Pike et al., 2009; Lastochkin et al., 2018).

The principal advantage of this work is the provision of a mathematical framework in which concepts of spatial context and association are explicit in a way that facilitates the interpretation of process. Much of the information that is contained within the altitude field cannot be inferred from a single location or some evaluation of an isotropic, fixed-scale neighborhood, but is interpreted from the spatial structure of relief variation in the process of manual geomorphological mapping. High-magnitude coupling of tectonic uplift, bedrock river incision, and mass wasting, for example, is not interpreted from high curvature, convergence, neighborhood variations in slope angle or azimuth, or these factors combined for a particular location or neighborhood, but in the spatially consistent association of a highly anisotropic zone of high convergence in context of steep, planar slope facets facing each other and perpendicular to the long-direction of convergence, and high mountain ridges that contribute to low topographic openness, particularly in basins with a high degree of side-branching in their drainage and valley networks (e.g., Parvis, 1950; Wilson and Bishop, 2013; Pereira-Claren et al., 2019). Such characterization depends on specific models for representing important terrain elements, the spatial relationships between terrain elements, and

how these forms and structural associations relate to process. This work bares the necessity of robust semantic models and uncertainty characterization for understanding mountain geodynamics, and this framework is modular in the sense that it can host new and updated models that describe geomorphic form and process-form relationships. A good understanding of geodynamics is notably at the heart of hazards mitigation practices, which is of special importance to communities that depend on mountain resources but are at risk due to flooding, mass wasting, and other hazards whose telltale signs are manifest in the spatial structure of topographic morphology (Hewitt and Liu, 2010; Bishop et al., 2012; Van Westen, 2013; Owen, 2018).

1.3 Research Activities

The objectives of this research are addressed in three primary research activities: (1) formalization and evaluation of a topographic morphological structural framework; (2) characterization and mapping of various glacial properties and supraglacial process regimes; and (3) simulation and modulation of cosmogenic nuclide production given cosmogenic nuclide measurements and hillslope and fluvial erosion models, which are driven by terrain feature and TMS properties. These research activities are represented in the chapters of this dissertation.

Chapter II represents the first research activity, which addresses hypotheses H_0 and H_1 by achieving sub-objective 1: formulating and evaluating a formal TMS framework. The utility of the framework is demonstrated in the central Karakoram, with special emphasis on general differentiation between fluvial bedrock incision and the broader valley floors and U-shaped valleys of past and present glaciation, based on the spatial, hierarchical structure of the topography. This activity includes semantically modeling and mapping elemental forms, slope facets, valley bottoms, basins, and eminences, and synthesizing structural information through topological analysis–that is, containment by higher-order entities and intersection with lower- or same-order entities, and associated order-variant properties relevant to specific processes.

Chapter III represents the second activity, which achieves sub-objective 2 and tests hypothesis H_1 by utilizing variations in topographic structure to map supraglacial ablation and transport process regimes in the central Karakoram through application of specific TMS frameworks. This

research activity seeks to gain insight into glacier system dynamics based on the small-scale topographic morphological structure of debris-covered glaciers across altitudes.

Chapter IV represents the third research activity, which tests hypothesis H_2 by addressing sub-objective 3 by characterizing topographic structure, predicting erosion rate trends using landscape evolution models, and comparing structure and simulated rates with estimates of erosion rate based on modeled Beryllium-10 cosmogenic isotope production rates and measured Beryllium-10 concentrations in select basins in the Hazara region of Kashmir, northeastern Pakistan. The purpose of this research activity is to investigate the relationship between topographic structure and erosion, to calibrate structure-erosion relationships with measured data, and to explain some discrepancies between modeled and measured erosion rates using topographic structure.

Chapter V concludes and summarizes the findings of this research effort, placing the TMS framework into the context of mountain geodynamics research, geomorphometry, and GIST.

2. MOUNTAIN PROCESS REGIME CHARACTERIZATION USING A TOPOGRAPHIC MORPHOLOGICAL STRUCTURAL FRAMEWORK

Abstract

Complex mountain geodynamics are difficult to decouple due to forcing factors, feedback mechanisms, and system couplings that arise from interacting atmospheric, surface, and tectonic processes. The operational multi-scale scale dependencies and process-form relationships that govern the spatio-temporal extent of process regimes, which in turn govern relief production, have yet to be adequately characterized and mapped. This research establishes a topographic morphological structural framework for representing and querying the spatial organizational structure of the topography that governs and is governed by mountain geodynamics. The spatial scale-dependent structure of the topography is accounted for using land-surface parameters and land-surface partitioning into distinct terrain units that represent important aspects of the geomorphological system. The properties and spatial topology of terrain units provide constraints for modeling process-form relationships, which are represented as process-form indices and synthesized using logistic regression to empirically detect glacial and bedrock river incision process regimes at the basin-scale for 31 basins in the Central Karakoram at about 80% accuracy. The topographic morphological structural framework approach provides a mechanism for tractable representation of scale-dependent topographic structure for automated characterization of the land surface, providing insight into polygenetic geomorphological systems and systems coupling through defined process-form relationships.

2.1 Introduction

Investigations into understanding mountain geodynamics and topographic process-form relationships have yielded a wealth of knowledge that has been incorporated into erosion and landscape evolution models (Tucker and Bras, 1998; Montgomery and Brandon, 2002; Sklar and Dietrich, 2004; Whipple, 2004; Roering et al., 2007; Balco et al., 2008; Tucker and Hancock, 2010; Gas-

parini and Brandon, 2011; Owen, 2018), geohazards and risk assessment (Clark and Burbank, 2010; Hewitt and Liu, 2010; Van Westen, 2013; Sharma et al., 2014; Owen, 2018), and provided insight into geologic structure and tectonics (Zámolyi et al., 2010; Dortch et al., 2011b; Duvall and Tucker, 2015; Gray et al., 2018; Owen, 2018; Sharma et al., 2018). Nevertheless, complex mountain geodynamic interactions are difficult to decouple due to forcing factors, a multitude of feedback mechanisms, and system couplings that arise from interactions between atmospheric, surface, and tectonic processes (Ritter et al., 2002; Turcotte and Schubert, 2002; Bishop et al., 2010). The operational scale dependencies and process-form relationships that govern the spatio-temporal extent of process regimes, relief production and topographic evolution have yet to be adequately characterized and mapped (González et al., 1995; Phillips, 2003; Rhoads, 2006; Phillips, 2007; Koppes and Montgomery, 2009; Bishop et al., 2012). Given that the topography inherently records polygenetic evolution caused by forcing factors in various coupled systems (Phillips, 2007; Bishop and Houser, 2016), progress in understanding geomorphological systems and mountain geodynamics can potentially be made based upon characterization of topographic properties and the spatial morphological structure of the topography, as the topography inherently represents past and modern events related to process regimes (Bishop et al., 2018; Lastochkin et al., 2018).

Variations in forcing-factor dynamics are clearly seen throughout the Himalaya, as the relief structure and spatial organization of topographic elements and terrain features are spatially diverse (Zeitler et al., 2001b; Scherler et al., 2014). Spatially heterogeneous coupling between lithology, crustal deformation, glaciation, fluvial transport, relief production, and orographic precipitation control topographic features, such as the size and shape of basins and the spatial density of ridge and drainage networks (Archer and Fowler, 2004; Bishop et al., 2010). Morphotectonic influences also govern crustal deformation and the spatial extent of shear zones, which have a distinct anisotropic expression in the fabric of the land surface, affecting such properties as basin elongation and symmetry, drainage density, ridge alignment, and mountain front sinuosity (Zeitler et al., 2001a; Dortch et al., 2011b; Roy et al., 2016; Gray et al., 2018; Divyadarshini and Singh, 2019; Wani et al., 2019, 2020).

Given the recent developments in remote-sensing technology and the availability of digital elevation models (DEMs), Earth scientists have new opportunities to mathematically characterize topographic properties and begin to assess the spatial structure of the topography. Progress to date has focused on addressing theoretical issues including scale dependencies (Bishop et al., 2012; Phillips, 2016; Bishop and Dobreva, 2017), equifinality (Beven, 1996; Phillips, 2007), indeterminant boundaries (Burrough and Frank, 1996), hierarchical organization (de Boer, 1992; Kocurek and Ewing, 2016; Phillips, 2016), forcing factors (Bishop et al., 2010; Koons et al., 2012), connectivity (Heckmann et al., 2015; Cossart and Fressard, 2017), and other issues related to the complexity of geomorphic systems (Ode et al., 2010; Bishop et al., 2012, 2018). Many geospatial technology solutions for characterizing the morphology of the land surface have focused on developing and using land-surface parameters and using pattern recognition and artificial intelligence for land-surface partitioning or other characterizations (Bishop et al., 2012; Jasiewicz and Stepinski, 2013; Houser et al., 2017; Bishop et al., 2018; Toulia et al., 2018; Juliani, 2019, e.g.,). While such technologies certainly improve our ability to characterize the topography and may be useful for some geomorphological mapping, they do not address the fundamental scale-dependent and semantic issues of formalizing certain geomorphological concepts, such as topographic structure, for diagnosing process-form relationships, which are necessary for gaining insight into coupled systems and the polygenetic evolution of the land surface. Consequently, geomorphological mapping remains challenging due to issues of scale, indeterminate boundaries, semantics, spatial coincidence, genetics, and spatial topology (Fisher and Wood, 1998; Deng, 2007; Evans, 2012; Bishop et al., 2012, 2018). The integration of mountain geomorphology, geomorphometry, and geographic information science and technology (GIST) is necessary to mathematically formalize the concept of topographic structure, including the generation of robust semantic models for topographic elements and frameworks that capture the scale-dependent, hierarchical spatial structuring for those elements.

Therefore, the overall objective of this research is to establish and investigate an operational geomorphometric framework for characterizing the spatial organizational structure of mountain to-

pography that governs and is governed by mountain geodynamics. Specifically, we account for the spatial scale-dependent structure of the topography by evaluating topographic properties that regulate surface processes and govern matter and energy fluxes on the landscape. We formalize various topographic spatial entities ("terrain units") that can be used for creating a system of key structural topographic elements to gain insight into the topographic morphological structure (TMS) that characterizes geomorphological systems in mountainous environments from several perspectives. Sub-objectives include:

- Formalize terrain units that represent diverse spatial entities, including slope-facets, ridges, valley floors, basins, and eminences.
- Establish a framework for the structural characterization of components of the TMS, based upon terrain units and their spatial topological relationships.
- Explore the use of structural information to represent process-form relationships and characterize glacial and bedrock river incision process regimes.

We evaluate our approach in the Central Karakoram, because the region's topography exhibits the characteristics of distinct glacial and fluvial process regimes with high-magnitude process rates (Owen, 1989; Shroder, 1993; Archer and Fowler, 2004; Barros et al., 2006; Seong et al., 2009b,a; Searle et al., 2010; Shroder et al., 2011; Wallis et al., 2016). It is not the objective of this research to map and characterize the entire study area, but to demonstrate a framework wherein structural information helps to produce process-related information for process regime characterization at the basin scale.

2.2 Background

2.2.1 Topographic Properties

Land-surface parameters (LSPs) are useful for representing various properties of the topography and for gaining insight into process-form relationships to infer surface, lithologic, and climatic conditions (González et al., 1995; MacMillan and Shary, 2009; Bishop et al., 2018). Altitude is

the most fundamental parameter for characterizing topography and is related to mass distribution and rock and sediment flux caused by surface processes that are governed by climate and tectonic forcing factors (González et al., 1995; Montgomery, 2001, 2002). First- and second-order derivatives of altitude, including slope angle, slope azimuth (aspect), and various measures of curvature, in addition to numerous indices, aim to characterize surface geometry in order to provide information about gravity-driven flow and surface exposure to atmospheric and exo-planetary particles and fields (Shary et al., 2002; Codilean, 2006; Olaya, 2009; Nugraha et al., 2015; Bishop et al., 2018). Many other empirical parameterization schemes specifically aim to characterize process, including surface irradiance (Proy et al., 1989; Bishop et al., 2019), exposure to wind and cosmic particles (Yokoyama et al., 2002; Codilean, 2006; Bishop et al., 2010, 2019), sedimentation (Gallant and Dowling, 2003; Grauso et al., 2018), flooding (e.g., Mahmood and Rahman, 2019), and mass wasting (e.g., Larsen and Montgomery, 2012; Nugraha et al., 2015; Buitrago and Martínez M., 2016).

The relationships between LSPs and surface processes are typically understood through empirical models (e.g., Montgomery, 2001; Montgomery and Brandon, 2002; Whipple, 2004; Roering et al., 2007). Though perhaps necessary to induce the behavior of natural systems, empiricism also makes it challenging to map process regimes and characterize systems-couplings (Bishop et al., 2012, 2018) because empirical models often require region-specific tuning of one or more parameters that represent inter-related but unknown factors associated with scale-dependent climatic, geologic, and surface conditions (e.g., stream power law parameters, Phillips, 1988, 2003; Whipple, 2004; Barros et al., 2006; Phillips, 2007). A more complete analysis of the spatial structure of the topography may permit the inference of empirical parameters or the development of more deterministic models, but this requires contextual information that must be acquired at one or more unknown or variable and anisotropic scales. Though research acknowledges issues of scale (Phillips, 1988; Shary et al., 2005; Bishop et al., 2012; Phillips, 2016; Bishop and Dobreva, 2017) and some researchers have attempted to characterize the length-scales of homogeneous patches (e.g., Tate and Wood, 2001; Drăguţ et al., 2010) and topographic anisotropy (Roy et al., 2016;

Newman et al., 2018), there remains no theoretical framework for synthesizing local and scale-dependent contextual topographic information to address issues of scale and empiricism for more reliably predicting the spacial extent and relative magnitude of surface processes.

2.2.2 Terrain Units

Most evaluation of the topography and its structure, particularly as it relates to genetic processes, relies on geomorphological spatial entities, such as drainage basins (Guth, 2011), drainage networks (Kirchner, 1993), eminences (Sinha and Mark, 2010), ridge networks (Werner, 1988; Rak et al., 2019), slopes (Schmidt and Dikau, 1999), elementary forms (Schmidt and Hewitt, 2004; Minár and Evans, 2008), and relief forms (Dikau, 1989). The size, shape, spatial organization, and topology of these terrain units are the basis of most conceptual models in geomorphology and are essential to gaining insight into the TMS and its relationship to polygenetic evolution (Bishop et al., 2012, 2018). That is, terrain units depict different aspects of the geodynamics and their relationships to each other and conditions defined with LSPs, such as valley-floor narrowing or abrupt change in orientation suggesting entrance into a new tectonic or lithologic regime, or elongate basins with asymmetric drainage suggesting a half-graben structure (Back and Strecker, 1998; Balázs et al., 2017).

Partitioning the topography into units of structural significance poses a significant challenge, however (Bishop et al., 2012). Manual mapping techniques, while generally believed to be robust, are challenged by subjectivity and big-data issues. Computational scale influences the degree of spatial generalization and the magnitude of uncertainty in estimating topographic properties and therefore directly influences the number, size, shape, boundaries, and properties of each derived terrain unit. The meanings of certain terrain units also depends on context and the mapper's experience (Fisher and Wood, 1998; Deng, 2007): A long, low-relief ridge may be a levee, glacial moraine, or dune, and often cannot be distinguished except by its proximity to channel-forms, placement in or at the mouth of a broad valley floor, the anisotropic spatial frequency and magnitude of like forms, or other contextual criteria. Contextual information is therefore imperative for deriving terrain units or giving them structural meaning (Schmidt and Dikau, 1999; Deng, 2007;

Lingua and Noardo, 2015).

Due to issues of scale, uncertainty, and lack of semantic clarity, the boundaries between terrain units are often indeterminate or fuzzy in nature (Burrough and Frank, 1996; Fisher and Wood, 1998; Bishop et al., 2012; Bishop and Dobreva, 2017). One approach has been to map terrain units as fuzzy fields of class-membership (e.g., Gallant and Dowling, 2003; Deng and Wilson, 2008; Straumann and Purves, 2011), though this poses a significant technical challenge for using terrain units for structural analysis. Process regimes are very well suited to mapping as fuzzy entities, however, as they might be inferred from an analysis of the TMS and are spatially coincident with other process regimes that do or did influence the topography of a region (Phillips, 2007). The fuzziness of process regimes are therefore very well suited for mapping systems-coupling and polygenetic evolution, as could be inferred from such studies as the sediment cascades of Heckmann and Schwanghart (2013) and the scale-based principal component analysis of Barrineau et al. (2016).

2.2.3 Topographic Morphological Structure

The TMS concept has pervaded scientific literature since the earliest days of geomorphology, referred to, in whole or in part, as "topographic structure" (Jenson and Domingue, 1988), "topographic grain" (Mitra and Marshak, 1988; Sărăşan et al., 2019), "watershed structure" (Band and Moore, 1995), "drainage (network) structure" (Turcotte et al., 2001; Ai, 2007), "landform structure" (Dehn et al., 2001), and "relief structure" (Dikau, 1989; Whipple, 2004). The TMS concept has been valuable for inferring geologic structure (Mitra and Marshak, 1988), tectonic stress (Mitra and Marshak, 1988), mass wasting (Larsen and Montgomery, 2012; Nugraha et al., 2015; Buitrago and Martínez M., 2016), flood patterns (Mahmood and Rahman, 2019; Park, 2020), precipitation patterns (Archer and Fowler, 2004; Dobreva et al., 2017), paleoglacierization (e.g., Blomdin et al., 2016), and many other phenomena that govern and are governed by the morphological properties of the topography. The primary method for TMS investigation is visual interpretation (Bishop et al., 2012; Blomdin et al., 2016; Lastochkin et al., 2018). Work to more quantitatively utilize the TMS includes parameterization of the land surface (Bishop et al., 2018), characterization of scale

(Drăguţ et al., 2010; Smith, 2010; Danesh-Yazdi et al., 2017), and empirical process-form relationships for modeling glacial, fluvial, hillslope, and tectonic processes (Tucker and Bras, 1998; Koons et al., 2002; Montgomery, 2002; Montgomery and Brandon, 2002; Whipple, 2004; Roering et al., 2007; MacGregor et al., 2009; Tucker and Hancock, 2010; Koons et al., 2012; Struth et al., 2017). A framework that encapsulates aspects of the TMS for interrogating the TMS for mapping and characterizing surface processes is sorely needed, however.

A significant challenge in the application of the TMS concept is that TMS has not been formalized or quantitatively defined, but qualitatively inferred to be the spatial organization of terrain entities (e.g., Dikau, 1989; Hallet, 1990; Werner, 2003; Kocurek and Ewing, 2016; Lastochkin et al., 2018) or the patterns in fields of topographic properties (e.g., Jenson and Domingue, 1988; Houser et al., 2017). Consider, for example, the concepts associated with the term "flow structure," which may be interpreted to be the field of flow direction, with or without flux magnitude, for water or sediment (e.g., Rhoads and Johson, 2018). The field may itself be considered a structure, as it describes the relationships between parts of the altitude and gradient fields (e.g., Turcotte et al., 2001; Cossart and Fressard, 2017). Alternatively, one might argue that flow has no structure until it is abstracted to distinct, spatially-related units: flow-convergent basins and flow-conducting drainages, or as networks of sources, links, and sinks (e.g., Heckmann et al., 2016). The distinction between these two perspectives is unclear because, in application, fields are commonly represented as grids or point clouds, which are themselves distinct, spatially-related units (DeMers, 2001), and systems of distinct units at one scale may function as fields at different scales. Another perspective is that structure is manifest in both fields and entities, both valid and inseparably connected (Cova and Goodchild, 2002). The ubiquitous yet abstruse TMS concept must be more rigorously defined and explored if it is to have a more direct and significant impact on mountain and general geomorphological research.

Some work has recognized the TMS as emergent out of the scale-variant hierarchical self-organization of tectonic and sedimentary systems which generate or modulate relief (de Boer, 1992; González et al., 1995; Werner, 2003; Ewing and Kocurek, 2010; Kocurek and Ewing, 2016).

For example, Zernitz (1932) provided an early summary of relationships between geologic structure and drainage patterns that continues to see use (e.g., Yang et al., 2020), and basins and watersheds are almost universally defined by the collateral relief-associations between adjacent samples of the altitude field (e.g., Jenson and Domingue, 1988; Liu et al., 2020). Graph theory provides a framework for perceiving the topography as an interconnected system of distinct parts (Heckmann et al., 2015; Cossart and Fressard, 2017), such as the landform-systems of Heckmann et al. (2016) and Heckmann and Schwanghart (2013) for investigating sediment cascades and systems coupling. From a hierarchy theory perspective, Dikau (1989) and Minár and Evans (2008) recognized that simpler terrain units could be perceived as components of higher-order units and aggregated for geomorphological mapping and more advanced terrain analysis. This spatial-hierarchical perspective is foundational to understanding the relationships between surface processes, boundary conditions, and scale-dependent controls (de Boer, 1992; Ewing and Kocurek, 2010; Bishop et al., 2012; Kocurek and Ewing, 2016; Bishop et al., 2018). Graph theory and hierarchy theory may therefore be suitable to serve as the foundation for a quantitative TMS theoretical framework that is capable of representing and interpreting the scale-dependent spatial organizational structure of the topography, where its structure incorporates the spatial topological relationships among morphological terrain units (Bishop et al., 2012).

2.3 Study Area

The Central Karakoram of northeastern Pakistan and western China (Fig. 2.1) was selected for this study for its striking relief, rising from valley floors at about 2 km above sea level to peaks in excess of 7 km above sea level (Seong et al., 2009a). Furthermore, the Central Karakoram exhibits diverse basin structures, which are governed by relatively poorly understood mountain geodynamics, including erosion and uplift rates, tectonic and deformation zones, and climate dynamics involving system coupling and radiative and precipitation forcing (Archer and Fowler, 2004; Barros et al., 2006; Seong et al., 2009a; Searle et al., 2010; Shroder et al., 2011; Bishop and Dobreva, 2017; Dobreva et al., 2017). Glacial behavior and altitudinal extent is highly spatially variable, with minimum glacier altitudes varying between about 2.5 and 4.5 km above sea level (Hewitt, 2005),

with fluvial and aeolian process regimes dominating at lower altitudes (Seong et al., 2009a).

Spanning the region are the Kilik Fault, the Main Karakoram Thrust (MKT) which accommodates the placement of the Euasian terrane over the Kohistan-Ladakh island arc terrane (Shroder, 1993; Roland et al., 2001; Searle et al., 2010), and the Karakoram Fault which accommodates right-lateral slip between the Karakoram and the greater Himalaya. The Karakoram is principally underlain by metamorphic and metasedimentary rock with numerous silica-rich intrusions (Shroder, 1993; Wandrey and Law, 1998; Searle et al., 2010; Shroder et al., 2011). The tectonics of the region continue to produce around 2-6 mm a^{-1} uplift (Shroder, 1993; Seong et al., 2009a), in addition to the numerous NW-SE thrust, strike-slip, and fold structures that span the region. These geological conditions, in conjunction with high-magnitude glaciation and bedrock river incision (Shroder, 1993; Seong et al., 2007, 2009a), are responsible for the extreme relief and unique and geographically variable topographic structure of the Central Karakoram, which exerts a significant control on the spatial distribution of precipitation from the Indian Monsoon that feed erosive processes associated with the Karakoram's glaciers and river systems (Archer and Fowler, 2004; Dobreva et al., 2017).

The tectonics and geologic structure of the region exert a strong first-order control on the anisotropic fabric of topographic relief in the Central Karakoram, manifest in numerous NW-SE-oriented ridges, valleys, and steep slopes (Fig. 2.2) and secondary structures (Owen, 1989). Steep terrain is associated with high-magnitude relief production due to the coupling of lithology, high-magnitude uplift, climate conditions, and glacial, fluvial, and mass wasting erosional processes (Shroder et al., 2011; Dobreva et al., 2017). The Hunza region in the western portion of the study area, for example, exhibits extreme relief, which appears to be associated with relatively erosive metasedimentary rock and rapid tectonic uplift (Derbyshire, 1996). These conditions are particularly pronounced where there is high-altitude glaciation and high-relief V-shaped valleys that are associated with rapid fluvial incision in tectonic uplift zones (Fig. 2.2). Better characterization of topographic structure and semantic modeling of process-form relationships may provide useful clues to better understanding the complex geodynamics of the Karakoram, such as the coupling of

the westerlies and monsoon, which governs precipitation distribution that in turn governs glacial, fluvial, and mass wasting erosion dynamics (Archer and Fowler, 2004; Seong et al., 2009a; Shroder et al., 2011; Dobreva et al., 2017).

2.4 Data and Methods

2.4.1 Data

This study utilizes the void-filled SRTMv3 DEM (30 m) (NASA JPL, 2013), which represents the altitude field that serves as the basis for all analysis in this research. Corrections to the DEM, such as peak and pit correction and low-frequency spatial filtering were not applied to avoid destruction of real but uncertain features and to promote the development of robust terrain unit-extraction models that are less sensitive to noise. The uncorrected DEM was then used to produce LSPs, terrain units, and other characterizations of topographic variation. Analysis of LSPs utilized large window sizes to mitigate the influence of potential errors that may exist in the DEM.

Modern glacierization is significant in assessing a basin's process-regime history. The glacier database of Rankl et al. (2014) is therefore utilized to represent the modern extents of glaciers. The GLIMS database (Raup et al., 2007) likewise attempts to capture the modern extents of glaciers in the study area, but Rankl et al. (2014) glacier extents are more conservatively confined to their basins and accurate for this region based upon visual comparison with satellite imagery. Modern glacier presence is utilized for defining process regime indices.

2.4.2 Framework

In order to investigate an aspect of the TMS in a way that is mathematically tractable, it is necessary to describe the spatial or functional relationships between different LSPs and terrain units. Let morphological conditions (i.e., topographic properties) and terrain units be collectively described as terrain elements. That is, a terrain element is an entity, a field, or an (artifically) abstracted portion of an entity or field such as a centroid, boundary point, sample point, or grid cell. Terrain elements are related by spatial topology or geomorphological function (e.g., sources and sinks Heckmann et al., 2016). Terrain elements and their relationships together define a graph-

like structure, where terrain elements serve as the vertices and their relationships serve as the edges.

The graph-like structure of terrain elements and their relationships represents a component of the greater TMS, or a topographic morphological component (TMC). A simple TMC representing flow structure can be represented by grid cells in a DEM, linked to the lowest-altitude adjacent grid cell (e.g., Cossart and Fressard, 2017). From this flow structure, drainage networks can be derived based on accumulated flow inferred from the flow structure (Liang and Mackay, 2000; Cossart and Fressard, 2017). More complex TMCs are hierarchical in nature, such as basins containing terrain units, which contain elementary forms (Dikau, 1989; Minár and Evans, 2008; MacMillan and Shary, 2009), which contain or reference points sampled from LSPs, which are each derived from a local neighborhood of altitude samples. From this perspective, the TMS is a hierarchical structure consisting of all topographic properties (i.e., represented with LSPs) and terrain units associated across all scales by spatial topology (e.g., adjacency, overlap, containment), spatial context, spatial association, and function (Fig. 2.3).

Any relational structure representing a subset of the TMS is a TMC that may facilitate inference of process-related information via well-defined process-form relationships (Bishop et al., 2012; Heckmann et al., 2015; Cossart and Fressard, 2017; Lastochkin et al., 2018; Rak et al., 2019). Each TMC is therefore a framework for investigating the TMS, where the terrain elements and inter-element relationships must be designed in a way that facilitates information extraction from the TMS. The framework used in this research is a minimal representation of a portion of the TMS, consisting of the altitude field, derivative LSPs, terrain units (including slope-facets, valley networks, and basins), and spatial topological relationships which provide constraints for detecting glacial and bedrock river incision process regimes (Fig. 2.4).

2.4.3 Land-Surface Parameters

Topographic properties are relevant for characterizing the structure of the topography. Many properties can be represented using LSPs and can characterize local and meso-scale properties that are also related to erosional processes or depict the distribution of a characteristic across space

(e.g., slope azimuth, anisotropy). In our demonstration of a TMS framework, which involves the generation of terrain units, development of criteria that describe terrain units, and spatial topological criteria for establishing a TMC, the following land-surface parameters are utilized:

- Altitude (z), represented in the DEM. Altitude is the fundamental information from which LSPs are derived and which constrains the extents of terrain units as a representation of ridges in altitude maxima and flow by path of maximum descent.

- Slope angle (θ_t), after Shary et al. (2002), with altitude gradients along the x and y axes determined using linear least-squares regression. Slope angle represents altitude-field organization in relation to gravity and associated surface processes. Specifically, θ_t is a component in defining slope-facet units, which are primary organizational units in partitioning the land surface into valley floors and eminences.

- Slope azimuth (φ_t), after Shary et al. (2002), with altitude gradients along the x and y axes determined using linear least-squares regression. Slope azimuth provides the directional component to slope attitude for slope-facet units, and guides low-frequency slope directionality that helps to connect the valley floor at steep valley confluences.

- Surface area (SA), after Jenness (2004). Surface area provides insight into local relief conditions and topographic ruggedness.

- Slope-azimuth convergence index (SACI) describes the degree to which local terrain slopes toward a location. As such, SACI is useful for characterizing channel-forms, glacier margins, and local depressions. SACI is similar to the convergence index implemented in GRASS GIS software, which seems to originate from Bauer et al. (1985), as cited in Jasiewicz (2020). This study's implementation of SACI is based solely on slope azimuth:

$$\text{SACI} = \frac{1}{4N} \sum_{i=0}^{N} (|\cos \varphi_{t,i} - cosi\varphi_{p,i}| + |\sin \varphi_{t,i} - \sin \varphi_{p,i}|), \tag{2.1}$$

  where $\varphi_{p,i}$ is the prototypical azimuth angle from the focus to the center of grid cell i.

- Slope-azimuth divergence index (SADI), which describes the degree to which local terrain slopes away from a location. SADI is consequently useful for characterizing ridge-forms and local mounds. SADI is computed as SACI with $\varphi_{p,i}$ in the opposite direction.

- Tangential curvature (K_{tan}), after Olaya (2009) with surface gradients approximated from a quadratic surface model obtained by multiple least squares regression (Wood, 1996). Tangential curvature represents convexity in the vertical plane perpendicular to the gradient direction, and as such is an effective tool for representing local ridge-like structures. This research utilizes K_{tan} to assess the planarity of certain slope-facet units.

- Mean curvature ($\bar{K}$), after Olaya (2009) with surface gradients approximated from a quadratic surface model obtained by multiple least squares regression (Wood, 1996). Mean curvature represents general convexity or "ridge-ness." Mean curvature is computed at a range of scales (11x11, 21x21, 41x41) in order to confine ridge units to just those areas that consistently exhibit convexity across that range of scales.

- Skyview factor (V_f), also called positive openness, is a proxy for meso-scale relief structure (Yokoyama et al., 2002; Wilson and Bishop, 2013; Bishop and Dobreva, 2017). As such, it is related to ridges , drainages, and erosion zones. Active, high-magnitude river incision tends toward low V_f compared to the broad glacial valley floors, for example. Because of the Karakoram's high-magnitude and complex relief structure, V_f was computed to a maximum distance of 20 km with a 1-degree azimuthal step size.

In order to achieve a level of generalization that reduces sensitivity to DEM error, all neighborhood operations are computed over an 11x11 computational window.

2.4.4 Terrain Units

We utilize object-oriented analysis of fundamental terrain units to adapt to the scale of natural topographic variation. The terrain units relevant to this research are presented in Table 2.1 and the methods for their derivation are subsequently described.

2.4.4.1 Slope-Facet Units

Slope-facet (SF) units represent homogeneous patches of slope attitude, similar in function to the slope units of Alvioli et al. (2020). The components of slope attitude are slope steepness (SS) and slope azimuth (SA). SS is represented by partitioning θ_t into five classes by ISODATA cluster analysis. The SS classification is useful for guiding aggregation for higher-order terrain units (e.g., valley floors are unlikely to contain steep slopes). SA is represented by partitioning the land surface into eight classes by ISODATA clustering of $\cos\varphi_t$ and $\sin\varphi_t$. SF are the spatial intersection of SS and SA.

2.4.4.2 Slope-Curvature Units

Slope-curvature units are homogeneous patches of various curvature parameters and are representative of zones of flow divergence and convergence (Dikau, 1989; Shary, 1995; Schmidt and Hewitt, 2004; Shary et al., 2005; MacMillan and Shary, 2009). This research utilizes the ridge (R) unit, which is based on the fact that any area with $K_{\text{mean}} > 0$ is inherently ridge-like, even if not prominently so. An object defined solely as $K_{\text{mean}} > 0$ may, however, extend beyond mountain ridges along a string of convex features, such as a mountain ridge that descends onto a debris slope which grades into a glacial moraine. Thus, it may be impossible to separate mountain ridges from ridge-forms in the valley floor based on convexity alone. Such ridge-form spatial linkages do not always hold across scales, however. Therefore, in order to capture small-scale ridge geometry as well as larger-scale breaks in convexity, R objects are defined as regions with positive mean curvature in all three of 11x11, 21x21, and 41x41 computational windows that also overlap either of the steepest two SS classes: that is, they must be both definitively convex and prominent. Holes inevitably appear in R due to scale disagreements in the curvature partition, and are filled at the risk of classifying small, high-altitude basins as R.

2.4.4.3 Slope-Azimuth Convergence and Divergence Units

Slope-azimuth convergence (SAC) units represent local topographic lows, such as channel-forms, supraglacial lakes, and swales. SAC units are consequently important components of the

valley network. Slope-azimuth divergence (SAD) units conversely represent topographic highs, such as ridge-forms, peaks, and mounds. SAD units are consequently important components of the ridge network. SAC and SAD units are zones of, respectively, SACI and SADI ≥ 0.62, where 0.62 is an approximate natural division between highly convergent/divergent forms and the background topography.

2.4.5 Valley-Floor Units and Networks

One of the most challenging modeling efforts in geomorphometry is valley floor (VF) extraction. Previous attempts to map VF have utilized fuzzy classification based on relative altitude, slope, and curvature (e.g., Gallant and Dowling, 2003; Straumann and Purves, 2011; Zhao et al., 2019) or by identifying abrupt breaks in slope and curvature (e.g., Gilbert et al., 2016), sometimes relying on *a priori* knowledge of a valley centerline or drainage network. Although these methods produce subjectively good local VF, broadly acceptable for identifying regions of non-negative sediment budget, these methods tend to produce disjoint VF networks, particularly where tributary valleys are exceptionally narrow or steep. Furthermore, the expression of landforms within or bounding the valley floor, such as alluvial fans, terraces, and one or more channel-forms complicates the mapping processes. These methods also require careful tuning and empirical selection of coefficients or thresholds for various morphometric parameters, making the approaches difficult to apply in diverse geographic regions. It is therefore necessary to develop a method for VF extraction that adapts to the scale-variant nature of complex mountain topography and minimizes parameter-tuning and dependency on *a priori* knowledge.

The approach for extracting VF units outlined here does not explicitly account for issues of complex forms within or at the edges of VFs, but aims to map the contiguous, connected valley structure. VF extraction is a delineation between eminence (Em) units and the VF that bounds Em. This occurs by identifying what is almost certainly Em and then growing the Em region into steep SF, prohibited by channel-forms represented by SAC units, at the risk of including some ridgeline breaks as part of the VF, such that:

1. All R units are declared as Em zones.

2. The Em partition is grown into the two steepest SS classes, barred by SAC.

3. The Em partition is grown into the middle-steepness SS class, barred by SAC. This is performed only after growth into the two steepest SS classes, because other it risks growth into moderate slopes than onto steep slopes which may exist as small features within VF, which disjoins a portion of the VF for the sake of encompassing such features as terrace edges or spurious landforms located within the VF. Because VF connectivity is a primary concern, small-scale Em that might exist within VF are ignored unless they also have an R-unit core.

4. Some tributary valleys have steep, non-convergent outlets, including some hanging valleys and alluvial fans, so a "bridge" is made between the lower VF and the tributary VF by tracing paths in the φ_t and $\varphi_t + \pi$ directions in non-VF locations. If the summed up- and down-slope path-lengths bridging two VF is less than 200 m, all grid cells on and adjacent to the path are removed from the Em partition.

5. Holes in the Em partition are filled except where the hole touches the edge of the dataset.

6. The Em partition is completed with a 5x5 morphological opening operation. VF occupy all of the negative (non-Em) space in the Em partition.

In order to analyze the VF network structure, a discrete, rather than zonal, representation of the VF was acquired via skeletonization. A new graph-based approach is used because other skeletonization approaches, such as using morphological operations (e.g., Saha et al., 2016; Alshehhi and Marpu, 2017), tend to segment networks, are direction-dependent (e.g., Ge et al., 2011), or are scale-dependent (e.g., Rak et al., 2019). The skeletonization process is outlined as:

1. Represent all grid cells in VF as vertices in a graph.

2. Create an edge between each vertex and its eight neighbors.

3. Identify "shapes" in the graph, or complete subgraphs that have no complete subgraph components (i.e., where clustering occurs).

4. Replace each shape with a vertex (a shape-vertex). Add edges between the shape-vertices of adjacent shapes, and between shape-vertices and vertices that are part of the shape but must be preserved to maintain local connectivity, which can be determined with a limited depth-first traversal. Certain arrangements in graph structure require special consideration, which must be addressed in order:

   (a) The vertex of a complete 3-graph with no shape neighbors is retained and adjacent only to the vertex reduced from the 3-graph.

   (b) Complete 3-graphs adjacent to at least two complete 4-graphs are not counted among shapes to be reduced.

   (c) The edges between any two of four complete 3-graphs are not retained if all four 3-graphs are also adjacent to a 4-graph.

   (d) Make a complete 4-graph out of two complete 3-graphs that share an edge and that neighbor no other shapes.

   (e) If a set of four complete 3-graphs each share an edge with two other 3-graphs in the set, discard their common vertex and make them a complete 4-graph.

   (f) If a set of complete 3-graphs share a vertex but not all share an edge with two of the other 3-graphs, these shapes are only treated as adjacent if they share an edge.

   (g) If two adjacent complete 4-graphs share all other edges with complete 3-graphs, the 3-graphs are only treated as adjacent to other 3-graphs with which they share an edge.

5. Repeat until there is no clustering. Skeletonization was limited to 500 iterations with manual resolution of rare emergent cases that preserve or exacerbate local clustering.

Due to computational limitations, the entire study area was divided into 500x500 tiles with 100-cell (3 km) overlap with adjacent tiles. Each tile was skeletonized and then merged, with errors

corrected manually. Cycles exist in the network because the VF classification is imperfect (some ridge saddles or passes were included in the valley network) and because some antecedent valleys exhibit a mid-valley divide. Cycles in the VF network are iteratively identified using depth-first traversal with backtracking (Tarjan, 1972) and broken by removing each cycle's maximum-altitude vertex. Additional errors are resolved manually, such as where the VF network crosses a divide but not in a cycle.

The skeletonized VF network is characterized by Strahler stream order (Ω_{VF}). This research utilizes Ω_{VF} as the basis for defining basin structure, but could also be utilized to evaluate other characteristics of the valley structure as independent of the drainage structure, particularly where multiple streams may occupy one valley.

2.4.5.1 Ridges and Ridgelines

Ridgelines are challenging to represent as continuous, linear structures due to complex ridge morphology which includes cols, saddles, passes, and other ridge-breaks at a variety of scales. Consequently, this study represents ridges in four ways, each providing benefits for different applications: (1) R units, (2) skeletonized SAD units, (3) DEM maxima, and (4) basin edges.

A discrete representation of the ridge network is obtained by skeletonization of SAD units using the approach outlined for VF. Some parts of the SAD-based ridge network exist within the VF, however. Ridgeline networks that have the majority of their vertices within VF are removed, and remaining networks have leaf-branches (vertex-chains that include a vertex with fewer than two neighbors) removed if the majority of vertices in that branch are located within the valley floor. The majority rule is used, rather than removing all vertices located within the valley floor, in order to preserve ridge connectivity, as VF derived in this study favor valley connectivity over ridge connectivity. The ridgeline network was then iteratively pruned of spurious branches of length < 500 m, as they are relatively insignificant to the eminence-scale structure. Ridgeline order, Ω_{Em}, was then determined by setting leaf-branches to $\Omega_{\mathrm{Em}} = 0$ and incremented Strahler-like at ridge-junctions. The resultant structure is broadly suitable for approximating ridgelines and representing the internal connectivity structure of eminences.

2.4.5.2 Basin Units

Basin (Ba) units are traditionally defined as watersheds, by their contributing area from pour points known *a prior* (e.g., Martz and Garbrecht, 1992, 1993; Liang and Mackay, 2000). The Ba utilized in this study's framework may differ from traditional basins or watersheds due to a focus on valley structure over drainage structure. A buffer is created from each VF-network vertex and labeled by Ω_{VF}, with higher-order buffers taking precedence. Each buffered area serves as the nucleus for a Ba unit. Small, isolated Ba units (single-cell objects) are sieved from the dataset. All non-Ba areas are then assigned to the first Ba unit encountered along the path of steepest descent. If a local pit is encountered, the pit area is filled until it "spills over" (e.g., O'Callaghan and Mark, 1984) and tracing continues from the spill-point. Ba unit order (Ω_{Ba}) is inherited from the original Ω_{VF}.

Relative position within a Ba unit is important for understanding its relationship to geodynamics. For example, the glacier accumulation zone represents a very different location from where glacial outwash occurs at lower altitudes. Some contextual concepts must therefore be represented and integrated into the research's framework:

- Basin mouth. While the outlets of watersheds might be defined at a particular pour-point, perhaps at or upstream from a stream junction, basin mouths occupy a portion of a Ba unit boundary and span the width of the valley floor. The mouth of a basin is therefore defined as the lowest-altitude intersection of Ba unit perimeter with VF units.

- Within-basin position. The "up-basin," "top of basin," "high-altitude portion" concepts of basin structure may be inaccurate, as they may be intended to refer to regions of moisture accumulation far from the mouth of the basin rather than the peaks of high-relief divides near the basin outlet. These notions generally imply a relief-related path-distance from the basin outlet measured parallel to the basin or valley centerline, though this raises numerous technical challenges associated with the determination of *which* centerline(s) in a branching basin structure. The use of a centerline directly is problematic because it ignores the com-

plexity associated with the geometry of the basin perimeter and its internal ridge structure. Any measure of within-basin distance suffers from the same semantic ambiguity. This research represents concepts of within-basin position or distance by breadth-first traversal of the basin area from some distance=0 point, line, or area, and sub-basin edges (without sub-basin mouths) behave as barriers to the traversal. Thus, up-basin distance (x_{Ba}) is measured from the basin mouth, out-basin distance (y_{Ba}) is measured from the valley centerline, up-slope distance ($y_{\text{Ba,Em}}$) is measured from the valley floor area, and from-ridge distance (y_{R}) is measured from the basin and sub-basin non-mouth boundaries. These distances could be measured as cumulative planimetric distance or surface-distance, depending on the objectives of the study. This research utilizes planimetric distance for intuitive interpretation set in the x-y plane.

- Basin main branch. Basin analysis is often restricted to only the central or most prominent branch or path from headwall to basin mouth (e.g., Montgomery, 2002; Brook et al., 2005; Anderson et al., 2006; Lin and Oguchi, 2009). The most intuitive way to determine this main branch is to capture discard the areas of all sub-basins except that which maximizes $x_t extBa$ among order $\Omega_{\text{Ba}} - 1$ sub-basins, and recursively repeating for the $\max x_{\text{Ba}}$ sub-basin.

2.4.5.3 Eminence Units

Eminence (Em) units are derived from the Em partition created during the VF unit extraction. Division of the Em partition into distinct Em units was based on the structure of the ridgeline. Each Em unit nucleates from a ridgeline network junction and captures all ridgeline network vertices to the minimum-altitude vertex between it and an adjacent ridgeline network junction. Areas within both the Em partition and a SAD unit are assigned to the Em unit of the nearest ridge-vertex. All other grid cells are assigned to the first Em unit encountered along the path of steepest ascent. All remaining unassigned areas in the Em partition are made into unique Em units and, if they share a boundary with other Em units, are merged with the Em with which they have the least separating boundary. The degree of boundary separation is defined as:

$$\text{sep}_{ij} = I(\text{B}_{ij}) * P(\text{B}_{ij}), \tag{2.2}$$

where B_{ij} is the set of cells adjacent to both Em units i and j, I is the distance between the point of maximum altitude in Em unit i and the point of maximum altitude in B_{ij}, and P is the difference in altitude between those two points. Thus, distal, low-altitude boundaries, or those that maximize isolation and prominence, separate Em units. Eminence order, Ω_{Em}, is inferred from the $\Omega_E m$ of the originating junction vertex. An eminence occupies the area of all lower-Ω_{Em} to which it is connected by the ridge network without crossing ridge-junctions of the same or higher order.

2.4.5.4 Valley Cross-Sectional Profile

Cross-sectional profiles aren't strictly terrain units, but pose interesting terrain unit-related issues that must be addressed within a topographic morphological structural framework. The shape of the cross-sectional or latitudinal valley profile has been recognized as a key indicator of glaciation or bedrock incision (James, 1996; Li et al., 2001; Montgomery, 2002; Prasicek et al., 2014). Valley cross-sectional profile-lines are typically subjectively drawn with the intent to maximize the angles between the profile-line and the orientations of the valley floor (represented by the trim-line, center-line, thalweg, or assumed flow-line) and/or bounding ridge orientation (e.g., Graf, 1970; Li et al., 2001; Montgomery, 2002; Pilotti, 2016), with the implicit goal of maximizing apparent slopes for greater insight into gravity-driven processes. These criteria are only sufficient where valley morphology is simple (Amerson et al., 2008), and beg several questions:

- *Which* valley floor? If the profile-line is confined to a basin, the valley structure of that basin may be complex. A profile-line may cross the valley floor of the main branch of a basin as well as those of tributary valleys of sub-basins, or the basin's main branch may change orientation and its valley floor may consequently cross a profile-line multiple times.

- *Which* ridges? Ridgelines may not be representative of the valley being characterized because they may not represent structures at an appropriate scale, such as those that might bound a sub-basin oriented orthogonal to the valley of interest, or may be discontinuous.

Ba units provide a framework for representing this issue of scale, but there is no theory or mechanism for determining which minimum or maximum hierarchical level, or Ω_{Ba}, of basin is most appropriate.

- What other factors make one potential profile-line more favorable than another for a valley cross-section? Are shorter, higher-relief, steeper profiles more favorable as indications that the profile is not oblique to the valley walls? Are these factors less, as, or more important than orientation relative to the valley floor, ridgeline, or each other?

The procedure employed in this study utilizes the altitude field and VF partition as primary constraints. The profile-line must cross only one contiguous patch of VF and the highest-altitude point between VF-patches along the profile-line indicates a ridge.

Potential profile-lines that pass through a particular sample location (the profile origin) are found by casting rays in opposite directions from the origin to the edges of the second patch of VF encountered by each ray. Ridge-points are marked on the resultant line as the highest-altitude points between VF. The potential profile-line is truncated to the length between two adjacent ridge-points that encompass the profile origin and one patch of VF. Potential profile-lines are collected in 1-degree azimuth steps.

Potential profile-lines are then compared with respect to their relative length, their slope-steepness, the orientation of the VF they cross, and the orientation of the ridges at their bounds.

Relative steepness in this context is defined as:

$$\theta_{\text{slope}} = 1 - \cos\left(\tan^{-1}\left(\frac{|\theta_L| + |\theta_R|}{2}\right)\right), \tag{2.3}$$

where θ_L and θ_R are the linear least-squares regression slope-gradients on the left and right sides of the VF partition in the profile, excluding VF.

Local valley floor azimuthal orientation (φ_{VF}) can be determined by taking the orthogonal of the minimum-length width-line of the local VF partition by casting rays in opposite directions from a sample point to the nearest edges of the valley floor; this study utilizes a 1-degree angular step-

size for this determination. The circular mean of all φ_{VF} intersected by the potential profile-line is obtained by:

$$\bar{\varphi}_{\text{VF}} = \frac{\pi}{2} - \text{atan2}\left(\sum \sin \varphi_{\text{VF}}, \sum \cos \varphi_{\text{VF}}\right). \tag{2.4}$$

Because profile-lines oblique or parallel to the valley orientation tend toward high variability in sampled φ_{VF}, potential profile-lines are favored when φ_{VF} dispersion (r_{VF}) is small:

$$r_{\text{VF}} = \sqrt{\left(\frac{\sum_i^N \cos \varphi_{\text{VF},i}}{N}\right)^2 + \left(\frac{\sum_i^N \sin \varphi_{\text{VF,i}}}{N}\right)^2}. \tag{2.5}$$

All potential profile-lines' bounding ridge-points are organized into a clockwise- or counter-clockwise-ordered series of vertices. Mean ridgeline orientation ($\bar{\varphi}_{\text{R}}$) is approximated as the circular mean ridgeline azimuth (see Eq. 2.4) within 500 m ridgeline-path distance of the potential profile's ridge-point.

The chosen valley cross-sectional profile-line is that which maximizes the function:

$$f_{\text{x-sec}} = \left(1 - \frac{L - L_{\text{min}}}{L_{\text{max}} - L_{\text{min}}}\right) \theta_{\text{slope}} r_{\text{VF}} \sin\left[\Delta^{180^\circ}\left(\varphi_{\text{prof}}, \bar{\varphi}_{\text{VF}}\right)\right] \sin\left[\Delta^{180^\circ}\left(\varphi_{\text{prof}}, \bar{\varphi}_{\text{R}}\right)\right], \tag{2.6}$$

where L is the potential profile-line's length, L_{max} and L_{min} are the maximum and minimum lengths of all potential profile-lines sharing the same origin, Δ^{180° is the circular difference function for 180° intervals, and φ_{prof} is the azimuthal orientation of the potential profile-line.

2.4.6 Process Regime Detection

The generation of diverse LSPs and terrain units are significant components both for exploring the TMS concept and for producing structural information for process-regime detection. That is, LSPs, the properties of terrain units, and the spatial relationships between LSPs and different terrain units are utilized to provide scale-constraints and topographic property information in order to produce process information through process-form relationships depicted in the literature (Fig.

2.4). Process-form relationships are represented by process-form indices and are synthesized via logistic regression modeling to detect glacial and bedrock river incision process regimes at the basin scale. Process-form indices are presented first, followed by the method by which logistic regression models were constructed and trained. It is important to note that the framework presented in this research produces only a minimal set of information for process-regime characterization, and that additional information could also be produced to increase the accuracy, spatial precision, and detail or process-regime characterization.

2.4.6.1 Process-Form Indices

Process-form indices used in this study are intended to highlight whether a basin's morphology is effectively the result of glacial and/or bedrock river incision process regimes. In order to avoid the complexity associated with sub-basin structure, the computation of all indices is constrained to the basin's main branch. Variables involved in the computation of process-form indices were evaluated to reduce multicollinearity in the indices that were used in logistic regression. Surface area (Jenness, 2004) is related to local relief characteristics and genetic processes, but was found to be collinear with both slope angle and skyview factor (Table 2.3) and was therefore not further explored in this study. Process-form indices are presented in Table 2.2. The methods for computing the U- vs. V-shape index and high-altitude erosion-surface index are described here because they are not easily described in a tabular format.

The U- vs. V-shape index compares morphological conditions in a valley cross-sectional profile to both protypical U- and V-shaped profiles, computed as:

$$\text{RMSE}_{\text{U}} = \sqrt{\frac{\sum_i^N \left[z_i - \left(z_t + \frac{z_R - z_t}{(x_R - x_t)^2}(x_i - x_t)^2 \right) \right]^2}{N}}, \tag{2.7}$$

$$\text{RMSE}_{\text{V}} = \sqrt{\frac{\sum_i^N \left[z_i - \left(z_t + \frac{z_R - z_t}{x_R - x_t}(x_i - x_t) \right) \right]^2}{N}}, \tag{2.8}$$

$$\mathrm{UV}^* = 1 - \frac{\mathrm{RMSE_U}}{\mathrm{RMSE_U} + \mathrm{RMSE_V}}, \tag{2.9}$$

where (x_t, z_t) are the profile-distance and altitude of the thalweg and (x_R, z_R) are the profile-distance and altitude of the ridge on the same side of the thalweg as x_i. Note that samples within the valley floor are omitted from this computation. The index is then transformed with a binary sigmoid to increase differentiation between likeness to U- and V-shapes:

$$\mathrm{UV} = \frac{1}{1 + e^{-5(2\mathrm{UV}^* - 1)}}. \tag{2.10}$$

The high-altitude erosion-surface index represents the notion that high-altitude, low-slope, low-curvature surfaces were likely emplaced by past glacial processes.

$$I_{es} = \max(0, \cos(2\theta_t)) \max\left(1, \min\left(0, 1 - \left|\frac{K_{\tan}}{1/dx}\right|\right)\right), \tag{2.11}$$

where dx is the resolution of the DEM, presuming that a prototypical ridge exhibits at least a 45-degree change in slope within the length of one grid cell.

2.4.6.2 Logistic Regression

The indexes indicated in Table 2.2 were utilized in logistic regression to derive a model for detecting glaciation at the basin scale, in the form:

$$\mathrm{P(glacial)} = 1/\left(1 + e^{-\left(\beta_0 + \beta_1 \bar{\theta}_{t,\mathrm{mid}} + \beta_2 \Delta\bar{V}_f + \beta_3 \max w_{\mathrm{VF}} + \beta_4 w_{\mathrm{VF}}/w_{\mathrm{V}} + \beta_5 \mathrm{U\bar{V}} + \beta_6 A_g/A_{\mathrm{VF}} + \beta_7 \max I_{es}\right)}\right), \tag{2.12}$$

where β_0, β_1, ... β_n are regression coefficients. A similar model is used for detecting bedrock river incision, P(fluvial), excluding $\bar{I}_{es}$. Training for both models was performed over 5 million iterations with six basins that exhibit different degrees of glacial and fluvial basin modification, scale, and structural complexity. Specifically, the model was trained on the Pasu (glacial), Baltoro (glacial), Virjerab (glacial), Hurimul (fluvial), Tang-i-Dur (fluvial), and Yarkand South (fluvial)

basins (Fig. 2.5). The small training sample size was intentional as extensive training should be unnecessary with metrics representing highly diagnostic process-form relationships at its simplest scale, and as variations from these end-members ought to manifest in the model's predicted process regime probabilities.

A total of 31 basins (Fig. 2.5), including the training basins, were evaluated using the logistic regression models with accuracy determined as the fraction of correct to total predictions (Fig. 2.5).

2.5 Results

2.5.1 Land-Surface Parameters

The LSPs utilized in this study were useful for generating various terrain units, as they uniquely characterize various topographic properties that are the results of high-magnitude surface processes and erosion-tectonics coupling 2.6. For example, high-magnitude erosion patterns by glacial and bedrock river incision are clearly depicted in Fig. 2.6A. Patterns of relatively low slopes are associated with the valley-floor network, and the spatial extent of low-slope distributions is highly indicative of glacial erosion and river incision. The relatively high magnitude of slope angles associated with basin sidewalls and headwalls clearly indicates the coupling of ersion and uplift throughout the Central Karakoram. More specifically, slope angles range from 0 (horizontal) to 72-degrees, highlighting the incredible rate of altitude gain within portions of the Karakoram range (particularly near K-2). Very high-angle slopes are spatially associated with high-relief ranges in proximity of the Kilik fault, in a swath spanning from Baltoro Glacier and K-2 northwest through the Hunza region. Because the Central Karakoram exhibits such high relief, low slope angle is highly diagnostic of valley floors (Fig. 2.6).

Slope azimuth patterns and the orthogonal orientation structure of basins (Fig. 2.6B) associated with the Karakoram's valley network, much of which is controlled by geologic structure and crustal deformation (Owen, 1989), also depict highly active erosion/uplift dynamics. Though any azimuthal component is important for defining any sort of terrain unit based on slope attitude, it is

particularly effective in parts of the Karakoram where there are relatively long stretches of homogeneous slope azimuth azimuth, potentially caused by long-term erosion or threshold slopes due to uplift-incision-mass movement coupling. It may be possible to define valley hillslopes and headwalls exclusively using slope-azimuth units and a valley-floor partitions due to notable patterns in slope azimuth where basins and eminences overlap. This metric also served as the basis for the computation of slope-azimuth convergence and divergence indices.

The slope-azimuth convergence and divergence indices were effective at highlighting channel- and ridge-forms (Fig. 2.6C. Qualitative interpretation of the land surface is strongly aided but such striking visual representations of the channel-form or drainage cores of basins and convergent glacier margins associated with the thermal dynamics at the ice-bedrock interface and supraglacial meltwater channels. The boundary between high-convergence and high-divergence areas and the rest of the topography is very fuzzy and disjoint along channel- and ridge-forms, however, otherwise basins may have been possibly derived by little more than spatial analysis of these indices.

Tangential and mean curvature did not play a direct role in partitioning the land surface except as comparison to prototypical ridge-like curvature and to define ridge objects as nuclei of eminences. Mean curvature is arguably more successful in this regard, as it was challenging to identify a strong threshold for prototypical "ridge-ness" with tangential curvature whereas mean curvature's interpretation was straight-forward as a simple representation of convexity.

The skyview factor is a proxy for meso-scale relief conditions, and it visually highlights ridges and broad (glaciated) valley floors (Fig. 2.6D). Areas of particularly low skyview factor include narrow V-shaped bedrock at high altitude caused by glacier erosion and uplift. More subtle drops in skyview factor occur where valleys narrow as the geomorphological systems transitions from one process regime to another, such as from glacial to fluvial, or when crossing geologic structures associated with high-magnitude uplift.

2.5.2 Terrain Units

Slope-facet units facilitate visual and computational interpretation of the land surface morphology by reducing slope angle and slope azimuth to a more abstract and manageable form. The

boundaries between slope-facet units are natural and reasonably accurate depictions between shallow and steep slopes and distinct valley walls, which makes them potent assets for representing valley floors and eminences (Fig. 2.7A). The spatial variability in slope-facet unit scale, geometry, and topology appear to occur in distinct spatial patterns, such as large and steep slope-facet units on the slopes of the Shimshal River valley, associated with high-magnitude bedrock river incision and uplift coupling, or smaller clusters of slope-facet units in regions of less pronounced tectonic influence or underlain by weaker sedimentary or metasedimentary rock, such as the region associated with the Yarkand (Raskam) River in the northeast portion of the study area. Some glaciated basins, such as the Momhil Glacier and Pasu Glacier basins, exhibit low slope-angle slope-facet units at high altitudes on the slopes of those basins.

Ridge units are not particularly useful representations of mountain ridges or ridgelines, because of their dependence on multi-scale agreement on local convexity and limitation of overlapping with only the steepest slope-facet units. They do serve well, however, as nuclei for eminences. As such, ridge units are largely intermediate units that serve a computational function more than a strictly geomorphological interpretation function.

Slope-azimuth convergence units and slope-azimuth divergence units also served intermediary roles in this research, the former acting as barriers in the process of mapping eminence regions and the latter as ridgelines that represent eminence organizational structure (Fig. 2.7B). Slope-azimuth convergence units in particular were crucial for producing well-connected, far-reaching valley-floor networks by extending the low-slope concept of valley-floor partitioning with smaller channel-forms. The effectiveness of these units in their intermediary roles indicates their significance as representations of drainages and ridges at a certain scales. They fall short of that ambition, however, because of their fuzzy and scale-dependent nature which produces structures that are spatially disjoint.

The modified skeletonized slope-azimuth divergence unit representation represents the ridgeline network well (Fig. 2.7B). Patterns of preferred orientation and elongation in the ridge-network may indicate tectonic regimes, much like in the valley-floor network. Difference in ridgeline and

ridgeline junction-point density, as well as ridgeline azimuth dispersion, may also be related to differences in lithology due to differences in erodibility, such as the difference in ridgeline structure between the eminence at the bend of the Hunza river west of Khupgar and the the eminences to the north and east of Khupgar. The ridgeline network produced in this study, however, is disjoint at larger scales due in part to the emphasis on a well-connected valley-floor network. Consequently, ridgeline networks are too disjoint to effectively represent eminence hierarchical structure or to serve as boundaries for basin delineation.

Valley-floor units represent a continuous, connected, branching valley network very well, spanning even steep valley floors and non-concave geometries at valley outlets (Fig. 2.8). Dramatic changes in valley-floor orientation and width appear to be associated with geologic structure, particularly evident along the Shaksgam River valley the tributaries to the Shigar River, and even in the Momhil glacier basins. Where valley-floor width abruptly narrows highlights changes in process regime, such as transitions from the wider valley floors of glaciated regions to the narrow bedrock river-incised valleys as is evident in the Baltoro, Batura, Hispar, Momhil, Khurdopin, and numerous other glacierized basins. Furthermore, a profusion of valley side-branching is suggestive of tectonic control (Parvis, 1950; Pereira-Claren et al., 2019), as is apparent in numerous basins throughout the Karakoram, of which the Tang-i-Dur basin is archetypal in this regard.

Basins conform well to the base DEM and form intuitive boundaries between meso- and macroscale conduits of surface-flow (Fig. 2.9A). Low-order basins ($\Omega_{\text{Ba}} < 3$), however, represent small-scale variations in the altitude field that may not have been well-captured in terrain units derived from LSPs produced at the 11x11 computational scale used for this study. Numerous basin characteristics, including elongation, asymmetry, sinuosity, and drainage structure suggest tectonic influence of basin development (e.g., Struth et al., 2017; Wani et al., 2019, 2020). The trio of glaciers north of Kupghar—Ghutuji Yar, Lupghar Yaz, and Momhil—in addition to the Mulungutti, Virjerab, and Khurdopin glaciers to the east, which reside in basins of unusual straightness and length in a zone that appears to be subject to rapid uplift as suggested by these basins' elongate structure and high relief. Basins on the north side of the Kilik and Karakoram faults, by comparison,

tend to be smaller and less elongate, suggesting some combination of relatively less uplift or more erosive lithology that permit processes of erosion to more efficiently reach equilibrium with the land-surface structure. As basin delineation occurs by accumulating area by path of steepest descent, the ridge-boundaries of this study's basins are very similar to those that would be acquired by any other D8 method (e.g., Jenson and Domingue, 1988; Liu et al., 2020), with the greatest difference being that the basins do not drain to single point, but to an arc defined by the buffer around the valley-floor network in the higher-order basin.

Though eminence structure was not specifically evaluated in this study, the partition and hierarchical structure of eminence units (Fig. 2.9B), according to ridgeline-connectivity structure, provides a useful theoretical abstraction for evaluating basin-eminence interactions. They provide, for example, an idea of the spatial density of dissection of the landscape related to erosion and rock-mass distribution related to relief production. Further research is required, however, to create a more definitive and useful eminence structural representation, particularly as it relates to eminence disjointedness and basin overlap (e.g., to represent specific valley-walls, such as the valley headwall).

2.5.3 Process Regime Detection

The coefficients for basin-scale glacial and bedrock river incision process-regime detection are presented in Table 2.4, predicted process regime probabilities are presented in Table 2.5, and the process-form indices for each basin are reported in Table 2.6. The glacial model is 90.32% accurate under the condition that P(glacial) ≥ 0.5 in dominantly glaciated basins and P(fluvial) < 0.5 if the basin does not exhibit strong fluvial characteristics. The bedrock river incision model is 80.65% accurate under the conditions that P(fluvial) ≥ 0.5 in dominantly fluvial basins and P(glacial) < 0.5 if the basin does not exhibit strong glacial characteristics.

2.6 Discussion

2.6.1 Land-Surface Parameters

This research utilized LSPs to represent local aspects of surface morphology, including altitude, slope angle, slope azimuth, convergence, divergence, and mean curvature, which have served primarily to abstract the land surface in specific terrain units that were utilized to represent the spatial topological and hierarchical structure of the topography. Generalization was achieved by using a large computational window for most LSPs, which effectively subdued complex local morphology and errors associated with the original DEM. All higher-level entities utilized in this study (valley floors, ridgelines, basins, and eminences) appear to demand a variable level of generalization in their constituent parameters, as they span a wide range of length-scales. SACI and SADI are particularly effective at capturing drainage and ridge networks but are flawed due to lack of continuity, and it is unclear if a variable-scale approach for computing SACI and SADI would promote better-connected and highly accurate representation of those features. SACI, for example, would not capture the slopes below hanging valleys as part of the drainage network at a divergence range of scales, and the process for obtaining valley-floor units required an alternative method for "bridging" otherwise disjoint portions of the valley floor.

LSPs were also key to glacial and bedrock river incision process regime detection, particularly relief (represented by both altitude and slope angle), tangential curvature, and skyview factor. Patterns of altitude variation in cross-sectional profiles have been utilized for decades as indicators of surface processes that had been active in shaping the land surface (James, 1996; Li et al., 2001; Montgomery, 2002; Montgomery and Brandon, 2002; Brook et al., 2005; Lin and Oguchi, 2009). Skyview factor likewise is a powerful tool for assessing mesoscale relief conditions, indicating regions of high-magnitude erosion-uplift coupling in the Central Karakoram (Fig. 2.6) and differentiating between the more exposed glacier valley surfaces and the more enclosed bedrock river-incised valleys (Bishop and Dobreva, 2017; Bishop and Houser, 2016; Bishop et al., 2018). Tangential curvature was a challenging parameter to utilize, however. Though it provided some

constraint for indicating whether a high-altitude, low-slope surface was ridge-like or not, the proper determination for what constitutes "sufficiently ridge-like" is unclear and likely scale-dependent, and many surfaces that ought to have been de-emphasized by their ridge-ness while searching to characterize high-altitude erosion surfaces were not, or were not unique to basins with predominantly glacial character.

Land-surface parameterization remains a powerful tool for evaluating land-surface dynamics, but required a framework of higher-order terrain units to give those parameters a spatial context to have specific process-related meaning, such as relative altitudinal position within a basin, or within a cross-sectional profile line. Additional parameterization may assist in representing topographic structural context, such as the valley-floor orientation or within-basin distance parameters utilized during this research. Future research should consider how land-surface parameterization might capture higher-order concepts of topographic context and structure, particularly as they relate to surface processes within the boundary conditions of their higher-level structural context (Kocurek and Ewing, 2016).

2.6.2 Terrain Units

The units utilized in this research represent topographic entities that are important to representing topographic morphological structure as it relates to large-scale glacial and bedrock river incision process regime characterization. These units are also only highly basic representations of geomorphological entities, demonstrating that high-level, structural geomorphic investigation is possible with coarsely-defined units with great potential for refinement and expansion. This research also demonstrates that the spatial topological and functional relationships between terrain units require careful thought and significant effort to represent consistently. Though not presented specifically as semantic models, the linkages between entity concepts and computed terrain units are straight-forward and represent a step toward semantic modeling of topographic entities for automated characterization and interpretation of the land surface. One omnipresent issue, however, is that of uncertainty associated with indeterminate boundaries.

Slope-facet unit boundaries are inherently uncertain because they depend strongly on the de-

gree of generalization at which their constituent slope-angle and slope-azimuth parameters were computed and on the statistical, rather than spatial, distribution of those parameters within the arbitrary extent of the region of interest. Consequently, slope-facet unit boundaries vary given a regional subset or overlapping region. Furthermore, different research objectives may also necessitate a different number of slope-steepness classes depending on relief conditions, and there is no inherently compelling reason to divide slope-azimuth classes into some approximation or transformation of the eight cardinal and ordinal directions—that is, twelve directions might serve just as well in a natural system and for research objectives that require more nuanced accounting of slope directionality. A more deterministic model for establishing slope-facet units is warranted. One approach to address this is to utilize curvature units, though these units are not representative of slope attitude and require arbitrary or empirical thresholds to represent planarity (Dikau, 1989; MacMillan and Shary, 2009). The slope units of Alvioli et al. (2020) appear to address the issue of dividing the terrain into homogeneous patches, but these slope units have unclear or nonspecific conceptual-representation.

Curvature units may, however, serve in some capacity as representations of ridges or drainages (e.g., Hooshyar et al., 2016). This study found it useful to separate valley-floor ridge-forms from mountain ridge-forms by identifying areas of convexity at multiple scales to create more disjoint features that could be filtered based on spatial association with steep slope-facet units. The arbitrary scales at which convexity was evaluated for ridge units, as well as the dependency on the empirically-determined boundaries of associated slope-facet units, raise questions regarding what may constitute more suitable representations of eminence-nuclei that account for both convexity and prominence, or what the optimal scale-range is for characterizing these objects for partitioning the land surface into eminences and valley-floors. Additionally, the necessity to fill holes in the ridge-unit classification due to scale-disagreements in local convexity—the same characteristic exploited to produce disjoint ridge-objects—is problematic because hole-filling may omit small, well-enclosed basins and under-represent the valley-floor network. More research is required to identify a more robust representation of mountain ridge-units.

Slope-azimuth convergence units and slope-azimuth divergence units were powerful representations of channel-forms and ridge-forms, respectively, but suffered from disjointedness when a threshold was applied to separate channel- and ridge-forms from "background" topography. The boundaries of slope-azimuth convergence units and slope-azimuth divergence units are fuzzy, their uncertainty stemming from the scale at which slope azimuth was computed and the scale at which the slope-azimuth indices were computed. It may be possible that a scale-adaptive approach may help more properly characterize these units in a more continuous network of convergence and divergent forms, or analysis that takes spatial context of like-forms into account (e.g., Hooshyar et al., 2016). Once continuous networks of slope-azimuth convergence units and slope-azimuth divergence units, or other complete and continuous representations of channel- and ridge-forms, basin extraction and basin- and eminence-structure characterization may be represented in much simpler, complete, and intuitive form. The diversity of "ridge" definitions utilized in this study both emphasizes that different models provide distinct advantages and indicates opportunity for more robust conceptual models and techniques.

The valley-floor units and networks employed in this research are highly accurate based on visual inspection. The valley floor extraction model is structurally based and did not depend on subjective or empirical thresholding of an index that may produce a disjoint valley-floor network (Gallant and Dowling, 2003), the necessity to forcibly remove river sinuosity (Zhao et al., 2019), or even correct the based DEM. The method operates, however, on limiting assumptions that make the exact boundaries of these units conceptually uncertain, though this issue is also inherent in other valley floor extraction algorithms (e.g., Gallant and Dowling, 2003; Zhao et al., 2019). The slope- and convergence-related parameters that define those boundaries are clear within the degree to which slope-facet and slope-azimuth convergence unit boundaries are certain, but whether valley-floors also capture talus piles, alluvial fans, mass wasting deposits, terraces, or other geomorphological features in whole or in part is unclear. For example, the valley floors of this study may include portions of alluvial fans and talus piles while excluding prominent terrace boundaries. The ambiguous forms at the margins of valley-floor units also necessitates "bridging" disjoint

valley-floor units, highlighting the necessity of utilizing spatial context in order to address geomorphic uncertainty and favor valley structure connectivity. That valley-floor network structure was achieved though a skeletonization method that worked to preserve network connectivity, but more research and development is necessary to mitigate manual error correction and to address the concept of "drainage divide" prior to Ba extraction in order to establish proper flow-connectivity in an overly-contiguous valley-floor network.

Different studies may benefit from implementing different models for representing geomorphic entities. For example, a pure flow-conceptualization of basin may prove more valuable for evaluating flux and matter-energy interactions, and so may favor traditional watershed delineation methods and ancillary or *a priori* representations of the drainage structure (e.g., Martz and Garbrecht, 1992, 1993; Liang and Mackay, 2000; Turcotte et al., 2001; Wilson and Bishop, 2013; Liu et al., 2020). Such watersheds were problematic for this study because ridge-to-ridge valley structure is difficult to parse in the lower extents because the lower portions of watersheds are defined by local flow rather than by prominent ridge-structure. This study's basin mouths are the most indeterminate portions of basin boundaries, as the uncertainty of their ridge-boundaries is inherited from DEM error. Smaller-order basins are separated from the basins that they contribute flow to based on the edges of buffers around the valley-floor network (Fig. 2.8). In general, this appears to work quite well, but there lacks a specific structural or functional conceptual model for what constitutes the mouth of a basin within a valley-based, rather than drainage-based, framework.

The boundaries of eminences share boundary uncertainty issues with floor-floor units, and more research is needed to address what types of geomorphic entities are entity-specific, which are valley-floor specific, which indicate a transition between the two, and under what conditions they are interchangeable. Eminence structure also requires more specific conceptualization as to what constitutes "ridge order" when there are no distinct "pour points," and a better mechanism for evaluating eminence structure with nearby but non-adjacent eminence units in order to represent eminence hierarchical structure. Such characterization helps to discriminate between hill, mountain, massif, and ranges to address geodynamic systems in the context of visual prominence,

sedimentary provenance, deflection of atmospheric flow, and orogensis (Fisher and Wood, 1998; Archer and Fowler, 2004; Barros et al., 2006; Deng and Wilson, 2008; Sinha and Mark, 2010), as well as to better character the spatial character of geomorphic dissection as it relates to coupled lithology-climate geodynamics.

2.6.3 Process Regime Detection

The TMS framework explored in this study captures an intuitive representation of the land surface through levels of abstraction up the topographic spatial hierarchy (Fig. 2.3), which is achieved with semantic modeling to generate and query a TMC for systematic field- and object-based process-regime mapping. Results from logistic regression reduction of process-form relationships defined with a TMS framework demonstrate accurate extraction of surface process information encoded in a DEM, generally only accessible by subjective spatial and thematic constraints obtained through human visual interpretation. Our results demonstrate that formalization of conceptual models for TMEs and process-form relationships that address issues of scale and spatial context are suitable for achieving high-level automated geomorphometric analysis.

Accuracy and specificity may be improved through further research and development of the TMS framework utilized in this study, including an expanded accounting of specific, process-related terrain units such as distinct channel-forms (e.g., Hooshyar et al., 2016), flood plains (e.g., Dodov and Foufoula-Georgiou, 2006), terraces (e.g., Trenc et al., 2019), and diverse moraines and other glacial- or fluvial-specific landforms. The terrain units employed in this study should also be refined to approach a more deterministic representation of topographic entities. The process-form indexes employed in this study are generally highly representative of valley and basin structure, though additional representation of process-form relationships would provide additional information for refining process regime detection. The process-form index utilized in this study that requires the most attention is that of characterizing high-altitude glacier erosional surfaces, particularly for sieving out slope facet units on ridge-tops.

Indeterminate boundaries and fuzzy objects can pose a challenge to establishing topological relationships between TMEs, but are useful representations of some TMS-interpreted information, as

the uncertainty or multiplicity of mapped process regimes for a particular area inherently suggests polygenesis (Phillips, 2007). High glacial and bedrock river incision process regime probability in the Hoh Lungma basin, for example, may be manifest in the basin's exhibition of glacial morphology in its higher altitudes as well as bedrock river incision at its lower altitudes (Fig. 2.5; Table 2.5). Alternatively, Momhil Glacier basin is also predicted to have a high probability of exhibiting characteristics of glacial and bedrock river incision process regimes, even though Momhil is a distinctly glacial basin, but one that is occupied by a surge-type glacier and in a region of very high relief production (Fig. 2.2; Kořínková et al., 2014; Bhambri et al., 2017). Consequently, Momhil exhibits characteristics of the "glacial buzzsaw" phenomenon due to coupling of rapid denudation, mass wasting, climate forcing, and tectonic forcing (Mitchell and Montgomery, 2006; Koppes and Montgomery, 2009; Dortch et al., 2011b; Kořínková et al., 2014; Dobreva et al., 2017; Wani et al., 2019, 2020). Thus, though Momhil is a glacial basin, it exhibits characteristics commonly attributed to fluvial processes, which calls into doubt whether valley cross-sectional shape is a characteristic of the corrasive agent or of relative denudation rate. Though this study's logistic regression models achieved about 80% accuracy, very few basins were characterized as both glacial and fluvial.

Additional nuance may be achieved with greater spatial detail in process-regime detection for process-regime mapping. For example, Ba-scale variables might be inherited or re-interpreted based upon spatial or structural context for analysis at the scale of slope-facet units. Properties that are not well-represented in portions of the basin, such as I_{es} and A_g/A_{VF} which are only viable when contained within or without valley-floor units, must be propagated based on relative position within the basin, such as propagating the degree of glacier-valley floor overlap at maximum value to adjacent objects with increasing x_{Ba}, and decay with decreasing x_{Ba}, representing the notion that if a glacial is mapped in a basin, then the basin has been glaciated with high confidence at all altitudes further up-basin and with decreasing confidence down-basin. Even if specific slope facet units might be characterized by only one process regime, their combination within the context of a containing basin or eminence permits characterization of basin polygenetic evolution and inher-

ited forms. Process regime detection may occur at successively finer scales through inheritance of certain properties from higher-order TMEs as boundary conditions, re-interpretation of other properties suitable to the finer scale, and propagation based on structural context.

2.6.4 Topographic Framework For Geodynamic Investigations

This study exhibits a small demonstration of a TMS framework for process-regime detection by representation of topographic properties and entities and their spatial associations. We have already discussed how simple process-regime detection may provide insight into polygenetic evolution and systems coupling. Earlier research has alluded to utilization of TMS frameworks for evaluating coupled systems by representing topographic morphometric entities as sources, links, or sinks in sediment cascades (e.g., Heckmann et al., 2015, 2016) and evaluation of process-form relationships across scales (Phillips, 1988; Kocurek and Ewing, 2016; Phillips, 2016).

Further parameterization of topographic properties, entity properties, spatial topological relationships, and functional geomorphological relationships, in addition to more deterministic and robust models for representing geomorphic concepts, can provide a basis for the development and evaluation of more advanced TMS frameworks for understanding mountain geodynamics. Tectonic and crustal deformation regimes, for example, may be highlighted in features and patterns of TMEs related to orogenesis, faulting, and volcanism, including zones of low skyview factor, high-relief slope-facet units, elongated basin units, a high degree of side-branching in valley and drainage networks, and regions of distinct anisotropic relief patterns (e.g., Bhat et al., 2013; Roy et al., 2016; Gray et al., 2018; Wani et al., 2019, 2020). Coupling between lithologic and climactic regimes may be highlighted by eminence structure, scale-dependent spatial clustering of ridge-junction points, and valley-network structure. Mass wasting process regimes may be highlighted by the spatial density and clustering of slope-azimuth convergence units and slope-azimuth divergence units in proximity to up-slope planar slope-facets and cone-shaped mound features along the perimeters of valley floors.

The workflow employed in this research, specifically the derivation of LSPs, extraction of terrain units, and the derivation of higher-order terrain units from lower-order units and parameters,

was decided based upon an understanding of target process regimes and how they manifest in the topography, established in the geomorphological literature. Decisions on the appropriate computational scale for computing LSPs, and on what terrain units are important for characterizing certain process regimes, must be made in context with scale-dependent geodynamic process-form relationships, understood at a conceptual level and formalized into semantic models. For example, the U- vs. V-shape as diagnostic of glacial erosion, depended on some notion of valley structure—that is, a valley must be defined, how a cross-section is drawn must be defined, and how U-ness or V-ness is determined must be defined. The definition of a valley further depended on concepts related to convergence and convexity in association with steep slope elements, which necessitated definitions for convergence, convexity, and slope at a scale appropriate to general mountain-valley shape. The choice of computational scale, and the extraction of some terrain units, is traditionally based on concepts of homogeneity and heterogeneity (Lucieer and Stein, 2005; Minár and Evans, 2008; Drăguţ and Eisank, 2011; Alvioli et al., 2020), though there exists no clear guidance on what constitutes an appropriate scale for achieving a suitable level of generalization for different applications, or what constitutes a sufficient level of homogeneity. Some more recent research aims to optimize LSP scale based on concepts of homogeneity or fractal self-organization (e.g., Bishop et al., 2012; Newman et al., 2018; Lindsay et al., 2019), but whether such approaches can be made applicable to all geomorphic systems, which span a wide range of scales, is unclear. An automated system capable of parsing a semantic query for "glacial process regime" would then reference a semantic model that incorporates this information. If the components of that model (LSPs, terrain units, process-form relationships) are well-defined and their semantic uncertainty well-characterized, then the uncertainty of the interpretation diminishes, and the application of those lower-order components will become clearer as the geodynamics become better understood.

A TMS framework can also be well-suited for representing the concept of topographic complexity, by capturing variability in metrics of scale (size, shape, orientation), spatial hierarchy (e.g., degree of nesting in higher-order objects), entity or system structure (e.g., valley order), entity spatial topology (e.g., component clustering), spatial density and organization (e.g., spatial

clustering), and diversity of processes that might be interpreted through various aspects of the TMS framework. Much more research is clearly needed to develop and evaluate semantic models and TMS frameworks that can provide us with much more information about the nature of various geomorphological system components.

2.7 Conclusions

The primary objective of this study was to establish and investigate an operational geomorphometric framework for characterizing the spatial organizational structure of mountain topography, motivated by a need to query that structure for process-related information. This objective was met through achieving three sub-objectives:

1. Formalize terrain units. Diverse land-surface parameters (LSPs) were utilized to derive slope-facet units, ridge units, and slope-azimuth convergence and divergence units, which in turn were utilized to derive higher-order terrain units, specifically valley-floor units and networks, ridgeline networks, basin units, and eminence units.

2. Establish a framework for structural characterization of the topographic morphological structure (TMS). This objective was met utilizing a graph-like representation of component LSPs, terrain units, and the spatial topological relationships between them.

3. Explore the use of structural information to represent process-form relationships and characterize glacial and bedrock river incision process regimes. Terrain units provide critical contextual information and spatial constraints for representing specific process-form relationships as process-form indices. The process-form indices were then synthesized via logistic regression modeling to detect glacial and bedrock river incision process regimes at the basin scale for 31 basins in the Central Karakoram at about 80% accuracy.

This research demonstrates the utility of the structural framework approach to assist in remote characterization of the TMS for obtaining process-related information that is presently only accessible through expert qualitative interpretation of the land surface. It also shows that such analysis

is strongly dependent on a considerable foundation of well-defined LSPs, terrain units, spatial topological relationships, and process-form relationships. There is a clear need for more robust methods for deriving LSPs, terrain units, and their relationships to one another that are internally consistent and universally applicable, and which minimize uncertainty. Additional LSPs, terrain units, and process-form relationships will also provide information necessary to improve the detail and accuracy of process-regime detection and other process-related characterizations. Research to develop the TMS framework concept must further aim to characterize process at finer scales, in various environments, for diverse research objectives, and detect other process regimes, including those related to mass wasting, tectonics and crustal deformation, lithology-climate coupling, fluvial corridors, and glacier ice-balance dynamics.

The TMS framework represents the spatial contextual information upon which process inference is dependent, and as such represents an important component of expert knowledge and bears implications for addressing issues of big-data, study replicability, and robotic exploration. As such, the TMS framework may be leveraged to gain a deeper understanding of geodynamics, including topographic complexity, polygenetic evolution, and the coupling of various geodynamic systems (e.g., lithology, tectonics, climate).

2.8 Acknowledgments

We are grateful for the assistance of Da Huo and Zhaohui Chi for theoretical and technical consultation. We thank Ryan Ewing, Lewis Owen, Andrew Klein, and Anthony Filippi for their disciplinary insight. This work was supported by Sandia National Laboratories; and the United States National Park Service; and the Department of Geography at Texas A&M University.

Tables

Table 2.1: Terrain units representing aspects of mountain geodynamics within a topographic morphological structural framework.

Terrain Unit	Symbol	Description	Relevance
Slope-azimuth units	SA	Zones of homogeneous slope azimuth.	Directional component of slope attitude and surface flow. Component of SF.
Slope-steepness units	SS	Zones of homogeneous slope angle.	Vertical component of slope attitude, related to the magnitude of surface processes and erosion-uplift coupling. Component of SF.
Slope-facet units	SF	Zones of homogeneous slope attitude.	Basic unit of local topographic organization, used to partition the land surface into VF and Em.
Ridge units	R	Zones of prominent, multi-scale convexity.	High-confidence locations of non-VF, for initializing VF-Em partition.
Slope-azimuth convergence units	SAC	Zones of high topographic convergence	Drainages and local depressions, for extending VF.
Slope-azimuth divergence units	SAD	Zones of high topographic divergence	Ridges and mounds, for representing ridgelines
Valley-floor units & networks	VF	Contiguous zones of low-slope or high topographic convergence.	Em boundaries and Ba connectivity structure.
Ridgeline networks	-	Skeletonized SAD approximation of ridgelines.	Eminence connectivity structure.
Basin units	Ba	Regions of flow convergence to VF, bounded by ridges	Moisture capture and confinement of gravity-driven surface processes. Principal unit for glacial and fluvial process regime detection.
Eminence units	Em	Conspicuously elevated regions bounded by VF	Orographic moisture capture and deflection. Large-scale Em related to orogenesis. Structure possibly related to climate-lithology interaction.

Table 2.2: Process-form indices representing relationships between topographic morphological structure and glacial and bedrock river incision process regimes. These indexes were computed only by evaluating the basin's main branch.

Symbol	Description	Relevance
$\bar{\theta}_{t,\text{mid}}$	Mean slope angle within the middle-third altitudes of the basin's valley floor.	Glaciated basins tend toward gentler valley floor slopes in their mid-altitudes compared to non-glaciated basins.
$\Delta\bar{V}_f$	Skyview difference index, the difference between mean skyview factor within the middle-third and upper-third altitudes of the basin's valley floor	Glaciated basins tend toward a decrease in skyview factor from high- to mid-altitudes due to the scale over which glacier erosion causes valley shape and relief. This pattern appears less correlated to bedrock river incision valleys.
$\max w_{\text{VF}}$	Maximum valley-floor width.	Glaciated valleys tend to widen at higher altitudes given greater ice mass distribution and fluxes over time, compared to the typically narrow valley floors of bedrock river-incised valleys (Amerson et al., 2008).
$w_{\text{VF}}/w_{\text{V}}$	Mean valley-floor width to valley width ratio, limited to the middle-third altitudes of the basin to avoid complexity in determining valley cross-section profile-lines near the basin headwalls and outlet.	This metric attempts to characterize the scale dependency of glacier erosion in basins which operates at larger scales than fluvial processes.
$\bar{\text{UV}}$	Mean valley U- vs. V-shape index.	Glaciated valleys tend toward U-shaped cross-sectional profiles given erosion dynamics and fluvial bedrock-incised valleys tend toward V-shaped profiles, which is also facilitated by uplift and mass movement coupling (Montgomery, 2002; Montgomery and Brandon, 2002).
A_g/A_{VF}	Fraction of mapped existing glacier occupying the basin's valley floor.	Modern glacierized surfaces are likely to have been shaped to glacier processes. Basins with a predominantly fluvial structure may be fed by glaciers at high altitude that occupy only a small fraction of the basin valley floor.
$\max I_{es}$	Maximum high-altitude erosion-surface index among slope facet units whose centroids lie on eminence slopes within the basin.	High-altitude, low-slope, low-curvature surfaces were likely emplaced during past glaciation.

Table 2.3: Pearson product moment correlation coefficients with variance inflation factor (VIF) shown in parentheses. The compared variables are indicated in Table 2.2, in addition to surface area, SA. Each evaluated sample is an altitude bin in one of Baltoro, Pasu, Virjerab, Hurimul, Tang-i-Dur, or Yarkand South basins. Values are confined to the valley floor and averaged within the altitude bin (except w_{VF}, which takes the maximum within the altitude bin). Bolded values are those that indicate a high degree of collinearity. A separate analysis (*) evaluated each basin separately and then averaged correlation coefficients across basins.

	$\sin\theta_t$	SA	V_f	UV	w_{VF}
SA	**0.8661 (4.00)**				
V_f	-0.8303 (3.22)	**-0.9019 (5.36)**			
UV	-0.6214 (1.63)	-0.7253 (2.11)	0.7723 (2.48)		
w_{VF}	-0.6742 (1.83)	-0.5007 (1.33)	0.6313 (1.66)	0.5313 (1.39)	
$w_{\text{VF}}/w_{\text{V}}$	-0.4893 (1.31)	-0.4901 (1.32)	0.6602 (1.77)	0.8243 (3.12)	0.6670 (1.80)
$SA*$	**0.8645 (4.39)**				
V_f*	-0.6811 (1.69)	-0.7370 (2.05)			
UV*	-0.1969 (1.20)	-0.3231 (1.25)	0.5594 (1.60)		
$w_{\text{VF}}*$	-0.5194 (1.40)	-0.4446 (1.28)	0.5821 (1.62)	0.3990 (1.22)	
$w_{\text{VF}}/w_{\text{V}}*$	-0.1514 (1.22)	-0.2326 (1.18)	0.5094 (1.61)	0.8129 (3.76)	0.5203 (1.51)

Table 2.4: Models for basin-scale glacial and bedrock river incision (fluvial) process regime detection in the Central Karakoram. Parameters are described in Table 2.2. These models were obtained by logistic regression over 5 million iterations, training on six basins exhibiting diverse degrees of glacial and fluvial characteristics.

Coefficient	Paired Parameter	Glacial Model Value	Fluvial Model Value
β_0	Intercept	-29.5528	51.4503
β_1	$\bar{\theta}_{t,\text{mid}}$	-18.6926	23.2574
β_2	$\Delta\bar{V}_f$	8.0630	-6.8316
β_3	$\max w_{\text{VF}}$	13.5618	0.4846
β_4	$w_{\text{VF}}/w_{\text{V}}$	0.0197	-0.0248
β_5	$\bar{\text{UV}}$	1.2604	8.3702
β_6	A_g/A_{VF}	22.5711	12.3267
β_7	$\bar{I}_{es}$	-29.4203	0.0000

Table 2.5: Basin-scale process regime analysis. Ω_{Ba} is the basin hierarchical order, A is basin planimetic area, A_{mb} is the area of the basin's main branch that was analyzed, "Glacial" and "Fluvial" are determinations of process regimes that the basin exhibits based on visual interpretation of the DEM and satellite imagery (X if that class is most characteristics of that basin, ~ if the basin exhibits strong indicators of that class), and P(Glacial) and P(Fluvial) are probabilities of process regime dominance predicted with a logistic regression model trained on the basins indicated with *.

Basin	Ω_{Ba}	A [km^2]	A_{mb} [km^2]	Glacial	Fluvial	P(Glacial)	P(Fluvial)
Baltoro*	6	1424	230	X		1.0000	0.0000
Batura	6	680	178	X		1.0000	0.0000
Biafo	6	834	168	X		1.0000	0.0000
Braldu	6	1254	127	X		1.0000	0.0000
Ghulkin	4	60	28	X		1.0000	0.0000
Hispar	6	1306	214	X		1.0000	0.0000
Lupghar	4	72	48	X		**0.0000**	**1.0000**
Momhil	4	179	92	X		0.8914	**0.8844**
Panmah	6	849	122	X		1.0000	0.0000
Pasu*	4	99	46	X		1.0000	0.0104
Shuijerab	4	137	53	X		**0.0587**	**0.8560**
Skamri	6	1088	143	X		1.0000	0.0000
Virjerab*	5	411	82	X		1.0000	0.0000
Hoh Lungma	6	259	40	X	~	0.9093	0.5536
(unnamed)	6	150	38	X	~	**0.1462**	0.1377
Chot Pert	5	121	24	~	X	0.0000	1.0000
Jaglot	5	181	25	~	X	0.0000	**0.4469**
Jaglot North	5	106	46	~	X	0.9003	**0.0000**
Koktash	5	175	45	~	X	0.0000	1.0000
Phuparash	5	129	47	~	X	0.9354	**0.0104**
Ramghat Pul	4	66	24	~	X	0.0000	1.0000
Sinakar	5	444	78	~	X	0.0000	1.0000
Dorchan	5	124	15		X	0.0000	1.0000
Hurimul*	5	230	43		X	0.0000	1.0000
Shaksgam	5	55	20		X	0.0000	1.0000
Tang-i-Dur*	5	402	63		X	0.0000	0.9899
Yarkand East	4	66	14		X	0.0000	1.0000
Yarkand North	4	58	15		X	0.0000	1.0000
Yarkand South*	4	83	18		X	0.0000	1.0000
Yarkand West	4	49	11		X	0.0000	1.0000
Yarkand upper	4	88	14		X	0.0000	1.0000

Table 2.6: Basin-scale process regime analysis. "Regime" is the determination of process regimes that the basin exhibits based on visual interpretation of the DEM and satellite imagery: "G" if glacial is most characteristics of the basin's morphology, "g" if the basin exhibits strong glacial indicators, "F" if fluvial is most characteristic of the basin, "f" if the basin exhibits strong indicators of river incision. The parameters in each column are described in Table 2.2.

Basin (Regime)	$\bar{\theta}_{t,\text{mid}}$	$\Delta\bar{V}_f$	$\max w_{\text{VF}}$	$w_{\text{VF}}/w_{\text{V}}$	$\bar{\text{UV}}$	A_g/A_{VF}	$\max I_{es}$
Baltoro (G)	0.0698	0.0728	7770	0.6356	0.8242	0.8443	0.9994
Batura (G)	0.0988	0.0341	4700	0.4720	0.8413	0.9240	0.9994
Biafo (G)	0.0607	0.1807	5983	0.7068	0.7989	0.9246	0.9999
Braldu (G)	0.1795	-0.0366	3398	0.4600	0.6610	0.0000	0.9997
Ghulkin (G)	0.3287	-0.0353	2731	0.2802	0.4237	0.8440	0.9994
Hispar (G)	0.0826	0.0527	4834	0.5561	0.8534	0.7861	0.9992
Lupghar (G)	0.1482	0.1552	1519	0.2714	0.7533	0.6081	0.9994
Momhil (G)	0.1617	0.0167	1836	0.3431	0.6320	0.8706	0.9994
Panmah (G)	0.0720	0.0787	3807	0.5330	0.8285	0.7772	0.9995
Pasu (G)	0.1169	0.0451	2089	0.4686	0.8187	0.8884	0.9994
Shuijerab (G)	0.1744	-0.0059	2156	0.4359	0.7075	0.3504	0.9969
Skamri (G)	0.0946	0.0094	3661	0.6047	0.8347	0.6080	0.9995
Virjerab (G)	0.0968	0.0229	4060	0.4959	0.7780	0.7609	0.9995
Hoh Lungma (G)	0.1505	0.0206	2117	0.5291	0.7533	0.5608	0.9992
(unnamed) (Gf)	0.2295	-0.0188	2331	0.3514	0.6221	0.3425	0.9993
Chot Pert (gF)	0.3268	-0.0535	1621	0.2863	0.5271	0.1864	0.9921
Jaglot (gF)	0.4145	-0.1470	2617	0.2885	0.2933	0.0000	0.9988
Jaglot North (gF)	0.2138	0.0019	2672	0.2872	0.6166	0.1995	0.9990
Koktash (gF)	0.3190	-0.0754	1853	0.2380	0.3664	0.3899	0.9982
Phuparash (gF)	0.2159	0.0586	2550	0.3541	0.5198	0.3690	0.9981
Ramghat Pul (gF)	0.4339	-0.1979	1440	0.2507	0.1838	0.0000	0.9988
Sinakar (gF)	0.3720	0.0477	1852	0.3118	0.6082	0.3583	0.9990
Dorchan (F)	0.3829	-0.0215	1641	0.1972	0.1425	0.0000	0.9914
Hurimul (F)	0.2539	-0.0178	1116	0.2446	0.3670	0.0038	0.9986
Shaksgam (F)	0.4150	-0.0797	947	0.3012	0.3027	0.0000	0.9995
Tang-i-Dur (F)	0.3056	-0.0927	2154	0.3568	0.3318	0.3538	0.9997
Yarkand East (F)	0.3567	-0.0770	1047	0.4620	0.5692	0.0000	0.9938
Yarkand North (F)	0.3626	-0.0627	810	0.2689	0.2656	0.0000	0.9915
Yarkand South (F)	0.4424	-0.1110	979	0.2402	0.1367	0.0000	0.9997
Yarkand West (F)	0.4292	-0.0971	659	0.3483	0.2535	0.0000	0.9939
Yarkand upper (F)	0.3113	-0.0311	1549	0.5030	0.4479	0.0000	0.9938

Figures

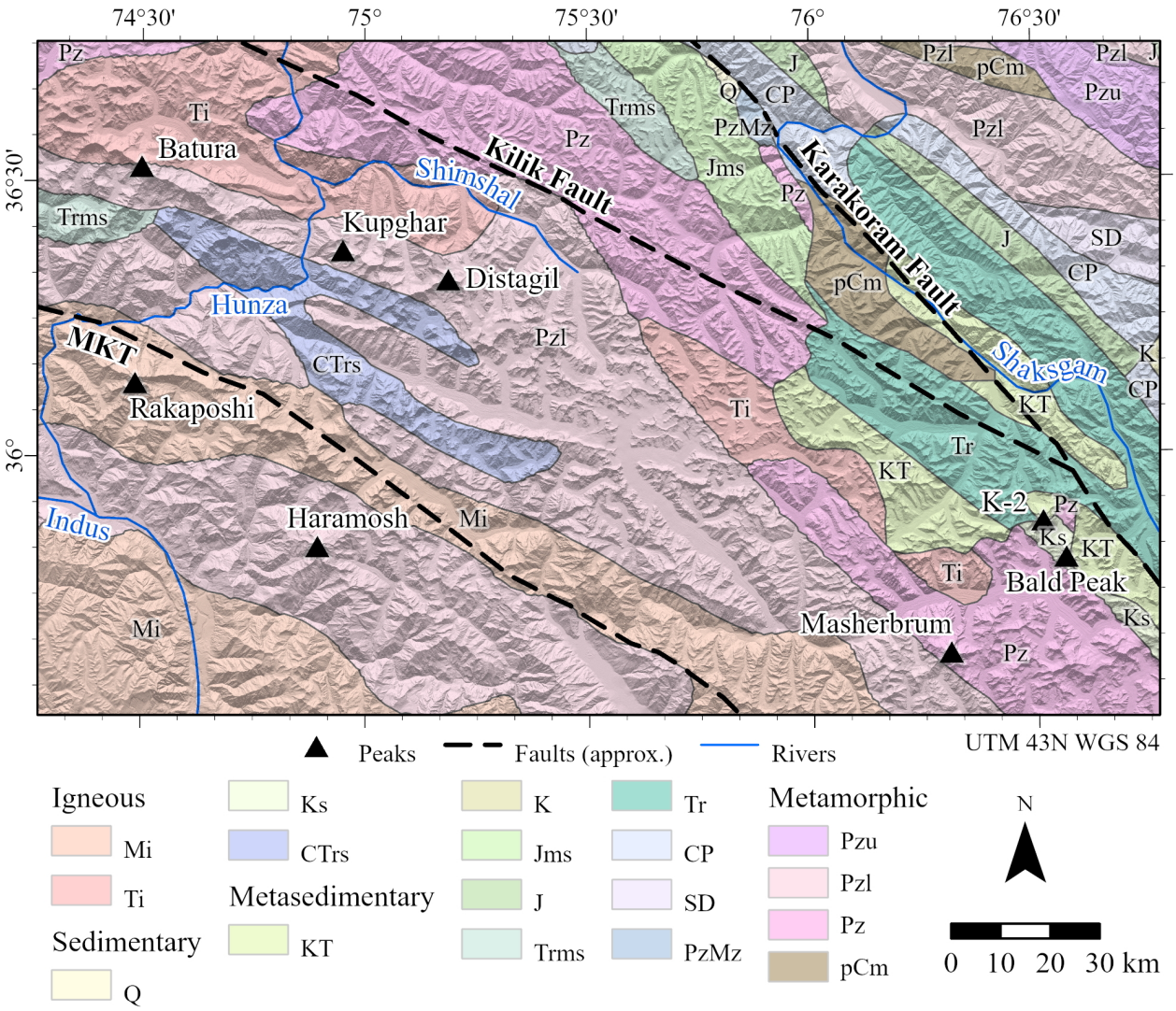

Figure 2.1: Simplified geologic map of the study area in the Central Karakoram, northeastern Pakistan and western China (data sourced or approximated from Wandrey and Law, 1998; Steinshouer et al., 1999; Zanchi and Gaetani, 2011; Mahar et al., 2014), overlaid on a hillshade derived from the SRTM DEM v3 (NASA JPL, 2013). Units are indicated by common symbols for their age, except pC = pre-Cambrian. Rock types are indicated as i = igneous, s = sedimentary, ms = metasedimentary, m = metamorphic, u = upper, and l = lower; all other units are undifferentiated. The line annotated as the Main Karakoram Thrust (MKT) also accommodates the Shyok Suture Zone and (approximately) the Shigar Fault.

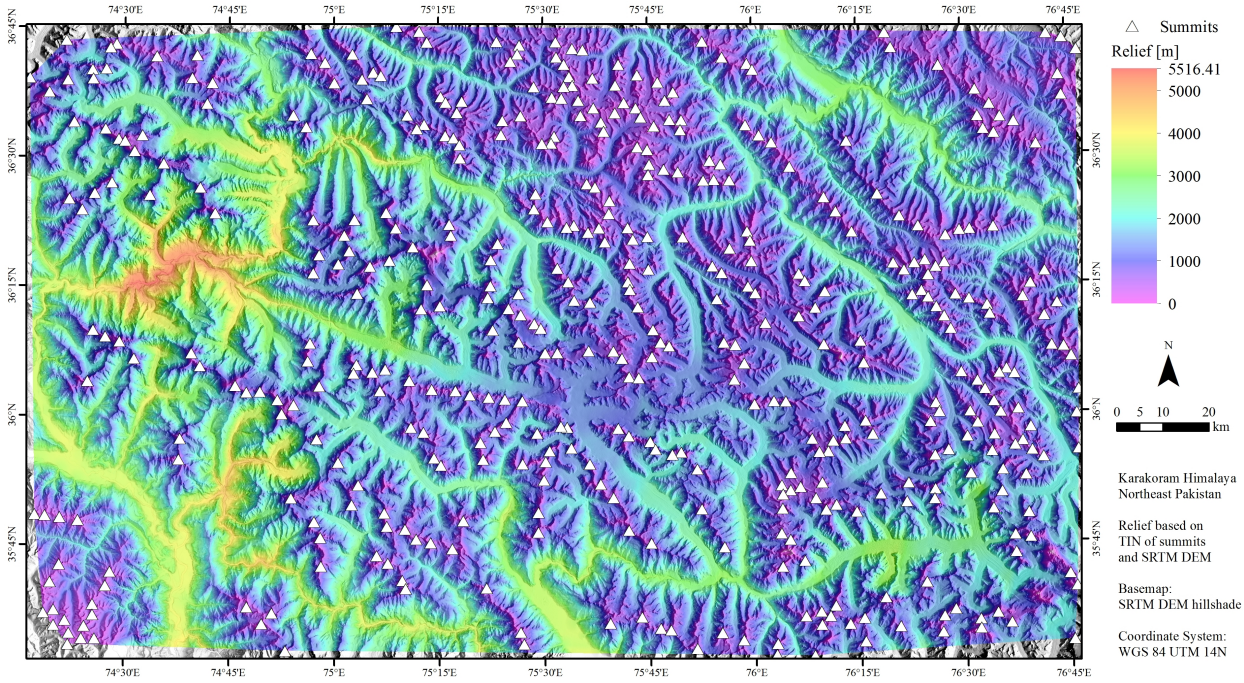

Figure 2.2: Map of minimum relief produced for the Central Karakoram. Relief is estimated as the difference between the SRTM DEM and a TIN surface generated from peaks that represent points of highest altitude within 1.5 km planimetric distance. Note the SW-SE-oriented topographic fabric and very high relief values near Rakaposhi and Haramosh.

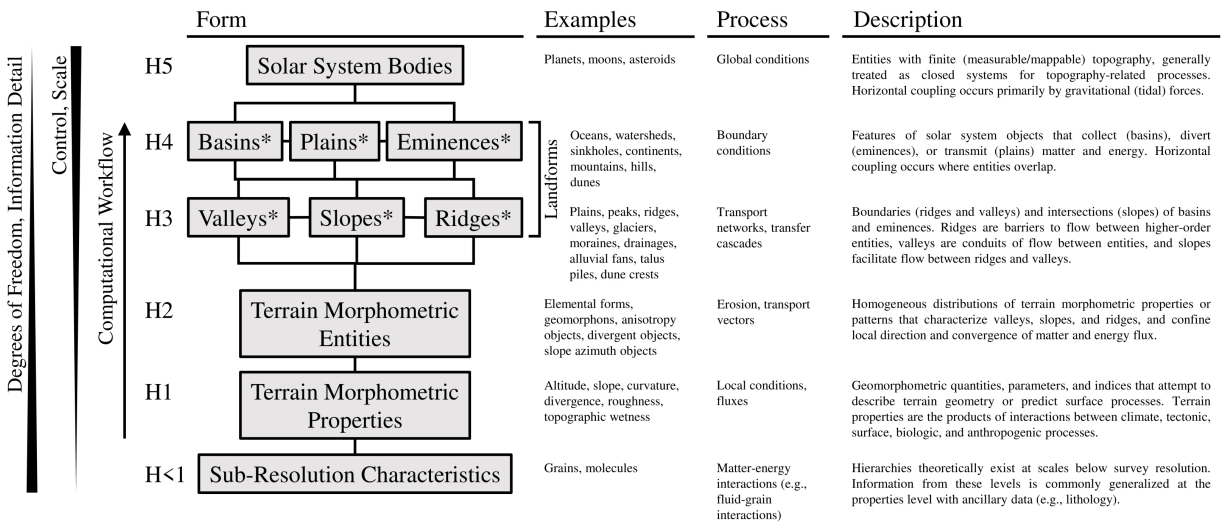

Figure 2.3: The general TMS spatial-hierarchical framework. H1, H2, ..., H5 represent organizational levels in the topographic hierarchy. Some entities (*) may be spatially nested inside an entity that exists at the same or lower hierarchical level but at a larger scale, such as dune eminences (H4) nested within a valley floor (H3).

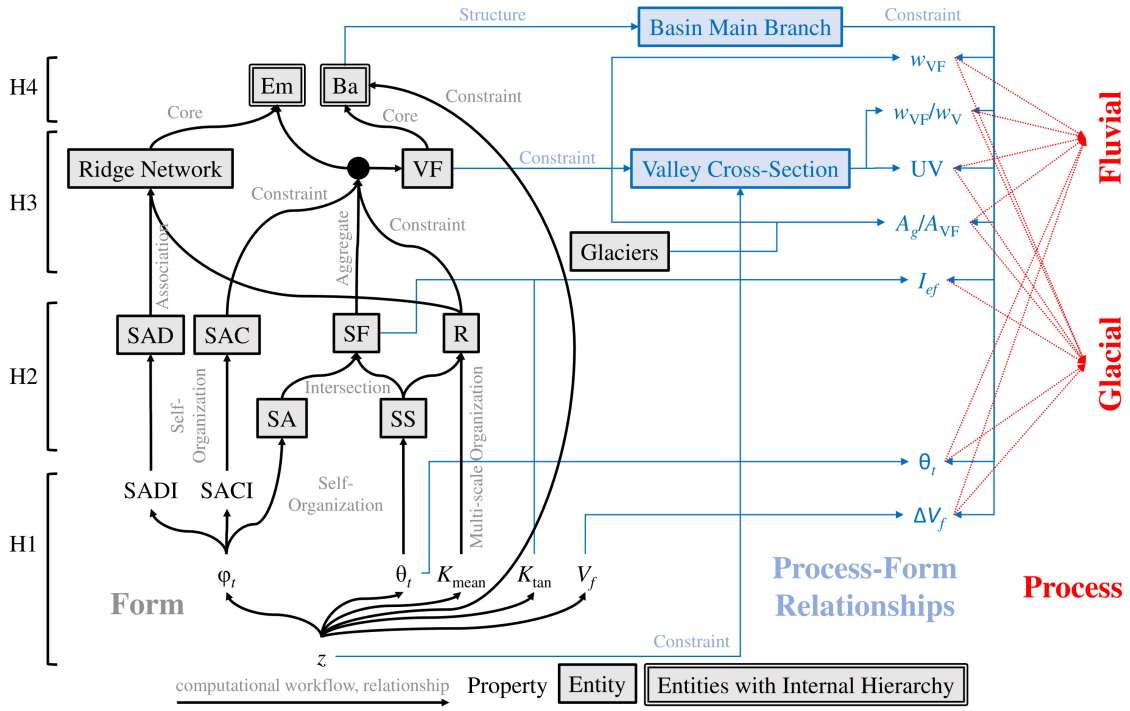

Figure 2.4: The generalized framework, or component of the topographic morphological structure, utilized to detect glacial and bedrock river incision (fluvial) process regimes. Arrows indicate the general workflow utilized in this study. Land-surface parameters are altitude (z), slope azimuth (φ_t), slope angle(θ_t), mean curvature (K_{mean}), tangential curvature (K_{tan}), skyview factor (V_f), slope-azimuth divergence index (SADI), and slope-azimuth convergence index (SACI). Terrain units are slope-azimuth divergence (SAD) units, slope-azimuth convergence (SAC) units, slope-azimuth (SA) units, slope-steepness (SS) units, slope-facet (SF) units, ridge (R) units, the ridge network, the valley floor (VF) network, eminence (Em) units, and basin (Ba) units. The basin main branch and valley cross-sections are utilized to constrain process parameters: valley-floor width (w_{VF}), valley-floor width to valley width ratio ($w_{\text{VF}}/w_{\text{V}}$), U-V valley shape index (UV), fraction of glacierized valley-floor area (A_g/A_{VF}), elevated erosional surface index (I_{es}), mean slope angle θ_t, and a skyview difference index (ΔV_f). The levels H1, H2, H3, and H4 represent hierarchical levels in the overall topographic morphological structure (Fig. 2.3).

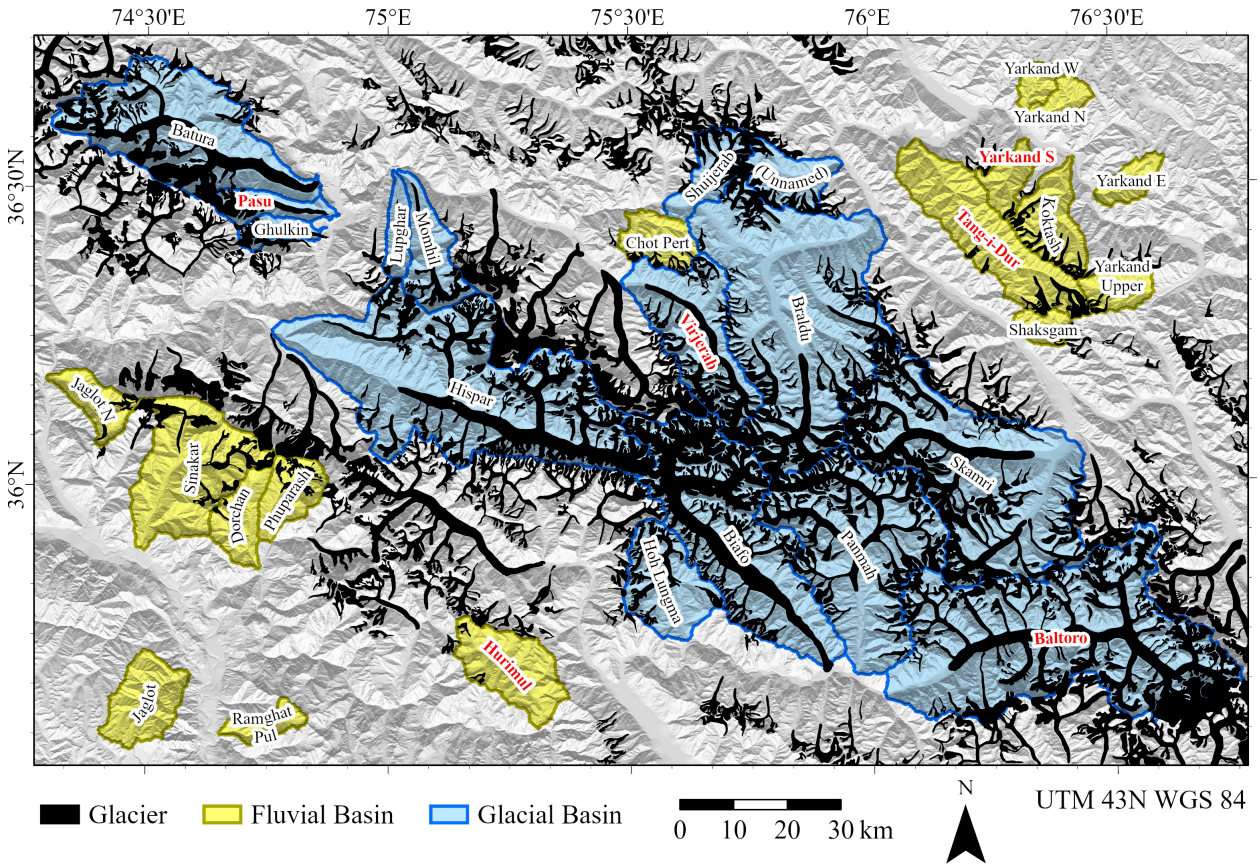

Figure 2.5: Map of basins selected for analysis, with modern glacier extents (Rankl et al., 2014), overlaid on a hillshade derived from the SRTM DEM (NASA JPL, 2013). Basins selected for training logistic regression models have their names depicted in red. Basin names are informal and derived from the names of glaciers, valleys, rivers, towns, or cities associated with or proximal to the basin.

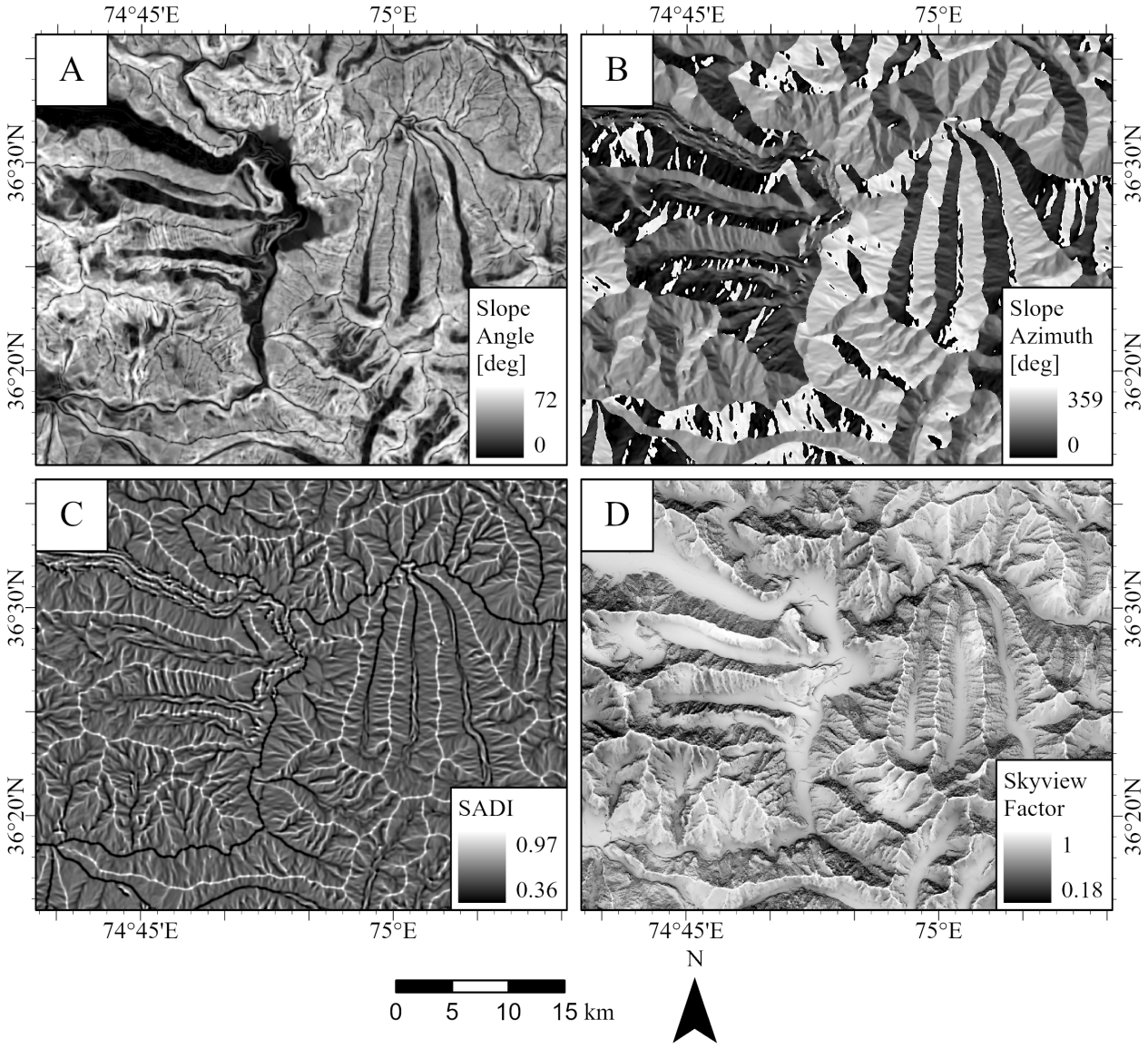

Figure 2.6: Select land-surface parameters at the confluence of the Hunza and Shimshal valleys: (A) Slope angle; (B) Slope azimuth; (C) Slope-azimuth divergence index (SADI); and (D) Skyview factor.

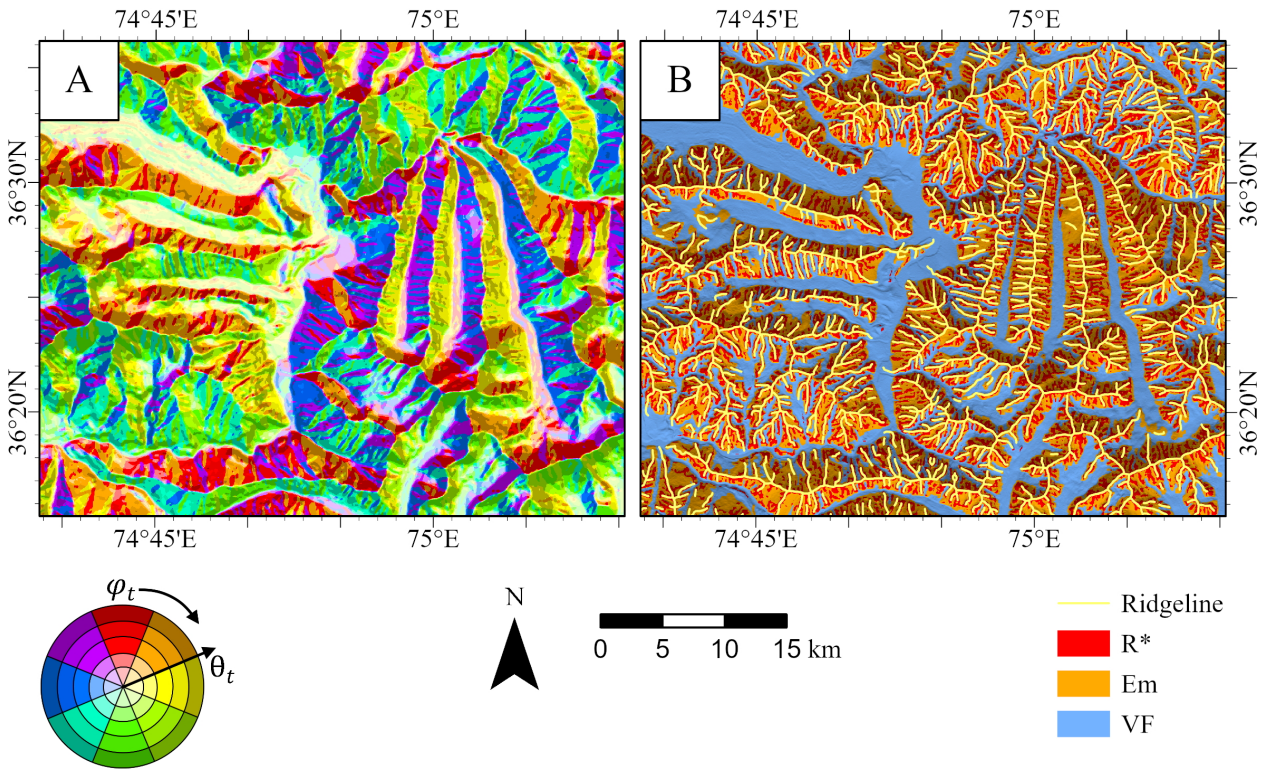

Figure 2.7: Select terrain units at the confluence of the Hunza and Shimshal valleys: (A) Slope-facet units, colored by slope azimuth (φ_t) and slope angle (θ_t); (B) Ridgeline networks drawn over ridge units ∩ slope-azimuth divergence units (R*) and the eminence (Em)-valley floor (VF) partition.

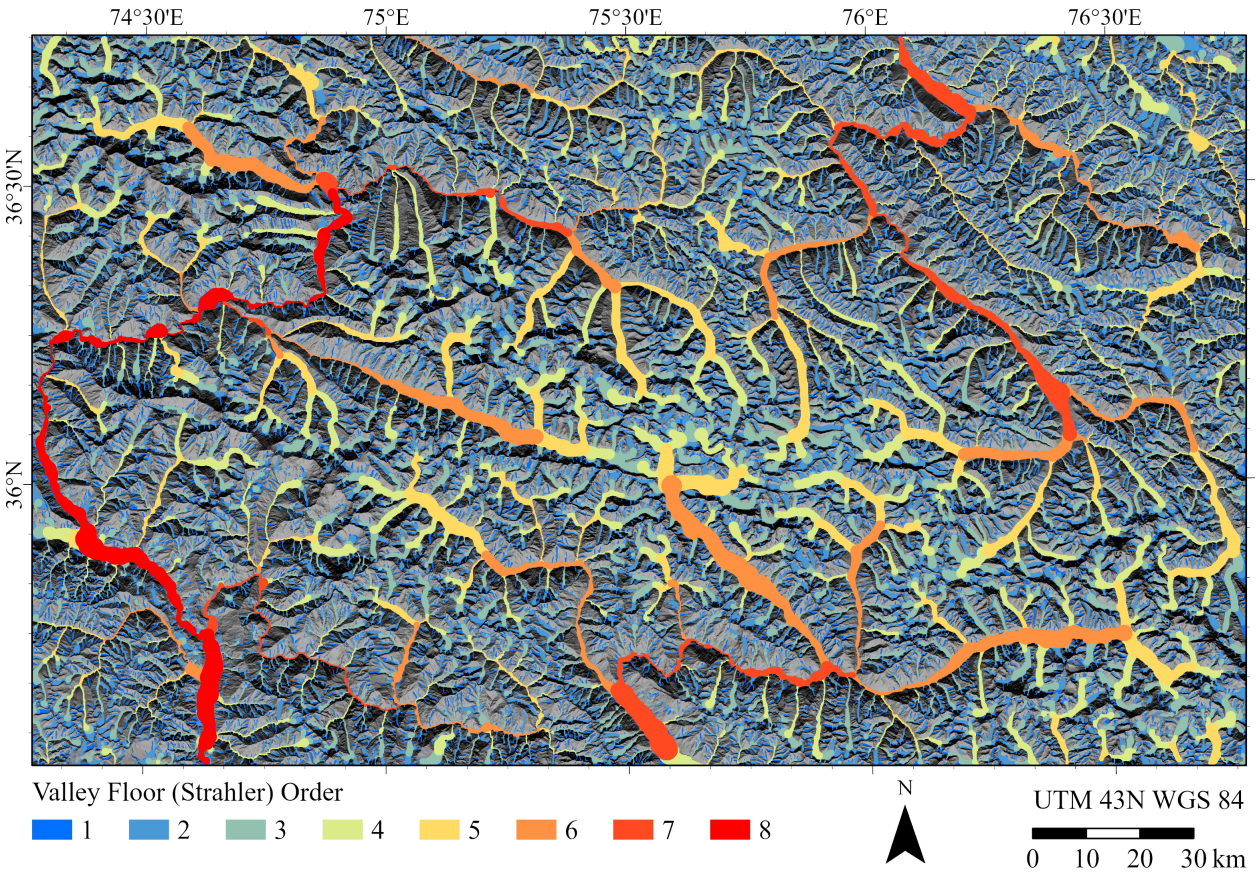

Figure 2.8: Valley floors, with the valley network characterized with Strahler's ordering.

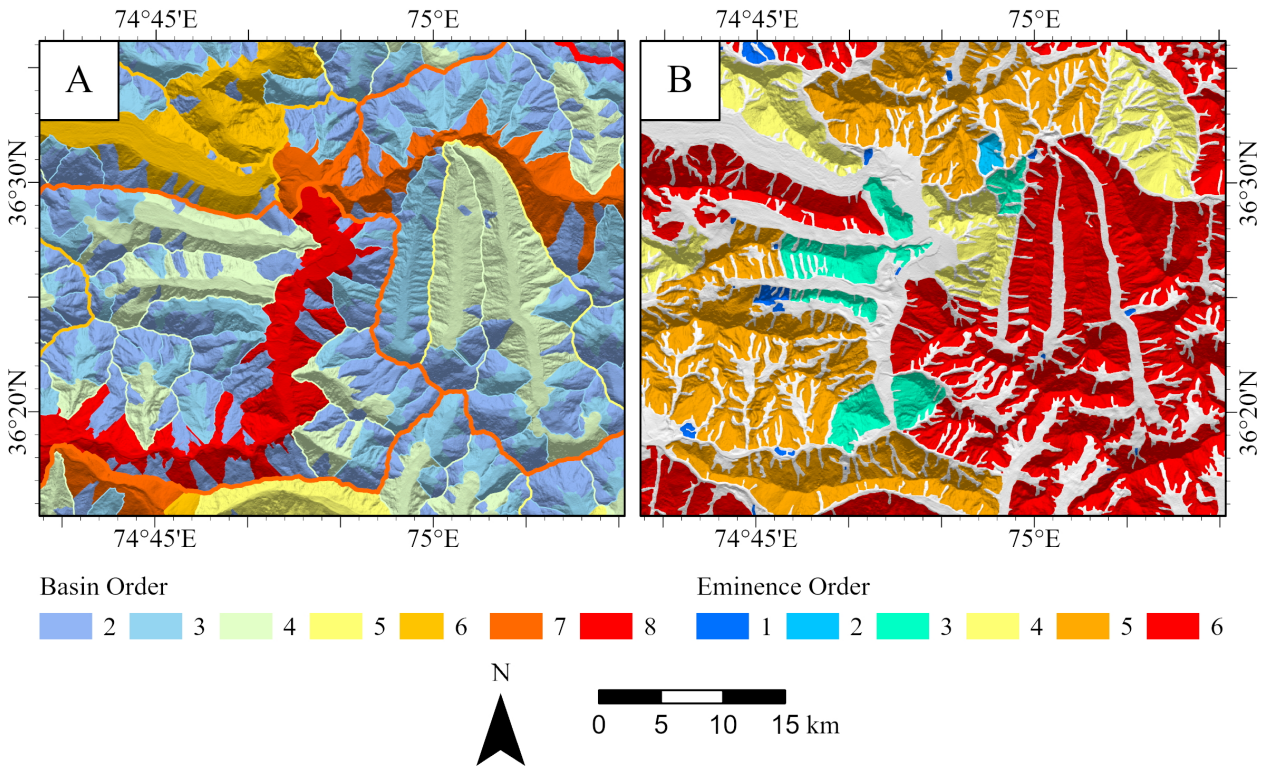

Figure 2.9: Terrain units at the confluence of the Hunza and Shimshal valleys: (A) Basin units, with fill colored by minimum basin hierarchical order and outline colored by maximum basin order; (B) Eminence units, colored by maximum eminence hierarchical order. Note that eminence order is strongly controlled by the connectivity of the ridgeline network and eminence adjacency.

3. UTILIZATION OF TOPOGRAPHIC STRUCTURE AND NETWORK ANALYSIS FOR CHARACTERIZING AND MAPPING GLACIER SURFACE PROCESS-REGIMES ON BALTORO GLACIER IN THE CENTRAL KARAKORAM

Abstract

Geomorphometric process-regime characterization and mapping is notoriously difficult, as diagnostic process-form relationships need to be established, mathematically formalized, and digitally represented. This can be accomplished by identifying variations in process-regimes that exhibit processes that govern surface morphological properties and are associated with specific terrain features with particular spatial topological relationships. This research characterizes process-regimes utilizing a topographic-morphological-structural approach that attempts to capture the spatial contextual information associated with terrain units and their spatial and functional relationships to each other within a graph-like framework. The process-regimes targeted in this research are regimes of glacial downwasting and supraglacial lake development that are characterized by hummocky glacier-surface topography due to heterogeneous ice ablation and sediment load, and regimes of intermoraine drainage and sediment transport that are characterized by well-organized moraine and longitudinal drainages due to glacier-ice flow. We utilize the void-filled SRTM DEM (v3, 30 m) in the area of the Baltoro Glacier, central Karakoram, to derive a slope-azimuth divergence index that serves as the basis for extracting spatially compact depression and mound units that represent components of hummocky topography associated with heterogeneous glacial downwasting, and elongate channel and ridge units that represent moraines and intermoraine drainages. For each grid cell location, we establish unique networks incorporating terrain units appropriate to each target process regime with linkages based on criteria of distance, direction, and flow-paths. We find that network characteristics related to network size, length, and anisotropy are effective for mapping the target process regimes. This simplistic demonstration highlights the potential for representing concepts of spatial context in a mathematical framework for mapping process regimes,

though future research is needed to address issues of scale, semantic uncertainty, criteria for establishing structure-relevant topology, the manifestation of process-form relationships in network structure, and visualization.

3.1 Introduction

The shape and organizational structure of any landscape is a product of complex tectonic and climatic forcing factors and feedbacks that evolve over time, making almost all landscapes a modification of inherited topography and polygenetic evolution (Phillips, 2003, 2007). Process regimes, or zones of dominance for a particular process or family of related processes operating on the land surface, can be recognized by specific landforms and the arrangements of those landforms (i.e., landform associations; Bhat et al., 2013; Prasicek et al., 2014; Lastochkin et al., 2018; Bishop et al., 2020). Such recognition of process regimes is common in geomorphology, as an understanding of what processes have and will operate where is necessary for assessing geohazards, planning and protecting infrastructure, securing water resources, and numerous other applications (Pike, 2000, 2002; Pike et al., 2009; Lastochkin et al., 2018; Bishop et al., 2018, 2020).

The boundaries or spatial extents of process regimes can be challenging to identify, however, though some modeling techniques attempt to capture some elements of process regimes, such as where slope over-steepening may indicate risk of mass wasting (Montgomery, 2001; Montgomery and Brandon, 2002; Gruber et al., 2009; Hewitt, 2009; Hewitt and Liu, 2010). Process-regime characterization and mapping is a notoriously difficult topic in geomorphometry, as diagnostic process-form relationships need to be established, digitally represented, and mathematically formalized (Bishop et al., 2012; Bishop and Houser, 2016; Bishop et al., 2018, 2020). This can be conceptually and computationally accomplished by identifying variations in process-regimes that exhibit processes that govern surface morphological properties, presence of specific terrain features, and the spatial relationships between those features. Mountain topography is particularly well-suited for process-regime mapping due to high relief and well-understood valley structure organized by distinct processes of tectonic uplift, crustal deformation, mass wasting, fluvial incision, and glacial erosion (Owen, 1989; Tomkin and Braun, 2002; Zámolyi et al., 2010; Bhat et al., 2013;

Gray et al., 2018; Wani et al., 2019, 2020).

Glacier surfaces also exhibit land-surface features associated with specific process-regimes. Considering the ablation zones of glaciers, process regimes can include: (1) debris-deposition zones, where englacial, supraglacial, and bed-load transport or deposition of sediment produce a depositionary environment, usually near the terminus; (2) rapid and spatially heterogeneous glacial thinning zones caused by relatively low surface slopes and the presence of supraglacial lakes and ice-cliff retreat, where rapid ablation due to water and transport of sediment causes downwasting (Huo et al., 2021); (3) rapid sediment transport zones in higher altitude areas, where moraines, moraine valleys, and supgraglacial streams rapidly ablate the surface and gravitational sediment fluxes, water runoff and thermal erosion increases relief and rapidly transports sediment to lower altitudes or off glacier at boundaries. These process-regimes overlap, such that the ablation dynamics encapsulate the overlap of these process-regimes, thereby causing polygenetic glacier-surface topographic evolution. Consequently, surface morphometric properties and glacier-surface terrain features are unique and can be linked to specific process-regime conditions.

Computationally, geomorphometry and the use of land-surface parameters can be used to characterize various properties, and object-oriented representation and analysis of land-surface features as terrain units can be used to characterize feature properties. The spatial distribution and topological relationships between land-surface features that are linked with process-regimes can then be characterized using network analysis (Heckmann et al., 2015; Phillips et al., 2015; Bishop et al., 2020). As such, networks of land-surface features are small components of the greater, location-dependent topographic morphological structure, and can provide insight into specific spatially-sensitive aspects of mountain geodynamics, as manifest in the presence and spatial organization of certain land-surface features. By utilizing process-form criteria, we can then mathematically formalize a process-morphological system by defining network architectures suited to capture important elements of a geomorphic system, including topological representation of such concepts as spatial context and association, and utilize network properties to differentiate process-regimes and investigate glacier-surface polygenetic evolution. This represents a significant improvement

in mapping that permits the study of the role of various surface processes in glacier-surface topographic evolution.

Therefore, the main objective of this research is demonstrate the use of a geomorphometric-network framework for characterizing and mapping glacier-surface process regimes on the surface of the large Baltoro Glacier in Pakistan. The specific process-regimes targeted in this research are zones of glacial downwasting and supraglacial lake development (PR-WL), associated with hummocky topography due to heterogeneous ablation dynamics, and zones of intermoraine supraglacial drainage and sediment transport (PR-DT), associated with well-organized lateral and medial moraines. Recognizing that there may be innumerable approaches to addressing the main objective, this study aims only for a conceptual demonstration that is achieved via several sub-objectives:

1. Establish land-surface parameters useful for characterizing the target process-regimes.
2. Extract terrain units from the chosen land-surface parameters that represent key features associated with the target process-regimes.
3. Utilize rudimentary criteria for establishing network architectures that incorporate process-regime-relevant terrain units and topological relationships between those terrain units.
4. Evaluate some basic network properties to roughly map the target-process regimes.

The Baltoro Glacier in the central Karakoram is selected for this study because its size makes it accessible for diverse remote sensing studies, its surface morphology exhibits end-member characteristics of both target process-regimes, and it has been recognized as a relatively stable glacier with no apparent features associated with unstable or atypical ice-flow (Rankl et al., 2014; Huo et al., 2020, 2021).

3.2 Background

3.2.1 Surface Processes and Process-Regimes

Regions of mountainous topography exhibit relatively high-magnitude process rates due to orographic moisture capture and gravitational potential energy which are governed by past or present orogenesis due to tectonic uplift and patterns of landscape evolution that are controlled by lithology, geologic structure, and climate. Mass wasting is prevalent throughout mountainous terrain, which couples with sediment transport along valley floors by moving water or ice, which transport material initially deposited by mass wasting. Glaciers at high altitude feed sediment and water to lower altitudes, and proglacial fluvial systems carve through glacial outwash and glacially-exposed bedrock. Sediment-transport dynamics are affected by these overlapping process-regimes where diverse tectonic, geologic, and climatic systems interact in a complex system of coupled system dynamics and process feedbacks (Phillips, 2003; Bishop et al., 2012; Bishop and Dobreva, 2017). These dynamics alter the morphology of the topography in predictable ways, yielding characteristic landforms, but in spatial scale and arrangements that are specific to conditions both inherited and imposed on the system at the time of formation (Phillips, 2007; Bishop et al., 2010).

The same principles apply to process-regimes that operate at smaller scales than tectonics or climate, though smaller-scale processes are dependent on the larger-scale conditions that define the boundary conditions of the system (Kocurek and Ewing, 2016). The glacier system is impacted by a variety of complex, interacting geodynamic systems, including the lithology of the mountains hosting glaciers, underlying geologic structure that controls the orientation and connectivity structure of glacial valleys, the valley structure that confines surface processes and governs orogenic moisture capture and sediment transport vectors, and climate forcings that control moisture accumulation and mechanical weathering (Archer and Fowler, 2004; Barros et al., 2006; Dobreva et al., 2017; Forsythe et al., 2017). The glacier surface itself is affected by debris from mass wasting that accumulates on the glacier surface and is self-organized into glacial moraines and intermoraine valleys by ice-flow and supraglacial meltwater (Gibson et al., 2017; Huo et al., 2021). The distri-

bution of glacier debris evolves over time with the movement of ice, mass wasting, and ice freeze-thaw, spatially and temporally heterogeneously affecting glacier surface albedo thermal insulation, albedo, and self-shadowing which results in complex patterns of surface ablation, supraglacial ponding and lake development, and supraglacial and englacial drainage (Shukla and Garg, 2019; Huo et al., 2021). Where glacial downwasting is most prevalent and supraglacial lakes and ice cliffs develop, the topography becomes complex and hummocky at the loss of well-defined linear moraine features which are present at higher altitudes. These erosional and depositional systems, driven by glacier-surface dynamics, present an excellent test case for process-regime mapping due to their distinct surface morphology.

3.2.2 Geomorphometry and Spatial Analysis

Geomorphometry is the discipline of numerically characterizing the properties of the land surface. Much of geomorphometry occurs through land-surface parameterization, or representation of the properties of the land surface based on spatial variations in the altitude field, such as slope angle, slope azimuth or aspect, and curvature (Shary et al., 2002; Olaya, 2009). This surface-property aspect of geomorphometry makes it suitable for mapping process-regimes by representing key features associated with those processes in numerical format. Moraines, for example, have high altitude compared to their immediate surroundings and are convex in nature, though other parameters may capture fundamental moraine characteristics, and a number of parameters might represent the hummocky topography associated with supraglacial lake formation, ice-cliff development, and surface debris redistribution in zones of glacial downwasting, including curvature variations, patterns of slope-azimuth variation, or a surface roughness parameter (Mark, 1975; Olaya, 2009; Lindsay et al., 2019).

Land-surface parameterization facilitates objective, empirical, or statistical partitioning of the land surface into distinct objects or terrain units related to a system of interest. The family of techniques utilized to extract and characterize spatial objects is called object-oriented analysis, and generally aims to enhance spatial analysis through abstraction and spatial generalization (Drăguţ and Blaschke, 2006; Minár and Evans, 2008; MacMillan and Shary, 2009; Alvioli et al., 2020). Meth-

ods of extracting objects include thresholding based on certain land-surface parameters (Drăguţ and Blaschke, 2006; MacMillan and Shary, 2009), pattern recognition (including diverse machine learning techniques, Hoeser and Kuenzer, 2020; Xie et al., 2020), spatial patterns (e.g., "geomorphons," Jasiewicz and Stepinski, 2013), representations of scale or homogeneity (e.g., Drăguţ et al., 2010; Drăguţ and Eisank, 2011), and region-growing based on some initial or nucleation conditions (Lucieer and Stein, 2005). Once objects are identified, various metrics can characterize their area, perimeter, shape, relief, and many other properties that might give insight into their nature or distinguish them from other spatial objects, such discriminating a medial moraine on a glacier's surface from an ice- or sediment-mound by the object's shape characteristics, and a supraglacial moraine from a hill or mountain-ridge by its topological relationship to a glacier's area (containment). Topographic features associated with surface processes may be represented as terrain units (topographic spatial objects) within a computational environment, and the properties of these units may then be used to identify and map the glacial process-regimes targeted in this study.

Network analysis is a developing branch of geomorphometry that is concerned with the spatial and functional relationships between structurally significant points or terrain units, largely in analysis of sediment cascades (Heckmann and Schwanghart, 2013; Heckmann et al., 2015), floodplain or catchment connectivity (Dodov and Foufoula-Georgiou, 2006; Barnes et al., 2020), and abstraction of system dynamics and system couplings (Heckmann et al., 2015; Phillips et al., 2015). Network analysis may also be a means of characterizing process-form relationships and, consequently, process-regimes, by providing a framework for evaluating the spatial structure of the surface, particularly by utilizing terrain units as components of that structural framework. The hummocky topography associated with zones of glacial downwasting due to glacier-surface energy-balance feedbacks and sediment redistribution (Huo et al., 2021) has a spatial structure of topographic mounds and depressions that is distinct, for example, from higher-altitude portions of a glacier that tend to be more organized into elongate and curvilinear moraines. Bishop et al. (2020) demonstrate the use of morphometric-object networks on the surface of Baltoro Glacier

as capable of highlighting areas associated with glacier surface processes in comparison with surrounding mountain slopes. This research intends to expand upon the network analysis presented in Bishop et al. (2020), as more research is needed in the area of geomorphometric network analysis (Bishop et al., 2018, 2020).

3.3 Study Area

We conduct our research within the central Karakoram of northeastern Pakistan (Fig. 3.1). The Karakoram is part of the western limb of the Himalayan orogenic belt. It is largely underlain by Oligocene and younger leucogranites, including the Baltoro granite batholith, uplifted to more than 8 km above sea level in some areas (Foster et al., 2010; Searle et al., 2010), in addition to the Mesozoic and Paleozoic phillites, schists, and dolomitic marbles and other carbonates that comprise the Karakoram Metamorphic Complex, which developed over much of the Cenozoic era (Searle et al., 2010; Zanchi and Gaetani, 2011). The Karakoram is notable for its high-altitude peaks, extreme relief, and complex topography, due to high-magnitude erosion and relief production associated with the coupling of atmospheric, surface and tectonic systems (Bishop et al., 2010; Kořínková et al., 2014; Wallis et al., 2016; Dobreva et al., 2017). It also exhibits extensive geohazard potential, as landsliding and valley-dammed and glacial-outburst catastrophic flooding has been documented (Hewitt and Liu, 2010).

The Karakoram is extensively glacierized and exhibits a large number of debris-covered glaciers (Raup et al., 2007; Rankl et al., 2014). Glaciers within the region are highly variable in size, and investigators have documented significant glacial fluctuations over relatively small areas, such that different glaciers span the spectrum of advancing to retreating (Bishop et al., 2014; Rankl et al., 2014; Bhambri et al., 2017; Dobreva et al., 2017). This is significantly different than glaciers further east in the Himalaya that are predominately downwasting and retreating, such that a significant spatial gradient across the Himalaya exists (Archer and Fowler, 2004; Bishop et al., 2014; Rankl et al., 2014; Bhambri et al., 2017). The high degree of spatial variability is thought to be due to variations in climate forcing caused by the Westerlies and the Monsoon, and the collective intersection of these two systems, where the westerlies dominate in the winter and spring, and the

monsoon during the summer (Archer and Fowler, 2004; Dobreva et al., 2017). In addition, the region is known as the "Karakoram Anomaly" (Hewitt, 2005), and investigators have indicated that glaciers within the region exhibit positive ice mass-balance conditions (Zanchi and Gaetani, 2011; Rankl et al., 2014), presumably due to mass loading and the intensification of the Westerlies and/or increased orographic precipitation given the extreme relief and complex topographic structure (Archer and Fowler, 2004; Hewitt, 2005; Dobreva et al., 2017; Forsythe et al., 2017). Furthermore, the region exhibits the highest number of surge-type glaciers in the world, presumably caused by a variety of internal glacier mechanisms and external forcings including mass loading and perhaps tectonics (Copland et al., 2009; Quincey et al., 2011, 2015; Farinotti et al., 2020). Variations in Karakoram glacier dynamics are highly spatially heterogeneous in terms of ablation rates, mass balance, velocity, and state (Hewitt, 2005; Rankl et al., 2014). The unique topographic conditions and variations in climate forcing and processes within the Karakoram make it ideal for exploring the relationships between topographic structure and climate-glacier dynamics, including assessing glacier state and surface processes, as well as estimating components of the glacier erosion system and denudation that governs mountain geodynamics.

Specifically, we focus on the Baltoro Glacier (Fig. 3.1). The Baltoro and other glaciers of the Karakoram are the largest and longest in the world outside the polar region. Like most of the Himalayan glaciers, Baltoro Glacier is debris-covered. It flows for more than 60 km and is commonly 2 km in width. Moving ice, spatially heterogeneous debris cover, and subtle but complex glacier-surface morphology has a positive feedback relationship with patterns of surface melt due to surface material and morphology interactions with both direct and indirect solar irradiance, including the development of supraglacial lakes which may evolve into supraglacial or englacial drainage conduits, and development of ice cliffs and redistribution of oversteepened mounds of debris (Gibson et al., 2017; Shukla and Garg, 2019; Huo et al., 2020, 2021). At higher altitudes, the Baltoro Glacier exhibits well-organized laterial and medial moraines which are fed by frequent mass wasting events associated with the oversteepened mountain topography of that region (Derbyshire, 1996; Seong et al., 2007, 2009b,a; Bishop et al., 2010; Searle et al., 2010; Shroder

et al., 2011). The distinctive surface morphological characteristics between the upper-altitude, well-organized moraine zone in juxtaposition with the complex hummocky glacier surface morphology of the ablation zone at lower altitudes on a such a large glacier makes the Baltoro Glacier an excellent target to study these phenomena with remotely sensed data.

3.4 Methods

3.4.1 Data

This research targets glacial processes, so glacier footprints are utilized to provide a spatial constraint for analysis. This study utilizes the glacier database of Rankl et al. (2014) due to its relatively high level of accuracy and more conservative glacier boundaries compared to those of the GLIMS database (Raup et al., 2007), as can be seen through comparison with satellite imagery. Only the footprint of the Baltoro Glacier is utilized in this study, which was modified to exclude all tributary glaciers and valleys except the Godwin-Austen Glacier, which is the widest and most prominent of the Baltoro Glacier's tributaries.

The void-filled version 3 of the Shuttle Radar Topography Mission digital elevation model (SRTMv3 DEM, 30 m; NASA JPL, 2013) was utilized to represent the altitude field to serves as the basis for all geomorphometric analysis accomplished in this research. The DEM was searched for local minimal and maxima exhibiting at least a 60 m difference from the mean of the neighboring cells in order to identify potentially erroneous altitude values and then to fill those cells with the means of their neighboring cells—no grid cells meeting or exceeding the 60 m criterion were identified in the targeted Baltoro and Godwin-Austen glacier areas. The DEM was therefore not modified with peak removal, pit filling, or general low-frequency spatial filtering, in order to preserve the complex, small-scale variations that represent glacier surface process-regimes targeted in this study. The DEM was then used to produce land-surface parameters, identify altitude extrema within terrain units, characterize relief, and analyze supraglacial flow-paths.

Satellite imagery was utilized as a basis for interpretation and validation for process-regime mapping. This study utilizes relatively cloud-free visible-to-near-infrared ASTER scenes (NASA

LP DAAC, 2015). Though the ideal is to utilize imagery near the time that the SRTM data were collected in 2000 (NASA JPL, 2013), atmospheric conditions in the Karakoram make it challenging to capture relevant cloud-free imagery. The Baltoro Glacier is relatively stable, however (Rankl et al., 2014), and imagery within several years of the DEM capture date record the same types of features and patterns being characterized via geomorphometry and in approximately the same areas, such as supraglacial lakes at lower altitudes and well-developed moraines at higher altitudes. The scenes utilized for this research were captured 6 October 2003 and 14 August 2004. The 2003 scene includes the easternmost extent of the glacier and required manual color adjustment to see glacier-surface features due to extensive snow cover that caused sensor saturation and bloom.

3.4.2 Land-Surface Parameters

Many land-surface parameters (LSPs) and approaches can be used to characterize diverse aspects of the topography. We utilize a simplistic approach that makes use of the altitude field, slope azimuth, and a prototypical index that characterizes the convergence and divergence patterns of the slope azimuth, which can be used to map features characteristic of hummocky topography and moraine-dominated glacier topography associated with the target process-regimes.

Altitude is the most fundamental LSP utilized in geomorphometry and is represented in the SRTM DEM utilized for this study. Alone, altitude represents spatial variations in rock and ice mass, exposure to certain altitude-controlled climate zones, and flow characterization by local altitude differences (Olaya, 2009). This study exploits altitude to compute other LSPs and define terrain-unit characteristics, including within-unit altitude extrema used as the basis for nodes in network analysis, and for defining flow-paths using the path of steepest descent (Jenson and Domingue, 1988; Koka et al., 2017).

Slope-azimuth attempts to represent the direction of the steepest average facing direction of a slope. Spatial patterns of slope-azimuth are therefore related to surface flow-lines and patterns of flow convergence and divergence. Slope-azimuth is computed in a 3x3 window, for observation of small-scale variations, after the method of Shary et al. (2002), with slope gradients along the x and y axes computed using least squares linear regression.

We characterize divergence and convergence in one metric using the slope-azimuth divergence index (SADI; Bishop et al., 2020):

$$SADI = 1.0 - \frac{\sum_{i=1}^{n} |\,(\cos\varphi_i - \cos\varphi_{i,p})\,| + |\,(\sin\varphi_i - \sin\varphi_{i,p})\,|}{(n-1)\,4}, \tag{3.1}$$

where φ_i represents the slope azimuth of grid cell i, and $\varphi_{i,p}$ represents the prototypical divergent direction from the origin of the computation window toward cell i, n represents the total number of grid cells in a window (excluding the center cell), and the denominator is a normalization factor based upon the window size and the maximum numerical difference that could be computed for a grid cell. SADI is computed over a 3x3 window in order to observe small-scale variations. The SADI index theoretically spans the interval [0,1], where larger values highlight debris mounds, ice cliffs, and ridges while low values indicate convergent conditions such as ponds, lakes, channels, and depressions. In practical application, the interval covered by SADI computed at the 3×3 scale is about [0.35,1].

3.4.3 Object-Oriented Analysis

Supraglacial debris loads and gravitational sediment fluxes produce variable debris depths which govern the magnitude of ablation (Gibson et al., 2017; Huo et al., 2021). Differential ablation alters the topography, thereby altering patterns of surface irradiance and subsequent ablation rates in a complex feedback loop (Huo et al., 2021). Meltwater produced by this dynamic flows across the surface, and can collect in supraglacial ponds that can evolve into lakes, which may further evolve or drain via englacial conduits given ice fracturing and the thermal properties of water that accelerate ice melt. The coupled ablation dynamics results in the lowering of the glacier surface due to water-ablation and the expansion of lakes, as water-level ablation undercuts the ice topography resulting in ice calving that generates ice-cliffs that surround many lakes. Ice cliffs rapidly retreat as they exhibit a very thin layer of debris and short-wave and long-wave adjacent terrain irradiance also facilitates rapid retreat given the anisotropic orientation of the ice cliff and its proximity to debris that exhibits relatively high temperatures and reflectivity (Huo et al., 2021).

Collectively, these ablation dynamics generate topographic depressions given past or present water accumulation, and debris mounds that exhibit higher altitudes due to differential ablation, erosion, deposition, ice cliffs, and ridges surrounding lakes and surface-drainage zones (Bishop et al., 2020). Consequently, topographic depressions and mounds may best represent this process-regime, as opposed to more elongate convergent and drainage features, such as moraines and supraglacial channels. This was broadly the approach of Bishop et al. (2020), but without specific indication of the method utilized for object extraction or use of object property constraints (e.g., size, shape) for sieving the set of objects.

This study utilizes object-oriented analysis to represent features associated with process-regimes as terrain units, which are further reduced to nodes for use in networks wherein the spatial arrangement of terrain units can be utilized to infer process-related information. These features can be accurately characterized and mapped using the SADI metric and object-oriented analysis confined to the footprint of the target glaciers. Specifically, terrain units utilized in this study are depression units, mound units, channel units, ridge units, and sink-points.

We utilize simplistic thresholds (0.48 and 0.70, or about two standard deviations about the SADI mean) of convergent and divergent features that favor small, compact features that may represent local depressions and higher-altitude debris mounds or portions of ice cliffs caused by differential ablation. We utilize spatial clumping to generate unique IDs for each depression and mound unit with queen's case contiguity. We then compute various properties that facilitate object sieving in multiple steps to remove objects that do not represent the fundamental features of the system. Specifically, we characterize each unit's size (area), minimum-area bounding box (for the degree of elongation and preliminary measure of orientation), and compactness. The minimum-area bounding box is found by a simple brute-force algorithm that identifies the minimum product of the distances between the nearest and furthest grid cells belonging to that unit in orthogonal directions, searching in 1° increments. Compactness is defined using an object-shape compactness index:

$$C = \frac{4\pi A}{P^2}, \tag{3.2}$$

where A and P are the unit's planimetric area and perimeter, respectively. The shape-compactness index spans the interval (0,1] where a 1 indicates a perfectly circular object. A unit is considered "elongate" in this study if the length of its long-axis is at least twice the length of its short-axis, and "compact" if $C < 0.5$.

Terrain units are then sieved in a series of steps:

1. Units smaller than 5 grid cells are omitted, as they may be structurally insignificant or related to DEM error.

2. Because elongate land-surface features may be discontinuous in terms of SADI-derived terrain units, elongate units are iteratively expanded to include other units in the direction of their bounding box's long axis. For each cell belonging to a divergent unit, a "bridge" is drawn between that cell and all other cells within 200 m belonging to a different divergent unit if the object is either elongate with no more than 30° different in long-axis orientation, or is compact (and its long-axis is therefore irrelevant or unreliable). The same is repeated for convergent units, and a union is made between divergent units and their bridges (except where a convergent unit or bridge exists) and between convergent objects and their bridges (except where a divergent unit or bridge exists). This is repeated until there are no unions to be made. This method of extending elongate objects might be considered its own form of limited network analysis, without the establishment of a formal network structure, by linking terrain units whose topological relationships are defined by rules that represent anisotropic spatial context.

3. Units that are not compact are omitted, as they are not representative of the depressions and mounds targeted for the glacial thinning and supraglacial lake process-regime.

In this way, we identify those terrain features that are the result of heterogeneous debris redistribution, differential ablation, and the evolution of supraglacial lakes associated with glacier

thinning and glacier-surface relief production. Each depression unit's centroid is set to the lowest-altitude location within the unit, and each mound unit's centroid is set to the highest-altitude location within the unit. Depression and mound unit 'centroids' serve as nodes for developing our network architecture for the PR-WL process-regime.

The PR-DT process-regime is more dominant at higher altitudes on relatively large glaciers, such as the Baltoro and Biafo glaciers in the central Karakoram, where relatively high ice-flow velocities, sediment flux, meltwater production, and water drainage produce intermoraine drainage and sediment transport systems that extends along flow-lines down the glacier profile. Surface features associated with PR-DT include parallel moraine-ridges that confine transportation conduits in interrmoraine valleys, which may or may not exhibit a supra-glacial stream, thereby enhancing relief and facilitating sediment and water transport down-glacier and off-glacier near the lateral portions of the glacier surface. The process dynamics associated with PR-DT generate a strong anisotropic fabric exhibiting linear-to-curvalinear moraine-ridges, and similarly-oriented valley bottoms or streams.

We utilize inclusive SADI thresholds (0.54 and 0.65, or about one standard deviation about the mean) to promote spatial continuity in the characterization of relatively linear features that are approximately parallel with the glacier flow-line and ice-flow direction, such as moraines and intermoraine valleys. We utilize spatial clumping to generate unique IDs for each channel and ridge unit, using queen's rule of spatial contiguity, and sieve them according to their area, extend elongate features in the same manner as in the process for deriving depression and mound objects, and finally omit units that are not elongate. For channel units, we identify sink-points, which are locations of the lowest altitude among their neighbors in a 3×3 window, which serve as locations for determining channel unit mean local elongation directions. If a channel unit does not contain a sink, its lowest-altitude location is utilized for this purpose. The local elongation direction is defined as the direction that maximizes the sum length of two rays in opposite directions until each ray encounters a grid cell that does not belong to that terrain unit, checking every 1°. The mean elongation direction of a channel unit is the circular mean of all local elongation directions

evaluated at each sink-point within the unit, weighted by the sum length of rays cast to the edge of the object in the local elongation direction and its opposite, accounting for diametric bimodal azimuthal distribution (opposite directions are treated as equivalent) with the angle-doubling method. The mean elongation direction is comparable to the orientation of the unit's bounding box, but is more sensitive to the unit's structure, whereas the bounding box is more useful for determining the degree of shape elongation. We also identify peak-points for each ridge unit, which are locations of the highest altitude among their neighbors in a 3×3 window, utilizing the maximum-altitude location of the ridge unit if it does not contain any peak-points. Peak-points contained within ridge units serve as a series of network nodes that depict those locations with maximum debris load, which characterizes differential ablation and sediment distribution along the entire length of the moraine.

Some network architectures may wish to incorporate flow characteristics associated with their constituent nodes and establish new nodes where these flow-lines terminate. Flow-line terminations occur both at sinks, which are associated with supraglacial ponds or lakes and moulins, and at the perimeter of the glacier, where flow is assumed to escape the glacier system. It may be advantageous to compute these locations prior to analysis for possible inclusion in networks. Specifically, these are locations of lowest altitude within a 3×3 window and all grid cells outside but adjacent to the glacier within a 3×3 window.

3.4.4 Network Analysis

3.4.4.1 Network Architecture and Process-Regime Characterization

Our approach to network development for all process-regimes consists of defining: (1) a root node, that serves as a starting point for establishing a network; (2) a spatial-topological framework that consists of identifying terrain units and linking them using basic criteria; and (3) computation of network parameters that characterize geometry and scale-dependent characteristics related to process-form relationships that characterize scale and system properties (e.g., connectivity or anisotropy). For all process-regimes, each grid cell on the glacier surface serves as a root node and

has a network associated with it.

For the PR-WL process-regime, we conceptualize that this regime is best represented by its hummocky topography due to spatially heterogeneous downwasting due to meltwater production and glacial surface morphology evolution feedbacks related to spatially heterogenous debris loading that governs spatial patterns of surface irradiance and surface-cover thermal dynamics (Huo et al., 2021). As such, we anticipate a high spatial density of depression and mound units, and short flow-path lengths from mound units to sink-points. A fixed distance is therefore utilized to identify nodes within an area—more nodes within a pre-defined radius indicates the high node density associated with the hummocky topography that is characteristic of this process-regime. The radius utilized for this study is 500 m, which permits a range of network structures to emerge due to spatially-dependent node proximity. The root node is first linked to depression nodes within 500 m of it where the link would not cross the glacier boundary. In this way, the root node is linked to depressions that serve as the lower-altitude base for this process-regime. We then link each depression node to all other depression nodes within 500 m, except where the link would cross the glacier boundary or a mound unit, to enable characterization of spatial density and system anisotropy. Each depression node is then linked to all mound nodes within 500 m of it if the link would not cross the glacier boundary, establishing the upper-altitude base for this process-regime. Collectively, this represents the spatial-topological framework of the network.

We then develop the process-morphology topological component of the network. This is accomplished by performing a flow-path analysis from each mound node that has been identified as part of the network, and accounts for the slope-azimuth direction and the deposition of debris and/or water. For each mound unit, we generate flow linkages using the path of steepest descent, constraining flow-paths' initial directions to each grid cell neighboring the mound unit centroid. Flow-path end-nodes are sink-points, which may be located at glacier boundaries or in depressions, convergent drainage pathways, or supraglacial streams. Only the shortest flow-path is retained for each mound-sink pair. This process-morphology linkage exhibits a very different shape and length compared to an euclidean-based linkage, thereby characterizing drainage, connectivity, and depo-

sitional conditions, thereby accounting for the nature of flow characteristics in the local system. Examples of the network architecture for this process-regime are displayed in Figures 3.2A-D.

To generate a network for the PR-DT process-regime, we again make use of a root-network node and spatially search for the nearest channel unit by performing a radial scan in 1° increments to a maximum distance of 500 m. This identifies the channel unit that defines the local orientation of the system. Note that a channel unit can be in between two ridge units, or adjacent to or on the glacier boundary. We search in directions orthogonal to the channel unit's mean elongation direction to search for divergent units that spatially bound the root node and determine if the system is bounded by divergent linear objects. We then connect the root node to each peak-point associated with the ridge unit or units (or ridge-unit centroid, if it contains no peak-points). Peak-point nodes are connected to all other peak-point nodes within the same ridge unit if the link would not cross the glacier boundary. In this way we establish the spatial topological framework for the upper-altitude bounds of the system with linkages that characterize the anisotropic nature of the system.

From each peak-point (or ridge-unit centroid, if it contains no peak-points), we then perform a flow-path analysis in directions orthogonal to the local elongation direction. This ensures that water and sediment flow-paths are orthogonally constrained by the two types of objects. Each flow-path terminates with a sink-node that becomes part of the network architecture. Examples of the network architecture for the PR-DT process-regime is displayed in Figure 3.3A-D.

3.4.4.2 Network Characteristics

Networks designed to encapsulate components of the geomorphological system and their spatial relationships represent frameworks for mathematically representing unique process-form relationships, including relationships that only emerge through spatial context and association. These relationships are explored with metrics representing network characteristics. There are countless characteristics that could be utilized. For a basic demonstration, we employ the following network properties:

- The number of nodes in the network. Networks designed to incorporate terrain units characteristic of a particular process-regime may exhibit a greater number of such related nodes.

- For a network architecture designed around a set scale, the number of nodes can also be broadly captured in more continuous fashion without a network architecture using various types of point-pattern analysis—this study utilizes the cosine-kernel point-intensity analysis (Bishop et al., 2020):

$$D_N = \sum_{i=1}^{n} \frac{1}{r^2} \frac{\pi}{4} \cos\left(\frac{\pi}{2} \frac{d_i}{r}\right), \tag{3.3}$$

  where n is the number of points within the radius of the kernel, r, and d_i is the distance between point i and the kernel origin.

- Mean flow-line length. Highly complex, hummocky topography theoretically tends toward short flow-lengths compared to well-organized, moraine-prevalent glacier surface topography.

- Link-anisotropy, which is represented as the inverse-dispersion of link-azimuths:

$$R = \sqrt{\left(\frac{\sum_{i=1}^{n} \sin \varphi_i}{n}\right)^2 + \left(\frac{\sum_{i=1}^{n} \cos \varphi_i}{n}\right)^2}, \tag{3.4}$$

  where n is the number of links in the sampled population and φ_i is the azimuth-angle of the i^{th} link. The angle-doubling method is used to account for the diametric bimodal distribution of azimuths (opposite directions are treated as equivalent). Link-anisotropy spans the interval [0,1], where 1 is more anisotropic (less dispersed). Highly anisotropic network links describe highly organized, direction-dependent environments, such as moraines and moraine valleys. Isotropy is the inverse of anisotropy.

Many other, more sophisticated network properties could be evaluated, but this research only aims to provide a proof-of-concept of the usage of networks to represent and explore aspects of

topographic structure in the context of process-regime mapping.

As networks were created for each grid cell in the glacier area, network characteristics can be visualized in comparison to LSPs and satellite imagery to determine which are best suited for mapping their respective process-regimes. It must be noted that different network architectures will mean that a particular root node may have limited access to features across the width of the glacier, thus general trends should be considered rather than very specific patterns. For example, the PR-DT process-regime only captures at most two ridge units in specific directions, and network characteristics may therefore display with sharp longitudinal and latitudinal cut-offs where different or no channel and ridge units may be encountered. Some networks may therefore be more suitable for general detection than for precise mapping without additional constraints.

3.5 Results

3.5.1 Land-Surface Parameters

Differences in spatial patterns of slope azimuth are immediately recognizable between the lower Baltoro Glacier (Fig. 3.4A), which is strongly affected by processes of heterogeneous ice ablation, supraglacial lake development, and surface sediment redistribution, in comparison to the upper glacier (Fig. 3.4B), which exhibits a strong anisotropic fabric associated with moraine development controlled by ice flow and supraglacial drainage. The glacier surface exhibits spatial variation in slope-azimuth at a dramatically different scale compared to the adjacent mountain slopes that is the result of glacial ice-surface processes versus the dominance of mass movement on the adjacent terrain.

The spatial patterns of SADI on the glacier surface also exhibits patterns of high-frequency spatial variation of local convergence/divergence slope orientation of the glacier surface in the lower glacier (Fig. 3.4C) compared to the strong anisotropic fabric that is characteristic of ice-flow and moraine development in the upper glacier (Fig. 3.4D). The spatial scale of SADI variation is also distinct between the glacier surface and the surrounding mountain slopes. Glacier margins are notably convergent, exhibiting low SADI values, and these areas exhibit the potential for representing

ice loss, as intermittent streams are found at the glacier boundary and there are thermal differences between ice and bedrock (Seong et al., 2009a; Huo et al., 2020). Depressions and channel-forms are also apparent with low SADI values, and mounds and ridge-forms are highlighted in high SADI values, where each zone of very high or low SADI values has a distinct geometry that facilitates interpretation of the topographic surface, strongly indicating that SADI appropriately characterizes surface features for object-representation of depression, channel, mound, and ridge features.

3.5.2 Terrain Units

Depression and mound units derived from SADI are abundant in areas that exhibit supraglacial lakes and complex surface features related to erosion, deposition, and heterogeneous ice melt (Fig. 3.2A), and at some glacier confluences in the lower-to-mid-glacier (Fig. 3.2B), in comparison to high-altitude locations that exhibit more organized topography in the mid- (Fig. 3.2C) to upper-glacier (Fig. 3.2D). Supraglacial debris is rarely distributed evenly and smoothly, as processes of ice flow, mass wasting, ablation of glacial ice, and intermittent surface runoff redistribute the supraglacial sediment load even in areas that exhibit well-organized glacier surface morphology (Gibson et al., 2017; Huo et al., 2020). Consequently, depression and mound units are common outside regions of high-magnitude downwasting. This may result in some areas outside of high-magnitude ablation zones to appear to have a high density of depression and mound units, potentially confusing object-oriented characterizations of process-regimes, as depicted in this research. The elongate-object extension process should mitigate this confounding factor, however by aggregating "strings" of such features. Future research may wish to pursue a more sophisticated approach for characterizing the spatial structure of glacier topographic features within an object-oriented framework in order to more uniquely characterize less dominant features and patterns and reduce confounding factors in analyses that depend upon semantic modeling of terrain units.

Channel and ridge units extracted from SADI represent their target moraine and intermoraine valley and supraglacial drainage features well. Though the complex spatial patterns of SADI in areas of intense glacial downwasting also yield some ridge and channel units (Fig. 3.3A), these features are generally more developed (more continuous) at the fringes of zones of intense glacial

downwasting (Fig. 3.3B), in the mid-glacier (Fig. 3.3C), and in the upper glacier (Fig. 3.3D). We note that channel and ridge units exhibit spurs, orthogonal to the main trace of each feature, sometimes connecting parallel terrain units. These spurs are common and represent a weakness in utilizing only SADI to represent elongate features. Spurs may be identified and pruned with additional structural analysis of these terrain units, although this was not necessary as our focus was to establish simple linkages to features associated with the system of interest, where more-developed elongate features indicate greater association with the intermoraine and supraglacial drainage process-regime. Such characteristics may, however, introduce uncertainty when using these results to map process-regimes and more sophisticated attempts at network analysis should account for these issues in mapping efforts.

3.5.3 Glacial Downwasting and Supraglacial Lake Regime

High spatial frequencies of depression and mound objects in the lower glacier contribute to networks with larger numbers of nodes and somewhat isotropic linkages in the lower glacier (Fig. 3.2A-B) given the specific fixed-distance criteria utilized in the PR-WL network architecture. Network mound-to-sink flow-lines tend to be short and appear to be predominantly in directions parallel or oblique to the flow-direction of the glacier. Lower-glacier network patterns are distinct from locations on the glacier surface that are dominated by elongate moraines and inter-moraine valleys in the upper glacier, where networks tend to be small and anisotropic, being starved of compact depression and mound units within the predefined search distance (Fig. 3.2C-D). Because flow-lines are dependent upon the presence of both depression and mound units, or locations where there locally exists high-frequency spatial surface variation, the lengths of flow-lines in PR-WL networks appear to be short regardless of process-regime.

The PR-WL network architecture used in this research is hierarchical in nature, such that a root-node connects to a set of nodes, each of which is connected to its own sub-network of nodes. This produces artifacts in the spatial presentation of network characteristics where each grid cell represents the root node of a unique network. In the case of the PR-WL process-regime, these artifacts manifest as overlapping and interfering circles centered on each depression node, since

these represent the first-level network components that a root node will link to based on a fixed distance (Fig. 3.5A). The spatial patterns of these artifacts are not conducive to process-regime mapping with smooth or continuous variation in network properties that could represent a particular process-regimes, but do facilitate mapping by providing insight into what locations on the glacier surface exhibit features that are diagnostically related to specific processes and/or process regime dynamics.

Regardless, the lower glacier is notably highlighted in comparison to the upper glacier by the number of nodes in each network (Fig. 3.5A), confirming that more depression and mound nodes characteristic of the PR-WL process-regime are found within the lower glacier, and thereby differentiates sections of the glacier where these characteristics are less dominant. A more continuous perspective of this network property is obtained with a map of node density using the cosine-kernal for point intensity mapping (Fig. 3.5B).

Other characteristics of various permutations of link-length and network anisotropy have not yielded consistent, convincing results. The isotropy of linkages representing flow-lines, for example (Fig. 3.5C), might be associated with the PR-WL process-regime, as predicted, but lacks the consistency, as well as the spatial coverage that would be desired for mapping purposes, due to accessibility of depression nodes within the fixed radius of any particular grid cell.

3.5.4 Intermoraine Drainage and Sediment Transport Regime

Networks constructed with the PR-DT network architecture exhibit patterns unique to each ridge unit and the root-channel-ridge geometry that governs the inclusion of ridge networks. Networks generally appear to become larger and more complex with increasingly distance up-glacier, with small, short ridges and few peak and sink nodes at lower altitudes (Fig. 3.3A) and very large ridges and associated nodes at middle (Fig. 3.3B-C) or higher altitudes (Fig. 3.3D). The capacity of the PR-DT network architecture to adapt to the scale of features of interest is a notable advantage in the characterization of systems associated with such scale-variant features. The splay of links from the root node to ridge peak-points has no obvious connection to the PR-DT process-regime, though these links are more isotropic if ridges of similar scale bound the root node and more anisotropic

with longer ridge units. The peak-peak links with each ridge unit are distinctly anisotropic except where long ridges pass large bends in the glacier (Fig. 3.3D). Network peak-to-sink flow-lines are notably orthogonal to the ridge structures for a brief distance (up to 250-300 m) before becoming parallel with the ridge and channel units (Fig. 3.3A-C). This flow behavior is predictable, given the initial constraint on initializing these flow-paths to directions perpendicular to the local ridge-unit orientation and the altitude gradient associated with ridge units. More sophisticated approaches might take advantage of these flow-patterns, such that paths that depart from ridge-perpendicular at shorter distances may characterize systems with less prominent moraines, and longer ridge- or channel-parallel portions of flow-lines may indicate more organized systems with fewer features associated with glacial downwasting, such as depressions, supraglacial ponds, or moulins.

The network architecture designed for the PR-DT process-regime is based on anisotropic access to terrain units rather than distance alone, and the spatial distribution of network characteristics is consequently indicative of the presence and geometry of targeted terrain units (Fig. 3.6A). As with PR-WL, the artifacts in this process-regime's network characteristics are not conducive to smooth or continuous process-regime mapping, but give insight into the zones that exhibit topographic features associated with the process-regime. Utilizing a more dynamic scale for identifying moraine features represented as ridge units also yields greater spatial coverage than the fixed-radius approach of the PR-WL networks.

As with PR-WL, the number of nodes in networks designed for the PR-DT process-regime highlights those areas in proximity to the most elongate and complex ridge units (Fig. 3.6A). Notably, this network characteristic highlights zones in the upper glacier where moraines dominate as well as zones in the lower-middle glacier where moraines are still prominent (Fig. 3.1A) and where there is also a small lapse in the hummocky topography associated with glacial downwasting and supraglacial lakes (Fig. 3.5B). The zone within about 10 km of the glacier terminus exhibits very few nodes pertaining to this network architecture, as do areas in the mid-glacier and on the Godwin-Austen Glacier.

Similar patterns are expressed in the mean length of network linkages representing flow-lines

(Fig. 3.5B). Areas with more organized, moraine-dominated topography should exhibit fewer local sinks and, consequently, longer flow-lines, and this appears to be captured in the upper- and mid-glacier areas. Long flow-lines become present again at the glacier terminus where the glacial system transitions to a more robust supraglacial fluvial system and flow-lines terminate at the glacier terminus rather than at more localized sink-points.

The anisotropy of links between ridge-unit peak-points also highlights the middle and upper glacier, as well as the Godwin-Austin glacier (Fig. 3.6C). The lower anisotropy of a portion of the upper glacier is associated with a ridge unit that passes through a ~90° bend in the glacier. This method of measuring anisotropy, though apparently capturing the anisotropic character of these features in many places associated with the PR-DT process-regime, clearly has limitations in zones of non-uniform glacier flow direction, and might be mitigated with adjustments within the context of glacier flow-lines or an inverse-distance weight on the anisotropy analysis.

3.6 Discussion

3.6.1 Land-Surface Parameters and Terrain Units

A persistent challenge in geomorphometric analysis is selecting the ideal or most appropriate scale for conducting terrain analysis, including window sizes for computing geomorphometric parameters and addressing issues of anisotropy (Shary et al., 2005; Bishop et al., 2012; Dobreva et al., 2017; Bishop et al., 2018, 2020). The 3×3 window used to compute slope azimuth and SADI was sufficient for this study, as the features of interest in this study were small-scale, though moraines would most likely be better represented at a scale that achieves greater generalization and greater feature connectivity and continuity (e.g., 5×5-11×11). The issue of window size and level of generalization is an issue that requires more investigation in the context of object-oriented and network analyses (Shary et al., 2005; Bishop et al., 2012; Phillips, 2016; Bishop and Dobreva, 2017; Bishop et al., 2018, 2020). Various investigators have also discussed the issue of characterizing the scale of local homogeneity (e.g., Drăguţ et al., 2010; Drăguţ and Eisank, 2011), but it is not clear when it is appropriate to add this degree of freedom to a field that, at-present,

struggles with developing diagnostic criteria for what constitutes a ridge, peak, valley floor, etc. (Fisher and Wood, 1998; Gallant and Dowling, 2003; Fisher et al., 2005; Deng, 2007; Deng and Wilson, 2008; Sinha and Mark, 2010; Lingua and Noardo, 2015; Hooshyar et al., 2016; Zhao et al., 2019). Clearly, semantic modeling efforts to address property and scale issues are sorely needed. Also regarding scale, some accounting for anisotropy was necessary to connect strings of isolated, divergent mounds to ridges, and strings of isolated, convergent depressions to channels, but moraines and supraglacial channels were still under-represented in this work. Some methods exist to evaluate the scale of homogeneity (Wu et al., 2000; Drăguţ et al., 2010; Smith, 2010), but it is not clear how this concept of sale relates to surface processes and dynamics. Despite these issues of scale, SADI computed at the 3×3 computational scale has facilitated superb representation of depression, mound, channel, and ridge units. The Bishop et al. (2020) networks that utilized SADI-derived objects appear to have been produced with a photogrammetric 15-m resolution DEM, and the 5×5 (75×75 m) generalization utilized for that work attempts to generalize near the 3×3 (90×90 m) scale utilized for this study. The finer-resolution dataset was able to represent features that exist at a higher spatial frequency, and so finer spatial resolutions may be better suited to evaluating the PR-WL process-regime, particularly in a more continuous fashion, if only because depression and mound units would be significantly more numerous. This may pose a problem, however, by complicating and disintegrating elongate objects, perhaps requiring a greater level of spatial generalization for their representation or a form of anisotropy or network analysis to identify which divergent or convergent units are components of larger, elongate features. This entangles issues of computational and representational scale with issues of landscape and landform semantics and ontology, and more semantic modeling in this regard is absolutely required.

The spurs off of elongate objects (Fig. 3.3B-C) highlight a short-coming of thresholding SADI to extract elongate terrain units. Small spurs and ridges flank most ridge-like features, but are generally not recognized as a component of the ridge's or ridge-network's structure, being small and easy to dismiss by a human analyst. In this analysis, they are not problematic because any link to a distinct moraine system serves the purpose of this study's demonstration. However, more

accurate and specific representations of these terrain units may be necessary for other characterizations of the glacial surfaces or the spatial organization of the glacial topography. Arguments may be made as to whether spurs represent an important component to feature spatial structure, such that the body of the terrain unit be filled out to the spurs' extent, or if the spurs ought to be removed, depending on whether the theoretical conceptualization of the research problem favors terrain units that represent channel- or ridge-like features as only their most divergent or convergent components or as fuller bodies, such as where volumetric analysis might be relevant. Because the margins of these features are uncertain, this issue raises an important semantic and ontological dilemma rooted in as-yet unsolved issues of indeterminate boundaries in geomorphology (Fisher and Wood, 1998; Brändli, 1996; Phillips, 1999; Fisher et al., 2005; Deng, 2007; Deng and Wilson, 2008; Bishop et al., 2012, 2020).

3.6.2 Glacial Downwasting and Supraglacial Lake Regime

The PR-WL network architecture designed for this study performs well where node count correctly highlights areas exhibiting supraglacial lakes and a break-down in moraine-dominated topography (compare Fig. 3.5 with satellite imagery in Fig. 3.2). These spatial patterns are also corroborated by field observations (Seong et al., 2009a; Bishop et al., 2010), satellite observations (Gibson et al., 2017), topographic analysis (Fig. 3.4; Bishop et al., 2020), and physics-based modeling of supraglacial meltwater production (Huo et al., 2021).

There are numerous other approaches that can be used to establish and characterize a network of terrain units for the PR-WL process-regime. An exhaustive discussion on all possibilities is neither possible nor productive in the current state of the discipline, but some key insights based upon this work can be clarified. Specifically: (1) the need for more sophisticated approaches in terrain unit extraction and identification; (2) methods for addressing spatial artifacts and uncertainty in network property maps; and (3) additional perspectives on using network architectures in representing geodynamic process-regimes.

The properties shown in Fig. 3.5A-B provide reasonable insight into where hummocky topography exists on the surface of Baltoro Glacier, and they are associated with zones where

supraglacial lakes occur on the glacier surface based on satellite image interpretation (Fig. 3.2A-B). The area at the confluence with the Godwin-Austen Glacier is also highlighted, however, because depressions and mounds are associated with, but not unique to, zones of glacial downwasting and the evolution of supraglacial lakes. The discrimination between ice cliffs and mounds would improve the characterization because of their associated with lakes. Further evaluation of spatial context, such proximity to a tributary glacier and the width or other properties of that tributary, may also help to discriminate between melt-related depressions and mounds and those associated with ice deformation at glacier confluences.

The spatial artifacts depicted in Fig. 3.5A and C do not communicate spatial uncertainty in mapping as clearly as a smoother, more continuous spatial function would. With the methods used in this research, a smooth, continuous field is impossible: A node is either a component of the network or it is not. A link either exists or it does not. A hierarchical network architecture can only exacerbate the issue of the step-wise spatial distribution of network characteristics, as any access to a high-level node immediately grants access to the full body of its sub-network. There may be methods to modulate this: (1) applying a low-frequency filter to the network properties map; (2) introducing weights based, for example, on distance from the root node, depth in the hierarchical network, or some comparison with a terrain unit's shape or orientation characteristics in relation to the root node or geographic point of analysis; (3) allowing for more scale-adaptive linkages, though this may only change the shape of the artifacts (compare Fig. 3.5A with Fig. 3.6A); or (4) discarding the notion of a root node entirely and relying on the more fundamental terrain-unit networks and growing (and attenuating) network properties from these lower-level network locations represented by network nodes, links, or convex hulls. The way toward better representation of spatial uncertainty with terrain-unit networks is unclear based upon this work and needs additional research, as well as the need to define what spatial uncertainty means in the context of spatial associations in relation to a network consisting of spatial entities.

The fixed search-distance utilized to construct networks for the PR-WL process-regime appears to be problematic from two perspectives: First, the fixed distance means that some areas

will simply not contain features of interest. Flow-line isotropy (Fig. 3.5C), or other measure of direction-dependence, may be a highly suitable network characteristic, for example, but it is impossible to say because the distribution of the property is more strongly controlled by the availability of depression-unit nodes in proximity to mound units than by the property itself. This also suggests that more representative features of the process regime should be represented (e.g., ice cliffs). The PR-WL network architecture may be suitable for evaluating the quantity of associated features in a region, but not for evaluating the natural structure of the topographic system. A distance-dependent mask or weight on a better-formed network may be more appropriate for evaluating network node spatial density than an entire network predicated upon that constraint. Second, the fixed distance was arbitrary. Natural systems are commonly distance- and direction-dependent. Attempting to characterize the structure of a natural system without any scale adaptation may explain why only point-density analysis was successful at mapping areas associated with the PR-WL process-regime (Fig. 3.5A), which does not require network representation (Fig. 3.5B). Therefore, networks that entirely rely on fixed scales may be incapable of representing the structure of a natural system unless there is sufficient iteration in radius-searching until a more robust structure emerges. This might have been accomplished with depression and mound units if the hierarchical structure were abandoned and depression- and mound-nodes iteratively searched for their counterparts, to the extent that new nodes could be discovered on the fringes of the network. One iteration from depressions to mounds does not appear to have been sufficient. More research exploring the distance- and direction-scale-dependency in geomorphic systems in warranted.

3.6.3 Intermoraine Drainage and Sediment Transport Regime

The PR-DT process-regime is well-represented with the network architecture designed to represent it and simple network characteristics (Fig. 3.6), and a composite index might be derived that combines node count, flow length, and link anisotropy into a process-regime index suitable for approximate mapping. The highlighted areas appear to correspond well with areas that exhibit distinct medial moraines and associated upper glacier stream channels that are highly characteristic of this process-regime (Figs. 3.1, 3.3; Seong et al., 2009a), even where that structure begins

to break down in the middle and lower glacier and the system transitions to greater dominance of glacier lake-related downwasting (Fig. 3.5A-B).

The Godwin-Austen Glacier was expected to yield a stronger PR-DT-related signal due to its long, straight ridge units. It appears that the rapid ice-flow regime of the Godwin-Austen Glacier may have precluded numerous local peak objects due to less of a debris load that more complex moraine structure might exhibit, which would have served as network nodes. The narrow glacier width and occasional local pits may have also terminated the flow-paths originating from local peaks earlier than seems to have occurred with flow-paths on the upper Baltoro Glacier surface. It may be possible that networks in the lower glacier may exhibit too-high a node count despite being relatively short due to more debris load and greater debris-load variability, which causes differential ablation and, consequently, more moraine peaks. Some accounting for terrain-unit characteristics in addition to network-structure characteristics is warranted. Mapping of the PR-DT process regime may also be improved with a more robust flow characterization that (1) accounts for the initial moraine-perpendicular flow-direction, and (b) is more permissive of overflow through shallow local pits and depressions thereby increasing flow-line length where the topography is more organized.

The spatial artifacts shown throughout Fig. 3.6 are shaped uniquely to the local conditions of accessibility to a channel unit, the orientation of that channel unit, and accessibility to ridge units in directions orthogonal to the long-axis of the channel unit. The near-ubiquity of channel and ridge units provides greater spatial coverage than what a fixed-radius search could provide which, in some instances, yields a more continuous-appearing network property map (Fig. 3.6B). These artifacts, however, do not conform well to mapping robust process-regime boundaries and do not communicate spatial uncertainty well, and numerical methods to account for root-node distance from network components, differences in link-orientation and terrain unit-orientation, and other characteristics may be taken into account to yield a more continuous mapping product.

3.6.4 Geomorphological Mapping

Networks of terrain units serve as representations of components of local topographic structure, which is inherently related to the processes associated to geomorphic features as indicative of past or present processes. Our approach characterizing a geomorphological system has limitations related to scale, semantics, and uncertainty, although our results clearly demonstrate the potential for mathematically tractable geomorphological mapping by representing topographic structure inherent in landform spatial associations. Furthermore, there is notable overlap between the PR-WL and PR-DT results (Figs. 3.5, 3.6), indicating that features associated with different, even end-member process-regimes may be found in locations where the topography is not at equilibrium with respect to only one dominant process-regime, or where a set of processes are not fully dominant. Thus, polygenetic evolution, system instability, and system-couplings may be characterized and mapped with this type of approach using a semantically-defined network of landform associations. Furthermore, this approach permits the encapsulation of process modeling to account for process rate distributions related to feedback mechanisms as characterized by Huo et al. (2021).

The differences between PR-WL and PR-DT networks and associated network characteristics are significant, even though both networks use terrain units based on similar concepts (SADI thresholds and object shape) and similar architectures (a hierarchy of an arbitrary root to terrain units to flow). The two network architectures differ principally on issues of scale. Specifically, the PR-WL network aims to represent systems at small, isotropic scales (Fig. 3.2), and this affected how terrain units were extracted, how they were linked together, and how they were analyzed. The PR-DT network architecture, on the other hand, exaggerates the anisotropy of the system, targeting only well-connected connected, highly elongate objects, and establishing linkages based on orthogonality to unit elongation directions (Fig. 3.3). This was appropriate for this study, because the two process regimes are, in many respects, end-members in terms of system isotropy. Other systems may likewise be characterized by their degree of anisotropy or length-scales, though this is unlikely to be true for all geomorphic systems.

Other process-regimes may be mapped and characterized with a framework that accounts for

topology and spatial context. Surge-type glaciers might be differentiated from non-surge-type glaciers, for example, by identifying surge lobes, moraine sinuosity, or surface signs of ice deformation associated with ice-flow velocity variation (Copland et al., 2009; Grant et al., 2009; Hewitt, 2009; Bhambri et al., 2017), with network architectures and terrain-unit and network properties that capture system sinuosity and surface complexity within context of tributary glaciers, steep slopes, valley depth, and so forth. Such mapping would reduce dependency on a historical precedent for surge activity and permit more accurate and widespread analysis of glacier-related hazards or glacier sensitivity to climate change (Hewitt, 2005, 2009; Huo et al., 2020, 2021). Other geomorphic process-regimes might be assessed through evaluation of ridge, drainage, and basin structures, including tectonic regimes associated with processes of crustal shear and uplift (Perron et al., 2008; Roy et al., 2016; Gray et al., 2018; Pereira-Claren et al., 2019; Wani et al., 2019, 2020; Różycka and Migoń, 2021). For example, crustal deformation is associated with narrow drainage systems in elongate basins (Wani et al., 2019, 2020), curving ridge-lines (Gray et al., 2018), and high relief (Montgomery and Brandon, 2002; Bhat et al., 2013; Bhambri et al., 2017), which features can be represented as terrain units or properties of terrain units and in networks aimed to represent the spatial contextual relationships of such features, including topological relationships (e.g., containment) and scale-dependency relationships (e.g., orthogonality).

We note that it appears that each process regime may be associated with a distinct structure, consisting of different or differently-defined land-surface parameters, terrain units, and spatial linkages. A more generalized network structure may be desirable, however, which attempts to encapsulate all topographic structure and can be analyzed to characterize diverse process regimes as manifest in that structure. That is, to represent not only distinct systems of depressions, mounds, channels, and ridges, but of slope elements, stream networks, valley networks, ridge structures, basins, eminences, and all coincident or related grid cells with their relevant geomorphometric properties, in a complex web of linkages defined by spatial topology, flow, and other spatial or functional relationships, and then to parse that complex graph of terrain elements for information regarding glacial downwasting, glacier surge, acceleration of overland flow, rapid bedrock river-

incision, mass wasting, crustal shear, or numerous other process regimes and indications of coupled systems. Such representation and interpretation of the land surface is multi-dimensional and multi-faceted, and very complex from numerous perspectives, including issues related to scale, semantics, landform ontology, and the geomechanics that govern process-form relationships (Bishop et al., 2012; Bishop and Dobreva, 2017; Bishop et al., 2020). This type of structure may depend on land-surface parameter and terrain unit definitions that are generalized, multi-purpose, and have well-characterized spatial and semantic uncertainty. Each process regime may be manifest in specific structures, which may be represented as components or sub-graphs of the more general graph of terrain elements. The networks generated for this research are examples of such components. A more generalized network approach will, however, help to standardize and normalize this type of analysis for numerous geometric and geodynamic applications, and permit semantic models of process-form relationships to be distinct from the design of the structure itself.

A number of key issues for mapping using network architectures for representing topographic structure and process-form relationships will need to be addressed in future research, however. Key issues identified in this study include:

- Semantic uncertainty of terrain units incorporated into analysis as structurally significant to the system of interest. This study utilized only very simplistic representations of land-surface features, but that simplicity leads to considerable uncertainty in what terrain units may represent. For example, are mounds isolated piles of debris, vestiges of ice in a zone of heterogenous ablation, or slightly more prominent heaps on an otherwise continuous moraine? Are moraines best characterized as elongate, divergent features, or do they also encompass locally non-divergent or convex slopes? An important topic of research is the characterization of the spatial extent and distribution of semantic uncertainty for certain land-surface features, both theoretically and technically, given a set of object-extraction techniques or semantic models. A better characterization of uncertainty, particularly as it relates to a specific technique, will guide the field toward best practices for the most accurate representation of land-surface features, which will reduce the uncertainty associated with any analysis relying

on digital representations of land-surface features.

- Network architectures, including what terrain units are part of the system and what criteria define their topology. This includes issues of scale, such as distance and orientation, which may depend on object or network size, shape, barriers between points, or other properties. Distances need not be euclidean, such that topology may be defined by functional relationships as part of a sediment cascade (Heckmann and Schwanghart, 2013) or viewsheds (Ode et al., 2010), for example. In general, linkages define any one feature's spatial association and context in relation to other features, and may be used for such queries as "is this feature at lower altitude than that feature?" as hummocky topography may exist below an adjacent or nearby planar slope, suggesting landslide, or "is this feature 'surrounded' by these other features" as a crater is suggested by the presence of compact basin surrounded by ridges in addition to its shape characteristics. The rules that define the topology of geomorphic systems requires more research.

- Structural characteristics associated with target phenomena and the spatial uncertainty and "fuzzification" of the analysis for mapping and characterization. Once a system of terrain units is established, how are notable organizational relationships represented mathematically? The use of a root node in this network served as a convenient means for establishing a network at any location, but also introduces linkages that may be irrelevant to the system of interest, unless the network is intended to seek information regarding the topographic structure in relation to that location, such as utilizing a basin's pour-point to define and evaluate its structure (Liang and Mackay, 2000; Wilson et al., 2012; Lastochkin et al., 2018; Liu et al., 2020). Further research is needed to understand how the structure of a system relates to human cognition of the organization of the land surface (e.g., Sinha and Mark, 2010) and process-form relationships, including land-surface connectivity (e.g., Heckmann et al., 2015; Phillips et al., 2015; Cossart and Fressard, 2017; Grauso et al., 2018) and complexity (McDonnell et al., 2007; Ode et al., 2010; Bishop and Dobreva, 2017) as it relates to surface

processes and their operational scales within the context of a location's local and regional geomorphology (Kocurek and Ewing, 2016).

3.7 Conclusions

The objective of this study was to investigate the use of topographic structure and network analysis for mapping glacier-surface process-regimes on the Baltoro Glacier. This has been generally accomplished for the glacial downwasting and supraglacial lake (PR-WL) process-regime that is characterized by hummocky glacier-surface topography due to heterogeneous ablation and sediment redistribution dynamics that give rise to and are accentuated by supraglacial lakes, ice cliffs, and uneven sediment cover in a positive feedback loop (Huo et al., 2020, 2021), and for the inter-moraine drainage and sediment transport (PR-DT) regime that is characterized by a well-organized system of lateral and medial moraines associated with supraglacial streams and inter-moraine valleys.

The hummocky topography of the PR-WL process-regime is represented by compact depression and mound units extracted from a small-scale slope-azimuth divergence index, and the network node density representing depressions and mounds highlights such regions well (Fig. 3.5A-B). The moraine-dominated topography of the PR-DT process-regime is represented by elongate channel and ridge units extracted from the slope-azimuth divergence index, and size, length, and orientation characteristics of network consisting of nodes representing ridge units and drainage patterns are effective at highlighting zones exhibiting the characteristics of the moraine-intermoraine system (Fig. 3.6).

The network representation of topographic spatial structure for characterizing process-form relationships is effective at mapping these process-regimes, and further research may introduce greater methodological sophistication to increase mapping precision and reduce uncertainty. Other process-regimes associated with a particular pattern of spatial organization of land-surface features, such as tectonic shear zones or landslides, are suitable for mapping based on structural criteria. It may be possible to extract specific relative or absolute process-related information from topographic structural networks as well, and presents an opportunity for future research in this

area.

Nevertheless, there are numerous issues that must be addressed to facilitate process-regime mapping. These include:

1. Scale, with respect to land-surface parameters. Land-surface parameters can be computed in numerous ways, with key considerations being the resolution of the dataset and the computational window size used for producing topographic properties. This study used a 90×90 m area to achieve detailed results. Mountain ridges and moraines are notably anisotropic features, however, and land-surface parameters capable of capturing those details may prove useful for more robust mapping of such features, as would research investigating theoretical and technical best-practices in relation to scale.

2. Scale, with respect to networks. The spatial contextual and functional relationships relevant to geomorphic systems and geodynamic process-regimes are commonly constrained by larger-scale conditions, such as ridgelines separating hydrological regimes or drainages and ridgelines confining mass wasting regimes on eminence slopes. We used glacier boundaries as such a constraint in this study. The scale-dependence at smaller scales can be less obvious, however, and depends strongly on the process-form or process-structure relationships being investigated. This study used a fixed scale for PR-WL regimes and a dynamic scale for PR-DT regimes, which dramatically influenced what terrain units could be reached from any given point within the glacier area, as well as the geometries of those networks and how network properties were interpreted spatially. The functional meaning of network links also dramatically depends on their derivation: The PR-WL network links were based on proximity, appropriate for building networks based on terrain unit spatial density, but the PR-DT network linkages were based on direction-dependence and terrain unit containment. Both process regimes evaluated in this study also used flow-lines to establish more functional rather than strictly euclidean relationships, as might be of interest in river networks and sediment cascades (Heckmann and Schwanghart, 2013; Phillips et al., 2015; Heckmann et al., 2015, 2016; Cossart and Fressard, 2017). The rules that govern linkages then affect

what network properties are useful for characterizing a particular process-regime, including whether clustering or interconnectivity is relevant, if network geometry supports evaluation of anisotropy, or if a spatial process-related sequence can be reliably inferred from a network's structure. These issues are nontrivial, and best practices have yet to be established in the context of geomorphic and geodynamic research. Furthermore, representing network properties spatially requires an additional consideration of scale to modulate and interpret spatial variability in network characteristics, including representation of spatial uncertainty associated with those characteristics.

3. Semantic uncertainty. This study utilized depressions, mounds, channels, and ridges as terrain units that represent land-surface features associated with the target process-regimes. Whether a mound was better represented as an extension of ridge, or if ridges should have frequent spurious appendages, challenges assumptions as to what these terrain units actually represent and, consequently, if networks consisting of these terrain units truly give insight into geodynamic systems of interest. More research is needed to develop robust semantic models and characterize semantic uncertainty for diverse land-surface features, in order to make any analysis based upon these features reliable and useful for geomorphometric analysis.

4. Topological criteria. The rules that define the organizational structure of a system are perhaps as important as the rules used to define the components of that system. Some relationships may be best defined by euclidean distance, least-cost paths, or functional relationships. Though a codification of these types of rules may be limiting, some taxonomy or classification of linkage-rule types in relation to their structural meanings would be a valuable contribution to the field for facilitating best-practice network representations of topographic structures.

5. Process-form relationships manifest in network characteristics. The web of interconnected terrain units only has meaning if the structure of the many linkages can be interpreted and

parsed into specific process-form relationships. Spatial organization can be characterized in innumerable ways—distance, direction, and clustering (interconnectivity) are only a few examples, and their relationship to process depends on characteristics of the system of interest, and are worth careful consideration. What it means for a particular geomorphological system to have a high clustering coefficient, or high average degree, or axial dependence on link orientation, or any other characteristic requires further research that must be conducted to focus the exploration of network characteristics to facilitate analyses based on the spatial organization of land-surface features.

A mathematical framework for representing concepts of spatial association, context, and organization between terrain units in mountain environments is a significant evolutionary step in geomorphometry. The process-form relationship is rarely dependent on only the presence of certain land-surface features but also on their process mechanics and organizational patterns, which can be interpreted in context with polygenetic evolution associated with inherited topography and coupled geodynamic systems. A spatial-contextual framework based upon semantic definitions will facilitate automated terrain classification and land-surface interpretation, which should benefit the various scientific disciplines and industries that depend upon robust characterization of the land surface (Pike, 2000, 2002; Pike et al., 2009; Bishop et al., 2012, 2020).

Figures

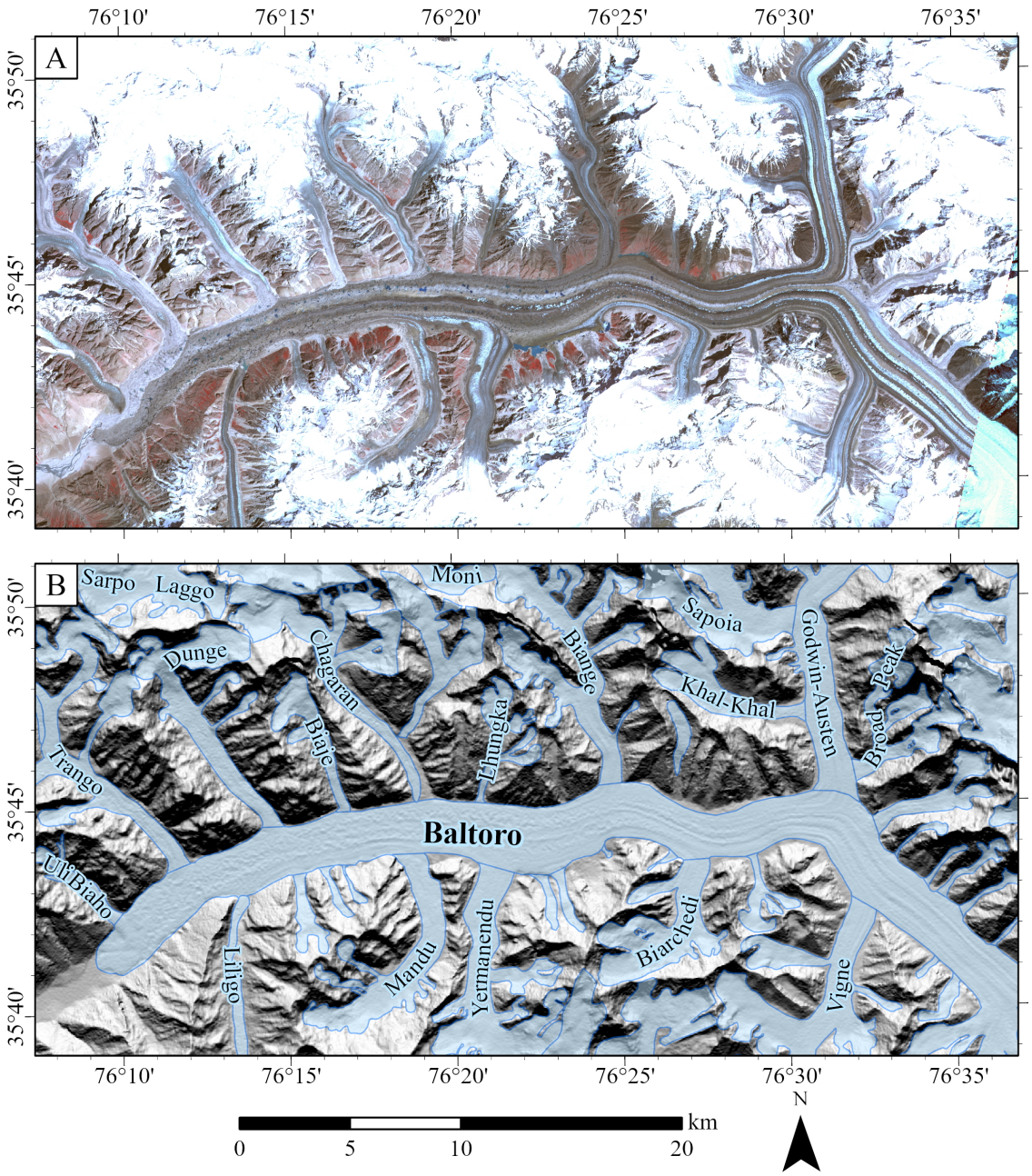

Figure 3.1: The Baltoro Glacier study area, shown in (A) ASTER false-color composite (RGB = Near-infrared, Red, Green), and (B) hillshade with annotated glaciers. ASTER imagery was captured 14 August, 2004 and, in the eastern most portion of the area, 6 October 2003, enhanced to account for poor image quality (NASA LP DAAC, 2015). The hillshade is derived from the void-filled SRTM DEM (30 m) (NASA JPL, 2013).

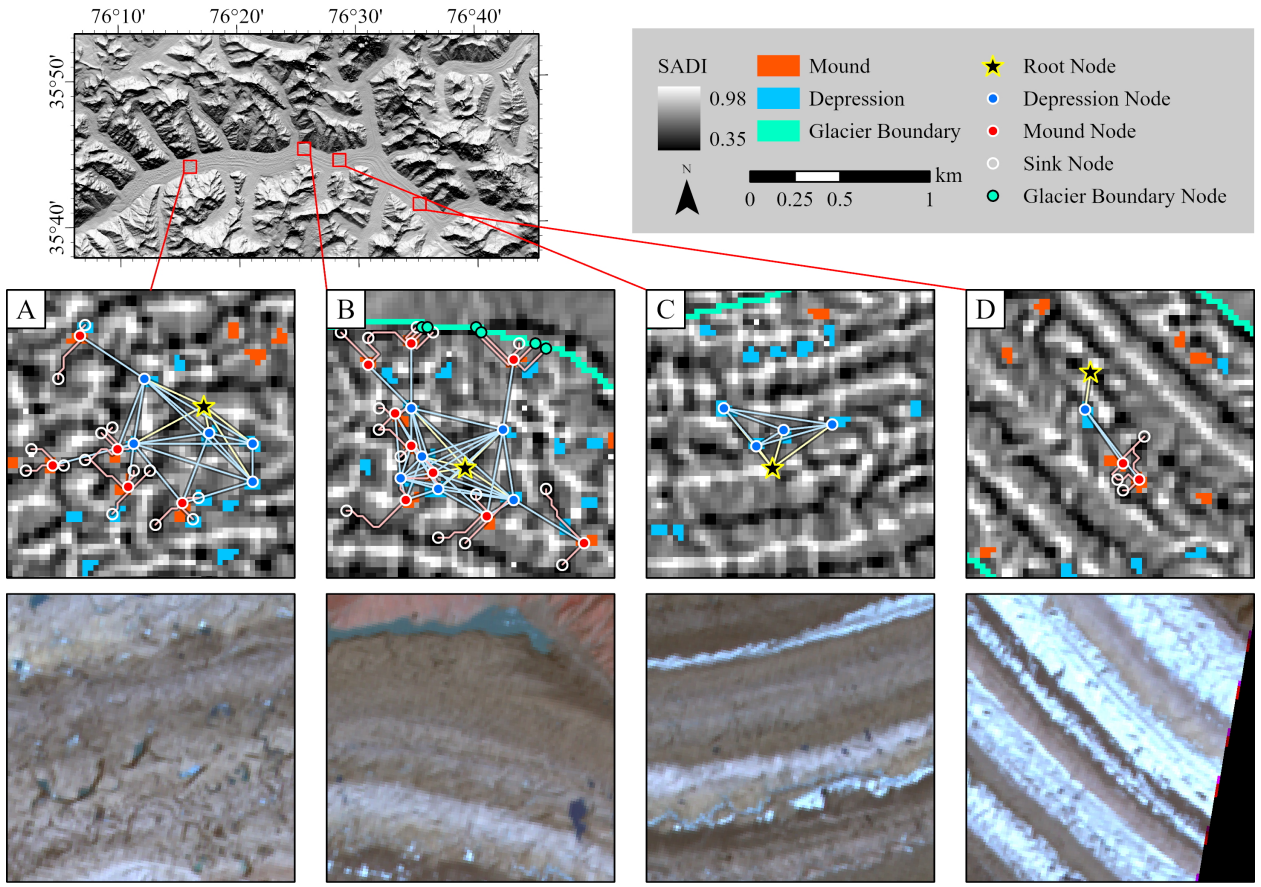

Figure 3.2: Networks constructed for identifying regions with the morphometric characteristics of glacial thinning and supraglacial lake process-regime, drawn over a map of the slope-azimuth divergence index (SADI). These networks consist of an arbitrarily-located root node, which links to nearby depression nodes (yellow lines), which link to other nearby depression nodes and mound nodes (blue lines), which then link to sink nodes via the path of steepest descent (red lines). Sample networks constructed with this architecture are shown: (A) in the lower glacier near the terminus, archetypal for this process-regime; (B) at the confluence of the Biange and Baltoro glaciers where glacier surface morphology is complex; (C) in the mid-glacier where glacier surface relief is well-organized; and (D) in the moraine-dominated upper glacier. False-color ASTER imagery (RGB = Near-infrared, Red, Green) is displayed to show surface features related to glacier surface processes, captured 14 August 2004 (NASA LP DAAC, 2015).

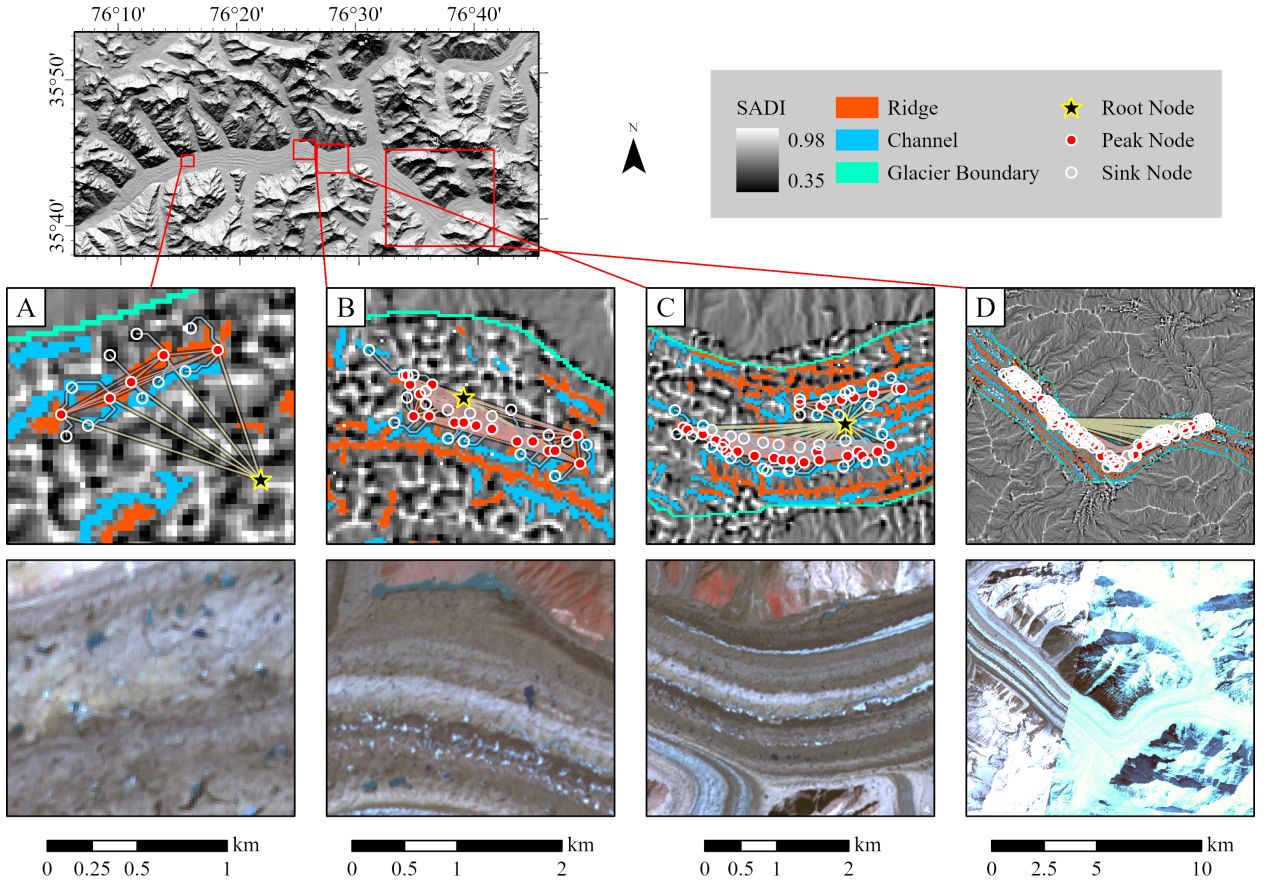

Figure 3.3: Networks constructed for identifying regions with the morphometric characteristics of the intermoraine drainage and sediment transport process-regime, drawn over a map of the slope-azimuth divergence index (SADI). These networks consist of an arbitrarily-located root node, which links to all local altitude maxima located within ridge units (moraines, approximately) on either side of it in directions orthogonal to the local direction of elongation of the nearest channel unit (yellow lines), each peak links to each other peak within the same ridge-form unit (red lines), and each peak links to sinks via the path of steepest descent (blue lines). Sample networks constructed with this architecture are shown: (A) in the lower glacier near the terminus where there are few elongate ridge or channel units; (B) at the confluence of the Biange and Baltoro glaciers where the morphological expression of moraines is relatively weak; (C) in the mid-glacier, where the glacier surface relief is well-organized into ridge- and channel-forms; and (D) in the moraine-dominated upper glacier. False-color ASTER imagery (RGB = Near-infrared, Red, Green) is displayed to show surface features related to glacier surface processes, captured 14 August 2004 and, below panel (D), 6 October 2003, which was enhanced to account for poor image quality caused by scene brightness due to snow cover (NASA LP DAAC, 2015).

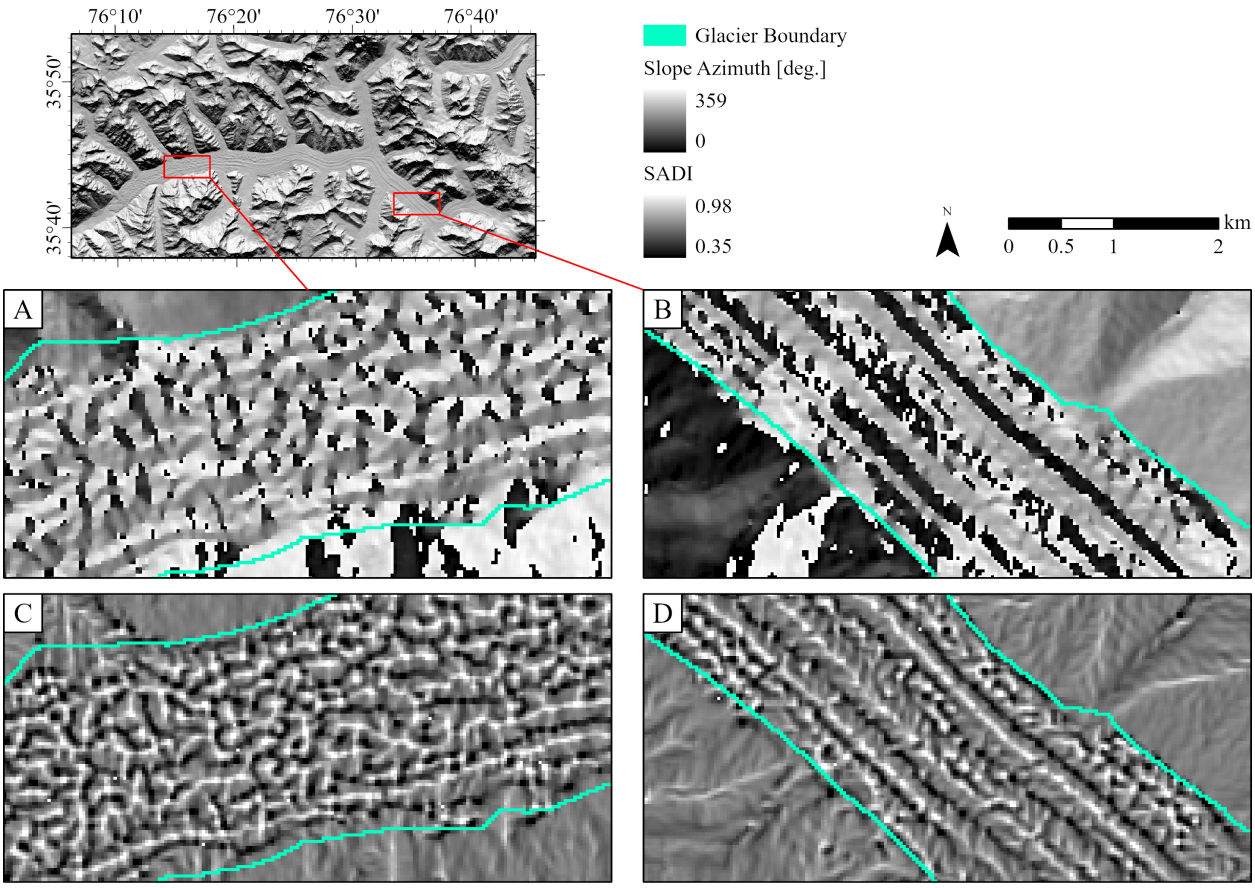

Figure 3.4: Slope azimuth in the lower (A) and upper (B) Baltoro Glacier, and slope-azimuth divergence index (SADI) in the lower (C) and upper (D) Baltoro Glacier, derived from the SRTM DEM (NASA JPL, 2013). Note that the lower glacier shows patterns of isotropic high-frequency variation, characteristics of hummocky topography related to heterogeneous glacier downwasting, in comparison to the more organized moraine-dominated topography associated with ice flow.

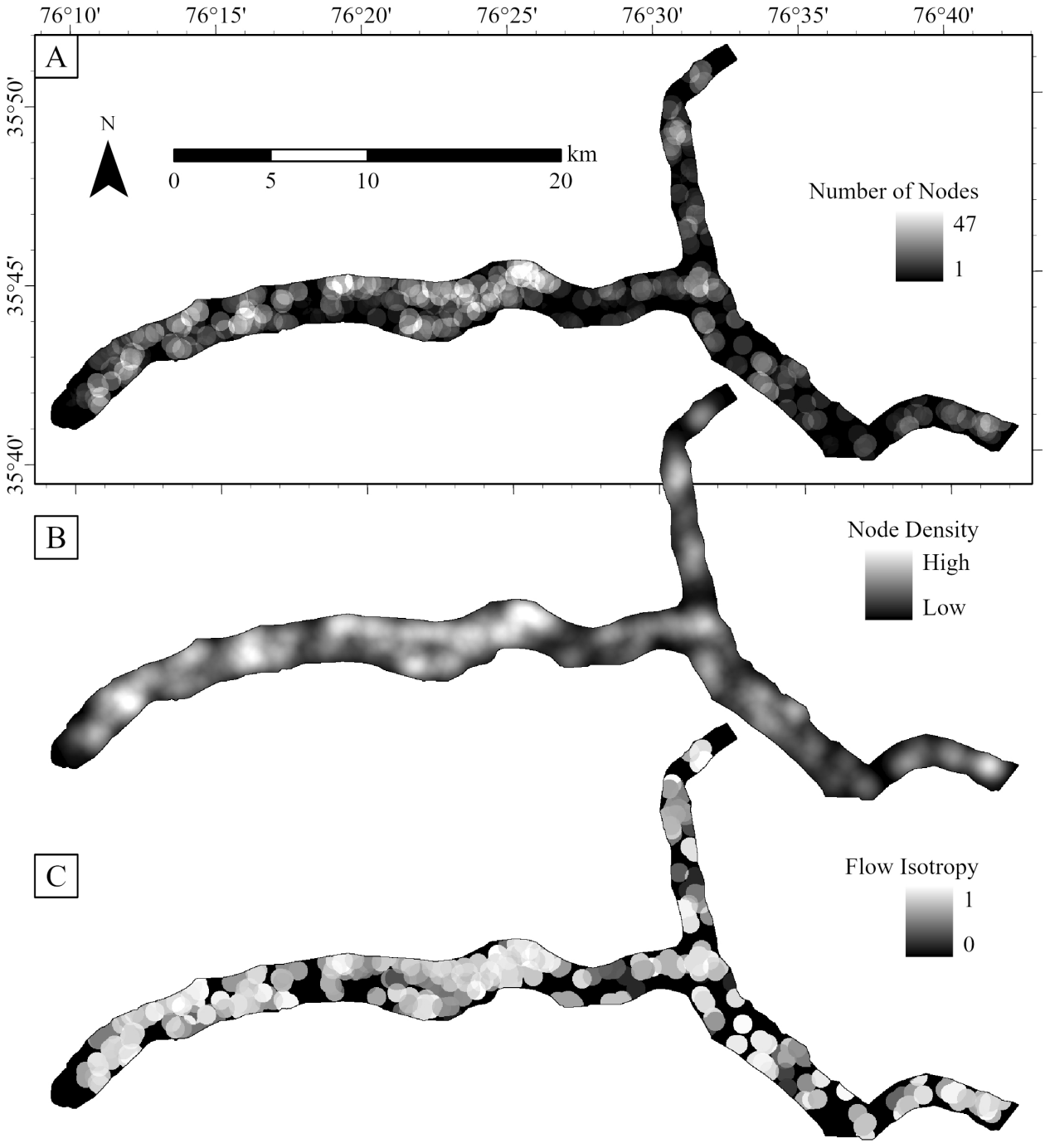

Figure 3.5: Network property maps for networks designed to represent the glacial downwasting and supraglacial lake process-regime, on the surfaces of the Baltoro and Godwin-Austen glaciers, where each grid cell serves as the root node for a network. Properties displayed are (A) the number of nodes represented in the network, (B) node point-density with a 1-km radius cosine kernel, and (C) network link-anisotropy for network linkages representing flow-lines. Examples of these networks are given in Fig. 3.2.

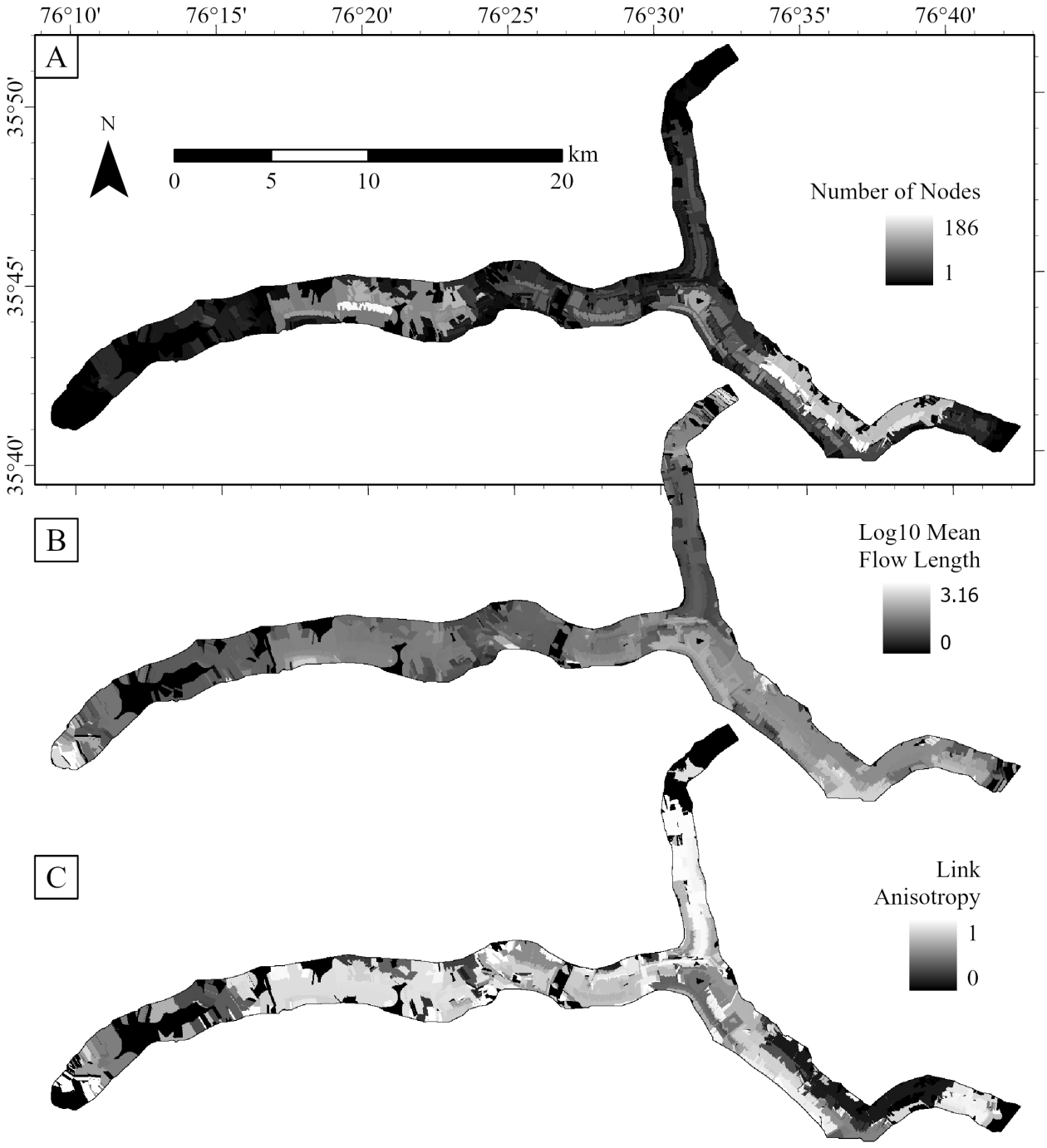

Figure 3.6: Network property maps for networks designed to represent the intermoraine supraglacial drainage and sediment transport process-regime, on the surfaces of the Baltoro and Godwin-Austen glaciers, where each grid cell serves as the root node for a network. Properties displayed are (A) the number of nodes represented in the network, (B) the mean length of network linkages representing flow-lines, and (C) network link-anisotropy for all peak-to-peak linkages. Examples of these networks are given in Fig. 3.3.

4. BASIN EROSION-RATE ASSESSMENT AND ESTIMATION USING TOPOGRAPHIC INFORMATION AND COSMOGENIC-BASED MODELING

Abstract

Mountain erosion geodynamics are complex and coupled with interacting geologic, climate, and topographic forcings. Considerable research has led to the development of robust models that relate erosion rate to land-surface parameters, such as slope, relief, and basin shape. Numerous other land-surface parameters have yet to be evaluated, however, and the influence of topographic conditions on the production of cosmogenic isotopes used to estimate erosion rates has yet to be adequately evaluated. Therefore, we evaluated relationships between numerous land-surface and terrain-unit parameters and both beryllium-10-based erosion rates and measured beryllium-10 concentrations, and explored the topographic modulation of modeled beryllium-10 production rates in the Hazara region in Kashmir, Pakistan. We found a lack of correlation between basin-averaged geomorphometric parameters with predicted erosion rate and with measured beryllium-10 concentration. We found a strong linear correlation between the modeled cosmogenic isotope production rates, including topography-modulated production rates, and measured concentrations of beryllium-10. The slope of the regression line between beryllium-10 production rate and beryllium-10 concentration has units of time, which we interpreted to be a regional characteristic exposure age to cosmic rays which, combined with topographic modulation, might be used to accurately predict beryllium-10 concentrations from modeled production rates, and predict erosion rates using remotely-sensed data and cosmogenic radionuclide theory. We therefore suggest that topographic modulation has potential for predicting cosmogenic nuclide concentrations which, with better understanding of characteristic timescales for beryllium-10 production, can also be used to predict erosion rates remotely based on topographic information and cosmogenic radionuclide theory.

4.1 Introduction

Mountain geodynamics involve the complex interaction of tectonic, climatic, and surface processes that control landscape morphology and erosion dynamics, but are difficult to decouple. Certain process rates can be inferred through the use of geochronology techniques, including mineral cooling ages by apatite thermochronometry and fission-track thermochronometry (Ehlers and Farley, 2003; Finnegan et al., 2008), denudation or exhumation rates by cosmogenic radionuclides (Vance et al., 2003; Reiners and Brandon, 2006), and exposure age dating by cosmogenic radionuclides and optically-stimulated luminescence techniques (Owen et al., 2001; Seong et al., 2007; Dortch et al., 2011a; Wintle and Adamiec, 2017). Numerous researchers have attempted to relate aspects of the local or basin-scale geomorphometric parameters to erosion rate estimates using these techniques, including such parameters as slope, relief, curvature, and basin shape (e.g., Ahnert, 1970; Roering et al., 1999; Montgomery, 2001; Montgomery and Brandon, 2002; Whipple, 2004; Roering et al., 2007; Hurst et al., 2012; DiBiase et al., 2010; DiBiase and Whipple, 2011; Bermúdez et al., 2013; Różycka and Migoń, 2021). These empirical relationships depend on erosion rate estimates that depend upon the steady-state assumption, even in active orogenic environments. A departure from modeled morphometric parameter-erosion rate relationships, or a lack of correlation, is often related to temporal or spatial differences in climate, and geologic, or geomagnetic conditions (Dunai, 2000, 2001; Montgomery and Brandon, 2002; Desilets et al., 2006; Stolar et al., 2007; Balco et al., 2008; DiBiase and Whipple, 2011; Portenga and Bierman, 2011; Bermúdez et al., 2013). There may be additional topographic characteristics related to relief production that have yet to be more fully explored, which may influence how erosion rates are calculated (von Blanckenburg, 2005; Bishop et al., 2020).

Landscape or topographic evolution models relate denudation to topographic parameters, sometimes coupled with ancillary climate data (Tucker and Hancock, 2010; Yang et al., 2015), thereby providing options for investigating topography-erosion relationships. Many of these relationships are empirical in nature, however, and ambiguous scaling factors and power-law coefficients do not or cannot account for the numerous interacting factors that influence causal topography-erosion

process mechanics (Whipple, 2004; Tucker and Hancock, 2010; Bishop et al., 2020). Topographic evolution models that make use of process mechanics, on the other hand, depend on parameters that cannot be known for every point on the land surface and cannot be reliably discerned with current data and techniques via remote sensing, such as soil thickness or rock mechanical properties (Sklar and Dietrich, 2004; Gruber et al., 2009; Tucker and Hancock, 2010). Further causal scale-dependent relationships to erosion have yet to be explored, however, which may improve upon scaling factors and challenge model assumptions (von Blanckenburg, 2005; Bishop et al., 2020).

The comparison of measured cosmogenic nuclide concentrations in relation to modeled cosmogenic nuclide production rate is popular for estimating the ages of surfaces and erosion rates (Lal, 1991; Stone, 2000; Owen et al., 2001; Codilean, 2006; Seong et al., 2007; Balco et al., 2008; Adams et al., 2009; Seong et al., 2009b,a). Basin-average erosion rates require an approximation of the average cosmogenic nuclide production rate throughout the entire basin (Schaller et al., 2001; von Blanckenburg, 2005; Codilean, 2006). The methods for determining production rate, however, depend upon assumptions of steady-state, and that the surface is eroded at a rate that is significantly slower than the timescales at which a cosmogenic nuclide is produced (Lal, 1991; Stone, 2000; Balco et al., 2008). The steady-state assumption infers that the topography either does not evolve heterogeneously or that its evolution has minimal impact on the cosmogenic production rate and erosion rate of the basin during the relevant time interval. This assumption, depending on basin size and the time scales involved, is absurd (Phillips, 1999, 2003; von Blanckenburg, 2005; Bishop et al., 2020) but necessary to assume given that the past state of the topography and other temporally variable factors are generally not known (Dunai, 2000, 2001; Desilets et al., 2006; Balco et al., 2008). Assuming that current conditions are representative and related to cosmogenic isotope production, however, it is unclear how various topographic factors alter the amount of isotopes present in any particular location. Specifically, fewer cosmogenic nuclides should be expected in locations subject to rapid sediment flux or high denudation rates. It is therefore necessary to investigate the modulation of cosmogenic nuclide production rates with topographic parameters to determine if this approach can predict basin-average nuclide concentrations that are related to real amounts

measured in the stream at the basin's outlet? More specifically, is there a relationship between geomorphometric parameters and measured cosmogenic nuclide concentration and erosion rate?

The objective of this research is to further explore aspects of topographic properties and spatial structure as they relate to cosmogenic isotope (beryllium-10) production and erosion rate. We explore this topic for basins in the vicinity of Muzaffarabad in Kashmir, Pakistan, which appear to have shared similar geologic and climate conditions for their relevant history. The main objective of this paper is supported by achieving five sub-objectives:

1. Represent terrain units that are important to topographic structure in mountainous environments using object-oriented analysis. Specifically, we represent slope structure using slope facets (slope-attitude units), the drainage network, and basins where samples have been collected for basin-average beryllium-10 cosmogenic production and erosion analysis.

2. Compute various land-surface and terrain-unit parameters representing such topographic characteristics as local and mesoscale relief, slope, topography-based sediment flux, near-surface failure potential due to topographic load, terrain unit area, terrain unit shape, and topographic organization (e.g., bifurcation ratio, hypsometric integral, fraction of steep slopes).

3. Model the production rate of beryllium-10 in select basins to predict erosion rate using measured beryllium-10 concentrations.

4. Statistically evaluate the relationships between land-surface and terrain-unit parameters and both predicted erosion rate and measured beryllium-10 concentrations.

5. Empirically evaluate the usage of land-surface parameters for modulating beryllium-10 production rates to approximate measured beryllium-10 concentrations.

4.2 Background

4.2.1 Erosion Dynamics and Topography

Landscape evolution and erosion dynamics are prominent aspects of terrain modeling (e.g., Tucker and Bras, 1998; Pike, 2002; Bishop et al., 2003; Pike et al., 2009; Tucker and Hancock,

2010; Dortch et al., 2011b; Bishop et al., 2012; Wilson and Bishop, 2013; Bishop et al., 2020; Różycka and Migoń, 2021) due to its relevance to such application domains as agriculture, hydrological resource management, and hazards mitigation (Pike, 2000; Pike et al., 2009; Wilson and Bishop, 2013; Bishop et al., 2018, 2020). There are strong relationships between aspects of the topography and erosion rate, most notably relief and slope angle as proxies for gravitational forcing (Ahnert, 1970; Roering et al., 1999; Montgomery and Brandon, 2002; Roering et al., 2007) and upstream area as a proxy water discharge (Whipple, 2004). Ahnert (1970) noted a linear relationship between basin slope or hillslope relief and erosion rate, for example, which was later identified as the low-relief portion of a nonlinear relationship between slope or relief and erosion rate (Roering et al., 1999; Montgomery and Brandon, 2002). The relationship between slope and erosion due to diffusive processes is given as:

$$\epsilon_{\text{diff}} = \frac{KS}{1 - \left(\frac{S}{S_c}\right)^2}, \tag{4.1}$$

where K is a scaling coefficient, S is the local slope gradient, and S_c is a critical or threshold slope gradient (relief is sometimes substituted for slope gradients; Ahnert, 1970; Montgomery and Brandon, 2002; DiBiase et al., 2010). For sediment-mantled topography, this empirical diffusion equation relating hillslope steepness or relief to sediment flux appears to be highly predictive, but relies on a scaling coefficient that may or may not account for complex scale- and location-dependent climate, tectonic, geologic, and biologic conditions that influence the erodibility of a landscape (Bishop et al., 2003; Phillips, 2003; Aalto et al., 2006; Phillips, 2007; Wohl, 2013; Bishop et al., 2018, 2020), each of which interact with each other and affect erosion dynamics in nonlinear ways (Burbank et al., 2003; Phillips, 2003; Wohl, 2013; Sweeney et al., 2015; Bishop et al., 2018, 2020). Furthermore, the limitation of selecting an arbitrary or empirical slope threshold complicates modeling efforts because it may not be clear how thick sediment cover may be, some areas may exhibit steeper-than-threshold slopes without obvious bedrock exposure, and non-diffusive processes such as landsliding may occur even in areas with shallow slopes (e.g., Burbank et al., 1996; Kamp et al.,

2008; Tucker and Hancock, 2010; Rempe and Dietrich, 2014).

Whipple (2004) summarizes empirical power-law models used to predict river incision, which use stream steepness and the area theoretically capable of contributing flow as a proxy for river discharge, such that:

$$\epsilon = K A_{\text{accum}}^{m} S^{n} \tag{4.2}$$

where A_{accum} is the planimetric area contributing flow and m and n are power coefficients that modulate the relative influence of the contributing area and local slope, respectively. The scaling coefficient, K, may be divided into numerous other scaling coefficients that attempt to represent erosional resistance, climate conditions, storm thresholds, the influence of sediment load, and so forth (Whipple, 2004; Gasparini and Brandon, 2011), but it remains unclear if these factors are truly separable or account for all topographic factors that influence denudation, such as adjacent hillslope properties and sediment supply (Burbank et al., 2003; Archer and Fowler, 2004; Bookhagen and Burbank, 2006; Gasparini and Brandon, 2011; Dobreva et al., 2017). More deterministic models attempt to avoid the ambiguity of empirical coefficients associated with the stream power law, but depend on other assumptions and additional parameters that may be difficult to represent or know, such as the size and composition of saltating grains, frequency of grain impact, the tensile strength of exposed bedrock, and the fraction of exposed bedrock (Sklar and Dietrich, 2001, 2004).

Topographic evolution models seek to combine one or more empirical or stochastic models for predicting land-surface altitude change over time. Tucker and Bras (1998), for example, combined the slope-diffusion model, the stream-power model, and three models for landsliding, which has proven notoriously difficult to predict (Guzzetti et al., 2006; Gruber et al., 2009; Tucker and Hancock, 2010; Aronica et al., 2012; Larsen and Montgomery, 2012; Goetz et al., 2015; Dao et al., 2020). Numerous parameterization schemes exist for predicting topographic evolution that attempt to account for gravitational, hydrological, glacial, and chemical weathering and erosion (MacGregor et al., 2000; Brocklehurst and Whipple, 2002; Roering, 2008; MacGregor et al., 2009; Tucker and Hancock, 2010; Booth and Roering, 2011; Shelef and Hilley, 2016; Bishop et al., 2018, 2020).

Empirical parameterization schemes are problematic because they do not cover causal effects such as lithologic properties, topographic stress, differential weathering due to geologic structure, and so forth, relying instead on geomorphometric proxies, ancillary data, and ambiguous scaling or power-law coefficients which cannot account for the ways in which causal factors may interact with each other in nonlinear ways (Whipple, 2004; Bishop et al., 2020). Process-mechanic approaches may not fully account for all causal factors and, for the causal factors that they do address, the values are largely unknown except at specific locations where they have been measured, such as grain size distribution, soil thickness, or rock mechanical properties (Tucker and Bras, 1998; Montgomery and Brandon, 2002; Whipple, 2004; Sklar and Dietrich, 2004; Gruber et al., 2009; Tucker and Hancock, 2010; Moon et al., 2017; Struth et al., 2017, 2019; Bishop et al., 2018, 2020). Many more scale-dependent topographic parameters or process-mechanics parameters need to be evaluated to determine if they exhibit a relationship with erosion (Bishop et al., 2020). If they do, this should improve upon scaling factors and challenging assumptions associated with empirical coefficients and temporal homogeneity or steady-state.

Issues of scale are pervasive throughout geomorphological modeling (Phillips, 1988; Shary et al., 2005; Bishop et al., 2012; Phillips, 2016; Bishop and Dobreva, 2017; Bishop et al., 2018, 2020). From the perspective of process modeling, Montgomery and Brandon (2002) and DiBiase et al. (2010) indicate that hillslope relief may be the more reliable parameter to relate to diffusive hillslope erosion, as it is less sensitive to the resolution of the altitude field dataset. The scale at which relief should be determined, including the distance- and direction-dependence of this measure (i.e., relief in a given window, variable window, flow-path between ridge and stream, or euclidean path between ridge and stream), is not clear (Ahnert, 1970; Montgomery and Brandon, 2002; DiBiase et al., 2010; Hurst et al., 2012). Such issues of scale extend to the representation of other parameters related to erosion, including the scale at which slope and curvature should be generalized (Wood, 1996; Shary et al., 2002, 2005; Hurst et al., 2012; Prasicek et al., 2014), characterization of topographic shielding (Codilean, 2006; Li, 2013), determination of homogeneity or surface roughness (Wu et al., 2000; Lindsay et al., 2019; Zhang et al., 2020), and representation of

topographic anisotropy (Roy et al., 2016; Newman et al., 2018). The relationship between basin area and erosion rate is also unclear: DiBiase et al. (2010) report a complete lack of correlation to basin area in their dataset, yet it contributes to stream-power erosion models (Whipple, 2004; Perron and Royden, 2013; Struth et al., 2017) and Syvitski and Milliman (2007) and Ali and de Boer (2008) report that erosion can be partially explained using basin area.

Despite issues associated with diverse models' empiricism, parameterization, and scale representation, there are clear relationships between topographic parameters and erosion rate which may be further exploited to modulate erosion rate estimates. Slope appears to be a consistent factor, as well as local or mesoscale relief (Ahnert, 1970; Tucker and Bras, 1998; Montgomery, 2001; Montgomery and Brandon, 2002; Whipple, 2004; Tucker and Hancock, 2010; Bishop and Dobreva, 2017; Bishop et al., 2018, 2020). Curvature may also serve as a useful parameter in certain conditions (Hurst et al., 2012; Moon et al., 2017). Drainage network characteristics are also affected by processes of erosion (Tucker and Bras, 1998; Perron et al., 2008; Sweeney et al., 2015; Pereira-Claren et al., 2019). Tectonic processes affect erosion rate and manifest in certain geomorphometrics, including parameters that describe basin size, shape, and hypsometry (Bhat et al., 2013; Różycka and Migoń, 2021).

Relief variability results in stress-field perturbations in the near surface that govern rock resistance to erosion (Molnar, 2004; St. Clair et al., 2015). Stress induced by topographic load has been investigated in various modeling efforts and its effect on near-surface fracturing has been validated in the field (Martel and Muller, 2000; Muller and Martel, 2000; Slim et al., 2015; St. Clair et al., 2015; Moon et al., 2017), including correlations between high modeled failure potential and near-surface and deep fracturing (St. Clair et al., 2015; Moon et al., 2020) and landslide size (Clark and Burbank, 2010; Li and Moon, 2021; van der Beek, 2021). Previous studies, however, have only qualitatively linked topographic load to erosion dynamics and denudation rates or have not established an empirical relationship between the two. Moon et al. (2017), for example, demonstrated a relationship between near-surface failure potential and low-frequency surface curvature, but do not establish an empirical relationship between the two, possibly because this is also dependent

on regional horizontal stresses, relief of local eminences, or other geographic or geological factors that were not accounted for. Li and Moon (2021) demonstrated a strong relationship between failure potential and landslide size, but does not relate topographic stress conditions to landslide frequency, making it difficult to apply directly to an erosion rate study, though Clark and Burbank (2010) relate landslide size to frequency. Clark and Burbank (2010) relate landsliding to rock p-wave velocity as a proxy for fracture intensity, though the exact relationship between fracture intensity and the stress field is unclear (though see St. Clair et al., 2015). This study therefore incorporates near-surface stress estimates in its analysis to investigate the relationship between stress induced by topographic load and erosion rate estimates.

4.2.2 Cosmogenic Radionuclide Approaches

Beryllium-10 is produced in quartz in rock and regolith in the uppermost ~3 m of Earth's surface via spallation reactions with cosmic rays and these reactions decrease exponentially with depth in the substrate (Lal, 1991). The average erosion rate is inversely proportional to the surface beryllium-10 concentration and is integrated over the time required to erode one cosmic ray penetration length (1 e-folding depth), ~100 and ~60 cm for regolith and bedrock, respectively (Lal, 1991; Granger et al., 1996). The erosion rate is given by:

$$\epsilon = \frac{\Lambda_r}{t_e} = \frac{\Lambda_r}{\left(\frac{C_{\mathrm{Be}}}{P_{\mathrm{Be}}(\lambda,z)}\right)}, \tag{4.3}$$

where Λ_r is the cosmic ray penetration length and t_e is the effective surface-exposure age of a sample, which is a function of the concentration of beryllium-10, C_{Be} [atoms g^{-1}], and the latitude- and altitude-dependent production rate of the nuclide, P_{Be} [atoms g^{-1} yr^{-1}]. These average beryllium-10 erosion rates are a measure of both physical and chemical denudation and typically reflect erosional processes over ~10^3 to 10^5 timescales (Bierman and Steig, 1996; von Blanckenburg et al., 2004). Stone (2000) refined the parameterization scheme of Lal (1991) by better scaling cosmogenic nuclide production rates by atmospheric depth and geomagnetic shielding, which are respectively approximated with altitude and latitude. Other methods exist for scaling cosmogenic

nuclide production rate, including methods to account for topographic shielding (e.g., Codilean, 2006; Li, 2013) and secular variation in the geomagnetic field (Dunai, 2000, 2001; Desilets et al., 2006; Balco et al., 2008).

The methods of measuring and interpreting *in situ* cosmogenic radionuclide concentrations have been applied to the scale of basins (von Blanckenburg, 2005; Dortch et al., 2011b; Bhat et al., 2013; Struth et al., 2017; Różycka and Migoń, 2021). Assumptions for this type of analysis are summarized by von Blanckenburg (2005), and are:

1. Denudation within the basin is uniform over time or, in other words, the basin is in steady state or in equilibrium with current conditions for the timescale at which it takes to transfer and mix sediment from all portions of the basin and deposit the sediment mixture at the basin mouth. This is a good assumption if sediment transport is not dominated by mass wasting, as in areas of high tectonic or rainfall activity, because a small area recently affected by landsliding might be over-represented in sediment at the basin outlet (von Blanckenburg, 2005; Grande et al., 2021).

2. Each area of the basin contributes quarks to the mixed sample proportional to the area's erosion rate, which is valid in settings of uniform lithology or where all lithologies erode at the same rate.

3. Contributing rock types contain similar grain size distributions and the released grain sizes are independent of the erosion process.

4. Quartz is not enriched on its way to the surface by preferential dissolution of other minerals.

5. Sediment storage in the basin is minimal, such that sediment transfer occurs on much shorter timescales than hillslope denudation. That is, transport from any location within the basin is effectively instantaneous. This is an issue of scale, as locations operating in regimes of slow sediment transfer (e.g., soil creep) and locations further from the basin mouth should have greater effective exposure time due to their longer transport time, thereby contributing disproportionately higher cosmogenic nuclide concentrations, artificially lowering the

basin-average erosion rate estimate. A lack of correlation between basin size and erosion rate predicted with cosmogenic nuclides (DiBiase et al., 2010) would suggest that this assumption generally holds true, but not so if basin size is a significant factor in erosion rate (Syvitski and Milliman, 2007; Ali and de Boer, 2008).

6. Denudation occurs far more rapidly than radioactive decay. For beryllium-10, this requires denudation rates in excess of 0.3 mm kyr$^{-}1$ (von Blanckenburg, 2005).

Not all assumptions will be met, but the method should yield relatively robust estimates regardless (von Blanckenburg, 2005). Though the sediment transfer rate assumption generally appears to hold, scale-dependence in terms of basin elongation and shape appear to be significant (Bhat et al., 2013; Różycka and Migoń, 2021). Such factors appear to be universally and appropriately related to tectonic activity and geologic control rather than scale-dependence (e.g., Bhat et al., 2013; Różycka and Migoń, 2021), exploiting a violation of the steady-state and minimal storage assumptions. The steady-state assumption, however, may itself be scale-dependent (Ahnert, 1994; Thorn and Welford, 1994; Montgomery and Brandon, 2002; Aalto et al., 2006; Wohl et al., 2014; Thoms et al., 2018), though the scale-dependency of steady-state or diverse types of equilibrium is not fully understood.

Surprisingly, there does not appear to be any attempts to modulate predicted cosmogenic nuclide production rates with topographic parameters except for a topographic shielding scaling factor. Specifically, locations exhibiting rapid erosion should yield fewer cosmogenic nuclides due to briefer exposure time before being mixed with the rest of the basin's sediment. The goal of this modulation would be to provide a more accurate prediction rate that, combined with a sensible (average) effective exposure time, could accurately predict the average cosmogenic nuclide concentration in the basin, comparable to what may be measured from river sediments at the basin outlet.

4.3 Study Area

This study focuses on the Hazara region of Kashmir, northern Pakistan, in the vicinity of Muzaffarabad and the confluence of the Neelum and Jhelum rivers (Fig. 4.1). The Köppen-Geiger climate classification for Muzaffarabad and sampled basins is Cfa (temperate, no dry season, hot summer; Beck et al., 2018). The region is warm and wet, with mean monthly rainfall in excess of 130 mm, being fed by seasonal monsoons (Salma et al., 2012). The regional topography is forested and steep (Fig. 4.2), with a mean slope angle of 25° and standard deviation of 11.5°, and a distinct NW-SE topographic grain that coincides with major structures that accommodate regional NE-SW shortening (Calkins et al., 1975; Kamp et al., 2008; Shah, 2015).

The study area appears to bear no direct influence of significant glaciation, being exclusively or nearly exclusively shaped by processes of fluvial incision and mass wasting. Regional glacier equilibrium lines appear to be at or above 4000 m, perhaps as low as about 3500 m at the maximum glacial advance in the Kashmir basin across the Pir Panjal range to the east (Shroder, 1993; Derbyshire and Owen, 1997). Kamp et al. (2008) indicates the presence of steep, high-altitude peaks associated with glaciation between the Neelum and Kunhar (Kaghan) rivers to the north. The highest-altitude peak within the study area is located between the Neelum and Jhelum rivers near the eastern extent of the study area, which may exhibit signs of relict glaciation. The steepest slopes appear to be related to fluvial incision and mass wasting processes (Kamp et al., 2008; Basharat et al., 2013, 2014).

The region's underlying lithology principally consists of the Lower Miocene mudstones and sandstones of the Murree Formation, and the Precambrian slates, shales, and limestones of the Hazara Formation west of the Jhelum and Kunhar rivers (Calkins et al., 1975; Thakur, 1998; Kamp et al., 2008; Basharat et al., 2013; Mughal et al., 2018; Dar et al., 2021). A narrow expression of the Cambrian carbonates and Late Miocene shales-to-conglomerates of the Muzaffarabad and Kamlial formations, respectively, underlies a thin area along the Kunhar River near the confluence of the Jhelum and Kunhar rivers (Calkins et al., 1975; Kamp et al., 2008; Basharat et al., 2013, 2014). The sandstones (quartzites and shales) of the mid-Paleozoic Tanawal Formation unconformably

overlie the Hazara Formation in the northwestern portion of the study area, just west of the Kunhar River (Kamp et al., 2008; Qasim et al., 2017). An exposure of the Mid-Late Miocene Kamlial Formation sandstones and mudstones occur in the souther-central portion of the study area (Kamp et al., 2008; Ullah et al., 2015). The northeast-dipping Kashmir Boundary Thrust or Kashmir Basin Thrust parallels the eastern branch of the Jhelum River in the study area (Kamp et al., 2008; Shah, 2015). The Main Boundary Thrust is a west-dipping structure that passes beneath Muzaffarabad and parallels the western branch of Jhelum River, and accommodates significant crustal shortening and uplift, and delimits the western boundary of the Hazara-Kashmir Syntaxis (Calkins et al., 1975; Kamp et al., 2008; Basharat et al., 2013; Shah, 2015; Vassallo et al., 2015). The climate, tectonic setting, geologic structure, and fine-grained and carbonate sediments make the region prone to slope failure and high-magnitude erosion rates (Kamp et al., 2008). All basins sampled for this study are underlain by the Murree Formation except for the west-most basin (Z-19), which is underlain by the Tanawal Formation in its northwestern half and Hazara Formation in its southeastern half, and the southern-most basin (Z-04), which is partially underlain by the Kamlial Formation along its eastern edge. It should be noted that the Murree Formation was found to be most prone to landslides following the 2005 Kashmir earthquake, and that many of these landslides were on shallow slopes (Kamp et al., 2008).

4.4 Methods

4.4.1 Field Sampling and Cosmogenic Isotope Methods

Sediment samples were collected in 2005 from seven streams that drain catchments throughout the region. We collected multiple 100-g-size sediment samples using a hand-held trowel to make up an ~2 kg sample, avoiding particles >2 cm in diameter, from active channel bars to a depth of a few cm to ensure complete sediment mixing (Niemi et al., 2005; Yanites et al., 2009). These were air-dried and packed in plastic bags. We avoided channel sediment from areas potentially influenced by local stream-bank slumps, landslides, and anthropogenic inputs. We note, however, that the region had been recently impacted by mass wasting following the Kashmir earthquake in

2005 (Kamp et al., 2008; Basharat et al., 2013, 2014).

Laboratory work to measure cosmogenic beryllium-10 was undertaken in the geochronology laboratories at the University of Cincinnati. We extracted quartz, and ultimately beryllium, from samples by standard methods of HF dissolution and column chromatography pioneered by Kohl and Nishiizumi (1992). Sediment particles <2 cm in diameter for each 2 kg sample were crushed and sieved to acquire a 250-500 μm particle size fraction. The crushed fraction was run through a Franz magnetic separator to help remove magnetic minerals and feldspars. The non-magnetic fractions were chemically leached using aqua regia for acid for more than 12 hours. This was followed by one or more 5% HF/HNO_3 leaches for about 24 hours. The remaining non-quartz minerals were removed using heavy liquid (lithium heteropolytungstate) separation to obtain the quartz separate. The purity of the quartz separate was examined under an optical microscope. The quartz was then leached in 1% HF/HNO_3. The pure quartz was spiked with a beryllium-9 carrier and dissolved in 48-50% HF. Blanks were also prepared at this stage and followed the same procedure as for the beryllium-9-spiked quartz. The quartz solution and blanks were taken to dryness in a fume hood. The samples were then fumed three times with $HClO_4$. The residue was then passed through anion and cation exchange columns to separate the beryllium fraction. $Be(OH)_2$ gel was precipitated from the beryllium fraction using NH_4OH. The $Be(OH)_2$ gel was rinsed and dried in acid-cleaned quartz crucibles for about 24 hours. Once dry, the samples were calcinated to BeO by ignition at 750 °C for 5 minutes. The BeO was mixed with Nb powder and loaded into steel accelerator mass spectrometer (AMS) targets. The beryllium-10 concentrations were determined from $^{10}Be/^{9}Be$ ratios measured by AMS at PRIME Laboratory at Purdue University with the 07KNSTD standard and beryllium-10 half-life of 1.36 Ma (Nishiizumi et al., 2007). $^{10}Be/^{9}Be$ blanks had ratios of ~3×10^{-15}.

4.4.2 Remote Sensing Data

Landsat-5 Thematic Mapper Level-2 (reflectance) imagery (path 150, row 036) was utilized to supplement topographic interpretation of the land surface and better understand general vegetation patterns using the Normalized Difference Vegetation Index (NDVI, Rouse et al., 1973; Jensen,

2000). Ideally, the satellite imagery used represents the surface near the time of sample collection, though this was not possible using Landsat data due to significant cloud cover and data availability. Two cloud-free scenes were used to observe the study area, one on 11 March 2009 (Fig. 4.1), and the other on 19 September 2009.

Version 3 of the Shuttle Radar Topography Mission, void-filled digital elevation model (SRTMv3 DEM) provides a highly accurate altitude field at 30 m spatial resolution (NASA JPL, 2013). The altitude field represented in the DEM is utilized as the basis for all geomorphometric analysis and hydrological characterization of the basins associated with field samples, including terrain unit extraction and characterization and the derivation of land-surface parameters. The DEM was not further modified except as described in the methods of this study.

4.4.3 Terrain Unit Extraction

Streams and hydrological basins are important aspects of the topographic structure associated with erosion and cosmogenic nuclide measurement, particularly in terms of transport dynamics and spatial containment of the geomorphological conditions associated with surface processes relevant to a particular sediment sample collected at the mouth of a basin. Streams and basins associated with cosmogenic radionuclide samples are obtained utilizing the Spatial Analyst Hydrology toolbox in ArcGIS Pro 2.8.2 software. The specific workflow was:

1. Process the DEM with the Fill tool to remove sinks in the dataset.

2. Compute flow-direction using the D8 method with the Flow Direction tool. Tools for characterizing streams and extracting the watershed require a D8 flow-direction raster.

3. Compute flow-accumulation using the Flow Accumulation tool.

4. Generate streams as a threshold of flow-accumulation ≥ 100 cells. We use this threshold to ensure streams are mapped through each sample location and are represented in each studied basin.

5. Generate unique stream reach IDs using the Stream Link tool and compute stream order using the Stream Order tool. These are used to compute stream bifurcation ratios.

6. Manually nudge field-sample locations onto nearby stream locations. The Snap Pour Point tool was not used because the distance for correction was different for each watershed, and some sample locations may have been erroneously snapped to streams draining the regional basin rather than representing the basin associated with the sample.

7. Generate basins using the Watershed tool.

To evaluate another aspect of topographic structure associated with basin erosion, this study extracts slope-facet units. Slope-facets are zones of relatively homogeneous slope attitude. Large, steep slope facets are indicative of threshold slopes associated with rapid erosion. The procedure for acquiring slope facets was:

1. Compute slope-angle (θ) and slope-azimuth (φ) rasters using the method of Shary et al. (2002), determining slope gradients via least-squares linear regression in a 5×5 window. The large window size generalizes the topography to mitigate the effects of DEM error and better represent these larger-scale features.

2. Partition the land surface into five slope-angle classes using the ISODATA algorithm on the slope-angle raster. Five classes are chosen to address the functional range in topographic steepness, such that the classes approximately represent the categories of near-horizontal, shallow, moderate, steep, and very steep slopes that might be found in mountainous terrain.

3. Partition the land surface, targeting eight slope-azimuth classes using the ISODATA algorithm on slope northerness ($\cos\varphi$) and slope easterness ($\sin\varphi$) rasters. The slope-azimuth classes approximately represent the cardinal and ordinal directions, adapted to the statistical distribution of slope azimuth in the study area.

4. Generate slope-facet classes by spatial intersection of the slope-angle and slope-azimuth classes.

5. Generate slope-facet units by spatial clumping using rook's rule spatial contiguity.

4.4.4 Land-Surface and Terrain-Unit Parameters

Numerous land-surface and terrain-unit parameters may be associated with erosion and other surface processes. This study evaluates many such parameters in relation to basin-average erosion rates estimated using beryllium-10 concentration measurements.

The land-surface parameters employed in this study are summarized with their equations in Table 4.1, with further descriptions here:

- Altitude (z), being related to climate forcing, and the production rate of cosmogenic nuclides. If all basins have approximately the same base-level, then z also indicates the degree to which a basin is elevated above base-level. Altitude is averaged for each basin.

- Slope angle (θ), which represents slope steepness and sediment flux by diffusive and gravity-driven processes. Slope angle is computed using the method of (Shary et al., 2002) in a 3×3 window, using linear regression to characterize slope gradients. The tangent of slope angle is averaged for each basin. The fraction of steep slopes exceeding 40° is also computed for each basin ($f\theta$), as a proxy for non-diffusive mass wasting slope processes.

- Hillslope relief (h), or local scale-dependent relief between the local ridge and drainage, which should be less sensitive to DEM resolution and has a strong relationship to erosion rate (Montgomery and Brandon, 2002). Hillslope relief is the altitude difference between the nearest stream and the first ridge encountered in the opposite direction. This is accomplished by casting a ray in opposite directions (this study uses 1° steps) and identifying stream and ridge locations in each ray, where a ridge is either the basin edge or the maximum-altitude location between two stream locations. If no stream is encountered between the ridges bounding the sample location, that direction is not used. Hillslope relief is averaged for each basin.

  DiBiase et al. (2010) cites Ahnert (1970) and Montgomery and Brandon (2002) for their method of computing neighborhood relief in a window with varying window size. This

method is not used in this study, as it is not clear how the window size should vary and it seems clear that the window is intended to represent the relief between a stream and the nearest ridge associated with the hillslope. Hurst et al. (2012) compute hillslope relief by tracing the path of steepest descent from ridge locations mapped using the method of Passalacqua et al. (2010) and filtered based on local slope angle and proximity to mapped roads, trails, and valley bottoms. This study does not replicate the method of Hurst et al. (2012) because of its numerous assumptions associated with DEM resolution, DEM smoothness, arbitrary distances to mapped features, incomplete representation of the ridgeline, and uncertainty with how mapped ridgelines might interact with mapped drainages of varying density, but we note that if a consistent ridge-to-drainage flow-path could be identified, it would be superior to our method, which assumes that the relevant hillslope relief can be discerned in a straight line between a mapped stream and a ridge as we have defined it.

- Mean curvature (K_{mean}). Hurst et al. (2012) identified a positive relationship between hilltop curvature and erosion rate and related it to sediment transport efficiency in basins associated with the hilltop. Moon et al. (2017) further demonstrated a relationship between low-frequency surface curvature and the depth of high fracture activity associated with high failure potential due to topographic load. Mean curvature is averaged both for the entire basin and for streams only ($K_{\text{mean},s}$).

- Skyview factor (V_f), or positive openness, which represents the degree of hemispherical shielding imposed by the topography (Yokoyama et al., 2002; Codilean, 2006). Low skyview factor values suggest high meso-scale relief, steep slopes, and/or narrow valleys that are associated with rapid erosion rates (Wilson and Bishop, 2013; Bishop and Dobreva, 2017; Bishop and Houser, 2016; Bishop et al., 2018). Skyview factor is computed to maximum distance of 10 km in 1° steps. In order to avoid aggregating values where there is minimal relief at high altitudes, skyview factor is averaged for all stream cells within each basin.

- Slope sediment flux (Q_m), which is the modeled erosion rate assuming sediment transport is

dominated by diffusive processes (Tucker and Bras, 1998; Roering et al., 1999; Montgomery, 2001; Montgomery and Brandon, 2002; Roering et al., 2007; DiBiase et al., 2010; Tucker and Hancock, 2010). This study utilizes 45° as the critical threshold slope angle and assumes that slopes steeper than 40° do not contribute significantly to diffusive sediment flux, being more prone to erosion by other mass movement processes. Sediment flux is scaled by an empirical coefficient, K, which is dependent on climate and geologic conditions, which are not well-constrained in this study. The general relationship between measured and modeled erosion rate is more important than the magnitude of modeled erosion rate in this study, however, so the value of K is largely irrelevant. The K coefficient is set to 10^{-2}. The surface slope sediment flux is scaled to the interval [0,1] for the entire study area and then averaged for each basin.

- Hillslope relief-based sediment flux (Q_h), which is similar in theory to Q_m, though perhaps less sensitive to DEM resolution (Montgomery and Brandon, 2002). The same coefficients used for Q_m are used for Q_h.

- Stream power law river incision (Q_s), which is the modeled erosion rate assuming the area of accumulated flow and slope-angle are sufficient to model average stream discharge (Tucker and Bras, 1998; Whipple, 2004; Tucker and Hancock, 2010; Gasparini and Brandon, 2011). The stream power law depends upon empirical coefficients, K, m, and n, which are related to the climate and geologic conditions of the study area. The general relationship between measured and modeled erosion rates is of interest to this study, however, rather than the magnitude of modeled erosion rate. This study assumes $K = 10^{-8}$, $m = 0.5$, and $n = 1$, assuming that the m and n coefficients in Stock and Montgomery (1999) and Gasparini and Brandon (2011) are broadly representative for any basin where conditions are not well-constrained. The modeled river incision rate is then scaled to the interval [0,1] for the entire study area, and averaged for each basin.

- Chi index (χ), which is an empirical index that integrates the accumulated flow across a

basin's drainage network and appears to be proportional to erosion rate (Perron and Royden, 2013; Mudd et al., 2014; Yang et al., 2015; Struth et al., 2017). The magnitude of χ depends on the ratio of reference flow-accumulating area and local flow-accumulating area; this study uses a reference area of 1 grid cell (900 m^2). Yang et al. (2015) introduce a precipitation rate parameter, but the spatial variability of precipitation rate in the study area in not known and so is ignored in this study, effectively by setting the ratio of the reference precipitation rate to precipitation rate to 1.

- The mean depth of high failure potential ($d_{\Phi=0.75}$), which is the depth at which failure potential due to topographic load is equal to 0.75 (after Moon et al., 2017, ; Fig. 4.3). Failure potential is the normalized ratio of principal stresses, such that:

$$\Phi = \left| \frac{\sigma_1 - \sigma_3}{\sigma_1 + \sigma_3} \right|, \tag{4.4}$$

where σ_1 and σ_3 are the most and least compressive principal stresses (St. Clair et al., 2015; Moon et al., 2017). Principal stresses are computed using a two-dimensional finite boundary element model using the methods of Martel and Muller (2000) and Slim et al. (2015), which are based upon the TWODD method of Crouch and Starfield (1983). The TWODD model was developed to model stress partitioning around (cohesionless) fractures. Martel and Muller (2000) and Muller and Martel (2000) adapted the TWODD model for topographic stress conditions, and Slim et al. (2015) expanded the model to account for arbitrary topography. This study treats the topography as a homogeneous medium with mechanical properties similar to fine-grained sedimentary rocks, such as might be found in the sandstones, shales, and carbonates that underlying the study area (Calkins et al., 1975; Kamp et al., 2008). Specifically, rock density is set to 2600 kg m^{-3}, Poisson's Ratio to 0.30, and Young's modulus to 20 GPa (e.g., Beer et al., 2006; Xu et al., 2016). This study also ignores horizontal stress, specifically aiming to understanding the relationship between stresses due to topographic load and erosion without emphasis on the magnitude

of that relationship. St. Clair et al. (2015) demonstrated that a relationship exists between topographically-induced stresses and near-surface fracturing using geophysical methods.

The use of terrain units enables structural characterization not afforded by statistical reduction alone by exploiting such properties as terrain unit size, shape, and topology. Terrain-unit characteristics are mathematically represented using the equations in Table 4.2. Specifically, the terrain-unit parameters utilized in this study are:

- Slope facet area (A_{SF}), as large slope facets suggest prominence of threshold slopes associated with rapid erosion. For each basin, the area of all slope facets with at least 50% overlap with the basin is averaged.

- Slope facet surface area ($A_{s,\mathrm{SF}}$), which integrates the vertical dimension into the terrain unit's measurements in a manner that is related to both relief and surface exposure to weathering and erosive agents. Surface area is anticipated to have a positive relationship with erosion rate. The surface area for slope facets with at least 50% overlap with the basin is averaged.

- Slope facet surface area ratio ($A_{\mathrm{SF}}/A_{s,\mathrm{SF}}$), which is a measure of normalized inverse relief. Slope facets with smaller ratios have greater relief and are more likely to contribute to erosion by gravity-driven processes. The surface-area ratio is averaged for all slopes with at least 50% overlap with the basin.

- Slope facet slope angle (θ_{SF}), which is related to patches of the land surface where rapid erosion occurs by diffusive or gravity-driven processes. A slope facet's slope angle is computed as described using the Shary et al. (2002) method, but using the natural extent of the terrain unit as a constraint rather than a fixed computational window size. For each basin, the slope angle of all slope facets with at least 50% overlap with the basin are averaged. The fraction of slope facets that exceed 40° is also counted for each basin ($f\theta_{\mathrm{SF}}$), as a proxy for erosion by landsliding or non-diffusive slope erosion.

- Stream slope (θ_s), which is related to stream power. Stream slope is averaged for each basin.

- Drainage density (D_d), which is related to landscape dissection and erosivity (Tucker and Bras, 1998; Oruonye et al., 2015; Sangireddy et al., 2016).

- Bifurcation ratio (R_b), which is related to the degree of geological control on a basin's hydrological structure (Wilson et al., 2012; Oruonye et al., 2015). Strong geological control suggests faults and folds, and potential for differential erosion associated with those structures. The average bifurcation ratio is determined for each basin.

- Basin length (L_B), which is associated with the length or size of the transport corridor associated with the basin. This parameter is defined in Bhat et al. (2013) and Różycka and Migoń (2021) as the maximum planimetric distance between the basin's outlet and any point on its perimeter, and is used for calculating a basin's elongation ratio. This study examines this parameter as a representation of basin scale.

- Basin planimetric area (A_B), as larger basins exhibit more potential erodible area. This parameter is used to evaluate basin scale in relation to beryllium-10 concentration and erosion rate.

- Basin surface area ($A_{s,B}$), which integrates the vertical dimension into the basin's area measurement in a manner that is related to both relief and surface exposure to weathering and erosive agents. Surface area is anticipated to have a positive relationship with erosion rate.

- Basin surface area ratio ($A_B/A_{s,B}$), where lower values are related to greater relief and area exposed to erosive agents.

- Relief (Δz), or the basin's altitude range. Relief is, in itself, a minimum approximation of the amount of relief that has been produced by the coupling of tectonic uplift and erosive processes. Furthermore, high relief is often accommodated with steep slope angles that are more prone to failure, diffusion, and fluvial transport. Basins relief is therefore expected to have a positive relationship with predicted erosion rate.

- Hypsometric integral (H_I), which has been thought to be related to the degree of dissection in a basin, and related to the degree at which a basin may be above base-level and at disequilibrium with its environment (Pike and Wilson, 1971; Bhat et al., 2013; Wani et al., 2020).

- Circularity ratio (C), or shape-compactness index, which is a measure of the degree to which an object's shape is similar to the shape of a circle. Low basin circularity is associated with high tectonic activity, rapid uplift, and consequent geologic control on basin morphology and rise above base-level (Różycka and Migoń, 2021).

- Elongation ratio (E), which is related to the degree of tectonic activity and associated geologic control on basin structure (Bhat et al., 2013; Różycka and Migoń, 2021).

- Distance-isotropy (I_x), which is the ratio of the area occupied by an adjusted radial-distance signal to the area of an isotropic signal. Distance-isotropy is computed as follows:

    1. In each direction φ from the basin centroid, identify the greatest planimetric distance, $x(\varphi)$, to the perimeter of the basin.
    2. Let the middle-distance be $x_{\text{mid}} = (\max x + \min x)/2$. For each direction φ, set $x(\varphi) = x_{\text{mid}} - |x(\varphi) - x_{\text{mid}}|$. That is, if x_{mid} represents the radius of the isotropic signal, every point on the signal is adjusted to be equal to or less than isotropic.
    3. Compute the area of the radial signal as the sum of the areas of the triangles between each φ, then divide the signal area by πx_{mid}^2.

    This study evaluates every direction with a step size of 1°. Distance-isotropy is fundamentally a scale parameter that characterizes the degree of planimetric direction-dependence within the basin. In practice, it aims to characterize similar patterns as the circularity ratio and elongation ratio: an anisotropic distance-signal suggests geological controls on basic structure and differential erosion associated with accompanying geologic structures.

- Relief-isotropy (I_R), which is the ratio of the area occupied by an adjusted radial-relief signal to the area of an isotropic signal. This is computed as distance-isotropy, but $x(\varphi)$ is instead the difference between minimum and maximum altitude within the basin area in that direction. Because this measure of isotropy is tied to the basin's relief structure, is should more accurately characterize a basin's morphodynamics: Strong relief anisotropy suggests a direction-dependent fabric of ridge height and valley depth associated with the magnitude of erosion operating within the basin.

4.4.5 Cosmogenic Nuclide and Erosion Rate Prediction Models

Muons and neutrons continuously and isotropically bombard the Earth's surface, occasionally causing spallation in the quartz crystals and creating cosmogenic nuclides. This increases the concentration of beryllium-10 in quartz grains at a predictable rate. The concentration of beryllium-10 is, therefore, inversely proportional to the rate at which it is exposed, weathered, transported, and stored where it is sampled (i.e., erosion). A sample of quartz grains sampled from a stream is assumed to be representative of the average eroded quartz in the catchment that contributes to sediment flux through the sample point (Lal, 1991; Saha et al., 2015). Estimation of basin-wide average erosion rates utilizing beryllium-10 concentrations requires knowledge of the average production rate in the basin, which is a function of the activity of the cosmogenic nuclide, latitude (or strength and inclination of the geomagnetic field), altitude (atmospheric depth), and (topographic) shielding (Lal, 1991; Stone, 2000; Dunai, 2000, 2001; Codilean, 2006; Desilets et al., 2006; Balco et al., 2008).

The production rate of cosmogenic nuclides are notably spatially and temporally variable, and particles are continuously irradiated as they are transported. Exposure-age dating and erosion-rate estimates consequently depend heavily on assumptions that the model parameters and the erosion rate are constant through time or represent a temporal mean that is sufficiently representative of long-term conditions (Lal, 1991; Dunai, 2001; Desilets et al., 2006; Balco et al., 2008). Numerous techniques based on these assumptions have been found to be robust in a range of topographic settings, including the Himalaya (Granger et al., 1996; Schaller et al., 2001; Vance et al., 2003;

Saha et al., 2015). Diverse models for predicting cosmogenic nuclide production rates are all broadly based on the methods of Lal (1991) and Stone (2000), but differ in terms of how production rates scale with altitude and secular variation (Dunai, 2000, 2001; Desilets et al., 2006; Balco et al., 2008). This study utilizes the scaling method of Stone (2000) because it appears to be the least prone to error for beryllium-10 (Balco et al., 2008).

Cosmic rays are attenuated by interacting with the atmosphere, so mean annual atmospheric pressure stands as a proxy for atmospheric depth. This study uses the ICAO Standard Atmosphere as represented in Balco et al. (2008), such that:

$$P_{\text{atm}}(z) = P_{\text{atm,0}} e^{-\frac{gM}{R\epsilon}[\ln T_0 - \ln(T_0 - \epsilon_l z)]}, \tag{4.5}$$

where $P_{\text{atm,0}}$ is atmospheric pressure at sea level (1013.25 hPa), T_0 is mean sea level temperature (288.15 K), ϵ_l is the adiabatic lapse rate (0.0065 K m$^{-}1$), g is acceleration due to gravity, M is the molar weight of air, and R is the gas constant, such that $\frac{gM}{R} = 0.03417$.

A geographic scaling factor for nuclide production by neutron spallation is then calculated as:

$$S_{sp}(\lambda, z) = a + be^{-P_{\text{atm}}(z)/150} + cP_{\text{atm}}(z) + dP_{\text{atm}}(z)^2 + eP_{\text{atm}}(z)^3, \tag{4.6}$$

where a, b, c, d, and e are coefficients derived from between index latitudes (λ) in the scaling equation coefficients table of Stone (2000) via linear interpolation to avoid overshooting as per Balco et al. (2008).

Scaling due to production by muons is calculated as:

$$S_{\mu}(\lambda, z) = \frac{M_0[1013.25 - P_{\text{atm}}(z)]}{242}, \tag{4.7}$$

where M_0 is a coefficient derived by linear interpolation from the scaling equation coefficients table of Stone (2000).

The production rate of beryllium-10 is then computed as:

$$P_{\mathrm{Be}}(\lambda, z) = P_0 S_t (f_{sp} S_{sp}(\lambda, z) + (1 - f_{sp}) S_{\mu}(\lambda, z)), \tag{4.8}$$

where P_0 is a reference production rate for beryllium-10 (4.96 atoms g^{-1} yr^{-1}; Balco et al., 2008), S_t is a scaling factor to account for topographic shielding (this study uses skyview factor; Yokoyama et al., 2002; Wilson and Bishop, 2013; Bishop and Dobreva, 2017; Bishop et al., 2018), f_{sp} is the fraction of production due to neutron spallation (assuming 0.978, as per Balco et al., 2008). Balco et al. (2008) also include a scaling factor for sediment thickness, but this is ignored in this study because samples were collected from the surface in stream beds and because cosmogenic production is only being modeled at the surface (cover thickness = 0). An additional muon-production term is ignored for the same reason. Once production rate is predicted, it can be averaged for the entire basin area and used to estimate a basin-average erosion rate using Eq. (4.3), assuming a rock-penetration depth for regolith (100 cm).

4.4.6 Statistical Analysis and Topographic Modulation

Because basin interiors are spatially heterogeneous, we wish to more accurately predict the concentration of cosmogenic nuclides at any given location given the modeled production rate. A specific and accurate prediction in terms of magnitude may not be possible in this study given the limitations of sample size and geographic diversity, but some trends may be discovered that demonstrate the possibility for topographic modulation with respect to geomorphometric variables.

First, we produced scatter plots to identify outlier samples and to examine apparent relationships between erosion rate and the parameters produced for this study (NDVI and the parameters detailed in Tables 4.1 and 4.2), as well as between the measured beryllium-10 concentrations and the same parameters. We then evaluated the strengths of those relationships using Pearson's product-moment correlation test in R software, using $\alpha = 0.05$ and $\alpha = 0.01$ as our significance levels. If a nonlinear relationship seems apparent, we also log-transformed parameter values to increase linearity. We also note the sign of relationships to help assess if they are relevant and can be explained.

Second, we utilize land-surface parameters to modulate cosmogenic production rate and assume reasonable average effective exposure times to predict the beryllium-10 concentration measured at the mouths of the studied basins, such that:

$$C_{\text{Be}} = M_t t_e P_{\text{Be}}, \tag{4.9}$$

where M_t the scaling coefficient for topographic modulation, and is applied on each grid cell rather than applied based on basin averages, as the topographic factors are location-dependent. Note that M_t may be perceived as either scaling the production rate or scaling the effective exposure time. That is, higher erosion rates associated with certain land-surface parameters effectively reduce cosmogenic isotope production because of shorter particle residence time under the conditions associated with those locations. Areas that have experienced recent landsliding might be associated with a positive M_t to address violations of the steady-state assumption noted by von Blanckenburg (2005), but this study focuses on erosion effects that would decrease effective nuclide production, so M_t is made a scaling factor in the interval [0,1].

We evaluate 7 different scenarios for computing M_t:

1. No modulation ($M_t = 1$).

2. Modulation using slope ($M_t = \cos\theta$). Slope has the strongest relationship to erosion rate and is employed in nearly every erosion model due to its clear relationship to gravity-controlled sediment flux (Ahnert, 1970; Roering et al., 1999; Turcotte and Schubert, 2002; Sklar and Dietrich, 2004; Whipple, 2004; Tucker and Hancock, 2010; Bishop et al., 2020).

3. Modulation using hilltop and stream curvature ($M_t = 1 - |K_{\text{mean},r,s}|$). Hurst et al. (2012) identified a positive relationship between hilltop curvature and erosion rate, and Moon et al. (2017) identified a negative relationship between mean curvature and the depth of intense fracturing. We represent these relationship by identifying the locations of the nearest bounding ridge and stream using the same method to characterize hillslope relief and taking the average of the absolute value of mean curvature at both locations.

4. Modulation using the diffusive sediment flux model ($M_t = 1 - Q_{m,\text{norm}}$). Diffusive sediment flux on hillslopes *is* modeled erosion rate and incorporates the slope parameter. Q_m is normalized to the maximum possible flux given the maximum slope used to represent diffusive slopes in this study (40°; steeper slopes use $M_t = 1.0$).

5. Modulation using the stream power sediment flux model ($M_t = 1 - Q_{s,\text{norm,Ba}}$). Stream power law sediment flux is modeled erosion rate and inherently incorporates the slope parameter. Unlike Q_m, Q_s has no definable maximum, as it scales with the size of the area contributing flow, so is normalized to the range of Q_s in each basin and is only applied to stream locations (non-stream locations use $M_t = 1.0$).

6. Modulation using the combination of diffusive and stream power flux models ($M_t = 1 - \max(1, Q_{m,\text{norm}} + Q_{s,\text{norm,Ba}})$). Hillslope and stream sediment flux are scaled independently as in the Q_m and Q_s scenarios, respectively, and are then combined and capped to 1.0.

7. Modulation using the depth of intense fracturing from modeled topographically-induced stress ($M_t = 1 - \frac{d_{\Phi=0.75}}{400}$). Deep zones of high failure potential, which have been correlated to high fracture intensity using geophysical methods (St. Clair et al., 2015), are more susceptible to weathering and erosion. This study normalizes fracture depth by dividing by an arbitrary 400 m, which exceeds the maximum depth predicted throughout the study area.

We then determine the degree of correlation between measured beryllium-10 concentrations and modulated production rate using Pearson's product-moment correlation test. An average effective exposure age may then applied to modulated production rate to estimate the beryllium-10 concentration for each basin for each modulation scenario. The relationship between each predicted beryllium-10 concentration and measured beryllium-10 concentration is the same as the relationship between production rate and measured beryllium-10 concentration, scaled linearly by the assumed averaged effective exposure age, so new information is not obtained by computing it for this study.

4.5 Results

4.5.1 Terrain Units and Land-Surface Parameters

Though notable issues exist regarding the D8 method of extracting stream networks (Tarboton, 1997; Turcotte et al., 2001), the stream networks mapped in the study area appear to be reasonable representations of the drainage network. The density of these networks is different for each basin but, while that may be an important characteristic associated with a drainage basin's genetics and geodynamic function (e.g., Wilson et al., 2012; Oruonye et al., 2015; Sweeney et al., 2015; Sangireddy et al., 2016), the drainage density is controlled by the choice of an arbitrary threshold for extracting the stream network based on area accumulating flow. The 100-cell threshold used for this study was driven by a desire to represent streams in every basin, and the threshold was necessary to ensure that even the smallest basin evaluated in this study contained a portion of the stream network. This choice yielded visually dense drainage networks throughout the study area. It is unclear what effect the choice of threshold has on the characterizations of the studied basins, except that measures directly dependent on distance and direction to a stream are sensitive to the spatial distribution of low-order streams, including this study's method for measuring hillslope relief.

The basins studied for this area are of diverse size and shape (Fig. 4.4), ranging from about 0.5 to 190 km^2 and averaging between about 1100 to 1500 m in elevation. Almost all studied basins are elongated with a high degree of side-branching in the stream networks that they contain. Basins associated with samples Z-04 and Z-19 are notably asymmetric. The basin associated with sample Z-20 appears to be a general exception, having a mean altitude of 2430 m, being somewhat circular in shape and exhibiting a more or less symmetric relief structure and dendritic drainage pattern. The basin associated with sample Z-01 is the smallest basin and almost lacks any mapped streams, making it difficult to assess its internal structure, its morphology appearing to be almost entirely driven by slope processes.

The statistical distribution of slope-azimuth yielded 6 slope-azimuth classes in the study area by

the ISODATA algorithm rather than the target 8 classes (Fig. 4.4), reflecting the strong azimuthal fabric in the region's topography. Slope facet units visually highlight the strong slope-azimuth dichotemy between north-northeast-facing slopes and south-southwest-facing slopes. Visual interpretation of slope facet units also highlights asymmetry in larger basins and along the Jhelum River (Fig. 4.4).

The study area spans about 3 km of relief, from the valley of the Jhelum river to the highest peak in the east (Fig. 4.5A). Compared to the ranges east and west of the Jhelum River, the eminence wedged between the bend in the Jhelum River, coincident with the Main Boundary Thrust and Kashmir Boundary Thrust, appears to be of generally lower altitude. This wedge is also distinct in visualization of slope angle (Fig. 4.5B), where the surrounding mountains tend to exhibit higher slope angles in comparison. Slope angle also appears to effectively demarcate the Kashmir Boundary Thrust, even northwest of Muzaffarabad and the confluence of the Jhelum and Neelum rivers. The differences between mountainous zones and associations with geologic structures are not as readily apparent in visual inspection of mean curvature (Fig. 4.5C), though the general topographic grain of the region is highlighted in the orientation of high-curvature ridges. Skyview factor highlights prominent ridges, and dark areas are associated with steep and narrow features (Fig. 4.5D). The wedge of terrain between the Main Boundary Thrust and Kashmir Boundary Thrust generally exhibits high skyview coefficient values in comparison with the surrounding mountains, coincident with the lower altitude and gentler slopes that contribute to greater openness in that area.

4.5.2 Beryllium-10 Production Rate and Erosion Rate Predictions

The modeled production rate of Beryllium-10 ranges from about 3.5 to 95 atoms g^{-1} yr^{-1} in the study area. Production rate is highly spatially heterogeneous with maximum values along ridgetops and the lowest values in narrow valleys with steep slopes (Fig. 4.6). Areas of low altitude also exhibit relatively low production rate, including basins associated with samples Z-01, Z-04, Z-05, and Z-06. The basin associated with sample Z-20 appears to have the highest modeled production rate.

Measured beryllium-10 concentrations and calculated effective exposure age and erosion rate

are presented in Table 4.3. The average erosion rate predicted for the basin associated with sample Z-01 appears to be at least twice as rapid as that of any other basin (Figs. 4.7 and 4.8). This prediction is likely due to a combination of the basin's small size, lack of a developed drainage system, low modeled production rate, and lack of scaling factors to account for local slope processes. The basin associated with sample Z-04 also appears to be an outlier in terms of basin-scale metrics, including process parameters Q_s and χ (Fig. 4.7) and basin parameters L_B, A_B, and $A_{s,B}$ (Fig. 4.8). Consequently, sample Z-01 was generally omitted from statistical analysis, as was sample Z-04 for tests involving the scale of the basin.

4.5.3 Topographic Modulation and Statistical Analysis

There does not appear to be a strong correlation between NDVI or any of the land-surface or terrain unit parameters evaluated in this study (Fig. 4.4). Some parameters in erosion rate-geomorphometric parameter space appear to possibly include sample Z-01 along their trend. Mean curvature, drainage density, basin circularity, basin elongation, and log-transformed relief reach significant levels in relation to predicted erosion rate if Z-01 is included in the analysis (Table 4.4). With these "significant" treatments taken into account, mean curvature appears to have a negative relationship (p-value ≈ 0.01) with erosion rate, which is supported by the findings of Moon et al. (2017) that relates curvature with zones of intense fracturing. Drainage density also appears to have an inverse relationship with erosion rate (p-value = 0.0407), suggesting that greater erosion occurs where there are fewer streams in relation to hillslopes, which is usually associated with greater geologic control on basin structure which can in turn be associated with tectonic forcing (Oruonye et al., 2015; Sangireddy et al., 2016; Różycka and Migoń, 2021). The inverse relationship between basin relief and erosion rate is contradictory, suggesting that erosion is greater where less relief has been produced (by erosion) and there is less gravitational potential energy to drive erosion. The small sample size and inclusion of the apparently spurious Z-01 sample, however, makes the statistical significance of these relationships dubious. There does not appear to be a relationship between erosion rate and parameters reduced at the basin scale in this dataset.

If we evaluate land-surface and terrain-unit parameters against measured beryllium-10 concen-

trations, we find that sample Z-20 is the most prominent outlier in terms of beryllium-10 concentration, having approximately three times the concentration of beryllium-10 compared to any other sample (Figs 4.9 and 4.10). This is likely explained by the basin's high altitude 4.6, as beryllium-10 concentration and basin mean altitude are correlated ($R^2 = 0.89$ and p-value 0.0015; Table 4.5). Because sample Z-20 appears to be an outlier, however, it is omitted from most tests, and sample Z-04 is also omitted from tests with parameters that are dependent upon basin scale (Q_s, χ, L_B, A_B, and $A_{s,B}$). The only parameter that appears to be statistically significant under these constraints is basin circularity ($R^2 = 0.72$ and p-value 0.0329), which has an inverse relationship with beryllium-10 concentration, contrary to what was anticipated, as less circular basins are associated with greater tectonic or geologic control and associated weathering and erosion (Różycka and Migoń, 2021). If sample Z-20 is included in the test, relief-based diffusive sediment flux also appears to be positively correlated with beryllium-10 concentration (p-value = 0.0028), though this contradicts our understanding of how beryllium-10 concentration should develop: greater sediment flux should yield a lower cosmogenic nuclide concentration because sediment is removed more rapidly and would consequently not have been exposed to cosmic rays as long as sediment in a system with less sediment flux. Mean curvature, mean stream curvature, drainage density, and basin relief are all near-significant (p-values = 0.0587, 0.0894, 0.0881, and 0.0678, respectively) with a weak ($R^2 \approx 0.56$) positive relationship with beryllium-10 concentration (Table 4.5), but these suggest that basins that are generally convex (longer and broader hilltops than gullies or streams), have a dense drainage structure, and high relief may have contributed greater amounts of beryllium-10, suggesting lower erosion rates, which is contrary to the expected relationships.

Land-surface and terrain-unit parameters reduced at the basin scale were not significantly correlated to measured beryllium-10 concentrations or predicted erosion rates using the Stone (2000) method for modeling beryllium-10 production rates.

Though lacking a dataset of spatially dense field measurements of erosion rate and up-stream-averaged cosmogenic isotopes, we can explore the concept of modeling spatially continuous erosion rates based on cosmogenic nuclide production. For example, basin-averaged skyview factor

does not have a relationship with basin-average erosion rate or beryllium-10 concentration in our dataset, but skyview factor is applied locally as a scaling coefficient to the beryllium-10 production rate everywhere in the basin, effectively modulating beryllium-10 production on a local scale even though this is not reflected in the basin average.

A challenge in modeling spatially continuous erosion rate based on cosmogenic nuclide production is knowing what effective exposure age is appropriate at each location. We could assume one, given ~2 kyr seems reasonable based on the production rate-beryllium-10 concentration relationship (Table 4.3). There is a strong linear correlation between modeled beryllium-10 production rates and measured beryllium-10, however (p-value = 0.0006; Table 4.6; Fig. 4.12), and the units of the slope of that regression line is in units of time, about 6.3 kyrs. The exact meaning of this quantity is unclear, but may serve as a characteristic exposure time for the region, and be used to predict cosmogenic nuclide concentration from modeled production rates. This linear correlation holds with the diverse scenarios explored for topographic modulation (p-values $\leq$ 0.0333 ; Table 4.6).

The spatial patterns of modulated production rate (Fig. 4.12) are comparable to those of unmodulated production rate estimates (Fig. 4.6), though modulation by measures computed by searching for the nearest ridge or stream locations (curvature and depth of high failure potential) produce a less smooth spatial pattern due to the scale-dependent, and sometimes imprecise, nature of the approach. Valley floors are generally de-emphasized the most using modulation by the stream power law sediment flux model and by the depth of high failure potential, though the latter generally reduces production-rate spatial variation among low-order streams and ridges at high altitudes. The spatial distribution of the concentration of beryllium-10, assuming constant exposure age or that the modulation applies to the exposure age instead of production rate, is the same as that for modulated production rate shown in Fig. 4.12, multiplied by as assumed average effective exposure age. The erosion rate at any location would therefore be linearly proportional to the inverse of the beryllium-10 production rates and assumed concentrations, as per Eq. (4.3).

Because effective exposure age is a scalar, the transformations from mean modulated produc-

tion rate to a prediction of mean beryllium-10 concentration, or from mean beryllium-10 concentration to mean erosion rate is linear. The relationships represented in Table 4.6 are therefore also representative of the relationship between measured beryllium-10 concentration and modeled beryllium-10 concentration.

4.6 Discussion

4.6.1 Land-Surface Parameters and Terrain Units

Some measure of uncertainty always exists with the discrete classification of landforms in a geographic information system (GIS) (Burrough and Frank, 1996; Deng, 2007; Bishop et al., 2012, 2018, 2020). The spatial character of streams and basins will differ with the method used to represent flow direction (Tarboton, 1997; Zhou and Liu, 2002) as well as the threshold used to distinguish streams from the background topography, though some methods exist to evaluate this (e.g., Ozulu and Gökgöz, 2018). This research used a simple and accessible method in a popular GIS and selected a threshold that best suited the objectives of the study by assuring that every sampled basin represented some portion of the drainage network, but doing so raised questions regarding the uncertainty of the approach. Any technique that uses mapped streams, including the identification of ridges, computation of hillslope relief, and modeling of topographic stress, is strongly dependent on the density of the stream network, which is directly influenced by the choice of threshold on the area contributing flow to any given location. The exact nature of this influence is unclear, except that the effects of topographic load are likely to be under-estimated because relatively less-prominent ridges between low-order streams are being identified as the ridges bounding the system, which may not be accurate. Future research should consider the impact of drainage density on stream network and adjacent slope characterization as it relates to the spatial scale of topographic features and phenomena being observed, which may be spatially variable.

Slope facets have notably uncertain boundaries because they are dependent on the statistical distribution of slope-angle and slope-azimuth angles in the dataset, which will be different for a

subset of those data, data representing a larger area, data at a different spatial resolution, and so forth. The collapse of two slope-azimuth classes into their adjacent classes, resulting in 6 slope-azimuth classes rather than the targeted 8, may not occur with other datasets overlapping the study area, or, if ISODATA is initialized with random class centers, then it may become impossible to exactly replicate another study's slope facets. A greater number of slope-azimuth classes will tend to reduce the average slope facet size and alter topological characteristics. Slope facets were generated as a representation of important components of the hillslope, but a more consistent or deterministic method of representing them would benefit future research that wishes to evaluate the structure of systems with threshold slopes.

We noted distinct differences in altitude, slope, and skyview factor parameters in a wedge of terrain bounded by the Jhelum River and major regional structures compared to those of the surrounding mountains. This suggests a strong geologic control on the topographic structure of these regions, which should also impact the erosion dynamics of the studied basins. Our dataset does not support any conclusion on what those causal factors are, but may explain our general lack of significant correlations between basin-averaged land-surface and terrain-unit parameters with erosion rate and beryllium-10 concentration. Future studies may wish to conduct careful investigation of topographic structure prior to sampling for better control on factors contributing to basin geometry and erosion dynamics. Otherwise, the spatial distributions of terrain-unit characteristics and land-surface parameters provide helpful insight related to the nature of spatially heterogeneous erosion in a region: slope-facets are particularly useful for interpreting topographic grain and basin asymmetry (Fig. 4.4), and slope angle and the skyview factor are useful in identifying the locations of major geologic structures and highlighting where process rates should potentially be high (Figs. 4.5B, D).

Given the exceptionally small sample size (governed by difficult logistics and time for field-work), we lack the statistical rigor to establish any conclusive evidence of topographic property control on erosion rate or the production of cosmogenic nuclides, but we are able to raise some interesting points and pose questions that need to be addressed in future research. There lacks a sig-

nificant correlation between geomorphometric parameters with either of erosion rate or beryllium-10 concentration (Tables 4.4 and 4.5) when averaged basin-wide, yet geomorphometric parameters (slope and mean curvature) and modeled parameters (diffusive sediment flux, modeled stream power law river incision, and predicted fracture depth based on modeling stress due to topographic load) are significant when applied locally prior to being averaged for each basin (with p-values $\leq$ 0.0333; Table 4.6). This dichotomy suggests that topographic process-form relationships are best evaluated at the scale at which those processes occur before they are aggregated up the topographic spatial hierarchy to the scale at which phenomena of interest can be feasibly field-validated. Further research with a larger sample size may be able to address this aspect of scale-dependence, including spatially frequent *in situ* sampling of cosmogenic isotopes within a basin among diverse topographic conditions in comparison to basin-average measurements, with care taken to account for factors related to lithology, tectonics, climate, and topographic structure.

The basins evaluated in this study are diverse in size, though significant relationships were not found between basin-scale parameters and erosion rate. This may be due to this study's small sample size, but DiBiase et al. (2010) also showed a lack of correlation between basin size and average erosion rate with a much larger sample size. They note, however, that their study was not designed to test that hypothesis, and others have identified some sort of scale-dependency (Syvitski and Milliman, 2007). It would be surprising that there would be no scale-dependency given that some of the most prominent metrics for simulating topographic evolution and evaluating erosion rate are dependent upon a measure of upstream area (Whipple, 2004; Tucker and Hancock, 2010; Struth et al., 2017). Perhaps cosmogenic nuclides are mostly or almost entirely contributed by slopes, as they reach higher altitudes and therefore are more exposed to cosmic rays than streams (Fig. 4.6), and may have longer residence times than particles transported by water. Landsliding and rockfalls can also bias erosion rate estimates based on cosmogenic nuclides, and it may be that the basins evaluated in this study and those evaluated by DiBiase et al. (2010) were strongly influenced by these processes. If not by mass wasting, a stream that incises more deeply because its discharge is supported by a larger watershed should incur a response of accelerated slope failure to maintain

threshold slopes above the rapidly incising stream, enforcing the scale dependency on erosion rate. Further research is required to better understand the scale dependence or independence of basin erosion dynamics, with a sufficiently large or specific sample population to account for lithologic, tectonic, biologic, and climate variables in addition to basin hierarchy (i.e., how do erosion factors change with nested sub-basins or when sampled repeatedly along the length of a stream?). Such research would also directly investigate the assumption of minimal within-basin sediment storage (von Blanckenburg, 2005), as particle irradiation from source to sample location should be strongly dependent on hillslope length and transport rates on those slopes.

Numerous other characters of the topography and its spatial structure have also not been evaluated in this study, and future studies may wish to explore other aspects topographic structure. For example, we noted the high degree of side-branching in some basins, yet this was not evaluated in this study. We also did not evaluate the properties of eminences overlapping the studied basins, including their relief, shape, and structural complexity (e.g., number of sub-eminences and peaks), which should have a profound relationship with stress fields due to topographic load and associated zones of intense fracture (Slim et al., 2015; Moon et al., 2017) and with climate due to orogenic moisture capture and deflection (Roe et al., 2002; Archer and Fowler, 2004). The relationships between factors causing or abetting erosion and geomorphometric parameters also need to be better understood. Failure potential due to topographic stress, for example, has been related to surface curvature (Moon et al., 2017), but there exists no model to relate the two, nor to relate near-surface fracture intensity to erosion rate. New land-surface parameters may capture some of these relationships, including rain shadow (if mean climate conditions are known), orientation and intensity of the topographic grain (e.g., Roy et al., 2016; Newman et al., 2018), curves or abrupt changes in drainage orientation or profile (Mudd et al., 2014; Gray et al., 2018; Jaiswara et al., 2019; Struth et al., 2019), measures of planarity of homogeneity that could help to characterize zones of mass wasting (Wu et al., 2000; Xiao et al., 2013). The spatial topological characteristics associated with different terrain units such as eminences, basins, ridges, slope facets, and river terraces may provide additional insights and provide much-needed spatial context to this type of

analysis, such as a planar slope facet on a high-relief eminence with either hummocky topography located below the planar slope facet and/or a stream in a V-shaped valley, collectively indicating a high likelihood of landslide or debris flow, regardless of the local slope angle or soil-moisture proxies (Tucker and Bras, 1998; Tucker and Hancock, 2010). This requires significant research for semantically modeling terrain units, establishing rules for linking terrain units in a topological network framework, and exploring the characteristics of these networks as they relate to mountain geodynamics.

4.6.2 Topographic Modulation of Cosmogenic Nuclide Production Rate for Estimating Erosion Rates

Using GIS methods to model cosmogenic nuclide production and predict erosion rates has been proven an effective way to evaluate average erosion conditions in numerous terrestrial environments (e.g., Granger et al., 1996; Schaller et al., 2001; von Blanckenburg, 2005; Codilean, 2006; Bishop et al., 2020; Różycka and Migoń, 2021). Cosmogenic nuclide production models presently only account for topographic factors in terms of those necessary to scale production rate by atmospheric depth or to characterize the degree of hemispherical shielding. In general, this appears to sufficient, as this study finds a significant linear relationship between modeled beryllium-10 production rate and measured beryllium-10 concentration without modulation (R^2 = 0.92 and p-value = 0.0006; Table 4.6), though our sample size is far too small to be conclusive on this point. Further research using a greater sample size may reveal the presence of nonlinear relationships, or that certain types of topographic modulation produce more linear or significant relationships than others, indicating that topographic control caused by erosion dynamics govern average basin cosmogenic isotope concentrations. Slope angle may help to explain more variation in the production rate-nuclide concentration, however, not only because slope angle is associated with gravitational and diffusive slope processes, but also because slope angle represents some degree of localized topographic self-shielding that may not be captured in the more general mesoscale topographic shielding, or represents additional surface area exposed to cosmic radiation. We also identified significant relationships using hilltop and stream curvature and modeled diffusive sediment flux,

stream power river incision, and depth of high failure potential for modulating beryllium-10 production rates. A best-practice modulation approach should be investigated for more accurate erosion rate characterizations, or even possibly a preliminary prediction of beryllium-10 concentration that may reduce uncertainty in erosion predictions using remote sensing and GIS techniques.

The linear relationship between production rate and beryllium-10 concentration is interesting, as the slope of that relationship is in units of time. We interpret this quantity to represent a characteristic exposure time to cosmic rays, though, if so, this characteristic exposure time tends to be about three to six times greater than the effective exposure time modeled according to Eq. (4.3), depending on the modulation method (compare tables 4.3 and 4.6). What is the relationship between this characteristic time and basin-average effective exposure times? What is implied by a non-zero intercept for this functional relationship? Further research with a larger sample size should evaluate this relationship across different scales, lithologies, and climate conditions to determine if it is truly an empirical relationship, or characterizes various forcings and/or processes. If a linear relationship can extend in space and time, then beryllium-10 concentrations can be predicted by knowing or assuming some characteristic timescale. This then begs the questions as to how a characteristic timescale might be discerned in relation to the magnitude and distribution of erosion rates, and the degree of timescale spatial scale-dependence. If topographic modulation can be used to more accurately characterize cosmogenic nuclide production rates in the context of surface processes, and if a characteristic timescale can be discerned with remote sensing data, then erosion rates may be accurately assessed using geospatial data and spatial analysis and modeling.

A few basins might be used to establish a characteristic timescale for a region where the lithology is relatively homogeneous, but numerous factors introduce theoretical complications to this notion. Specifically, production rates are spatially and temporally dependent on numerous factors, including basin-scale morphometrics, local-scale morphometrics, landscape morphological evolution, tectonics, lithology, biota, climate forcing, and secular variation. Secular variation in the context of cosmogenic radionuclides is particularly of concern in the geomorphological community because it is not well constrained, and a key criticism of techniques that propose to leverage it

for cosmogenic radionuclide production rate estimation (e.g., Balco et al., 2008). Furthermore, if the effective production rate of cosmogenic radionuclides is strongly impacted by basin morphology, and if that morphology evolves significantly over the relevant timescale (e.g., a few thousands years; Tables 4.3, 4.6), then a reconstruction of past topography, in context with other temporally variant factors (e.g., paleoclimate, geomagnetic field variation) is also necessary to predict nuclide concentration. More knowledge on this aspect of landscape evolution dynamics will therefore depend on tests of the steady-state and minimal storage assumptions in cosmogenic radionuclide studies (von Blanckenburg, 2005). It is unclear how significant these factors influence erosion estimates, however, given that cosmogenic radionuclide methods have been found to be robust even in very dynamic Himalayan environments (Granger et al., 1996; Schaller et al., 2001; Vance et al., 2003; Saha et al., 2015), and additional research is required to characterize the sensitivity of effective nuclide production to landscape morphology.

4.7 Conclusion

The main objective of this research was to explore aspects of topographic properties and spatial structure as they relate to cosmogenic isotope production and basin-average erosion rates. Our principal finding is that basin-averaged land-surface and terrain-unit parameters do not correlate well with predicted erosion rate or measured beryllium-10 concentrations with our dataset, but that topographic modulation of modeled beryllium-10 production on a per-grid-cell basis does establish statistically significant correlations with measured beryllium-10 concentrations. Furthermore, we identified a strong linear relationship between modeled beryllium-10 production rate and measured beryllium-10 concentration, where the slope of that regression line is in units of time and may represent a regional characteristic exposure age or timescale which, in conjunction with modeled cosmogenic nuclide production rates and topographic modulation, might be used to predict beryllium-10 concentrations anywhere in a basin.

We used simple and accessible methods for representing the land surface with terrain units, and the resultant drainage network, basin structure, and slope-attitude representation appear to be effective at representing these aspects of topographic structure and lend themselves well to visual

interpretation of the land surface (Fig. 4.4). We encountered issues that introduced uncertainty into our analysis associated with the empirical or arbitrary selection of thresholds for extracting the stream network, and the method of dividing the topography into slope-steepness and slope-azimuth classes for generating slope-facet units, which depends on the scale-dependent statistical distribution of topographic parameters. More robust characterizations of the drainage network and partitioning of the land surface based on slope attitude should reduce uncertainty and increase study replicability and applicability of these important components of topographic structure.

Visual interpretation of geomorphometric parameters, particularly slope angle and skyview factor, was useful for recognizing zones of distinct geologic control. Cosmogenic modeling provided visual confirmation and insight into the degree that altitude controls cosmogenic isotope production. Because beryllium-10 samples are representative of basin-scale conditions, we averaged geomorphometric parameters for each basin for comparison to predicted erosion rates and measured beryllium-10 concentrations, but did not find relationships that were significant and could be explained, except for a positive relationship between mean altitude and beryllium-10 concentration which was expected. We conclude that our sample size is too small to make any definitive statements regarding basin-averaged geomorphometrics in comparison with erosion rate and beryllium-10 concentration.

Although significant correlations between geomorphometric parameters and predicted erosion rates and measured beryllium-10 concentrations were not found, there is a significant correlation between topography-modulated beryllium-10 production rates and measured beryllium-10. This suggests that although geomorphometric parameters cannot explain the variance in basin-average erosion rates or measured beryllium-10 concentrations when reduced at the basin scale, they do have a significant relationship with measured beryllium-10 concentrations when applied at the local scale. This suggests that topographic modulation has the potential to be used to predict beryllium-10 concentrations throughout a basin if a characteristic exposure age could be determined for a region, which we interpret to be the slope of the regression line between beryllium-10 production rate and beryllium-10 concentration. Future research should explore this concept because, if a

relationship between basin-average cosmogenic nuclide concentration and production rate can be established, it could be used for estimating cosmogenic nuclide concentrations at any location. If both cosmogenic nuclide concentrations and production rates can be modeled, then erosion rates based on cosmogenic isotope theory might be inferred by remote sensing alone, opening up new options for erosion prediction for very large datasets in challenging locations.

This work represents preliminary research regarding the investigation of functional relationships between topographic properties, erosion rates, and cosmogenic nuclides. Larger sample sizes will help to determine if such relationships are linear or non-linear given the coupled dynamics of erosion involving climate, topography, surface processes and tectonics. Given our findings, we recommend:

- Development of methods to characterize uncertainty in calculating topographic parameters that depend upon the drainage network, particularly as it relates to scale-dependencies associated with low-order streams (e.g., the effect on variation in hillslope relief).

- Development of methods to characterize the spatial uncertainty associated with the boundaries of land-surface classifications or objects partitioned using k-means, ISODATA, or other unsupervised method. The slope facet units utilized in this study are powerful landscape characterizations for assessing the size and orientation fabric of the topography, but are difficult to repeat or have different meaning within the context of a dataset with a different statistical distribution of slope-attitude parameters. Future research would benefit from a more deterministic method for extracting these objects.

- Investigation of the fast-transport, or minimal storage, assumption inherent in erosion studies based on cosmogenic nuclide production rates.

- Investigation of the scale-dependence of cosmogenic radionuclide methods for estimating erosion rate with a robust sample population that includes basins and sub-basins spanning and sampling along a stream's length, controlling for geologic and climate factors.

- Investigation of the relationship between cosmogenic nuclide production rate and nuclide concentration. The slope of that relationship is in units of time, and a better understanding of what this length of time means may facilitate location-dependent predictions of cosmogenic nuclide concentrations.

- A larger-scale investigation on the use of topographic parameters for modulation of local cosmogenic radionuclide production. Proper accounting for topographic parameters in cosmogenic nuclide production will facilitate accurate cosmogenic radionuclide concentration predictions at the basin and finer scales, and provide greater insight into erosion dynamics.

- Investigation into the usage of frameworks for representing the spatial topological structure of terrain units and their relationships to erosion processes and erosion rate estimates, including semantic modeling of terrain units, development of rules for relating terrain units topologically, and exploration of the properties of such topological structures in relation to erosion rates and causal mechanisms.

Tables

Table 4.1: Evaluated land-surface parameters that are relevant to erosion.

Parameter	Symbol	Equation	Relevance
Land-Surface Parameters			
Altitude	z	–	Climate forcing and cosmogenic nuclide production.
Slope	θ	$\tan^{-1}\sqrt{\left(\frac{\delta z}{\delta x}\right)^2+\left(\frac{\delta z}{\delta y}\right)^2}$	Gravitational forcing.
Hillslope Relief	h	$z_r - z_s$	Landscape dissection (Montgomery and Brandon, 2002).
Mean Curvature	K_{mean}	(Olaya, 2009)	Related to near-surface fracturing (Moon et al., 2017) and sediment flux (Hurst et al., 2012).
Skyview Factor	V_f	$\sum_{\varphi=0}^{2\pi}\cos^2(\varphi, r)\Delta\varphi/(2\pi)$	Relationship with steep or narrow features associated with rapid erosion (Wilson and Bishop, 2013; Bishop and Dobreva, 2017).
Process Parameters			
Slope Sediment Flux	Q_m	$\frac{K\tan\theta}{1-(\tan\theta/\tan\theta_c)^2}$	Sediment flux due to diffusive processes (Roering et al., 1999; Montgomery and Brandon, 2002).
Relief Sediment Flux	Q_h	$\frac{Kh}{1-(h/h_c)^2}$	Relief-based approximation of diffusive sediment flux (Montgomery and Brandon, 2002).
River Incision	Q_s	$KA_{\text{accum}}^m(\tan\theta)^n$	Stream power law incision rate (Whipple, 2004).
Chi Index	χ	$\int_0^x\left(\frac{A_0}{A_{\text{accum},x}}\right)^{m/n}\mathrm{d}x$	Proportional to erosion rate (Struth et al., 2017).
Depth of High Failure Potential	$d_{\Phi=0.75}$	(see text)	Topographic stress exacerbates weathering (St. Clair et al., 2015; Moon et al., 2017).

z_r is local ridge altitude, z_s is local stream altitude, φ is slope azimuth (after Shary et al., 2002), $\Delta\varphi$ is azimuth step-size, r is maximum search radius, K is a scaling coefficient, θ_c is the critical threshold slope angle, h_c is the critical relief, m and n are power-law coefficients (assumed to be 0.5 and 1, respectively, after Stock and Montgomery, 1999; Gasparini and Brandon, 2011), A_0 is a reference area (1 grid cell or 900 m^2), and $A_{\text{accum},x}$ is flow-accumulation area at up-stream distance x. This study computes χ for all stream cells as $\sum\left(A_0/A_{\text{accum}}\right)^{m/n}\Delta\bar{x}$, where $\Delta\bar{x}$ is the mean distance between stream cells, as per Perron and Royden (2013).

Table 4.2: Terrain-unit parameters that are relevant to erosion and evaluated in this study.

Parameter	Symbol	Equation	Relevance
Slope Facet Parameters			
Area	A_{SF}	–	Large slope facets associated with threshold slopes.
Surface Area	$A_{s,\text{SF}}$	(Jenness, 2004)	Relief and general exposure.
Surface Area Ratio	$A_{\text{SF}}/A_{s,\text{SF}}$	$A_{\text{SF}}/A_{s,\text{SF}}$	Normalized $A_{s,\text{SF}}$.
Slope	θ_{SF}	as θ (Table 4.1)	Rapid erosion on steep slopes.
Drainage Network Parameters			
Slope	θ_s	as θ (Table 4.1)	Stream power.
Drainage Density	D_d	N_s/N_B	Related to landscape dissection and erosivity (Tucker and Bras, 1998; Oruonye et al., 2015; Sangireddy et al., 2016).
Bifurcation Ratio	R_b	$\sum_{i=0}^{N-1} \frac{R_{b,i}/R_{b,i+1}}{N-1}$	Higher values suggest greater geological control (Wilson et al., 2012; Oruonye et al., 2015) (i.e., differential erosion potential).
Basin Parameters			
Length	L_B	$\max x(pp, P)$	Size of the transport corridor.
Area	A_B	–	Erodible footprint.
Surface Area	A_s	(Jenness, 2004)	Relief and exposure.
Surface Area Ratio	$A_B/A_{s,B}$	$A_B/A_{s,B}$	Smaller values indicate more surface area to erode.
Relief	Δz	$\max z - \min z$	Minimum relief produced.
Hypsometric Integral	H_I	$(\bar{z} - \min z)/\Delta z$	High values suggest basin is generally above base-level.
Circularity Ratio	C	$4\pi A_B/P_B^2$	Low values associated with rapid uplift and drop in base level (Różycka and Migoń, 2021).
Elongation Ratio	E	$\frac{2\sqrt{A_B/\pi}}{L_B}$	Low values associated with tectonic activity (Bhat et al., 2013).
Distance-Isotropy	I_x	$A_{r,x}/A_{\circ,x}$	Anisotropy suggests geological controls and differential erosion.
Relief-Isotropy	I_R	$A_{r,R}/A_{\circ,R}$	Anisotropy suggests geological controls and differential erosion.

N_s is the number of stream cells, N_B is the number of basin cells, $R_{b,i}$ is the number of streams of order i, $x(pp, P)$ is planimetric distance between the basin pour-point and its perimeter, z is altitude, P_B is basin perimeter length, $A_{r,x}$ is adjusted radial planimetric-distance-based area of the basin, $A_{\circ,x}$ is isotropic radial planimetric-distance-based area of the basin, $A_{r,R}$ is adjusted radial relief-based area of the basin, and $A_{\circ,R}$ is isotropic radial relief-based area of the basin.

Table 4.3: Beryllium-10 measurements and calculations for samples in the study area.

Sample	Quartz Weight g	Be Carrier Weight g	$^{10}Be/^{9}Be$ $(\times 10^{-15})$	^{10}Be Concentration atoms mg^{-1}	^{10}Be Production* atoms g^{-1} yr^{-1}	Effective Exposure yr	Erosion Rate** mm yr^{-1}
Z-01	29.4488	0.4984	3.546 ± 0.487	5.437 ± 0.747	9.449	575 ± 79	0.869 ± 0.105
Z-04	29.3390	0.4619	18.644 ± 1.248	26.593 ± 1.781	13.048	2038 ± 136	0.245 ± 0.015
Z-05	29.7201	0.4639	19.554 ± 1.629	27.653 ± 2.304	9.657	2863 ± 239	0.175 ± 0.013
Z-06	29.3252	0.4610	9.014 ± 0.675	12.838 ± 0.962	9.368	1370 ± 103	0.365 ± 0.025
Z-17	15.3196	0.4151	10.254 ± 1.383	25.172 ± 3.395	13.194	1908 ± 257	0.262 ± 0.031
Z-19	29.1395	0.4208	15.704 ± 2.178	20.546 ± 2.850	10.814	1900 ± 264	0.263 ± 0.032
Z-20	24.6755	0.4285	62.214 ± 7.173	97.881 ± 11.285	22.492	4352 ± 502	0.115 ± 0.012

*Production rates were calculated using the method of Stone (2000).

**Erosion rates were calculated using the method of Lal (1991), assuming 100 cm as the penetration depth of cosmic rays in regolith.

Table 4.4: Regression line intercept (b) and slope (m) with Pearson's product-moment correlation coefficients (r) and significance results to test relationships with estimated basin-average erosion rate. Parameters are described in Tables 4.1 and 4.2, with parameter categories separated by a horizontal line. Omitted outlier samples are indicated in the comments column.

Parameter	b	m	r	t	p-value	comments
NDVI	0.0103	0.1441	0.1097	0.2207	0.8361	3/11/2009; omit Z-01
NDVI	-0.0047	0.4107	0.4067	0.8904	0.4236	9/19/2009; omit Z-01
$\bar{z}$	0.0831	-2.4E-5	-0.6896	-1.9043	0.1296	omit Z-01
$\bar{\theta}$	0.1084	-0.0024	-0.5098	-1.1851	0.3016	omit Z-01
$f\theta$	0.0555	-0.1665	-0.6586	-1.7505	0.1549	omit Z-01
$\bar{K}_{\text{mean}}$	0.0481	-0.7402	-0.0581	-0.1164	0.9129	omit Z-01
$\bar{K}_{\text{mean}}$	0.0610	-13.8526	-0.8872	-4.3006	**0.0077	
$\bar{K}_{\text{mean},s}$	4.0E-4	-0.0909	-0.3755	-0.8102	0.4633	omit Z-01
$\bar{K}_{\text{mean},s}$	-0.1358	-0.7242	-0.8642	-3.8400	*0.0121	
$\bar{h}$	0.0429	-0.0001	-0.6188	-1.5753	0.1903	omit Z-01
$\bar{V}_{f,s}$	-0.1828	0.2643	0.4566	1.0264	0.3627	omit Z-01
$\bar{Q}_m$	0.0942	-0.1622	-0.5007	-1.1567	0.3118	omit Z-01
$\bar{Q}_h$	0.0806	-0.9086	-0.6442	-1.6847	0.1673	omit Z-01
$\bar{Q}_s$	0.0525	-47.5717	-0.1490	-0.2610	0.8110	omit Z-01, Z-04
χ	0.0499	-5.4E-4	-0.1267	-0.2212	0.8391	omit Z-01, Z-04
$\bar{d}_{\Phi=0.75}$	0.0880	-0.0003	-0.5619	-1.3584	0.2459	omit Z-01
$\bar{A}_{\text{SF}}$	0.0813	-6.6E-6	-0.3431	-0.7305	0.5056	omit Z-01
$\bar{A}_{s,\text{SF}}$	0.0871	-6.8E-6	-0.4392	-0.9777	0.3836	omit Z-01
$A_{\text{SF}}/A_{s,\text{SF}}$	-0.2730	0.3530	0.3985	0.8690	0.4339	omit Z-01
$\bar{\theta}_{\text{SF}}$	0.0943	-0.0022	-0.3904	-0.8482	0.4441	omit Z-01
$f\theta_{\text{SF}}$	0.0616	-0.4502	-0.6161	-1.5644	0.1928	omit Z-01
$\bar{\theta}_s$	0.0786	-0.0020	-0.4597	-1.0353	0.3590	omit Z-01
D_d	0.1091	-1.2637	-0.5043	-1.1681	0.3077	omit Z-01
D_d	0.2738	-4.4802	-0.7751	-2.7429	*0.0407	
$\bar{R}_b$	0.0433	0.0026	0.0424	0.0849	0.9364	omit Z-01
L_B	0.0495	-0.0004	-0.0544	-0.0943	0.9308	omit Z-01, Z-04
A_B	0.0495	-0.0001	-0.0959	-0.1669	0.8781	omit Z-01, Z-04
$A_{s,B}$	0.0501	-0.0001	-0.1225	-0.2138	0.8444	omit Z-01, Z-04
$A_B/A_{s,B}$	-0.2125	0.2945	0.5452	1.3007	0.2632	omit Z-01
Δz	0.0656	-1.3E-5	-0.3886	-0.8435	0.4465	omit Z-01
$\ln \Delta z$	0.5803	-0.0731	-0.8271	-3.2909	*0.0217	
H_I	-0.0377	0.1912	0.6254	1.6028	0.1842	omit Z-01
C	0.0743	-0.0818	-0.2596	-0.5376	0.6194	omit Z-01
E	0.1035	-0.0911	-0.5222	-1.2246	0.2879	omit Z-01
I_x	0.0856	-0.0736	-0.6334	-1.6371	0.1769	omit Z-01
I_R	0.0448	0.0059	0.0377	0.0754	0.9435	omit Z-01

*=significant at $\alpha \leq 0.05$; **=significant at $\alpha \leq 0.01$

Table 4.5: Regression line intercept (b) and slope (m) with Pearson's product-moment correlation coefficients (r) and significance results to test relationships between geomorphometric parameters and sampled beryllium-10 concentrations representing basin sedimentary output. Parameters are described in Tables 4.1 and 4.2, with parameter categories separated by a horizontal line. Omitted outlier samples are indicated in the comments column.

Parameter	b	m	r	t	p-value	comments
$\bar{\text{NDVI}}$	-1.07E5	5.40E5	0.4743	1.0774	0.3419	3/11/2009; omit Z-20
$\bar{\text{NDVI}}$	-4.44E4	2.53E5	-0.0661	-0.1325	0.9010	9/19/2009; omit Z-20
$\bar{z}$	-1.12E4	24.0700	0.5909	1.4649	0.2168	omit Z-20
$\bar{z}$	-5.67E4	60.5100	0.9420	6.2741	**0.0015	
$\bar{\theta}$	3.88E3	6.51E2	0.1563	0.3164	0.7675	omit Z-20
$f\theta$	1.70E4	1.46E5	0.4253	0.9399	0.4005	omit Z-20
$\bar{K}_{\text{mean}}$	2.06E4	1.99E6	0.7951	2.6220	0.0587	omit Z-20
$\bar{K}_{\text{mean},s}$	5.14E4	1.10E5	0.7448	2.2320	0.0894	omit Z-20
$\bar{h}$	-7.70E3	1.76E2	0.5218	1.2233	0.2884	omit Z-20
$\bar{V}_{f,s}$	7.52E4	-6.30E4	-0.1481	-0.2994	0.7795	omit Z-20
$\bar{Q}_m$	7.93E3	4.35E4	0.1644	0.3334	0.7556	omit Z-20
$\bar{Q}_h$	-5.83E3	8.25E5	0.5355	1.2682	0.2735	omit Z-20
$\bar{Q}_h$	-5.39E4	2.43E6	0.9250	5.4437	**0.0028	
$\bar{Q}_s$	1.20E4	7.51E7	0.5835	1.2444	0.3017	omit Z-04, Z-20
χ	1.53E4	76.8600	0.4174	0.7955	0.4844	omit Z-04, Z-20
$\bar{d}_{\Phi=0.75}$	5.10E4	-2.60E2	-0.7035	-1.9795	0.1189	omit Z-20
$\bar{A}_{\text{SF}}$	1.15E4	1.6700	0.1444	0.2919	0.7849	omit Z-20
$\bar{A}_{s,\text{SF}}$	9.52E3	1.8550	0.1755	0.3566	0.7394	omit Z-20
$A_{\text{SF}}/A_{s,\text{SF}}$	1.47E5	-1.40E5	-0.2198	-0.4506	0.6756	omit Z-20
$\bar{\theta}_{\text{SF}}$	2.43E4	-2.30E2	-0.0499	-0.0998	0.9253	omit Z-20
$f\theta_{\text{SF}}$	2.90E4	-3.43E5	-0.5546	-1.3330	0.2534	omit Z-20
$\bar{\theta}_s$	8.76E3	7.48E2	0.2569	0.5316	0.6231	omit Z-20
D_d	-1.33E4	7.24E5	0.7468	2.2457	0.0881	omit Z-20
$\bar{R}_b$	4.04E4	-1.26E4	-0.4580	-1.0304	0.3610	omit Z-20
L_B	9.70E3	1.64E3	0.6568	1.5088	0.2285	omit Z-04, Z-20
A_B	1.46E4	3.47E2	0.4659	0.9119	0.4291	omit Z-04, Z-20
$A_{s,B}$	1.45E4	3.11E2	0.4715	0.9260	0.4227	omit Z-04, Z-20
$A_B/A_{s,B}$	1.14E5	-1.05E5	-0.2099	-0.4294	0.6897	omit Z-20
Δz	6.53E3	10.8800	0.7792	2.4861	0.0678	omit Z-20
H_I	3.20E3	3.80E4	0.3057	0.6420	0.5558	omit Z-20
C	5.48E4	-1.05E5	-0.8481	-3.2015	*0.0329	omit Z-20
E	5.47E4	-5.64E4	-0.7095	-2.0139	0.1143	omit Z-20
I_x	3.49E4	-3.10E4	-0.3249	-0.6870	0.5299	omit Z-20
I_R	3.45E3	3.68E4	0.5239	1.2300	0.2861	omit Z-20

*=significant at $\alpha \leq 0.05$; **=significant at $\alpha \leq 0.01$

Table 4.6: Regression line intercept (b) and slope (m) with Pearson's product-moment correlation coefficients (r) and significance results to evaluate the correlation between modeled production rates [atoms g^{-1} yr^{-1}] and beryllium-10 concentration [atoms mg^{-1}]. Note that the slope of this relationship is in units of thousands of years, and may represent regional characteristic effective exposure time to cosmic rays.

Modulation Method	b	m	r	t	p-value
No modulation	-48.436	6.307	0.9607	7.7411	**0.0006
Slope ($cos\theta$)	-50.640	7.150	0.9629	7.9832	**0.0005
Curvature ($1 - \lvert K_{\text{mean},r,s} \rvert$)	-47.867	8.476	0.9595	7.6136	**0.0006
Diffusive flux ($1 - Q_{m,\text{norm}}$)	-73.910	11.260	0.9522	6.9697	**0.0009
Stream power flux ($1 - Q_{s,\text{norm,Ba}}$)	-47.859	6.322	0.9588	7.5489	**0.0006
Combined flux ($1 - \max(1, Q_{m,\text{norm}} + Q_{s,\text{norm,Ba}})$)	-58.759	9.495	0.9615	7.8283	**0.0005
Fracture depth ($1 - \frac{d_{\Phi=0.75}}{400}$)	-97.960	16.570	0.7932	2.9125	*0.0333

*=significant at $\alpha \leq 0.05$; **=significant at $\alpha \leq 0.01$

Figures

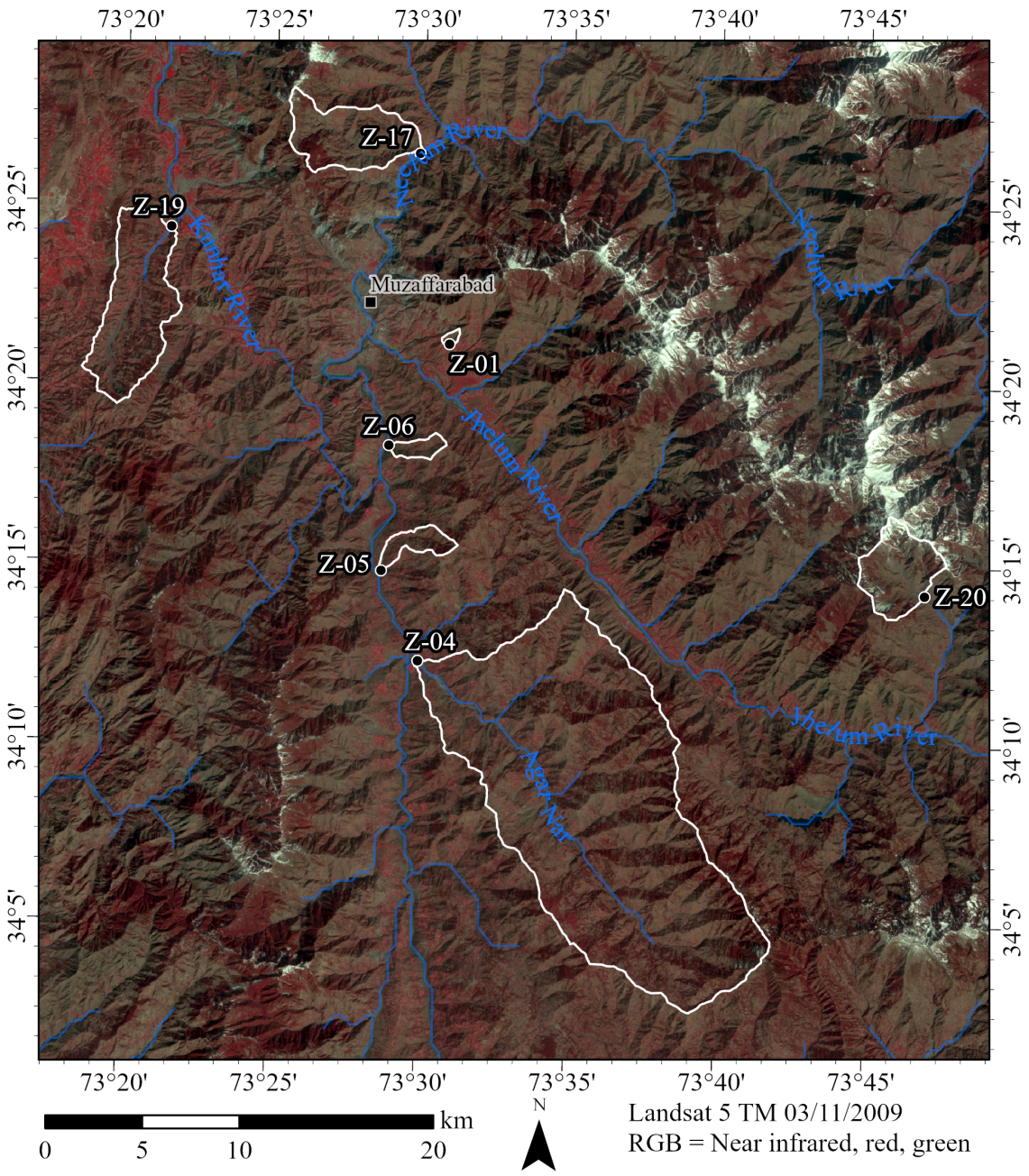

Figure 4.1: Map of sample sites and associated basins in relation to rivers (modified from Andreadis et al., 2013) on Landsat-5 TM Level-2 satellite imagery (11 March 2009; DOI: 10.5066/F7KD1VZ9).

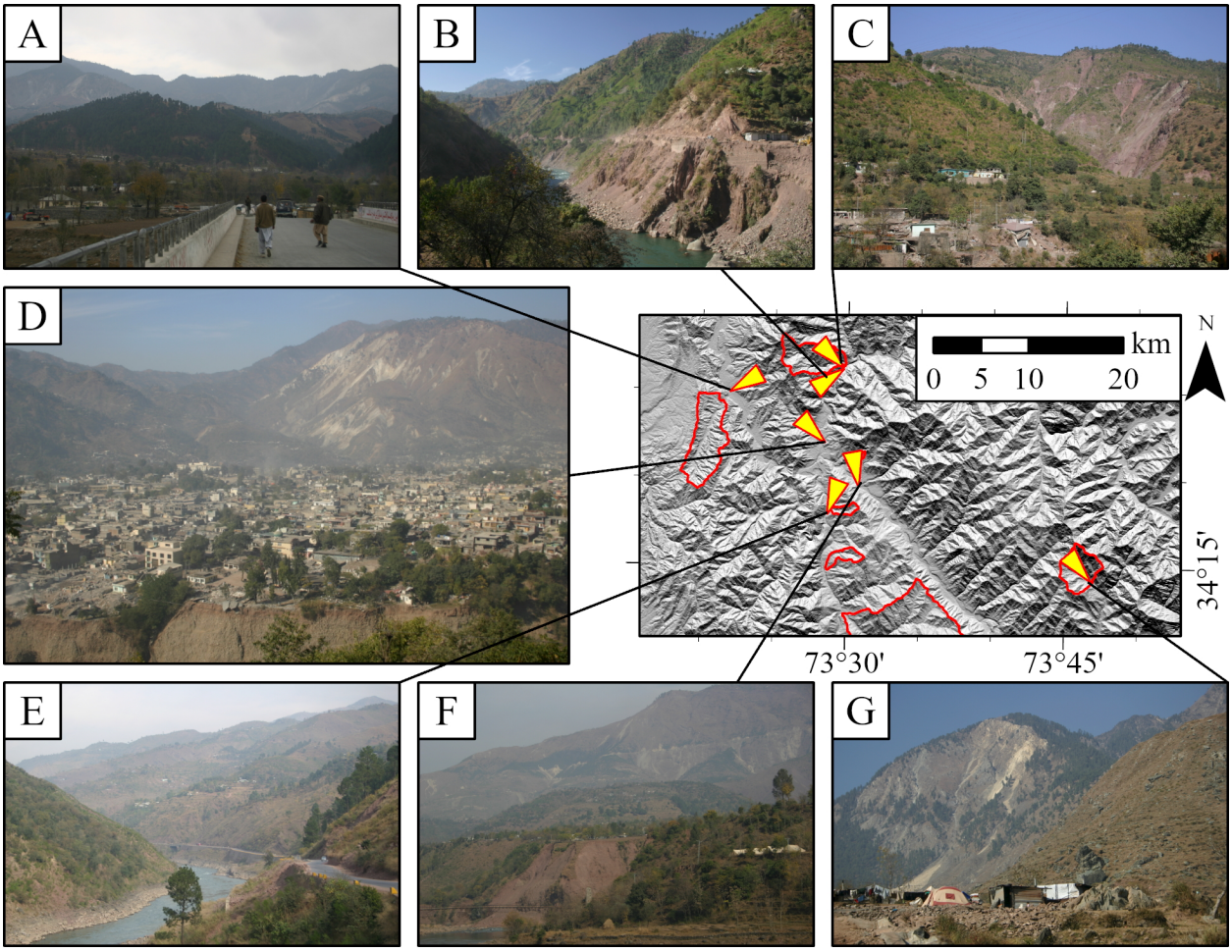

Figure 4.2: Photos showing the topography and land-surface conditions in the study area. A location map is given with photo directions shown in the widening direction of triangles superimposed on a hillshade of the study area; studied basins are outlined in red. Photo locations are: (A) near sample Z-19, looking east across the Kunhar River; (B) near sample Z-17, looking south down the Neelum River; (C) near sample Z-17, looking toward the basin represented by Z-17; (D) a view looking northwest across Muzaffarabad; (E) near sample Z-06, looking north up the Jhelum River and across the basin associated with sample Z-06; (F) south of sample Z-01, looking north across the Jhelum River (the basin associated with sample Z-01 is behind the prominent tree on the right of the photo); and (G) near sample Z-20, looking northwest across the basin associated with Z-20. Note the generally steep and vegetated terrain

.

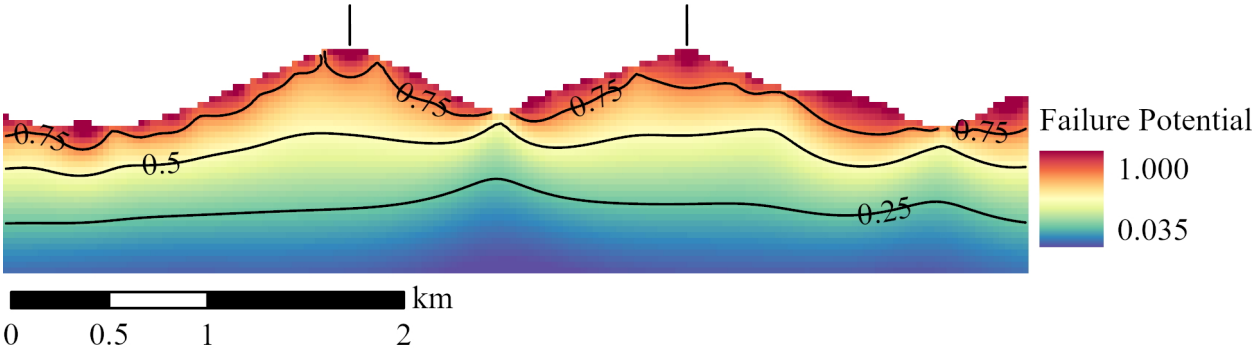

Figure 4.3: Example topographic cross-section with modeled failure potential (no vertical exaggeration). The depth of high failure potential is associated with zones of high fracturing (St. Clair et al., 2015). For all stream locations, this study averages the depth of the 0.75 contour between the ridges bounding the stream (vertical ticks).

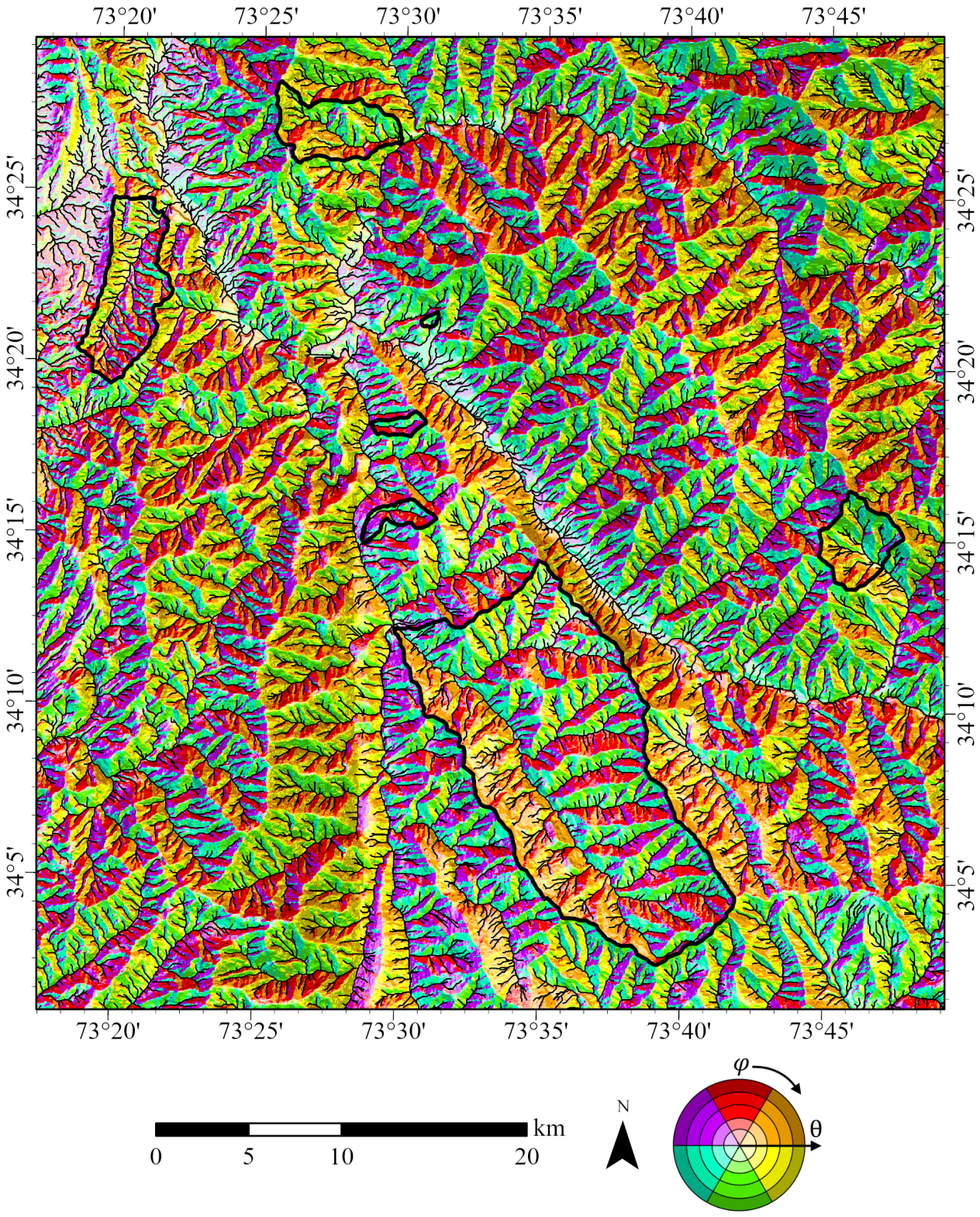

Figure 4.4: Terrain units in the study area. Streams are thin black lines, studied basins have thick black outlines, and slope-facets are displayed with hue and value indicating slope-azimuth (φ) and slope-angle (θ) classes, respectively.

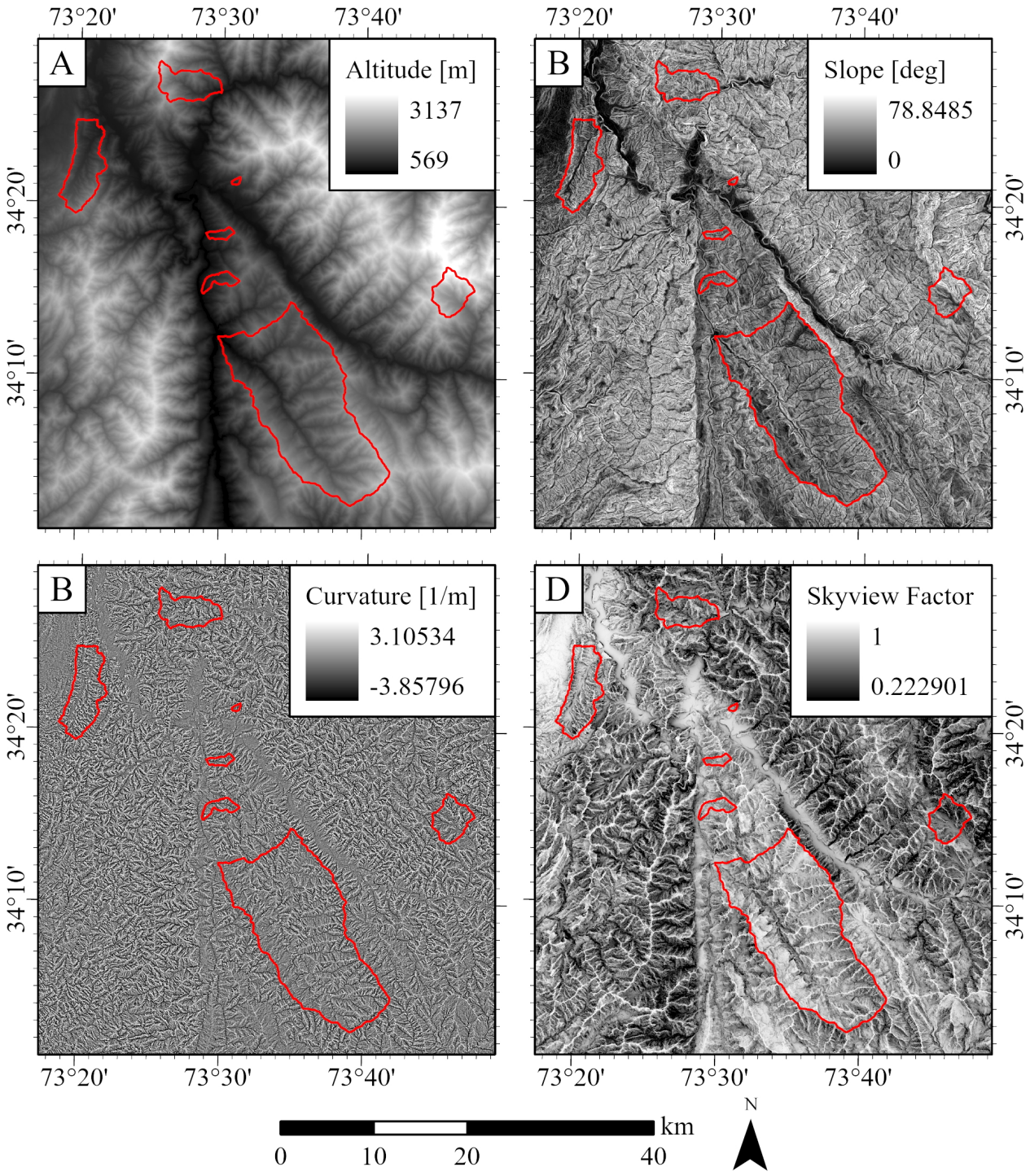

Figure 4.5: Land-surface parameters used to compare against erosion rate: (A) altitude; (B) slope angle; (C) mean curvature; and (D) skyview factor. Basins evaluated in this study are outlined in red.

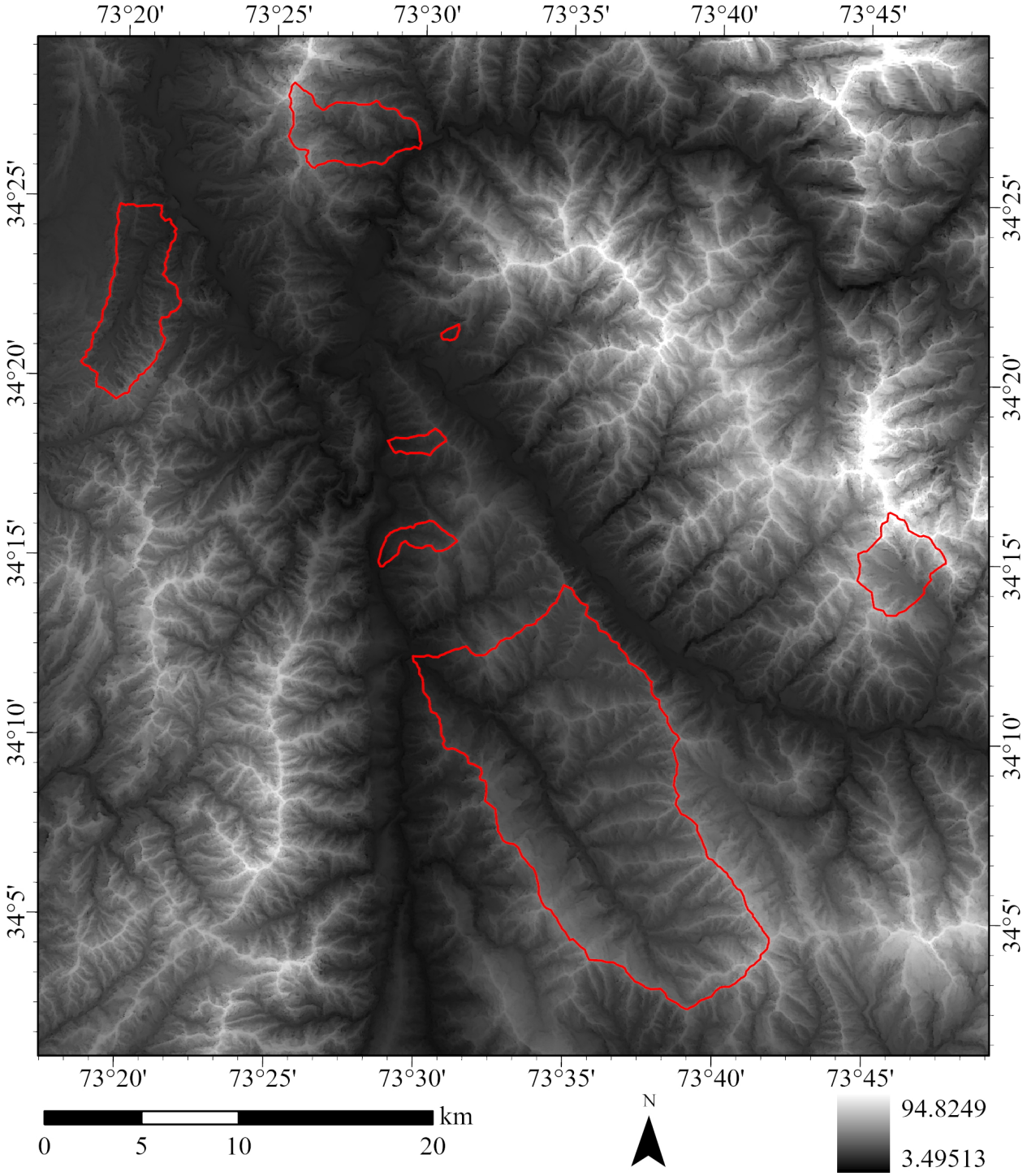

Figure 4.6: Modeled beryllium-10 Production rate [atoms g^{-1} yr^{-1}], using the methods of Lal (1991) and Stone (2000), after Balco et al. (2008). Studied basins are outlined in red.

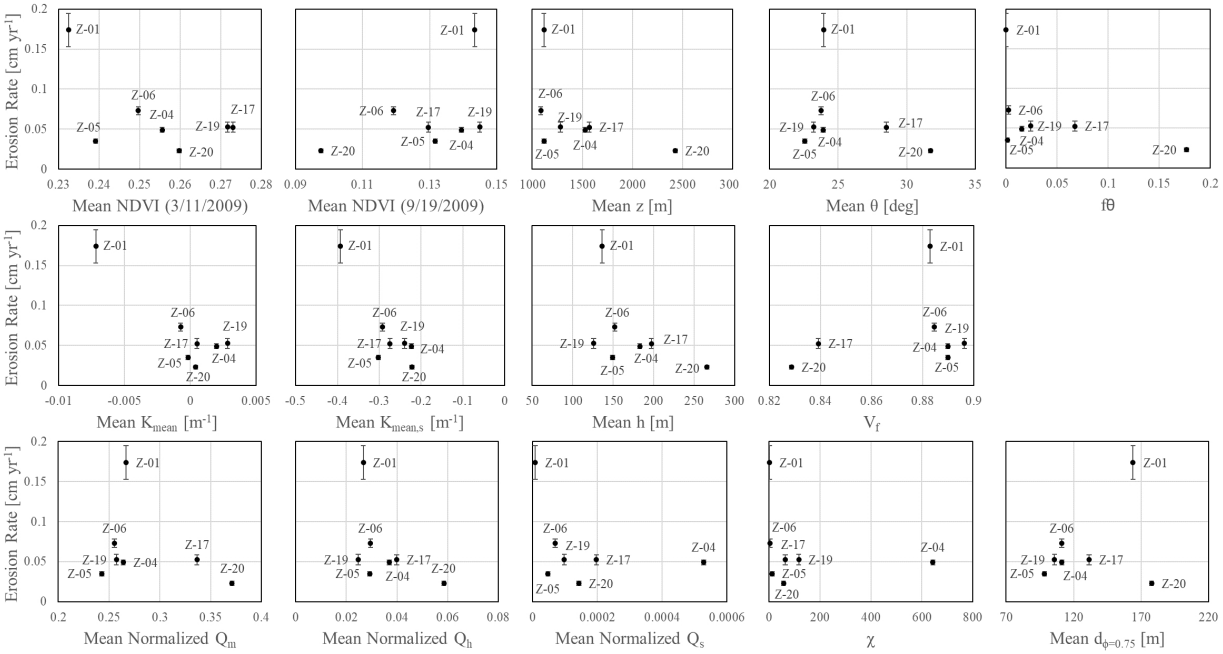

Figure 4.7: Beryllium-10-derived erosion rate versus NDVI and morphometric parameters at the basin scale. Parameters are explained in Table 4.1, with $f\theta$ being the fraction of steep ($\geq 40°$) slopes.

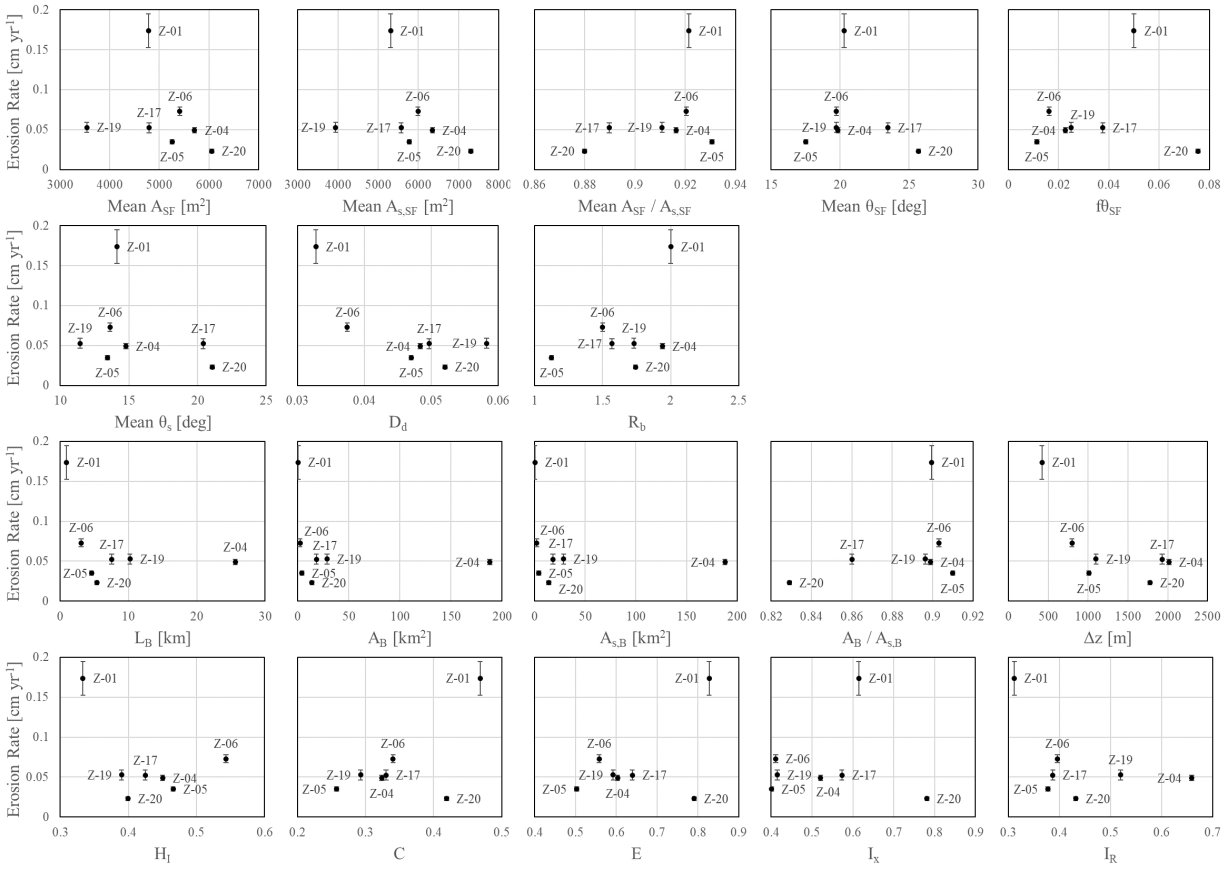

Figure 4.8: Beryllium-10-derived erosion rate versus terrain-unit morphometric parameters at the basin scale. Parameters are explained in Table 4.2, with $f\theta_{\mathrm{SF}}$ being the fraction of steep ($\geq 40°$) slope facet units within the basin.

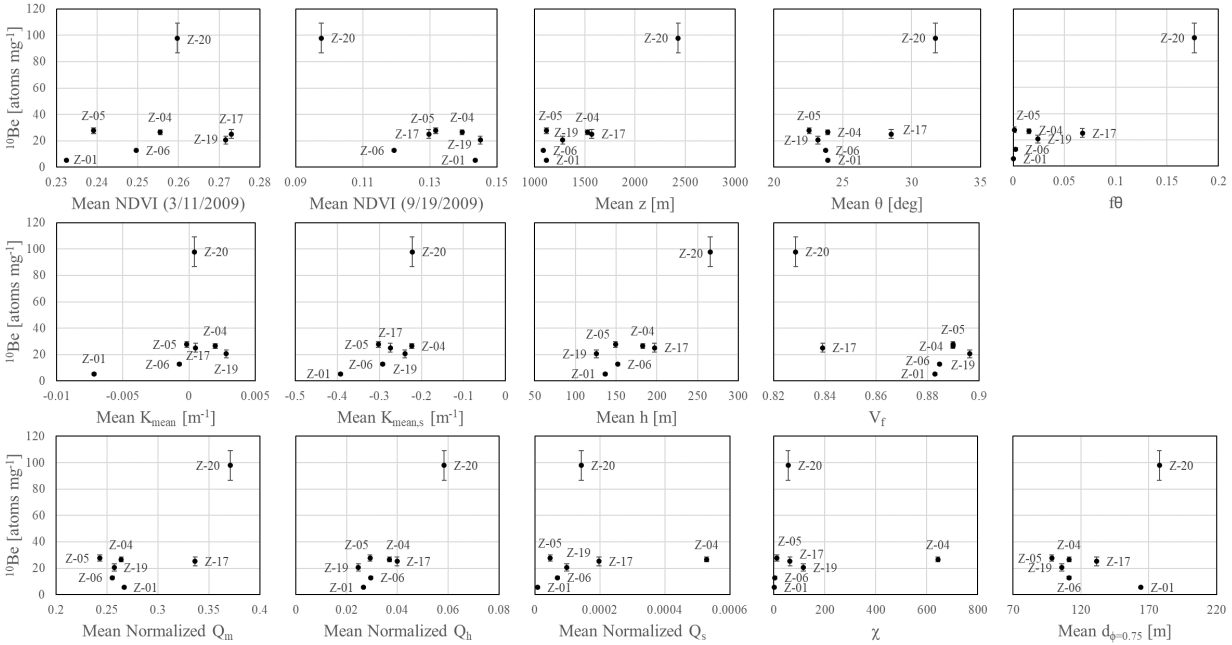

Figure 4.9: Measured Beryllium-10 concentration versus NDVI and morphometric parameters at the basin scale. Parameters are explained in Table 4.1, with $f\theta$ being the fraction of steep ($\geq 40°$) slopes.

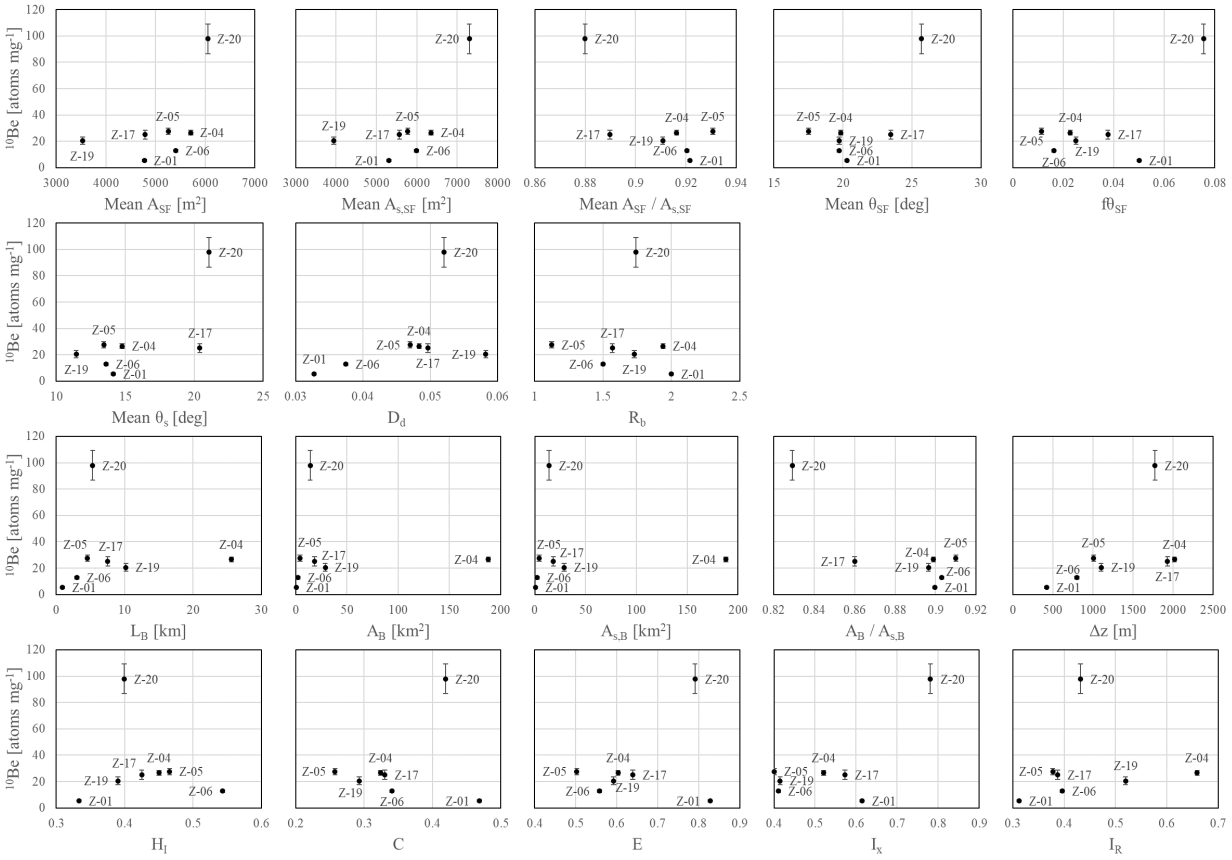

Figure 4.10: Measured Beryllium-10 concentration versus terrain-unit morphometric parameters at the basin scale. Parameters are explained in Table 4.2, with $f\theta_{SF}$ being the fraction of steep ($\geq 40°$) slope facet units within the basin.

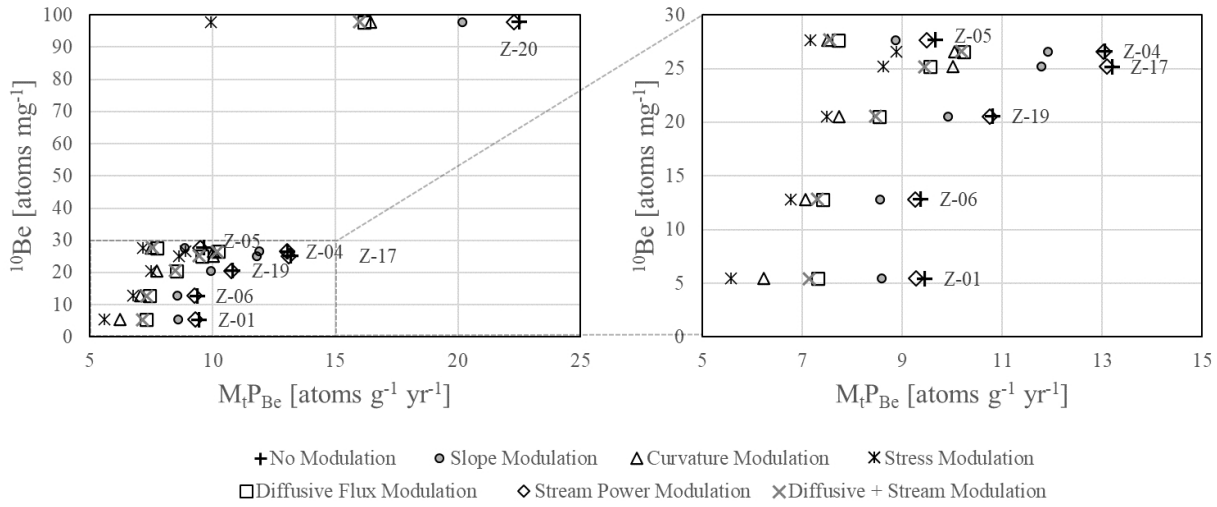

Figure 4.11: Average topography-modulated production rate of beryllium-10 (M_tP_{Be}) versus the measured concentration of beryllium-10. Note that topographic modulation has a nonlinear effect on erosion rate, which cannot be achieved through basin-averaging of scaling parameters. Also note the approximately linear relationship between modeled production rate and beryllium-10 concentration, and that the slope of this line is in units of time.

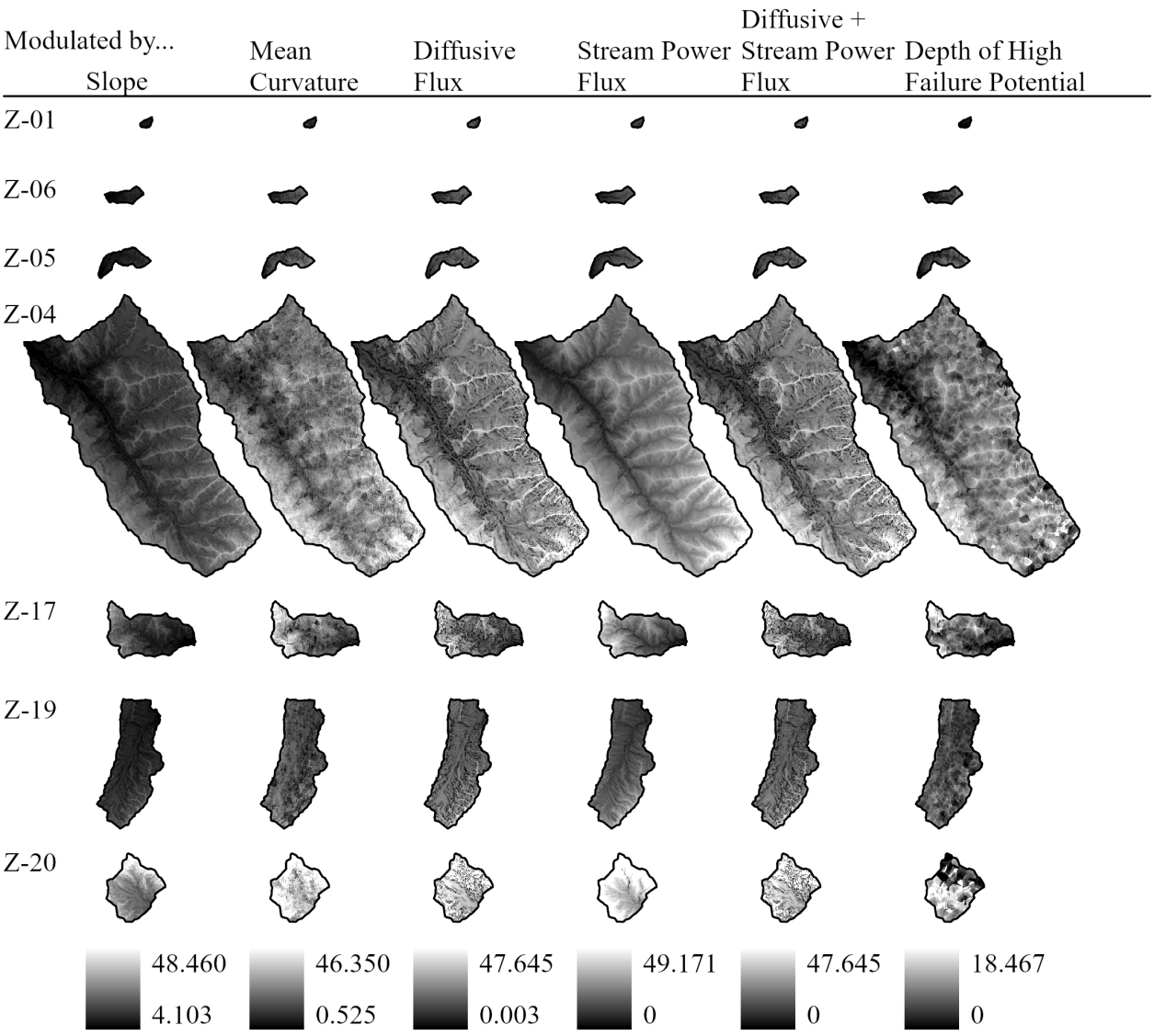

Figure 4.12: Beryllium-10 production rate modulated by geomorphometric parameters in studied basins [atoms g^{-1} yr^{-1}].

5. SUMMARY AND CONCLUSIONS

Mountain geodynamics are notoriously complex, as they involve the coupling of climate, surface, and tectonic processes that are related to processes of relief production and, consequently, landscape genetics. That is, processes that alter spatial patterns of relief variation are constrained by boundary conditions that are related to the spatial structure of the topography at a range of scales that are hierarchically (self-) organized (Phillips, 1988; de Boer, 1992; Werner, 2003; Ewing and Kocurek, 2010; Kocurek and Ewing, 2016; Phillips, 2016; Lastochkin et al., 2018; Barnes et al., 2020). The notion of the existence of topographic morphological structure (TMS) is not new, nor is the idea of using that structure for mapping landforms and process regimes (e.g., Werner, 2003; Lastochkin et al., 2018). What is lacking, however, is the bridge between those concepts and the modeling of that scientific knowledge and theory in a mathematical or computational framework that can exploit the complex scale-dependent hierarchical structure of the topography for advanced scientific investigation (Bishop et al., 2012, 2018, 2020). The formalization of topographic spatial structure and organization in a mathematical framework facilitates the interpretation of location- and scale-dependent geodynamics, even in remote areas, and is relevant in geological resource exploration, water resource management, and hazards mitigation (Pike, 2000; Bishop et al., 2018, 2020).

Key issues in this pursuit are identified in Chapter I, specifically: (1) from a mountain geodynamics perspective, we do not know where relief production occurs or the magnitude of the processes that generate relief except at specific sample locations; (2) from a geographic information science and technology (GIST) perspective, geometric and process-related characterizations of the topography are limited in the insight they can provide because they are scale-dependent and yield little information related to the causal factors that drive topographic evolution; and (3) from a geomorphology perspective, a digital elevation model (DEM) contains much of the information necessary for an expert to interpret landscape dynamics and infer driving factors, but we lack the methods for quantifying the same spatial patterns and relationships, as they are entangled in issues

of length-scale, anisotropy, inherited topography, empiricism, uncertainty, indeterminate boundaries, semantics, ontologies, and interoperability. Consequently, there exists no formal framework for representing complex, scale-dependent topographic structure in a way that can be used to describe geodynamic systems and infer process regimes.

The primary objective of this research was therefore to improve understanding of process-form relationships that can be used to characterize mountain geodynamics in northeastern Pakistan. That is, this research demonstrates certain concepts and techniques that facilitate representation and interpretation of topographic spatial structure and indicates research directions for approaching the goal of fully autonomous land-surface interpretation for mapping process regimes. As such, this research intersects both the geomorphology and GIST disciplines. The primary objective of this research was supported by three sub-objectives: (1) conceptualize, design, and implement a TMS framework that permits the characterization of terrain entities and spatial relationships for subsequent TMS network analysis; (2) evaluate TMS frameworks to gain insight into the spatial constraints that govern the operational scale dependencies of glacier-surface process regimes; and (3) evaluate the use of terrain entities and topographic information in comparison to measured beryllium-10 concentrations and modeled beryllium-10 production rates to better understand the relationship between TMS and erosion rates.

These objectives facilitated the testing of three hypotheses: (H_0) the TMS is not related to landscape genetics; (H_1) the spatial organization of terrain entities and patterns of geomorphometric parameters can be used to characterize surface process regimes; and (H_2) a TMS framework facilitates the prediction of erosion rates. Three research activities addressed the objectives and tested the hypotheses of this research, which are represented in Chapters II, III, and IV, respectively: (1) formalization and evaluation of a TMS framework; (2) characterization and mapping of select glacial process regimes; and (3) simulation and modulation of cosmogenic nuclide production rates in the context of topographic parameters and erosion within select basins.

5.1 Key Findings

The objectives, hypotheses, and activities associated with this research can be generalized to the notion of modeling process-form relationships. In Chapter II, a generalized framework is presented that proposes that both topographic fields and entities be considered within a graph-like framework, or a web of locations and entities, each with their associated properties, connected by spatial topology (i.e., overlap, adjacency, and proximity). Such a graph then reaches across hierarchical levels of topographic structure (e.g., a slope-angle grid cell is located within a slope facet on a slope that is contained within a valley that is contained within a basin which is contained within higher-order basins that intersect an eminence structure) and within in the same hierarchical level (e.g., slope facets are connected in a web of spatial adjacencies, and ridges are associated with other ridges in the same eminence). This TMS can be characterized by patterns of field properties, manifest in land-surface parameters (e.g., altitude, slope angle, curvature, openness), entity properties (e.g., landform relief, surface area, elongation), object-based reductions of fields (hypsometry, parameter-altitude profiles), and the properties of the spatial-topological graph of the TMS.

Chapter II demonstrated the use of the TMS framework for mapping terrain units and using topological properties (largely containment) to represent key process-form relationships that describe basin structure in relation to bedrock river incision and to glaciation. This required some object-based reduction of geomorphometric properties (e.g., mean slope, high-altitude "erosion surfaces" with low slope), object-based reduction of geomorphometric properties based on spatial context within high-level objects (e.g., the difference in skyview factor between different parts of the basin), intersection of spatially coincident objects (fraction of valley floor area occupied by glaciers), and contextual inference for orientation information (e.g., determination of valley orientation for valley width, valley floor width, and valley cross-sectional shape). Though the process described in Chapter II was not fully automated, it lays out the framework for achieving a fully automated process. One of the greatest challenges in automating landscape interpretation is the need to for more robust, deterministic semantic models for each landform, for establishing systems of

landforms, and for each process-form relationship. The TMS framework facilitated the spatial aggregation of simpler terrain units (ridges and slope facets) into more complex terrain units (valley floors and eminences) by providing necessary spatial context to, for example, what "steep" and "higher altitude" meant with respect to other like objects. Geomorphological mapping is itself an interpretive exercise (e.g., Campagna and Warner, 2018; Whitmeyer and Dordevic, 2020), and Chapter II demonstrates the power of the TMS framework to interpret elementary components of the land surface into functionally meaningful landform objects with a model for representing spatial context and addressing scale-dependence with object-oriented analysis. Much more semantic modeling research is required, however, to create a robust set of tools and procedures to represent important topographic entities, characterize spatial and semantic uncertainty associated with modeled features and process-form relationships, and perform spatial contextual analysis in a way that is accessible, interoperable, and replicable. In summary, key findings from the research activity represented in Chapter II are:

- Definitions of landforms and landform measurement (i.e., how to decide on a cross-section line) provided in the literature are insufficient for modeling the same features and interpretive processes: Specific semantic models are required.

- The TMS is highly complex, even in seemingly simply-structured basins, consisting of a web of innumerable spatially coincident fields and entities, but finite components of the TMS can be represented in a mathematical and computational framework related to particular process regimes.

- The TMS framework that was conceptualized, designed, and implemented in Chapter II is a suitable framework for representing the concepts of spatial context and association, which may be leveraged for further landscape characterization. This achieves sub-objective 1, demonstrates hypothesis H_0 (the TMS is unrelated to landscape genetics) as false and H_1 (the TMS can be used to characterize process regimes) as correct within the context of this study (predicting predominant glacial erosion or bedrock river incision at the basin scale in a

high-relief mountain environment), and plausible for other landscapes and process regimes.

Chapter III focused almost exclusively on designing specific network architectures and exploring their properties for process-related information that is wholly dependent on spatial context. That is, it was not enough to identify a nearby depression or mound, which might be related to a supraglacial lake or ice cliff. Instead, the process regime is characterized by many such features in close proximity. Likewise, elongate divergent units (~moraines) were only significant if an elongate convergent unit (~inter-moraine valley or supraglacial drainage) was nearby and if the divergent units existed in directions perpendicular to the elongation direction of the convergent unit. This was a crude way to represent the anisotropic structure of parallel moraines and intermoraine valleys that is easily identified by visual interpretation and related to supraglacial drainage and intermoraine sediment flux.

- Process regimes that exhibit distinct and unique spatial morphological signatures can be represented using simple and imperfect terrain units and networks designed to represent the specific process regime, and identified by reduction of network properties. The glacial downwasting and supraglacial lake regime was best characterized by the spatial density of depression and mound nodes, with visually isotropic networks. The characteristics that were best representative of the supraglacial drainage process regime were the number of peaks located within the elongate divergent units (indicative of larger, more continuous divergent units), the inverse dispersion in the orientations of network links between those peak locations (link-anisotropy), and the length of flow-paths from peak locations to local topographic sinks.

- Networks are effective for representing simple geomorphological systems and facilitating process-regime mapping. Some key issues must be addressed, however, to make network analysis more feasible for general process-regime mapping. The length-scale and direction-dependence at which land-surface parameters are computed, networks are confined, and topological relationships are established must be selected for each process regime in each

environment in which they are being mapped, and future research may wish to discover more general frameworks to process-regime mapping and characterization. Issues of scale alone introduce considerable spatial and semantic uncertainty in what terrain units represent and how networks are structured, and make these methods highly empirical and difficult to port to different study areas: future research should invest in developing robust semantic models and characterizing the spatial and semantic uncertainty associated with those models.

- The research represented in Chapter III effectively accomplished sub-objective 2 and demonstrated that H_1 is plausible by providing a framework for exploring and establishing the spatial constraints and scale-dependencies of glacier-surface process regimes using object-oriented analysis and rudimentary network analysis. Only a few network characteristics were explored in Chapter III, but many more could be investigated for more specific and reliable process-form relationships, including characteristics of clustering, symmetry, terrain-unit similarity, and others that might describe spatial patterns or changes in texture, orientation, or boundary conditions that are related to processes.

Chapter IV reduced the TMS concept to evaluations of geomorphometric parameters in the context of cosmogenic radionuclide theory at the basin scale in order to explore the erosion-parameter relationship at the same scale at which we had beryllium-10 samples. Key findings from Chapter IV are:

- Our sample population proved insufficient for establishing any relationships between land-surface and terrain-unit parameters and either modeled erosion rate or measured beryllium-10 concentration when land-surface parameters are reduced at the basin-scale.

- A linear relationship between beryllium-10 production rate and measured beryllium-10 concentration was identified. The slope of the regression line of this relationship has units of time, and was interpreted as a characteristic timescale for irradiation by cosmic rays for producing beryllium-10, which might be used to predict average beryllium-10 concentration based on spatially modeling cosmogenic isotope production and therefore predicting

erosion rates. Before this relationship can be used to predict beryllium-10 concentration, more research is required to better understand this relationship, confirm its statistical significance, and identify its degree of linearity under different geologic, climate, and topographic conditions.

- The production rate-nuclide concentration relationship was also significant when production rate was modulated with slope angle, hilltop- and stream-curvature, modeled diffusive sediment flux (Roering et al., 1999; Montgomery and Brandon, 2002), modeled stream power law bedrock river incision (Whipple, 2004) and the depth of intense fracturing due to modeled subsurface stress due to topographic load (Slim et al., 2015; St. Clair et al., 2015). The degree to which modulation by these parameters improve the prediction of cosmogenic nuclide production requires a more robust sample population.

- Sub-objective 3 (evaluating the use of terrain entities and topographic information to better understand relationships between TMS and erosion rates based on cosmogenic radionuclide theory) was not met conclusively: a larger sample size with more control for geologic, climate, and topographic conditions is required to thoroughly evaluate the TMS-erosion rate relationship. A spatial relationship between the TMS and genetic processes exists, given that H_0 was disproven and H_1 was demonstrated plausible in Chapters II and III, but the relationship between the TMS and erosion rate, the crux of H_2, requires further testing.

5.2 Future Research

Numerous issues have been raised in each chapter of this research, and more research is needed to improve mapping and characterization capability. The most notable avenues for future research that are essential for investigating the TMS in relation to process regimes and mountain geodynamics are:

- Semantic modeling of specific landforms and process-form relationships. Many landforms relevant to landscape genetics and ongoing processes have been identified and qualitatively

described in the geomorphology literature (an exhaustive literature search on the topic is not productive here, but see Church, 2010; Ritter et al., 2002; Smith and Mark, 2003; Phillips, 2007; MacMillan and Shary, 2009; Lastochkin et al., 2018). The computational extraction of these landforms is, however, fraught with challenge. Most work in the area of mapping landforms is accomplished by thresholding land-surface parameters (e.g., Shary et al., 2005; MacMillan and Shary, 2009), pattern-recognition approaches (e.g., Jasiewicz and Stepinski, 2013; Xiao et al., 2013; Sărăşan et al., 2019), limited contextual analysis (Lucieer and Stein, 2005; Drăguţ and Blaschke, 2006), and neural network or machine learning approaches (e.g., Xie et al., 2020; Rubanenko et al., 2021). Future geomorphometric analysis would benefit from deterministic approaches because they test and encapsulate our understanding of what constitutes specific landforms and their relationships to landscape genetics (Dehn et al., 2001; Deng, 2007) and because robust models should be applicable on any dataset representing any region on any planet for many applications, rather than relying on training datasets of indeterminate size and variation to address the many natural deviations from what may be considered typical.

- Characterization and communication of semantic uncertainty associated with land-surface parameters, terrain units, and geodynamic interpretations. A distinct vagueness presently permeates much of the geomorphometry discipline with respect to how or why features and relationships are defined, how well a terrain unit might represent its target landform (Fisher and Wood, 1998; Evans, 2012; Bishop et al., 2020; Sofia, 2020), or how well a process-form relationship might predict the extent and magnitude of relevant process regimes, which makes it difficult to communicate how models differ or are more suited for particular applications. Chapter II, for example, discusses issues associated with the valley floor partition, particularly that it is unclear whether it includes such features as talus cones, alluvial fans, the edges of alluvial terraces, or other peripheral forms. It is also unclear whether such features *should* be included in a representation of the valley floor, or if these objects should constitutes the valley floor boundary. Chatper III also discusses some uncertainty related

to spatial relationships established with certain network designs, which limit networks by some fixed length-scale, which challenged visual interpretation of some network properties because they were more influenced by spatial artifacts that by the network properties themselves. Well-defined models that are highly representative of their target morphological concepts (i.e., with low or well-characterized semantic uncertainty) are crucial for improving scientific communication and for achieving robust and interoperable geomorphometric mapping and geodyanmic characterization.

- Characterization and communication of spatial uncertainty associated with land-surface parameters, terrain units, and geodynamic interpretations. Spatial uncertainty relates to topics of fuzzy objects and indeterminate boundaries (Burrough and Frank, 1996; Cheng, 2002; Fisher et al., 2005; Deng and Wilson, 2008; Goodchild, 2017). Characterization of terrain units and process regimes as fuzzy objects or objects with indeterminate boundaries will help to better understand where true overlap and ambiguity exist, which may be related to landscape inheritance, polygenetic evolution, and system coupling (Bishop et al., 2003; Phillips, 2007; Bishop et al., 2012; Barrineau et al., 2016; Bishop et al., 2020). Representation of terrain units as fuzzy objects introduces new challenges of representing spatial topology and understanding spatial structure, however (though see Liu and Shi, 2006; Shi and Liu, 2007). While semantic uncertainty for terrain units and process-form relationships should be minimized, this may not be possible or desirable for spatial uncertainty for some terrain units or process characterizations, including process-regime mapping, because it is this fuzziness that indicates the fringes of geodynamic systems, the intersection and coupling of systems that relief in relief production, and indicate regions where land-surface morphology is not well explained by current models, each of which presents opportunities for further research to broaden and deepen our understanding of geodynamic systems.

- Scale adaptivity, or identification of (locally) relevant or appropriate scales for different geomorphic mapping and interpretation applications. Issues of scale were a consistent chal-

lenge in this research, including: (1) the appropriate application-specific level of generalization when computing geomorphometric parameters; (2) the minimum size that a terrain unit must be to be considered relevant to the study study; (3) the directions that should be considered when characterizing a system of terrain units; (4) the distances and directions that are relevant to obtain certain process-related information; (5) the scale at which specific process-related patterns should be attributed to the more general landscape (e.g., how to handle the spatial artifacts in the results of Chapter III). Such determinations of scale were empirical or, at worst, arbitrary but related to the objectives of each study. Once terrain units could be extracted, many issues of scale became irrelevant: spatial adjacency, spatial containment, and unit shape addressed many of these issues. Other researchers have already made great strides in characterizing spatial scale-dependence (Wu et al., 2000; Tate and Wood, 2001; Smith, 2010; Newman et al., 2018; Zhang et al., 2020), but we continue to lack a distinct method for determining a most appropriate scale for analysis, which may differ from location to location and from application to application. If a form may exist as different features at multiple scales (e.g., eolian ripples, dunes, and super-dunes), and features may themselves exist at a wide range of scales (e.g., dunes on different planets; Claudin and Andreotti, 2006), they must all be mapped and hierarchically sorted in order to sieve out all but the features of interest or to make sense of their structure if they are all of interest. In some ways, this avenue of research must generate methods to parse and interpret between semantically similar and ontologically linked concepts and features. Scale-adaptability must also address anisotropic patterns (Bishop et al., 2012; Jasiewicz and Stepinski, 2013; Roy et al., 2016; Newman et al., 2018; Bishop et al., 2018, 2020).

- More robust erosion rate investigations specifically aimed at understanding how topography modulates erosion rates and influences measurements of cosmogenic radionuclides. The research presented in Chapter IV raises questions that can be answered with a more robust population of cosmogenic isotope samples, with control for lithologic, tectonic, climate, and topographic factors. Specifically: (1) What relationships exist between land-surface and

terrain-unit parameters and erosion rate and cosmogenic nuclide concentration? (2) How do approximations of erosion rate and measurements of cosmogenic nuclides differ with respect to basin scale? In other words, a direct test of the minimal-storage assumption. (3) What is the empirical relationship between basin-averaged modeled cosmogenic nuclide production and measured cosmogenic nuclide concentration, and can that relationship be used to predict nuclide concentrations and erosion rates? (4) Does the modulation of cosmogenic nuclide production rates with topographic information significantly improve the accuracy of erosion rate estimates?

Land-surface morphology is clearly only one component of terrain or Earth-system structure, and additional geospatial data would provide the observations that give necessary context for further assessing geodynamics. Multi- or hyper-spectral data provides access to mineralogical information that can be leveraged to distinguish between soil and bedrock, providing spatial and thematic constraints for evaluating different types of mass wasting and sediment flux, or be considered in context of ecosystem, climate, and topographic conditions to accurately predict weathering and erosion patterns (Parvis, 1950; Ahnert, 1970; Montgomery and Brandon, 2002; Clark et al., 2003; Yamaguchi and Naito, 2003; Roering et al., 2007; Imbroane et al., 2007; Bishop et al., 2014, 2019). Data from the electromagnetic spectrum also gives access to direct and indirect information regarding climate and ecology, including the presence and turbidity of water, ice- or snow-cover, and the type, density, and health of vegetation (Jensen, 2000; Wohl, 2013). Drunken trees detected with LiDAR and high-resolution imagery will augment the detection of permafrost thaw or low-velocity landslides, for example (e.g., Ilinca and Gheuca, 2011; Schuur and Abbott, 2011; Salleh et al., 2018). As drone and robotic agents develop, the difference between field and remote observations will blur, and fine-resolution, highly precise observations will provide information from perspectives that cannot be achieved from high-flying aircraft or spacecraft. Furthermore, geophysical data, such as magnetic and gravity anomalies, provide important hints regarding the three-dimensional geological environment and help to predict lithological variation, igneous intrusions, or geologic structure due to tectonics that can explain patterns in landscape dissection

and basin structure (e.g., Decker and Smithson, 1975; Zeitler et al., 2001a; Bishop, 2007; Simons and Olhede, 2013). The incorporation of additional information will doubtless provide important contextual information that can be used to differentiate between landforms with similar morphology (e.g., dunes vs. drumlins; kettle-lakes vs. karst-environment ponds) and gain insight into other geodynamic systems, which could be incorporated into a high-dimensional Earth-system structure, of which topographic morphological structure is a component, and leveraged to reduce uncertainty and gain insight into geodynamic systems that cannot be well understood through land-surface morphology alone.

Overall, this research represents the integration of spatial information into geomorphometric analysis for better understanding process-form relationships in mountain environments. The TMS framework provides a mechanism for representing topographic structure utilizing semantic modeling, topology, and network analysis for reducing complex spatial information to key parameters that are related to landscape genetics. With additional research, we may gain greater insight into where relief production occurs, the magnitude of processes that generate relief, the scale-dependencies and boundary conditions of geodynamic processes, greater insight into the factors that drive relief production, and a better understanding of system couplings that influence the polygenetic evolution of the land surface. Next steps in this research are to improve upon landform, structure, and process-form semantic models, improve upon the characterization of semantic and spatial uncertainty, further develop theory on scale adaptivity for geomorphic applications, and investigate topography-erosion relationships, specifically targeting scale assumptions and the efficacy of topographic modulation for more accurate erosion rate estimations.

REFERENCES

Aalto, R., Dunne, T., and Guyot, J. L. (2006). Geomorphic controls on andean denudation rates. *Journal of Geology*, 114:85–99.

Adams, B., Dietsch, C., Owen, L. A., Caffee, M. W., Spotila, J., and Haneberg, W. C. (2009). Exhumation and incision history of the lahul himalaya, northern india, based on (u-th)/he thermochronometry and terrestrial cosmogenic nuclide methods. *Geomorphology*, 107:285–299.

Ahnert, F. (1970). Functional relationships between denudation, relief, and uplift in large mid-latitude drainage basins. *American Journal of Science*, 268(3):243–263.

Ahnert, F. (1994). Equilibrium, scale and inheritance in geomorphology. *Geomorphology*, 11:125–140.

Ai, T. (2007). The drainage network extraction from contour lines for contour line generalization. *ISPRS Journal of Photogrammetry and Remote Sensing*, 62:93–103.

Ali, K. F. and de Boer, D. H. (2008). Factors controlling specific sediment yield in the upper indus river basin, northern pakistan. *Hydrological Processes*, 22:3102–3114.

Alshehhi, R. and Marpu, P. R. (2017). Hierarchical graph-based segmentation for extracting road networks from high-resolution satellite images. *ISPRS Journal of Photogrammetry and Remote Sensing*, 126:245–260.

Alvioli, M., Guzzetti, F., and Marchesini, I. (2020). Parameter-free delineation of slope units and terrain subdivision of italy. *Geomorphology*, 358:107124.

Amerson, B. E., Montgomery, D. R., and Meyer, G. (2008). Relative size of fluvial and glaciated valleys in central idaho. *Geomorphology*, 93:537–547.

Anderson, R. S., Molnar, P., and Kessler, M. A. (2006). Features of glacial valley profiles simply explained. *Journal of Geophysical Research*, 3:F01004.

Andreadis, K. M., Schumann, G. J.-P., and Pavelsky, T. (2013). A simple global river bankfull width and depth database. *Water Resources Research*, 49(10):7164–7168.

Archer, D. R. and Fowler, H. J. (2004). Spatial and temporal variations in precipitation in the upper

indus basin, global teleconnections and hydrological implications. *Hydrology and Earth System Sciences*, 8(1):47–61.

Aronica, G. T., Biondi, G., Brigandì, G., Cascone, E., Lanza, S., and Randazzo, G. (2012). Assessment and mapping of debris-flow risk in a small catchment in eastern sicily through integrated numerical simulations and gis. *Physics and Chemistry of the Earth*, 49:52–63.

Back, S. and Strecker, M. R. (1998). Asymmetric late pleistocene glaciations in the north basin of the baikal rift, russia. *Journal of the Geological Society*, 155:61–69.

Balázs, A., Granjeon, D., Matenco, L., Sztanó, O., and Cloetingh, S. (2017). Tectonic and climatic controls on asymmetric half-graben sedimentation: Inferences from 3-d numerical modeling. *Tectonics*, 36:2123–2141.

Balco, G., Stone, J. O., Lifton, N. A., and Dunai, T. J. (2008). A complete and easily accessible means of calculating surface exposure ages or erosion rates from $^{1}0$be and $^{2}6$al measurements. *Quaternary Geochronology*, 3:174–195.

Band, L. E. (1989). Spatial aggregation of complex terrain. *Geographical Analysis*, 21(4):279–293.

Band, L. E. and Moore, I. D. (1995). Scale: Landscape attributes and geographical information systems. *Hydrological Processes*, 9:401–422.

Barnes, R., Callaghan, K. L., and Wickert, A. D. (2020). Computing water flow through complex landscapes—part 2: Finding hierarchies in depressions and morphological segmentations. *Earth Surface Dynamics*, 8:431–445.

Barrineau, P., Dobreva, I., Bishop, M. P., and Houser, C. (2016). Deconstructing a polygenetic landscape using lidar and multi-resolution analysis. *Geomorphology*, 258:51–57.

Barros, A. P., Chiao, S., Lang, Timothy, J., Burbank, D., and Putkonen, J. (2006). From weather to climate—seasonal and interannual variability of storms and implications for erosion processes in the himalaya. In Willet, S. D., Hovius, N., Brandon, M. T., and Fisher, D., editors, *Tectonics, Climate, and Landscape Evolution: Geological Society of America Special Paper 398*, pages 17–38. Geological Society of America, Boulder, Colorado, USA.

Barsch, D. and Caine, N. (1984). The nature of mountain geomorphology. *Mountain Research and Development*, 4(4):287–298.

Basharat, M., Rohn, J., Baig, M. S., and Khan, Muhammad Rustam ands Schleier, M. (2013). Large scale mass movements triggered by the kashmir earthquake 2005, pakistan. *Journal of Mountain Science*, 11(1):19–30.

Basharat, M., Rohn, J., Baig, M. S., and Khan, M. R. (2014). Spatial distribution analysis of mass movements triggered by the 2005 kashmir earthquake in the northeast himalayas of pakistan. *Geomorphology*, 206:203–214.

Bauer, J., Rohdenberg, H., and Bork, H.-R. (1985). Ein digitales reliefmodell als vorraussetzung fuer ein deterministisches modell der wasser-und stoff-fluesse. In Bork, H.-R. and Rohdenburg, H., editors, *Landschaftsgenese und Landschaftsoekologie H. 10, Parameteraufbereitung fuer deterministische Gebiets-Wassermodelle, Grundlagenarbeiten zu Analyse von Agrar-Oekosystemen*, pages 1–15. Selbstverlag Abteilung für Physische Geographie und Landschaftsökologie der Technischen Universität Braunschweig, Braunschweig, Germany.

Beck, H. E., Zimmermann, N. E., McVicar, T. R., Vergopolan, N., Berg, A., and Wood, E. F. (2018). Present and future köppen-geiger climate classification maps at 1-km resolution. *Scientific Data*, 5:180214.

Beer, F. P., Johnston, E. R., and De Wolf, J. T. (2006). *Mechanics of Materials: Fourth Edition in SI Units*. McGraw-Hill, New York, NY, USA.

Bermúdez, M., van der Beek, P. A., and Bernet, M. (2013). Strong tectonic and weak climatic control on exhumation rates in the venezuelan andes. *Lithosphere*, 5(1):3–16.

Beven, K. (1996). Equifinality and uncertainty in geomorphological modelling. In Rhoads, B. L. and Thorn, C. E., editors, *Proceedings of the 27th Binghamton Symposium in Geomorphology*, New York, NY, USA. Wiley.

Bhambri, R., Hewitt, K., Kawishwar, P., and Pratap, B. (2017). Surge-type and surge-modified glaciers in the karakoram. *Nature Scientific Reports*, 7:15391.

Bhat, F. A., Bhat, I. M., Sana, H., Iqbal, M., and Mir, A. R. (2013). Identification of geomorphic

signatures of active tectonics in the west lidder watershed, kashmir himalayas: Using remote sensing and gis. *International Journal of Geomatics and Geosciences*, 3(1):164–176.

Bierman, P. and Steig, E. J. (1996). Estimating reates of denudation using cosmogenic isotope abundances in sediment. *Earth Surface Processes and Landforms*, 21(2):125–139.

Bishop, M. P., Bonk, R., Kamp, Jr., U., and Shroder, Jr., J. F. (2001). Terrain analysis and data modeling for alpine glacier mapping. *Polar Geography*, 25(3):182–201.

Bishop, M. P., Bush, A. B. G., Copland, L., Kamp, U., Owen, L. A., Seong, Y. B., and Shroder, Jr., J. F. (2010). Climate change and mountain topographic evolution in the central karakoram, pakistan. *Annals of the Association of American Geographers*, 100(4):772–793.

Bishop, M. P., Bush, A. B. G., Furfaro, R., Gillespie, A. R., Hall, D. K., Haritashya, U. K., and Shroder Jr., J. F. (2014). Theoretical foundations of remote sensing for glacier assessment and mapping. In Kargel, J. S., Leonard, G. J., Bishop, M. P., Kääb, A., and Raup, B. H., editors, *Global Land Ice Measurements from Space*. Springer-Verlag, Berlin.

Bishop, M. P. and Dobreva, I. D. (2017). Geomorphometry and mountain geodynamics: Issues of scale and complexity. In Quattrochi, D. A., Wentz, E. A., Lan, N. S.-N., and Emerson, C. W., editors, *Integrating Scale in Remote Sensing and GIS*, pages 189–228. CRC Press.

Bishop, M. P. and Houser, C. (2016). Geomorphological mapping and geospatial technology. *International Encyclopedia of Geography: People, the Earth, Environment and Technology*, pages 1–13.

Bishop, M. P., James, L. A., Shroder, Jr., J. F., and Walsh, S. J. (2012). Geospatial technologies and digital geomorphological mapping: Concepts, issues and research. *Geomorphology*, 137:5–26.

Bishop, M. P. and Shroder, Jr., J. F. (2000). Remote sensing and geomorphometric assessment of topographic complexity and erosion dynamics in the nanga parbat massif. In Khan, M. A., Treloar, P. J., Searle, M. P., and Jan, M. Q., editors, *Tectonics of the Nanga Parbat Syntaxis and the Western Himalaya*, volume 170 of *Special Publications*, pages 181–199. The Geological Society of London, London, UK.

Bishop, M. P., Shroder, Jr., J. F., and Colby, J. D. (2003). Remote sensing and geomorphometry

for studying relief production in high mountains. *Geomorphology*, 55:345–361.

Bishop, M. P., Young, B. W., Colby, J. D., Furfaro, R., Schiassi, E., and Chi, Z. (2019). Theoretical evaluation of anisotropic reflectance correction approaches for addressing multi-scale topographic effects on radiation-transfer cascade in mountain environments. *Remote Sensing*, 11:2728.

Bishop, M. P., Young, B. W., and Huo, D. (2018). Geomorphometry: Quantitative land-surface analysis and modeling. In Wohl, E. and Scott, E., editors, *Reference Module in Earth and Environmental Sciences*. Elsevier, New York, NY, USA.

Bishop, M. P., Young, B. W., Huo, D., and Chi, Z. (2020). Spatial analysis and modeling in geomorphology. In *Reference Module in Earth Systems and Environmental Sciences*. Elsevier.

Bishop, P. (2007). Long-term landscape evolution: linking tectonics and surface processes. *Earth Surface Processes and Landforms*, 32:329–365.

Blomdin, R., Heyman, J., Stroeven, A. P., Hättestrand, C., Harbor, J. M., Gribenski, N., Jansson, K. N., Petrakov, D. A., Ivanov, M. N., Alexander, O., Rudoy, A. N., and Walther, M. (2016). Glacial geomorphology of the altai and western sayan mountains, central asia. *Journal of Maps*, 12(1):123–136.

Böhner, J. and Antonić, O. (2009). Land-surface parameters specific to topo-climatology. In Hengl, T. and Reuter, H. I., editors, *Geomorphometry: Concepts, software, applications*, volume 33 of *Developments in Soil Science*, pages 195–226. Elsevier, New York, NY, USA.

Bookhagen, B. and Burbank, D. W. (2006). Topography, relief, and trmm-derived rainfall variations along the himalaya. *Geophysical Research Letters*, 33:L08405.

Booth, A. M. and Roering, J. J. (2011). A 1-d mechanistic model for the evolution of earthflow-prone hillslopes. *Journal of Geophysical Research*, 116:F04021.

Boucher, S. and Zimányi, E. (2010). An ontology-based geodatabase interoperability platform. In Schorlemmer, M., Gruninger, M., and Euzenat, J., editors, *Cases on Semantic Interoperability for Information Systems Integration*, pages 294–315. IGI Global, Hershey, PA, USA.

Brändli, M. (1996). Hierarchical models for the definition and extraction of terrain features. In

Burrough, P. and Frank, A. U., editors, *Natural objects with indeterminate boundaries*, pages 257–270. Taylor & Francis, London, UK.

Brocklehurst, S. H. and Whipple, K. X. (2002). Glacial erosion and relief production in the eastern sierra nevada, california. *Geomorphology*, 42(1–2):1–24.

Brook, M. S., Purdie, H. L., and Crow, T. V. H. (2005). Valley cross-profile morphology and glaciation in park valley, tararua range, new zealand. *Journal of the Royal Society of New Zealand*, 35(4):399–407.

Buitrago, J. Y. and Martínez M., L. J. (2016). Digital elevation models (dem) used to assess soil erosion risks: A case tudy in boyaca, colombia. *Agronomia Colombiana*, 34(2):239–249.

Burbank, D. W., Blythe, A. E., Putkonen, J., Pratt-Sitaula, B., Gabet, E., Oskin, M., Barros, A., and Ojha, T. P. (2003). Decoupling of erosion and precipitation in the himalayas. *Nature*, 426:652–655.

Burbank, D. W., Leland, J., Fielding, E., Anderson, R. S., Brozovic, N., Reid, M. R., and Duncan, C. (1996). Bedrock incision, rock uplift and threshold hillslopes in the northwestern himalayas. *Nature*, 379:505–510.

Burrough, P. A. and Frank, A. U. (1996). *Geographic objects with indeterminate boundaries*, volume 2 of *GISDATA*. Taylor & Francis, Bristol, PA, USA.

Calkins, J. A., Offield, T. W., Abdullah, S. K. M., and Ali, S. T. (1975). Geology of the southern himalaya in hazara, pakistan, and adjacent areas. *United States Geological Survey Professional Paper*, 716-C:28.

Campagna, D. J. and Warner, T. A. (2018). Introduction to digital-mapping laboratory exercise. *Journal of Geoscience Education*, 44(5):576–580.

Cheng, T. (2002). Fuzzy objects: their changes and uncertainties. *Photogrammetric Engineering and Remote Sensing*, 68(1):41–49.

Church, M. (2010). The trajectory of geomorphology. *Progress in Physical Geography*, 34(3):265–286.

Clark, B. A. and Burbank, D. W. (2010). Bedrock fracturing, threshold hillslope, and limits to the

magnitude of bedrock landslides. *Earth and Planetary Science Letters*, 297:577–586.

Clark, R. N., Swayze, G. A., Livo, K. E., Kokaly, R. F., Sutley, S. J., Dalton, J. B., McDougal, R. R., and Gent, C. A. (2003). Imaging spectroscopy: Earth and planetary remote sensing with the usgs tetracorder and expert systems. *Journal of Geophysical Research*, 108(E12):5131.

Claudin, P. and Andreotti, B. (2006). A scaling law for aeolian dunes on mars, venus, earth, and for subaqueous ripples. *Earth and Planetary Science Letters*, 252(1–2):30–44.

Codilean, A. T. (2006). Calculation of the cosmogenic nuclide production topographic shielding scaling factor for large areas using dems. *Earth Surface Processes and Landforms*, 31(6):785–794.

Copland, L., Pope, S., Bishop, M. P., Shroder, Jr., J. F., Clendon, P., Bush, A., Kamp, U., Seong, Y. B., and Owen, L. A. (2009). Glacier velocities across the central karakoram. *Annals of Glaciology*, 50(52):41–49.

Cossart, É. and Fressard, M. (2017). Assessment of structural sediment connectivity within catchments: insights from graph theory. *Earth Surface Dynamics*, 5:253–268.

Cova, T. J. and Goodchild, M. F. (2002). Extending geographical representation to include fields of spatial objects. *International Journal of Geographical Information Science*, 16(6):509–532.

Crouch, S. L. and Starfield, A. M. (1983). *Boundary Element Methods in Solid Mechanics*. George Allen and Unwin Ltd., London, UK.

Danesh-Yazdi, M., Tejedor, A., and Foufoula-Georgiou, E. (2017). Self-dissimilar landscapes: Revealing the signature of geologic constraints of landscape dissection via topologic and multiscale analysis. *Geomorphology*, 295:16–27.

Dao, D. V., Jaafari, A., Bayat, M., Mafi-Gholami, D., Qi, C., Moayedi, H., Phong, T. V., Ly, H.-B., Le, T.-T., Trinh, P. T., Luu, C., Quoc, N. K., Thanh, B. N., and Pham, B. T. (2020). A spatially explicit deep learning neural network model for the prediction of landslide susceptibility. *Catena*, 188:104451.

Dar, Q. U. Z., Renhai, P., Ghazi, S., Sajid, Z., Wahab, A., Zubair, R. A., and Aziz, T. (2021). The precambrian hazara formation from hazara mountains, northern pakistan. *Arabian Journal of*

Geosciences, 14:134.

de Boer, D. H. (1992). Hierarchies and spatial scale in process geomorphology: A review. *Geomorphology*, 4:303–318.

Decker, E. R. and Smithson, S. B. (1975). Heat flow and gravity interpretation across the rio grande rift in southern new mexico and west texas. *Journal of Geophysical Research*, 80(17):2542–2552.

Dehn, M., Gärtner, H., and Dikau, R. (2001). Principles of semantic modeling of landform structures. *Computers & Geosciences*, 27:1005–1010.

DeMers, M. N. (2001). *GIS Modeling in Raster*. Wiley, New Jersey, USA.

Deng, Y. (2007). New trends in digital terrain analysis: Landform definition, representation and classification. *Progres in Physical Geography*, 31(4):405–419.

Deng, Y. and Wilson, J. P. (2008). Multi-scale and multi-criteria mapping of mountain peaks as fuzzy entities. *International Journal of Geographic Information Science*, 22(2):205–218.

Derbyshire, E. (1996). Quaternary glacial sediments, glaciation style, climate and uplift in the karakoram and northwest himalaya: review and speculations. *Palaeogeography, Palaeoclimatology, Palaeoecology*, 120(1–2):147–157.

Derbyshire, E. and Owen, L. A. (1997). Quaternary glacial history of the karakoram mountains and northwest himalayas: A review. *Quaternary International*, 38–39:85–102.

Desilets, D., Zreda, M., and Prabu, T. (2006). Extended scaling factors for in situ cosmogenic nuclides: New measurements at low latitude. *Earth and Planetary Science Letters*, 246:265–276.

DiBiase, R. A. and Whipple, K. X. (2011). The influence of erosion thresholds and runoff variability on the relationships among topography, climate, and erosion rate. *Journal of Geophysical Research*, 116:F04036.

DiBiase, R. A., Whipple, K. X., Heimsath, A. M., and Ouimet, W. B. (2010). Landscape form and millennial erosion rates in the san gabriel mountains, ca. *Earth and Planetary Science Letters*, 289:134–144.

Dikau, R. (1989). The application of a digital relief model to landform analysis in geomorphology. In Raper, J., editor, *Three dimensional applications in GIS*, pages 51–77. CRC Press.

Divyadarshini, A. and Singh, V. (2019). Investigating topographic metrics to decipher structural model and morphotectonic evolution of the frontal siwalik ranges, central himalaya, nepal. *Geomorphology*, 337:31–52.

Dobreva, I. D., Bishop, M. P., and Bush, A. B. G. (2017). Climate-glacier dynamics and topographic forcing in the karakoram himalaya: Concepts, issues and research directions. *Water*, 9:405.

Dodov, B. A. and Foufoula-Georgiou, E. (2006). Floodplain morphometry extraction from a high-resolution digital elevation model: A simple algorithm for regional analysis studies. *IEEE Geoscience and Remote Sensing Letters*, 3(3):410–413.

Dortch, J. M., Dietsch, C., Owen, L. A., Caggee, M. W., and Ruppert, K. (2011a). Episodic fluvial incision of rivers and rock uplift in the himalaya and transhimalaya. *Journal of the Geological Society, London*, 168:783–804.

Dortch, J. M., Owen, L. A., Schoenbohm, L. M., and Caffee, M. W. (2011b). Asymmetrical erosion and morphological development of the central ladakh range, northern india. *Geomorphology*, 135:167–180.

Drăguţ, L. and Blaschke, T. (2006). Automated classification of landform elements using object-based image analysis. *Geomorphology*, 81:330–344.

Drăguţ, L. and Eisank, C. (2011). Object representations at multiple scales from digital elevation models. *Geomorphology*, 129:183–189.

Drăguţ, L., Tiede, D., and Levick, S. R. (2010). Esp: a tool to estimate scale parameter for multiresolution image segmentation of remotely sensed data. *International Journal of Geographical Information Science*, 24(6):859–871.

Dunai, T. J. (2000). Scaling factors for production rates of in situ produced cosmogenic nuclides: a critical reevaluation. *Earth and Planetary Science Letters*, 176:157–169.

Dunai, T. J. (2001). Influence of secular variation of the geomagnetic field on production rates of

in situ produced cosmogenic nuclides. *Earth and Planetary Science Letters*, 1993:197–212.

Duvall, A. R. and Tucker, G. E. (2015). Dynamic ridges and valleys in a strike-slip environment. *Journal of Geophysical Research: Earth Surface*, 120:2016–2026.

Ehlers, T. A. and Farley, K. A. (2003). Apatite (u-th)/he thermochronometry: methods and applications to problems in tectonic and surface processes. *Earth and Planetary Science Letters*, 206(1–2):1–14.

Evans, I. S. (2012). Geomorphometry and landform mapping: What is a landform? *Geomorphology*, 137:94–106.

Ewing, R. C. and Kocurek, G. (2010). Aeolian dune-field pattern bondary conditions. *Geomorphology*, 114:175–187.

Farinotti, D., Immerzeel, W. W., de Kok, R. J., Quincey, D. J., and Dehecq, A. (2020). Manifestations and mechanisms of the karakoram glacier anomaly. *Nature Geoscience*, 13:8–16.

Finnegan, Noah J. ad Hallet, B., Montgomery, D. R., Zeitler, P. K., Stone, J. O., Anders, A. M., and Yuping, L. (2008). Coupling of rock uplift and river incision in the namche barwa-gyala peri massif, tibet. *GSA Bulletin*, 120(1/2):142–155.

Fisher, P. and Wood, J. (1998). What is a mountain? or the englishman who went up a boolean geographical concept but realized it was fuzzy. *Geography*, 83(3):247–256.

Fisher, P., Wood, J., and Cheng, T. (2005). Fuzziness and ambiguity in multi-scale analysis of landscape morphometry. In Petry, F. E., Robinson, V. B., and Cobb, M. A., editors, *Fuzzy Modeling with Spatial Information for Geographic Problems*, pages 209–232. Springer.

Forsythe, N., Fowler, H. J., Li, X.-F., Blenkinsop, S., and Pritchard, D. (2017). Karakoram temperature and glacial melt driven by regional atmospheric circulation variability. *Nature Climate Change*, 7:664–670.

Foster, D. A., Gleadow, A. J. W., and Mortimer, G. (2010). Rapid pliocene exhumation in the karakoram (pakistan) revealed by fission-track thermochronology of the k2 gneiss. *Geology*, 22:19–22.

Gallant, J. C. and Dowling, T. I. (2003). A multiresolution index of valley bottom flatness for

mapping depositional areas. *Water Resources Research*, 39(12):1347.

Gasparini, N. M. and Brandon, M. T. (2011). A generalized power law approximation for fluvial incision of bedrock channels. *Journal of Geophysical Research*, 116:F02020.

Ge, X., Safa, I., Belkin, M., and Wang, Y. (2011). Data skeletonization via reeb graphs. In Shawe-Taylor, J., Zemel, R., Bartlett, P., Pereira, F., and Weinberger, K., editors, *Advances in Neural Information Processing Systems*, volume 24, pages 837–845. Neural Information Processing Systems Foundation, Inc., San Diego, CA, USA.

Gibson, M. J., Glasser, N. F., Quincey, D. J., Mayer, C., Rowan, A. V., and Irvine-Fynn, T. D. L. (2017). Temporal variations in supraglacial debris distribution on baltoro glacier, karakoram between 2001 and 2012. *Geomorphology*, 295:572–585.

Gilbert, J. T., Macfarlane, W. W., and Wheaton, J. M. (2016). The valley bottom extaction tool (v-bet): A gis tool for delineating valley bottoms across drainage networks. *Computers & Geosciences*, 97:1–14.

Goetz, J. N., Brenning, A., Petschko, H., and Leopold, P. (2015). Evaluating machine learning and statistical prediction techniques for landslide susceptibility modeling. *Computers and Geosciences*, 81:1–11.

González, C., Ortigosa, L., Martí, C., and Gacía-Ruiz, J. M. (1995). The study of the spatial organization of geomorphic processes in mountain areas using gis. *Mountain Research and Development*, 15(3):241–249.

Goodchild, M. F. (2017). Imprecision and spatial uncertainty. In Shekhar, S., Xiong, H., and Zhou, X., editors, *Encyclopedia of GIS*. Springer, Switzerland.

Goodchild, M. F., Yuan, M., and Cova, T. J. (2007). Towards a general theory of geographic representation in gis. *International Journal of Geographic Information Science*, 21(3):239–260.

Graf, W. L. (1970). The geomorphology of the glacial valley cross section. *Arctic and Alpine Research*, 2(4):303–312.

Grande, A., Schmidt, A. H., Bierman, P. R., Corbett, L. B., López-Lloreda, C., Willenbring, J., McDowell, W. H., and Caffee, M. W. (2021). Landslides, hurricanes, and sediment sourcing

impact basin-scale erosion estimates in luquillo, puerto rico. *Earth and Planetary Science Letters*, 562:116821.

Granger, D. E., Kirchner, J. W., and Finkel, R. (1996). Spatially averaged long-term erosion rates measured from in situ-produced cosmogenic nuclides in alluvial sediment. *Journal of Geology*, 104(3):249–257.

Grant, K. L., Stokes, C. R., and Evans, I. S. (2009). Identification and characteristics of surge-type glaciers on novaya zemlya, russian arctic. *Journal of Glaciology*, 55(194):960–972.

Grauso, S., Pasanisi, F., and Tebano, C. (2018). Assessment of a simplified connectivity index and specific sediment potential in river basins by means of geomorphometric tools. *Geosciences*, 8:48.

Gray, H. J., Shobe, C. M., Hobley, D. E. J., Tucker, G. E., Duvall, A. R., Harbert, S. A., and Owen, L. A. (2018). Off-fault deformation rate along the southern san andreas fault at mecca hills, southern california, inferred from landscape modeling of curved drainages. *Geology*, 46(1):59–62.

Gruber, S., Huggel, C., and Pike, R. (2009). Modeling mass movements and landslide susceptibility. In Hengl, T. and Reuter, H. I., editors, *Geomorphometry: Concepts, software, applications*, volume 33 of *Developments in Soil Science*, pages 527–550. Elsevier, New York, NY, USA.

Guth, P. L. (2011). Drainag basin morphometry: a global snapshot from the shuttle radar topography mission. *Hydrology and Earth System Sciences*, 15:2091–2099.

Guzzetti, F., Reichenbach, P., Ardizzone, F., Cardinali, M., and Galli, M. (2006). Estimating the quality of landslide susceptibility models. *Geomorphology*, 81:166–184.

Hallet, B. (1990). Spatial self-organization in geomorphology: From periodic bedforms and patterned ground to scale-invariant topography. *Earth-Science Reviews*, 29:57–75.

Heckmann, T., Hilger, L., Vehling, L., and Becht, M. (2016). Integrating field measurements, a geomorphological map and stochastic modelling to estimate the spatially distributed rockfall sediment budget of the upper kaunertal, austrian central alps. *Geomorphology*, 260:16–31.

Heckmann, T. and Schwanghart, W. (2013). Geomorphic coupling and sediment connectivity in

an alpine catchment–exploring sediment cascades using graph theory. *Geomorphology*, 182:89–103.

Heckmann, T., Schwanghart, W., and Phillips, J. D. (2015). Graph theory—recent developments of its application in geomorphology. *Geomorphology*, 243:130–146.

Hewitt, K. (2005). The karakoram anomaly? glacier expansion and the 'elevation effect,' karakoram himalaya. *Mountain Research and Development*, 25(4):332–340.

Hewitt, K. (2009). Rock avalanches that travel onto glaciers and related developments, karakoram himalaya, inner asia. *Geomorphology*, 103:66–79.

Hewitt, K. and Liu, J. (2010). Ice-dammed lakes and outburst floods, karakoram himalaya: Historical perspectives on emerging threats. *Physical Geography*, 31(6):528–551.

Hoeser, T. and Kuenzer, C. (2020). Object detection and image segmentation with deep learning on earth observation data: A review-part i: Evolution and recent trends. *Remote Sensing*, 12:1667.

Hooshyar, M., Wang, D., Kim, S., Medeiros, S. C., and Hagen, S. C. (2016). Valley and channel networks extraction based on local topographic curvature and *k*-means clustering of contours. *Water Resources Research*, 52:8081–8102.

Houser, C., Bishop, M. P., and Wernette, P. (2017). Short communication: Multi-scale topographic anisotropy patterns on a barrier island. *Geomorphology*, 297:153–158.

Huo, D., Bishop, M. P., and Bush, A. B. G. (2021). Understanding complex debris-covered glaciers: Concepts, issues, and research directions. *Frontiers in Earth Science*, 9:652279.

Huo, D., Bishop, M. P., Young, B. W., Chi, Z., and Haritashya, U. K. (2020). Numerical modeling issues for understanding complex debris-covered glaciers. In *Reference Module in Earth Systems and Environmental Systems*. Elsevier.

Hurst, M. D., Mudd, S. M., Walcott, R., Attal, M., and Yoo, K. (2012). Using hilltop curvature to derive the spatial distribution of erosion rates. *Journal of Geophysical Research*, 117:F02017.

Ilinca, V. and Gheuca, I. (2011). The red lake landslide (ucigaşu mountain, romania). *Carpathian Journal of Earth and Environmental Sciences*, 6(1):263–272.

Imbroane, A., Melenti, C., and Gorgan, D. (2007). Mineral explorations by landsat image ratios.

Ninth International Symposium on Symbolic and Numeric Algorithms for Scientific Computing, pages 335–340.

Jaiswara, N. K., Kotluri, S. K., Pandey, A. K., and Pandey, P. (2019). Transient basin as indicator of tectonic expressions in bedrock landscape: Approach based on matlab geomorphic tool (transient-profiler). *Geomorphology*, 346:106853.

James, L. A. (1996). Polynomial and power functions for glacial valley cross-section morphology. *Earth Surface Processes and Landforms*, 21:413–432.

Jasiewicz, J. (2003-2020 (accessed July 14, 2020)). Grass gis 7.8.4dev reference manual: r.convergence. `https://grass.osgeo.org/grass78/manuals/addons/r.convergence.html`.

Jasiewicz, J. and Stepinski, T. F. (2013). Geomorphons–a pattern recognition approach to classification and mapping of landforms. *Geomorphology*, 182:147–156.

Jenness, J. S. (2004). Calculating landscape surface area from digital elevation models. *Wildlife Society Bulletin*, 32(3):829–839.

Jensen, J. R. (2000). *Remote Sensing of the Environment: An Earth Resource Perspective*. Pearson Education, New Jersey, USA.

Jenson, S. K. and Domingue, J. O. (1988). Extracting topographic structure from digital elevation data for geographic information system analysis. *Photogrammetric Engineering and Remote Sensing*, 54(11):1593–1600.

Juliani, C. (2019). Automated discrimination of fault scarps along an arctic mid-ocean ridge using neural networks. *Computers and Geosciences*, 124:27–36.

Kamp, U., Growley, B. J., Khattak, G. A., and Owen, L. A. (2008). Gis-based landslide susceptibility mapping for the 2005 kashmir earthquake region. *Geomorphology*, 101:631–642.

Kasprak, A., Caster, J., Bangen, S. G., and Sankey, J. B. (2017). Geomorphic process from topographic form: Automating the interpretation of repeat survey data in river valleys. *Earth Surface Processes and Landforms*, 42:1872–1883.

Kirchner, J. W. (1993). Statistical inevitability of horton's laws and the apparent randomness of

stream channel networks. *Geology*, 21:591–594.

Kocurek, G. and Ewing, R. C. (2016). Trickle-down and trickle-up boundary conditions in eolian dune-field pattern formation. In Budd, D. A., Hajek, Elizabeth, A., and Purkis, S. J., editors, *Autogenic Dynamics and Self-Organization in Sedimentary Systems, Special Publication*, volume 106, pages 5–17. SEPM.

Kohl, C. P. and Nishiizumi, K. (1992). Chemical isolation of quartz for measurement of in situ-produced cosmogenic nuclides. *Geochimica et Cosmochimica Acta*, 56(9):3583–3587.

Koka, S., Anada, K., and Yaku, T. (2017). Algorithm for ridge and valley detects in terrain maps. *Journal of Computational Methods in Sciences and Engineering*, 17:S95–S110.

Koons, P. O., Upton, P., and Barker, A. D. (2012). The influence of mechanical properties on the link between tectonic and topographic evolution. *Geomorphology*, 137:168–180.

Koons, P. O., Zeitler, P. K., Chamberlain, C. P., Craw, D., and Meltzer, A. S. (2002). Mechanical links between erosion and metamorphism in nanga parbat, pakistan himalaya. *American Journal of Science*, 302:749–773.

Koppes, M. N. and Montgomery, D. R. (2009). The relative efficacy of fluvial and glacial erosion over modern to orogenic timescales. *Nature Geoscience*, 2:644–647.

Kořínková, D., Svojtka, M., and Kalvoda, J. (2014). Rate of erosion and exhumation of crystalline rocks in the hunza karakoram defined by apatite fission track analysis. *Acta Geodynamica Geomaterialia*, 11(3(175)):235–253.

Lal, D. (1991). Cosmic ray labeling of ersion surfaces: *in situ* nuclide production rates and erosion models. *Earth and Planetary Science Letters*, 104:424–439.

Larin-Fonseca, R. and Garea-Llano, E. (2010). Topological relations as rule for automatic generation of geospatial application ontology. In *Proceedings of the VII Jornadas para el Desarrollo de Grandes Aplicaciones de Red*.

Larsen, I. J. and Montgomery, D. R. (2012). Landslide erosion coupled to tectonics and river incision. *Nature Geoscience*, 5:468–473.

Lastochkin, A. N., Zhirov, A. I., and Boltramovich, S. F. (2018). System-morphological ap-

proach: Another look at morphology research and geomorphological mapping. *Geomorphology*, 303:486–503.

Li, G. K. and Moon, S. (2021). Topographic stress control on bedrock landslide size. *Nature Geoscience*, 14:307–313.

Li, Y., Liu, G., and Cui, Z. (2001). Glacial valley cross-profile morphology, tian shan mountains, china. *Geomorphology*, 38:153–166.

Li, Y.-k. (2013). Determining topographic shielding from digital elevation models for cosmogenic nuclide analysis: a gis approach and field validation. *Journal of Mountain Science*, 10(3):355–362.

Liang, C. and Mackay, D. S. (2000). A general model of watershed extraction and representation using globally optimal flow paths and up-slope contributing areas. *International Journal of Geographical Information Science*, 14(4):337–358.

Lin, Z. and Oguchi, T. (2009). Longitudinal and transverse profiles of hilly and mountainous watersheds in japan. *Geomorphology*, 111:17–26.

Lindsay, J. B., Newman, D. R., and Francioni, A. (2019). Scale-optimized surface roughness for topographic analysis. *Geosciences*, 9:322.

Lingua, A. and Noardo, F. (2015). A semantic geodatabase for environment analysis: Extraction, management and sharing of earth and water information in gis. In Grueau, C. and Rocha, J. G., editors, *Proceedings of the 1st International Conference on Geographic Information Systems Theory, Applications and Management*, pages 213–220. SCITEPRESS.

Liu, K. and Shi, W. (2006). Computing the fuzzy topological relations of spatial objects based on induced fuzzy topology. *International Journal of Geographical Information Science*, 20(8):857–883.

Liu, K., Song, C., Ke, L., Jiang, L., and Ma, R. (2020). Automatic watershed delineation in the tibetan endorheic basin: A lake-oriented approach based on digital elevation models. *Geomorphology*, 358:107127.

Lucieer, A. and Stein, A. (2005). Texture-based landform segmentation of lidar imagery. *Interna-*

tional Journal of Applied Earth Observation and Geoinformation, 6:261–270.

MacGregor, K. R., Anderson, R. S., Anderson, S. P., and Waddington, E. D. (2000). Numerical simulations of glacial-valley longitudinal profile evolution. *Geology*, 28(11):1031–1034.

MacGregor, K. R., Anderson, R. S., and Waddington, E. D. (2009). Numerical modeling of glacial erosion and headwall processes in alpine valleys. *Geomorphology*, 103:189–204.

MacMillan, R. A. and Shary, P. A. (2009). Landforms and landform elements in geomorphometry. In Hengl, T. and Reuter, H. I., editors, *Geomorphometry: Concepts, software, applications*, volume 33 of *Developments in Soil Science*, pages 227–254. Elsevier, New York, NY, USA.

Mahar, M. A., Mahéo, G., Goodell, P. C., and Pavlis, T. L. (2014). Age and origin of post collision baltoro granites, south karakoram, north pakistan: Insights from in-situ u-pb, hf and oxygen isotopic record of zircons. *Lithos*, 205:341–358.

Mahmood, S. and Rahman, A.-u. (2019). Flash flood susceptibility modeling using geomorphometric and hydrological approaches in panjkora basin, eastern hindu kush, pakistan. *Environmental Earth Sciences*, 78:43.

Mark, D. M. (1975). Geomorphometric parameters: A review and evaluation. *Physical Geography*, 57(3/4):165–177.

Martel, S. J. and Muller, J. R. (2000). A two-dimensional boundary element method for calculating elastic gravitational stresses in slopes. *Pure and Applied Geophysics*, 157:989–1007.

Martz, L. W. and Garbrecht, J. (1992). Numerical definition of drainage network and subcatchment areas from digital elevation models. *Computers & Geosciences*, 18(6):747–761.

Martz, L. W. and Garbrecht, J. (1993). Automated extraction of drainage network and watershed data from digital elevation models. *Water Resources Bulletin*, 29(6):901–908.

McDonnell, J. J., Sivapalan, M., Vaché, K., Dunn, S., Grant, G., Haggerty, R., Hinz, C., Hooper, R., Kirchner, J., Roderick, M. L., Selker, J., and Weiler, M. (2007). Moving beyond heterogeneity and process complexity: A new vision for watershed hydrology. *Water Resources Research*, 43:W07301.

Minár, J. and Evans, I. S. (2008). Elementary forms for land surface segmentation: The theoretical

basis of terrain analysis and geomorphological mapping. *Geomorphology*, 95:236–259.

Mitchell, S. G. and Montgomery, D. R. (2006). Influence of a glacial buzzsaw on the height and morphology of the cascade range in central washington state, usa. *Quaternary Research*, 65:96–107.

Mitra, G. and Marshak, S. (1988). *Basic methods of structural geology*. Prentice Hall, New Jersey, USA.

Moglen, G. E. and Bras, R. L. (1995). The effect of spatial heterogeneities on geomorphic expression in a model of basin evolution. *Water Resources Research*, 31(10):2613–2623.

Molnar, P. (2004). Interactions among topographically induced elastic stress, static fatigue, and valley incision. *Journal of Geophysical Research*, 109:F02010.

Montgomery, D. R. (2001). Slope distributions, threshold hillslopes, and steady-state topography. *American Journal of Science*, 301:432–454.

Montgomery, D. R. (2002). Valley formation by fluvial and glacial erosion. *Geology*, 30(11):1047–1050.

Montgomery, D. R. and Brandon, M. T. (2002). Topographic controls on erosion rates in tectonically active mountain ranges. *Earth and Planetary Science Letters*, 201:481–489.

Moon, S., Perron, J. T., Martel, S. J., Goodfellow, B. W., Ivars, D. M., Hall, A., Heyman, J., Munier, R., Näslund, J.-O., Simeonov, A., and Stroeven, A. P. (2020). Present-day stress field influences bedrock fracture openness deep into the subsurface. *Geophysical Research Letters*, 47:e2020GL090581.

Moon, S., Perron, J. T., Martel, S. J., Holbrook, W. S., and St. Clair, J. (2017). A model of three-dimensional topographic stress with implications for bedrock fractures, surface processes, and landscape evolution. *Journal of Geophysical Research: Earth Surface*, 122:823–846.

Mudd, S. M., Attal, M., Milodowski, D. T., Grieve, S. W. D., and Valters, D. A. (2014). A statistical framework to quantify spatial variation in channel gradients using the integral method of channel profile analysis. *Journal of Geophysical Research: Earth Surface*, 119:138–152.

Mughal, M. S., Zhang, C., Du, D., Zhang, L., Mustafa, S., Hameed, F., Khan, M. R., Zaheer, M.,

and Blaise, D. (2018). Petrography and provenance of the early miocene murree formation, himalayan foreland basin, muzaffarabad, pakistan. *Journal of Asian Earth Sciences*, 162:25–40.

Muller, J. R. and Martel, S. J. (2000). Numerical models of translational landslide rupture surface growth. *Pure and Applied Geophysics*, 157:1009–1038.

NASA JPL (2013). Nasa shuttle radar topography mission 1 arc second, version 3 [data set].

NASA LP DAAC (2015). Aster level 1 precision terrain corrected registered at-sensor radiance v003 [data set].

Newman, D. R., Lindsay, J. B., and Cockburn, J. M. H. (2018). Measuring hyperscale topographic anisotropy as a continuous landscape property. *Geosciences*, 8:278.

Niemi, N. A., Oskin, M., Burbank, D. W., Heimsath, A. M., and Gabet, E. J. (2005). Effects of bedrock landslides on cosmogenically determined erosion rates. *Earth and Planetary Science Letters*, 237(3–4):480–498.

Nishiizumi, K., Imamura, M., Caffee, M. W., Southon, J. R., Finkel, R. C., and McAninch, J. (2007). Absolution calibration of ^{10}be ams standards. *Nuclear Instruments and Methods in Physics Research Section B: Beam Interactions with Materials and Atoms*, 258(2):403–413.

Nugraha, H., Wacano, D., Dipayana, G. A., Cahyadi, A., Mutaqin, B. W., and Larasati, A. (2015). Geomorphometric characteristics of landslides in the tinalah watershed, menoreh mountains, yogyakarta, indonesia. *Preocedia Environmental Sciences*, 28:578–586.

O'Callaghan, J. F. and Mark, D. M. (1984). The extraction of drainage networks from digital elevation data. *Computer Vision, Graphics, and Image Processing*, 28(3):323–344.

Ode, Å., Hagerhall, C. M., and Sang, N. (2010). Analyzing visual landscape complexity: Theory and application. *Landscape Research*, 35(1):111–131.

Olaya, V. (2009). Basic land-surface parameters. In Hengl, T. and Reuter, H. I., editors, *Geomorphometry: Concepts, software, applications*, volume 33 of *Developments in Soil Science*, pages 141–169. Elsevier, New York, NY, USA.

Oruonye, E. D., Ezekiel, B. B., Atiku, H. G., Baba, E., and Musa, N. I. (2015). Drainage basin morphometric parameters of river lamurde: Implication for hydrologic and geomorphic processes.

Journal of Agriculture and Ecology Research International, 5(2):1–11.

Owen, L. A. (1989). Neotectonics and glacial deformation in the karakoram mountains and nanga parbat himalaya. *Tectonophysics*, 163:227–265.

Owen, L. A. (2018). Earth surface processes and landscape evolution in the himalaya: a framework for sustainable development and geohazard mitigation. In Pant, N. C., Ravindra, R., Srivastava, D., and Thompson, L. G., editors, *The Himalayan Cryosphere: Past and Present*, Geological Society, London, Special Publications 462, pages 169–188. The Geological Society of London, London, UK.

Owen, L. A., Gualtieri, L., Finkel, R. C., Caffee, M. W., Benn, D. I., and Sharma, M. C. (2001). Cosmogenic radionuclide dating of glacial landforms in the lahul himalaya, northern india: defining the timing of late quaternary glaciation. *Journal of Quaternary Science*, 16(6):555–563.

Ozulu, İ. M. and Gökgöz, T. (2018). Examining the stream threshold approaches used in hydrologic analysis. *International Journal of Geo-Information*, 7(6):201.

Park, E. (2020). Characterizing channel-floodplain connectivity using satellite altimetry: Mechanism, hydrogeomorphic control, and sediment budget. *Remote Sensing of Environment*, 243:10.1016/j.rse.2020.111783.

Parvis, M. (1950). Drainage pattern significance in airphoto identification of soils and bedrocks. *Highway Research Board Bulletin*, 28:36–62.

Passalacqua, P., Trung, T. D., Foufoula-Georgiou, E., Sapiro, G., and Dietrich, W. E. (2010). A geometric framework for channel network extraction from lidar: Nonlinear diffusion and geodesic paths. *Journal of Geophysical Research*, 115:F01002.

Pereira-Claren, A., Gironás, J., Niemann, J. D., Passalacqua, P., Mejia, A., and Escauriaza, C. (2019). Planform geometry and relief characterization of drainage networks in high-relief environments: An analysis of chilean andean basins. *Geomorphology*, 341:46–64.

Perron, J. T., Dietrich, W. E., and Kirchner, J. W. (2008). Controls on the spacing of first-order valleys. *Journal of Geophysical Research*, 113:F04016.

Perron, J. T. and Royden, L. (2013). An integral approach to bedrock river profile analysis. *Earth Surface Processes and Landforms*, 38:570–576.

Phillips, J. D. (1988). The role of spatial scale in geomorphic systems. *Geographical Analysis*, 20(4):308–317.

Phillips, J. D. (1999). Edge effects in geomorphology. *Physical Geography*, 20(1):53–66.

Phillips, J. D. (2003). Sources of nonlinearity and complexity in geomorphic systems. *Progress in Physical Geography*, 27(1):1–23.

Phillips, J. D. (2007). The perfect landscape. *Geomorphology*, 84:159–169.

Phillips, J. D. (2016). Vanishing point: Scale independence in geomorphological hierarchies. *Geomorphology*, 266:66–74.

Phillips, J. D., Schwanghart, W., and Heckmann, T. (2015). Graph theory in the geosciences. *Earth-Science Reviews*, 143:147–160.

Pike, R. J. (2000). Geomorphometry–diversity in quantitative surface analysis. *Progress in Physical Geography*, 24(1):1–20.

Pike, R. J. (2002). A bibliography of terrain modeling (geomorphometry), the quantitative representation of topography—supplement 4.0. Open-file report 02-465, United State Geological Survey.

Pike, R. J., Evans, I., and Hengl, T. (2009). Geomorphometry: A brief guide. In Hengl, T. and Reuter, H. I., editors, *Geomorphometry: Concepts, software, applications*, volume 33 of *Developments in Soil Science*, pages 3–30. Elsevier, New York, NY, USA.

Pike, R. J. and Wilson, S. E. (1971). Elevation-relief ratio, hypsometric integral, and geomorphic area-altitude analysis. *Geological Society of America Bulletin*, 82(4):1079–1084.

Pilotti, M. (2016). Extraction of cross sections from digital elevation model for one-dimensional dam-break wave propoagation in mountain valleys. *Water Resources Research*, 52:52–68.

Portenga, E. W. and Bierman, P. R. (2011). Understanding earth's eroding surface with $^{1}0$be. *GSA Today*, 21(8):4–10.

Prasicek, G., Otto, J.-C., Montgomery, D. R., and Schrott, L. (2014). Multi-scale curvature for

automated identification of glaciated mountain landscapes. *Geomorphology*, 209:53–65.

Proy, C., Tanré, D., and Deschamps, D. Y. (1989). Evaluation of topographic effects in remotely sensed data. *Remote Sensing of Environment*, 30(1):21–32.

Qasim, M., Ding, L., Khan, M. A., Umar, M., Jadoon, I. A. K., Haneef, M., Baral, U., Cai, F., Shah, A., and Yao, W. (2017). Late neoproterozoic-early palaeozoic stratigraphic succession, western himalaya, north pakistan: Detrital zircon provenance and tectonic implications. *Geological Journal*, 53(5):1–22.

Quincey, D. J., Braun, M., Glasser, N. F., Bishop, M. P., Hewitt, K., and Luckman, A. (2011). Karakoram glacier surge dynamics. *Geophysical Research Letters*, 38:L18504.

Quincey, D. J., Glasser, N. F., Cook, S. J., and Luckman, A. (2015). Heterogeneity in karakoram glacier surges. *Journal of Geophysical Research: Earth Surface*, 120:1288–1300.

Rak, R., Kwapień, J., Oświęcimka, P., Zięba, P., and Drożdż, S. (2019). Universal features of mountain ridge networks on earth. *Journal of Complex Networks*, 0000:1–21.

Rankl, M., Kienholz, C., and Braun, M. H. (2014). Glacier changes in the karakoram region mapped by multimission satellite imagery, links to geotiff and esri shape file. *PANGAEA*. Supplement to: Rankl, M et al. (2014): Glacier changes in the Karakoram region mapped by multimission satellite imagery. The Cryosphere, 8(3), 977–989, doi:10.5194/tc-8-977-2014.

Raup, B. H., Racoviteanu, A., Khalsa, S. J. S., Helm, C., Armstrong, R., and Arnaud, Y. (2007). The glims geospatial glacier database: a new tool for studying glacier change. *Global and Planetary Change*, 56:101–110.

Reiners, P. W. and Brandon, M. T. (2006). Using thermochronoloy to understand orogenic erosion. *Annual Review of Earth and Planetary Science*, 34:419–466.

Rempe, D. M. and Dietrich, W. E. (2014). A bottom-up control on fresh-bedrock topography under landscapes. *PNAS*, 111(18):6576–6581.

Rhoads, B. L. (2006). The dynamic basis of geomorphology reenvisioned. *Annals of the Association of American Geographers*, 96(1):14–30.

Rhoads, B. L. and Johson, K. K. (2018). Three-dimensional flow structure, morphodynamics, sus-

pended sediment, and thermal mixing at an asymmetrical river confluence of a straight tributary and curving main channel. *Geomorphology*, 323:51–69.

Ritter, D. F. (1988). Landscape analysis and the search for geomorphic unity. *GSA Bulletin*, 100(2):160–171.

Ritter, D. F., Kochel, R. C., and Miller, J. R. (2002). *Process Geomorphology*. Waveland Press, Long Grove, IL, USA.

Roe, G. H., Montgomery, D. R., and Hallet, B. (2002). Effects of orographic precipitation variations on the concavity of steady-state river profiles. *Geology*, 30(2):143–146.

Roering, J. J. (2008). How well can hillslope evolution models "explain" topogrpahy? simulating soil transport and production with high-resolution topographic data. *Geological Society of America Bulletin*, 120(9/10):1248–1262.

Roering, J. J., Kirchner, J. W., and Dietrich, W. E. (1999). Evidence for nonlinear diffusive sediment transport on hillslopes and implications for landscape morphology. *Water Resources Research*, 35(3):853–870.

Roering, J. J., Perron, J. T., and Kirchner, J. W. (2007). Functional relationships between denudation and hillslope form and relief. *Earth and Planetary Science Letters*, 264:245–258.

Roland, Y., Mahéo, G., Guillot, S., and Pecher, A. (2001). Tectono-metamorphic evolution of the karakorum metamorphic complex (dassu-askole area, ne pakistan): exhumation of mid-crustal ht-mp gneisses in a convergent context. *Journal of Metamorphic Geology*, 19:717–737.

Rouse, J. W., Haas, R. H., Schell, J. A., and Deering, D. W. (1973). Monitoring vegetation systems in the great plains with erts. In Freden, S. C., Mercanti, E. P., and Becker, M. A., editors, *Proceedings of the Third Earth Resources Technology Satellite-1 Symposium, NASA SP-351*, pages 309–318.

Roy, S. G., Koons, P. O., Osti, B., Upton, P., and Tucker, G. E. (2016). Multi-scale characterization of topographic anisotropy. *Computers & Geosciences*, 90:102–116.

Różycka and Migoń, P. (2021). Morphometric properties of river basins as indicators of relative tectonic activity—problems of data handling and interpretation. *Geomorphology*, 389:107807.

Rubanenko, L., Pérez-López, S., Schull, J., and Lapôtre, M. G. A. (2021). Automatic detection and segmentation of barchan dunes on mars and earth using a convolutional neural network. *IEEE Journal of Selected Topics in Applied Earth Observations and Remote Sensing*, (Early Access):1.

Saha, P. K., Borgefors, G., and di Baja, G. S. (2016). A survey on skeletonization algorithms and their applications. *Pattern Recognition Letters*, 76:3–12.

Saha, S., Sharma, M. C., Murari, M. K., Owen, L. A., and Caffee, M. W. (2015). Geomorphology, sedimentology and minimum exposure ages of streamlined subglacial landforms in the nw himalaya, india. *Boreas*, 45(2):284–303.

Salleh, M. R. M., Rahman, M. Z. A., Ismail, Z., Khanan, M. F. A., and Razak, K. A. (2018). Multi-resolution remote sensing data in landslide activity inventory mapping. *IOP Conference Series: Earth and Environmental Science*, 169:012083.

Salma, S., Rehman, S., and Shah, M. A. (2012). Rainfall trends in different climate zones of pakistan. *Pakistan Journal of Meteorology*, 9(17):37–47.

Sangireddy, H., Carothers, R. A., Stark, C. P., and Passalacqua, P. (2016). Controls of climate, topography, vegetation, and lithology on drainage density extracted from high resolution topography data. *Journal of Hydrology*, 537:271–282.

Sărăşan, A., Józsa, E., Ardelean, A. C., and Drăguţ, L. (2019). Sensitivity of geomorphons to mapping specific landforms from a digital elevation model: A case study of drumlins. *Area*, 51(2):257–267.

Schaller, M., von Blanckenburg, F., Hovius, N., and Kubik, P. W. (2001). Large-scale erosion rates from in situ-produced cosmogenic nuclides in european river sediments. *Earth and Planetary Science Letters*, 188(3–4):441–458.

Scherler, D., Bookhagen, B., and Strecker, M. R. (2014). Tectonic control on $^{1}0$be-derived erosion rates in the garhwal himalaya, india. *Journal of Geophysical Research: Earth Surface*, 119:1–23.

Schmidt, J. and Dikau, R. (1999). Extracting geomorphometric attributes and objects from digital

elevation models—semantics, methods, future needs. In Dikau, R. and Saurer, H., editors, *GIS for Earth Surface Systems*, pages 153–173. Borntraeger, Berlin, Germany.

Schmidt, J. and Hewitt, A. (2004). Fuzzy land element classification from dtms base on geometry and terrain position. *Geoderma*, 121:243–256.

Schumm, S. A. and Lichty, R. W. (1965). Time, space, and causality in geomorphology. *American Journal of Science*, 263:110–119.

Schuur, E. A. G. and Abbott, B. (2011). High risk of permafrost thaw. *Nature*, 480:32–33.

Searle, M. P., Parrish, R. R., Thow, A. V., Noble, S. R., Phillips, R. J., and Waters, D. J. (2010). Anatomy, age and evolution of a collisional mountain belt: the baltoro granite batholith and karakoram metamorphic complex, pakistani karakoram. *Journal of the Geological Society, London*, 167:183–202.

Seong, Y. B., Bishop, M. P., Bush, A., Clendon, P., Copland, L., Finkel, R. C., Kamp, U., Owen, L. A., and Shroder, J. F. (2009a). Landforms and landscape evolution in the skardu, shigar and braldu valleys, central karakoram. *Geomorphology*, 103:251–267.

Seong, Y. B., Owen, L. A., Bishop, M. P., Bush, A., Clendon, P., Copland, L., Finkel, R., Kamp, U., and Shroder, Jr., J. F. (2007). Quaternary glacial history of the central karakoram. *Quaternary Science Reviews*, 26:3384–3405.

Seong, Y. B., Owen, L. A., Caffee, M. W., Kamp, U., Bishop, M. P., Bush, A., Copland, L., and Shroder, J. F. (2009b). Rock of basin-wide rockwall retreat in the k2 region of the central karakoram defined by terrestrial cosmogenic nuclide $^{1}0$be. *Geomorphology*, 107:254–262.

Shah, A. A. (2015). Kashmir basin fault and its tectonic significance in nw himalaya, jammu and kashmir, india. *International Journal of Earth Science*, 104:1901–1906.

Sharma, C. S., Mishra, A., and Panda, S. N. (2014). Assessing impact of flood on river dynamics and susceptible regions: Geomorphometric analysis. *Water Resources Management*, 28:2615–2638.

Sharma, G., Champati ray, P. K., and Mohanty, S. (2018). Morphotectonic analysis and gnss observations for assessment of relative tectonic activity in alaknanda basin of garhwal himalaya,

india. *Geomorphology*, 301:108–120.

Shary, P. A. (1995). Land surface in gravity points classification by a complete system of curvatures. *Mathematical Geology*, 27(3):373–390.

Shary, P. A., Sharaya, L. S., and Mitusov, A. V. (2002). Fundamental quantitative methods of land surface analysis. *Geoderma*, 107:1–32.

Shary, P. A., Sharaya, L. S., and Mitusov, A. V. (2005). The problem of scale-specific and scale-free approaches in geomorphometry. *Geographia Fisica e Dinamica Quaternaria*, 28:81–101.

Shelef, E. and Hilley, G. E. (2016). A unified framework for modeling landscape evolution by discrete flows. *Journal of Geophysical Research: Earth Surface*, 121:816–842.

Shi, W. and Liu, K. (2007). A fuzzy topology for computing the interior, boundary, and exterior of spatial objects quantitatively in gis. *Computers and Geosciences*, 33:898–915.

Shroder, Jr., J. F. (1993). *Himalaya to the Sea*. Routledge, London, UK.

Shroder, Jr., J. F., Owen, L. A., Seong, Y. B., Bishop, M. P., Bush, A., Caffee, M. W., Copland, L., Finkel, R. C., and Kamp, U. (2011). The role of mass movements on landscape evolution in the central karakoram: Discussion and speculation. *Quaternary International*, 236:34–47.

Shukla, A. and Garg, P. K. (2019). Evolution of a debris-covered glacier in the western himalaya during the last four decades (1971-2016): A multiparametric assessment using remote sensing and field observations. *Geomorphology*, 341:1–14.

Simons, F. J. and Olhede, S. C. (2013). Maximum-likelihood estimation of lithospheric flexural rigidity, initial-loading fraction and load correlation, under isotropy. *Geophysical Journal International*, 193:1300–1342.

Sinha, G. and Mark, D. (2010). Cognition based extraction and modeling of topographic eminences. *Cartographica*, 45(2):105–112.

Sklar, L. S. and Dietrich, W. E. (2001). Sediment and rock strength controls on river incision into bedrock. *Geology*, 29(12):1087–1090.

Sklar, L. S. and Dietrich, W. E. (2004). A mechanistic model for river incision into bedrock by saltating bedload. *Water Resources Research*, 40:W06301.

Slim, M., Perron, J. T., Martel, S. J., and Singha, K. (2015). Topographic stress and rock fracture: a two-dimensional numerical model for arbitrary topography and preliminary comparison with borehole observations. *Earth Surface Processes and Landforms*, 40:512–529.

Smith, A. (2010). Image segmentation scale parameter optimization and land cover classification using the random forest algorithm. *Journal of Space Science*, 55(1):69–79.

Smith, B. and Mark, D. M. (2003). Do mountains exist? towards an ontology of landforms. *Environment and Planning B: Planning and Design*, 30:411–427.

Smith, M. J., Hillier, J. K., Otto, C.-J., and Geilhausen, M. (2013). Geovisualization. In Bishop, M. P. and Shroder, J., editors, *Treatise on Geomorphology*, volume 3 of *Remote Sensing and GIScience in Geomorphology*, pages 299–325. Academic Press, San Diego, CA, USA.

Sofia, G. (2020). Combining geomorphometry, feature extraction techniques and earth-surface processes research: The way forward. *Geomorphology*, 355:107055.

St. Clair, J., Moon, S., Holbrook, W. S., Perron, J. T., Riebe, C. S., Martel, S. J., Carr, B., Harman, C., Singha, K., and Richter, D. d. (2015). Geophysical imaging reveals topographic stress control of bedrock weathering. *Science*, 350(6260):534–538.

Steinshouer, D. W., Qiang, J., McCabe, P. J., and Ryder, R. T. (1999). Maps showing geology, oil and gas fields and geologic provinces of the asia pacific region. Open-file report 97-470F, United States Geological Survey.

Stock, J. D. and Montgomery, D. R. (1999). Geologic constraints on bedrock river incision using the stream power law. *Journal of Geophysical Research*, 104(B3):4983–4993.

Stolar, D., Roe, G., and Willett, S. (2007). Controls on the patterns of topography and erosion rate in a critical orogen. *Journal of Geophysical Research*, 112:F04002.

Stone, J. O. (2000). Air pressure and cosmogenic isotope production. *Journal of Geophysical Research*, 105(B10):23,753–23,759.

Straumann, R. K. and Purves, R. S. (2011). Computation and elicitation of valleyness. *Spatial Cognition and Computation*, 11(2):178–204.

Struth, L., Garcia-Castellanos, D., Viaplana-Muzas, M., and Vergés, J. (2019). Drainage network

dynamics and knickpoint evolution in the ebro and duero basins: From endorheism to exorheism. *Geomorphology*, 327:554–571.

Struth, L., Teixell, A., Owen, L. A., and Babault, J. (2017). Plateau reduction by drainage divide migration in the eastern cordillera of columbia defined by morphometry and $^{1}0$be terrestrial cosmogenic nuclides. *Earth Surface Processes and Landforms*, 42:1155–1170.

Sweeney, K. E., Roering, J. J., and Ellis, C. (2015). Experimental evidence for hillslope control of landscape scale. *Science*, 349:51–53.

Syvitski, J. P. M. and Milliman, J. D. (2007). Geology, geography, and humans battle for dominance over the delivery of fluvial sediment to the coastal ocean. *The Journal of Geology*, 115:1–19.

Tarboton, D. G. (1997). A new method for the determination of flow directions and upslope areas in grid digital elevation models. *Water Resources Research*, 33(2):309–319.

Tarjan, R. (1972). Depth-first search and linear graph algorithms. *Society for Industrial and Applied Mathematical (SIAM) Journal on Computing*, 1(2):146–160.

Tate, N. J. and Wood, J. (2001). Fractals and scale dependencies in topography. In Tate, N. J. and Atkinson, P. M., editors, *Modelling Scale in Geographic Information Science*, pages 35–51. Wiley, New York, NY, USA.

Thakur, V. C. (1998). Structure of the chamba nappe and position of the main central thrust in kashmir himalaya. *Journal of Asian Earth Sciences*, 16(2–3):269–282.

Thoms, M. C., Piégay, H., and Parsons, M. (2018). What do you mean, 'resilient geomorphic systems'? *Geomorphology*, 305:8–19.

Thorn, C. E. and Welford, M. R. (1994). The equilibrium concept in geomorphology. *Annals of the Association of American Geographers*, 84(4):666–696.

Tomkin, J. H. and Braun, J. (2002). The influence of alpine glaciation on the relief of tectonically active mountain belts. *American Journal of Science*, 302:169–190.

Toulia, E., Kokinou, E., and Panagiotakis, C. (2018). The contribution of pattern recognition techniques in geomorphology and geology: The case study of tinos island (cyclades, aegean,

greece). *European Journal of Remote Sensing*, 51(1):88–99.

Trenc, N., Matoš, B., Velić, J., and Perković, D. (2019). Application of gis procedure for river terrace extraction from a lidar-based digital elevation model: The sava river valley nw of zagreb, croatia. *The Mining-Geology-Petroleum Engineering Bulletin*, 34(1):59–70.

Tucker, G. E. and Bras, R. L. (1998). Hillslope processes, drainage density, and landscaope morphology. *Water Resources Research*, 34(10):2751–2764.

Tucker, G. E. and Hancock, G. R. (2010). Modelling landscape evolution. *Earth Surface Processes and Landforms*, 35:28–50.

Turcotte, D. L. and Schubert, G. (2002). *Geodynamics*. Cambridge University Press, Cambridge, UK, 2 edition.

Turcotte, R., Fortin, J.-P., Rousseau, A. N., Massicotte, S., and Villeneuve, J.-P. (2001). Determination of the drainage structure of a watershed using a digital elevation model and a digital river and lake network. *Journal of Hydrology*, 240:225–242.

Ullah, K., Arif, M., and Tahir Shah, M. (2015). Petrography and geochemistry of the kamlial formation, southwestern kohat plateau, pakistan: implications for paleoclimate of the western himalayas. *Turkish Journal of Earth Sciences*, 24:276–288.

van der Beek, P. (2021). Stressed rocks cause big landslides. *Nature Geoscience*, 14:260–263.

Van Westen, C. J. (2013). Remote sensing and gis for natural hazards assessment and disaster risk management. In Shroder, J. and Bishop, M. P., editors, *Treatise on Geomorphology*, volume 3 of *Remote Sensing and GIScience in Geomorphology*, pages 259–298. Academic Press, Sand Diego, CA, USA.

Vance, D., Bickle, M., Ivy-Ochs, S., and Kubik, P. W. (2003). Erosion and exhumation in the himalaya from cosmogenic isotope inventories of river sediments. *Earth and Planetary Science Letters*, 206(3–4):273–288.

Vassallo, R., Mugnier, J.-L., Vignon, V., Malik, M. A., Jayangondaperumal, R., Srivastava, P., Jouanne, F., and Carcaillet, J. (2015). Distribution of the late-quaternary deformation in northwestern himalaya. *Earth and Planetary Science Letters*, 411:241–252.

von Blanckenburg, F. (2005). The control mechanisms of erosion and weathering at basin scale from cosmogenic nuclides in river sediment. *Earth and Planetary Science Letters*, 237:462–479.

von Blanckenburg, F., Hewawasam, T., and Kubik, P. W. (2004). Cosmogenic nuclide evidence for low weathering and denudation in the wet, tropical highlands of sri lanka. *Journal of Geophysical Research: Earth Surface*, 109(F3):F03008.

Wallis, D., Carter, A., Phillips, R. J., Parsons, A. J., and Searle, M. P. (2016). Spatial variation in exhumation rates across ladakh and the karakoram: New apatite fission track data from the eastern karakoram, nw india. *Tectonics*, 35:704–732.

Wandrey, C. J. and Law, B. E. (1998). Maps showing geology, oil and gas fields and geologic provinces of south asia. Open-file report 97-470C, United States Geological Survey.

Wani, A. A., Bali, B. S., Bhat, G. R., and Hussain, N. (2020). Impact of tectonics on drainage network evolution of suru basin, kargil n/w himalaya, jammu and kashmir, india. *Environmental Earth Sciences*, 79(26):13.

Wani, A. A., Bali, B. S., and Lone, S. (2019). Drainage characteristics of tectonically active area: An example from mawar basin, jammu and kashmir, india. *Journal Geological Society of India*, 93:313–320.

Werner, B. T. (2003). Modeling landforms as self-organized, hierarchical dynamical systems. In Wilcock, P. R. and Iverson, R. M., editors, *Prediction in Geomorphology*, volume 135, pages 133–150. American Geophysical Union, Washington, DC, USA.

Werner, C. (1988). Formal analysis of ridge and channel patterns in maturely eroded terrain. *Annals of the Association of American Geographers*, 78(2):253–270.

Whipple, K. X. (2004). Bedrock rivers and geomorphology of active orogens. *Annual Review of Earth and Planetary Sciences*, 32:151–185.

Whitmeyer, S. J. and Dordevic, M. (2020). Creating virtual geologic mapping exercises in a changing world. *Geosphere*, 17(1):226–243.

Wilson, J. P. and Bishop, M. P. (2013). Geomorphometry. In Bishop, M. P. and Shroder, J., editors, *Treatise on Geomorphology*, volume 3 of *Remote Sensing and GIScience in Geomorphology*,

pages 162–186. Academic Press, San Diego, CA, USA.

Wilson, J. S. J., Chandrasekar, N., and Magesh, N. S. (2012). Morphometric analysis of major sub-watersheds in aiyar and karai pottanar basin, central tamil nadu, india using remote sensing and gis techniques. *Bonfring International Journal of Industrial Engineering and Managment Science*, 2(1):8–15.

Wintle, A. G. and Adamiec, G. (2017). Optically stimulated lumiescence signals from quartz: A review. *Radiation Measurements*, 98:10–33.

Wohl, E. (2013). The complexity of the real world in the context of the field tradition in geomorphology. *Geomorphology*, 200:50–58.

Wohl, E., Gerlak, A. K., Poff, N. L., and Chin, A. (2014). Common core themes in geomorphic, ecological, and social systems. *Environmental Management*, 53:14–27.

Woldenberg, M. J. (1969). Spatial order in fluvial systems: Horton's laws derived from mixed hexagonal hierarchies of drainage basin areas. *Geological Society of America Bulletin*, 80:97–112.

Wood, J. (1996). Scale-based characterisation of digital elevation models. In Parker, D., editor, *Innovations in GIS 3*, pages 163–176. Taylor and Francis, London, UK.

Wu, J., Jelinski, D. E., Luck, M., and Tueller, P. T. (2000). Multiscale analysis of landscape heterogeneity: Scale variance and pattern metrics. *Geographic Information Sciences*, 6(1):6–19.

Xiao, C., Tian, Y., Li, T., and Gao, Z. (2013). Dem-based slope unit derivation. In *21st International Conference on Geoinformatics*. IEEE.

Xie, Z., Haritashya, U. K., Asari, V. K., Young, B. W., Bishop, M. P., and Kargel, J. S. (2020). Glaciernet: A deep-learning approach for debris-covered glacier mapping. *IEEE Access*, 8.

Xu, H., Zhou, W., Xie, R., Da, L., Xiao, C., Shan, Y., and Zhang, H. (2016). Characterization of rock mechanical properties using lab tests and numerical interpretation model of well logs. *Mathematical Problems in Engineering*, 2016:5967159.

Yamaguchi, Y. and Naito, C. (2003). Spectral indices for lithologic discrimination and mapping

by using the aster swir bands. *International Journal of Remote Sensing*, 24(22):4311–4323.

Yang, R., Suhail, H. A., Gourbet, L., Willet, S. D., Fellin, M. G., Lin, X., Gong, J., Wei, X., Maden, C., Jiao, R., and Chen, H. (2020). Early pleistocene drainage pattern changes in eastern tibet: Constraints from provenance analysis, thermochronometry, and numerical modeling. *Earth and Planetary Science Letters*, 531:115955.

Yang, R., Willett, S. D., and Goren, L. (2015). In situ low-relief landscape formation as a result of river network disruption. *Nature*, 520:526–529.

Yanites, B. J., Tucker, G. E., and Anderson, R. S. (2009). Numerical and analytical models of cosmogenic radionuclide dynamics in landslide-dominated drainage basins. *Journal of Geophysical Research: Earth Surface*, 114(F1):F01007.

Yokoyama, R., Shirasawa, M., and Pike, R. J. (2002). Visualizing topography by openness: A new application of image processing to digital elevation models. *Photogrammetric Engineering and Remote Sensing*, 68(3):257–263.

Zámolyi, A., Székely, B., Draganits, E., and Timár, G. (2010). Neotectonic control on river sinuosity at the western margin of the little hungarian plain. *Geomorphology*, 122:231–143.

Zanchi, A. and Gaetani, M. (2011). The geology of the karakoram range, pakistan: the new 1:100,000 geological map of central-western karakoram. *Italian Journal of Geosciences*, 130(2):161–262.

Zeitler, P. K., Koons, P. O., Bishop, M. P., Chamberlain, C. P., Craw, D., Edwards, M. A., Hamidullah, S., Jan, M. Q., Khan, M. A., Khattak, M. U. K., Kidd, W. S. F., Mackie, R. L., Meltzer, A. S., Park, S. K., Pecher, A., Poage, M. A., Sarker, G., Schneider, D. A., Seeber, L., and Shroder, J. F. (2001a). Crustal reworking at nanga parbat, pakistan: Metamorphic consequences of thermal-mechanical coupling facilitated by erosion. *Tectonics*, 20(5):712–728.

Zeitler, P. K., Meltzer, A. S., Koons, P. O., Craw, D., Hallet, B., Chamberlain, C. P., Kidd, W. S. F., Park, S. K., Seeber, L., Bishop, M. P., and Shroder, J. (2001b). Erosion, himalayan geodynamics, and the geomorphology of metamorphism. *GSA Today*, pages 4–9.

Zernitz, E. R. (1932). Drainage patterns and their significance. *The Journal of Geology*, 40(6):498–

521.

Zhang, X., Xiao, P., and Feng, X. (2020). Object-specific optimization of hierarchical multiscale segmentations for high-spatial resolution remote sensing images. *ISPRS Journal of Photogrammetry and Remote Sensing*, 159:308–321.

Zhao, Y., Wu, P., Li, J., Lin, Q., and Lu, Y. (2019). A new algorithm for automatic extraction of valley floor width. *Geomorphology*, 335:37–47.

Zhou, Q. and Liu, X. (2002). Error assessment of grid-based flow routing algorithms used in hydrological models. *International Journal of Geographical Information Science*, 16(8):819–842.